

| | |
|----------------------|---|
| Title | Iterative reconstruction as a novel method of radiation dose reduction at computed tomography in patients with Crohn's disease |
| Authors | O'Neill, Siobhán B. |
| Publication date | 2016 |
| Original Citation | O'Neill, S. B. 2016. Iterative reconstruction as a novel method of radiation dose reduction at computed tomography in patients with Crohn's disease. PhD Thesis, University College Cork. |
| Type of publication | Doctoral thesis |
| Rights | © 2016, Siobhán B. O'Neill. - http://creativecommons.org/licenses/by-nc-nd/3.0/ |
| Download date | 2024-05-08 01:54:03 |
| Item downloaded from | https://hdl.handle.net/10468/2608 |



Iterative Reconstruction as a Novel Method of Radiation Dose Reduction at Computed Tomography in Patients with Crohn's Disease

Siobhán Bernadette O' Neill

MB MCh BAO BMedSc MRCPI FFR(RCSI)

January 2016

This thesis is submitted for a PhD degree in Medicine from the National University of Ireland, University College Cork, School of Medicine and Health.

Supervisor: Professor Michael M. Maher

Head of Department: Professor Michael M. Maher

Table of contents

| | |
|--|-------|
| List of tables | V |
| List of figures | VII |
| Declaration | XII |
| Acknowledgements | XV |
| Dedication | XVIII |
| Abstract | XIX |
| Brief Introduction | XXII |
| <hr/> | |
| Chapter 1: Background | 1 |
| Techniques and Principles of Computed Tomography | 3 |
| CT History | 3 |
| CT Technology | 4 |
| Attenuation | 6 |
| Hounsfield Units | 6 |
| CT Scanner Set-up | 8 |
| Multi-detector CT | 8 |
| Helical Scanning | 9 |
| Data Acquisition | 10 |
| Image Processing | 11 |
| Filters | 11 |
| Automated Tube Current Modulation | 12 |
| Radiation Dose Concerns | 13 |
| CT Radiation Dose | 13 |
| Factors Affecting Radiation Dose | 17 |
| Image Reconstruction: Traditional and Novel Algorithms | 19 |
| Traditional Algorithms | 19 |
| Novel Algorithms | 21 |
| The Iterative Renaissance | 23 |
| Vendor Differences | 24 |
| Adaptive Statistical Iterative Reconstruction | 26 |
| Model Based Iterative Reconstruction | 28 |
| Image Quality Performance | 30 |
| Radiation Dose Metrics and their Measurement | 34 |
| CT Dosimetry | 34 |
| Image Quality Parameters and their Measurement | 38 |
| Parameters of Image Quality in CT | 38 |

| | |
|---|-----|
| Objective Evaluation | 40 |
| Subjective Evaluation | 41 |
| Potential for Bias | 43 |
| Evaluation Scales | 44 |
| Research Subjects | 46 |
| Aims of this Thesis | 48 |
| Aims | 48 |
| Hypotheses | 48 |
| Specific Objectives of the Individual Chapters | 49 |
| <hr/> | |
| Chapter 2: Evaluation of Iterative Reconstruction in phantom and cadaveric models with varying CT acquisition protocols with eventual development of a modified dose protocol for CT of abdomen and pelvis. | 51 |
| Introduction | 52 |
| Methods | 57 |
| Results | 71 |
| Discussion | 85 |
| Protocol Selection | 91 |
| <hr/> | |
| Chapter 3: A prospective feasibility study of sub-millisievert abdominopelvic CT using adaptive statistical iterative reconstruction in Crohn's disease | 97 |
| Introduction | 98 |
| Methods | 106 |
| Results | 120 |
| Discussion | 137 |
| <hr/> | |
| Chapter 4: Determining the optimal strength of adaptive statistical iterative reconstruction to apply to a modified dose CT protocol in patients with Crohn's disease | 145 |
| Introduction | 146 |
| Methods | 148 |
| Results | 155 |
| Discussion | 167 |

| | |
|--|-----|
| Chapter 5: A prospective feasibility study of sub-millisievert abdominopelvic CT using model based iterative reconstruction in Crohn's disease | 173 |
| Introduction | 174 |
| Methods | 176 |
| Results | 185 |
| Discussion | 202 |
| Chapter 6: Dose-equivalent CT with model based iterative reconstruction as a replacement for the abdominal radiograph in patients with Crohn's disease | 209 |
| Introduction | 210 |
| Methods | 214 |
| Results | 218 |
| Discussion | 227 |
| Chapter 7: Quantitative comparison of tissue attenuation values across traditional and novel reconstruction algorithms | 233 |
| Introduction | 234 |
| Methods | 237 |
| Results | 249 |
| Discussion | 261 |
| Conclusions | 265 |
| References | 272 |
| Appendices | 299 |
| Ethical Approval Documentation | 300 |
| Index | 303 |

List of Tables

| | |
|------------|---|
| Table 1.1: | Approximate range of CT numbers for a section of common tissues |
| Table 1.2: | Average effective doses for various diagnostic radiology procedures |
| Table 1.3: | CT technical parameters and effects on radiation dose |
| Table 1.4: | A summary of the currently available iterative reconstruction algorithms |
| Table 1.5: | A summary of the main benefits and pitfalls of ASiR and MBIR |
| Table 1.6: | A brief summary of performance evaluation studies of iterative reconstruction algorithms |
| Table 1.7: | A summary of CT dose descriptors and the CT parameters that affect them |
| Table 1.8: | The fundamental determinants of image quality in CT systems |
| Table 2.1: | Standard scan parameter applied to all CT acquisition protocols |
| Table 2.2: | Mean radiation doses for the anthropomorphic phantom with each CT protocol |
| Table 2.3: | How radiation dose correlates with image quality indices across the four reconstruction algorithms |
| Table 2.4: | Radiation dose and image quality parameters for 'standard-of-care' CT of abdomen and pelvis |
| Table 2.5: | Summary of the input parameters, radiation dose and image quality of the selected protocols |
| Table 3.1: | Patient demographics and clinical characteristics |
| Table 3.2: | Harvey-Bradshaw Index of Crohn's disease activity |
| Table 3.3: | Crohn's disease activity score |
| Table 3.4: | A summary of the radiation dose from modified and conventional dose CT protocols and the absolute and percentage dose reductions achieved |
| Table 3.5: | A summary of radiation dose from modified and conventional dose CT protocols for patients categorised by BMI <25kg/m ² of BMI ≥25kg/m ² |
| Table 3.6: | Lesions detected on conventional dose CT |
| Table 3.7: | Crohn's disease activity score |
| Table 4.1: | Patient demographics and clinical characteristics |
| Table 5.1: | Crohn's disease activity score |
| Table 5.2: | Patient demographics and clinical characteristics |

| | |
|------------|---|
| Table 5.3: | A summary of the radiation dose from modified and conventional dose CT protocols and the absolute and percentage dose reductions achieved |
| Table 5.4: | A summary of radiation dose from modified and conventional dose CT protocols for patients categorised by BMI <25kg/m ² of BMI ≥25kg/m ² |
| Table 5.5: | Crohn's disease related CT findings demonstrated on the method of reference reads |
| Table 5.6: | Comparison of median Crohn's disease activity scores between modified dose CT with MBIR and conventional dose CT with ASiR 40% |
| Table 5.7: | Cohen's Kappa agreement scores for CDAS and clinical findings comparing modified dose CT with MBIR and conventional dose CT with ASiR 40% with the method of reference read and with each other for each reader |
| Table 5.8: | Comparison of extra-intestinal CT findings between modified dose CT with MBIR and conventional dose CT with ASiR 40% for each reader |
| Table 6.1: | Summary of radiation dose for the modified dose CT protocol |
| Table 6.2: | Summary of the Crohn's disease related image findings on each modality |
| Table 7.1: | CTP404 sensitometry target specifications |
| Table 7.2: | Patient demographics and clinical characteristics |
| Table 7.3: | Standard scan parameters applied to all CT acquisition protocols |
| Table 7.4: | Anatomical sites in patients at which regions of interest were placed to measure objective image noise |

List of Figures

- Figure 1.1: CT scanner set-up
- Figure 1.2: Schematic of x-ray tube and detector set-up
- Figure 1.3: The Hounsfield scale of CT numbers
- Figure 1.4: Axial and helical mode CT scanning
- Figure 1.5: Global collective radiation dose from medical exposures
- Figure 1.6: Schematic representation of the steps of iterative reconstruction
- Figure 2.1: Kyoto anthropomorphic phantom positioning on the CT table
- Figure 2.2: Lateral and antero-posterior CT localiser radiographs of the Kyoto phantom
- Figure 2.3: Schematic set-up of the Catphan 600 phantom on the CT table
- Figure 2.4: Photographs of the Catphan 600 phantom in position on the CT table
- Figure 2.5: The CTP528 Catphan module
- Figure 2.6: The CTP515 Catphan module
- Figure 2.7: Schematic summarising the CT scanning parameters used for each of the CT acquisition protocols
- Figure 2.8: Attenuation and objective noise measurements in anthropomorphic phantom, cadaver and live human subject
- Figure 2.9: Slice levels in phantom (A) and cadaver (B) where regions of interest were placed to measure attenuation and objective noise
- Figure 2.10: Variations of radiation dose in terms of DLP, CTDI_{vol}, SSDE and effective dose with tube current, tube voltage and noise index
- Figure 2.11: Scatter graph of mean attenuation in the anthropomorphic phantom with each reconstruction algorithm
- Figure 2.12: Scatter graph of mean objective image noise in the anthropomorphic phantom with each reconstruction algorithm
- Figure 2.13: Scatter graphs of mean absolute (A) and percentage (B) objective image noise reduction in the anthropomorphic phantom with each reconstruction algorithm
- Figure 2.14: Scatter graph of mean signal to noise ratio in the anthropomorphic phantom with each reconstruction algorithm
- Figure 2.15: Scatter graph of median contrast resolution in the Catphan phantom with each reconstruction algorithm
- Figure 2.16: Scatter graph of median contrast to noise ratio in the Catphan phantom with each reconstruction algorithm
- Figure 2.17: Scatter graph of median spatial resolution in the Catphan phantom with each reconstruction algorithm
- Figure 3.1: Measurement of lateral (A) and antero-posterior (B) patient skin-to-skin diameters on the CT localiser images at the midslice level

- Figure 3.2: Column bar graph summarising the effective doses overall and for the BMI subgroups with both conventional and modified dose CT protocols
- Figure 3.3: Modified (A) and conventional (B) dose CT images of acute enteritis
- Figure 3.4: Modified (A) and conventional (B) dose CT images of acute proctitis
- Figure 3.5: Modified (A) and conventional (B) dose CT images of mesenteric lymphadenopathy
- Figure 3.6: Modified (A) and conventional (B) dose CT images of a pericolonic abscess
- Figure 3.7: Modified (A) and conventional (B) dose CT images of an enterocolic fistula
- Figure 3.8: Modified (A) and conventional (B) dose CT images of an incidentally detected case of cervical carcinoma with hydroureter and hydronephrosis
- Figure 3.9: Diagnostic acceptability of conventional and modified dose CT images
- Figure 3.10: Distribution and severity of streak artefact on conventional and modified dose CT images
- Figure 3.11: Subjective image noise on conventional and modified dose CT images
- Figure 3.12: Contrast resolution on conventional and modified dose CT images
- Figure 3.13: Boxplot of overall objective noise for conventional and modified dose CT protocols
- Figure 3.14: Mean objective noise at 5 distinct anatomical levels on conventional and modified dose CT images
- Figure 3.15: Signal to noise ratio for conventional and modified dose CT images
- Figure 4.1: Schematic of the reconstructed series yielded from the conventional and modified dose CT raw data
- Figure 4.2: The Advantage workstation
- Figure 4.3: Screenshot of the image review set-up for assessment of image quality indices
- Figure 4.4: Mean subjective diagnostic acceptability (A), contrast resolution (B) and streak artefact (C) with increasing strengths of ASiR for modified dose CT imaging
- Figure 4.5: Mean subjective image noise scores for increasing strengths of ASiR for modified dose CT imaging
- Figure 4.6: Mean absolute (A) and percentage (B) reduction in subjective image noise for increasing strengths of ASiR for modified dose CT imaging

- Figure 4.7: Mean objective image noise scores for increasing strengths of ASiR for modified dose CT imaging
- Figure 4.8: Mean absolute (A) and percentage (B) reduction in objective image noise for increasing strengths of ASiR for modified dose CT imaging
- Figure 4.9: Mean attenuation with increasing strengths of ASiR for modified dose CT imaging
- Figure 4.10: Mean signal to noise ratio with increasing strengths of ASiR for modified dose CT imaging
- Figure 4.11: The impact of BMI grouping on image quality indices of diagnostic acceptability (A), contrast resolution (B), streak artefact (C), subjective image noise (D) and objective image noise (E)
- Figure 5.1: The effective doses overall and for the BMI subgroups with both conventional and modified dose CT protocols
- Figure 5.2: Bar chart of the number of patients within each Crohn's disease activity score grade.
- Figure 5.3: Line graph demonstrating objective noise across reconstruction protocols
- Figure 5.4: Box and whisker plots demonstrating absolute (A) and percentage (B) noise reductions achieved with ASiR 40% and 70% and MBIR with modified dose CT
- Figure 5.5: Stacked bar graphs demonstrated the distribution of subjective noise (A), diagnostic acceptability (B), contrast resolution (C), spatial resolution (D) and streak artefact (E) for each of the reconstruction protocols
- Figure 5.6: Active Crohn's enteritis demonstrated on modified dose CT reconstructed with FBP (A), ASiR 40% (B), ASiR 70% (C) and MBIR (D) with conventional dose CT with FBP (E) for comparison
- Figure 5.7: Active Crohn's colitis demonstrated on modified dose CT reconstructed with FBP (A), ASiR 40% (B), ASiR 70% (C) and MBIR (D) with conventional dose CT with FBP (E) for comparison
- Figure 5.8: An end ileostomy demonstrated on modified dose CT reconstructed with FBP (A), ASiR 40% (B), ASiR 70% (C) and MBIR (D) with conventional dose CT with FBP (E) for comparison
- Figure 5.9: An ileo-ileal fistula with local perforation demonstrated on modified dose CT reconstructed with FBP (A), ASiR 40% (B), ASiR 70% (C) and MBIR (D) with conventional dose CT with FBP (E) for comparison
- Figure 5.10: Two Crohn's related abscesses demonstrated on modified dose CT reconstructed with FBP (A), ASiR 40% (B), ASiR 70% (C) and MBIR (D) with conventional dose CT with FBP (E) for comparison
- Figure 5.11: An incidental porcelain gallbladder demonstrated on modified dose CT reconstructed with FBP (A), ASiR 40% (B), ASiR 70% (C)

and MBIR (D) with conventional dose CT with FBP (E) for comparison

- Figure 6.1: Schematic summarising the study population
- Figure 6.2: Column bar graph summarising the effective radiation doses for abdominal radiograph and modified dose CT, with conventional dose CT and mean standard of care CT dose for comparison
- Figure 6.3: Column bar graph summarising the effective dose for abdominal radiation and modified dose CT, stratified for BMI values of $<25\text{kg/m}^2$ and $\text{BMI} \geq 25\text{kg/m}^2$
- Figure 6.4: Summary of the number of normal and abnormal examinations for each imaging modality
- Figure 6.5: Acute enteritis demonstrated on modified dose CT with MBIR.
- Figure 6.6: Acute enteritis with a non-obstructing stricture demonstrated on modified dose CT with MBIR.
- Figure 6.7: Sacroiliitis demonstrated on modified dose CT with MBIR.
- Figure 6.8: Incidental indeterminate low attenuation pancreatic lesion demonstrated on modified dose CT with MBIR.
- Figure 7.1: The CTP404 module of the Catphan 600 phantom
- Figure 7.2: Series reconstructed from the phantom and cadaveric raw data
- Figure 7.3: Series reconstructed from the clinical patient raw data
- Figure 7.4: The CTP404 module of the Catphan 600 phantom with regions of interest drawn in all 8 sensitometry targets
- Figure 7.5: Slice levels in phantom (A) and cadaver (B) where regions of interest were placed to measure attenuation and objective noise
- Figure 7.6: Slice levels in clinical patients where regions of interest were placed to measure attenuation and objective noise
- Figure 7.7: Attenuation and objective noise measurements in anthropomorphic phantom, cadaver and live human subject
- Figure 7.8: Graphical representation of the mean overall attenuation values of each of the sensitometry targets of the CTP404 module of the Catphan phantom
- Figure 7.9: Box plot of attenuation values in the sensitometric targets in the CTP404 module across all nineteen of the acquisition protocols
- Figure 7.10: Scatter graph demonstrating the mean attenuation from a composite of the 8 sensitometric targets in the CTP404 module with each reconstruction algorithm
- Figure 7.11: Line plot of the mean attenuation for each of the individual sensitometric targets across reconstruction algorithms
- Figure 7.12: Scatter graph demonstrating the mean attenuation for a composite of 5 anatomical sites in the anthropomorphic phantom with each reconstruction algorithm

- Figure 7.13: Scatter graph demonstrating the mean attenuation for a composite of 5 anatomical sites in the five cadavers with each reconstruction algorithm
- Figure 7.14: Box and whisker plot of attenuation at 13 sites in clinical patients with each reconstruction algorithm
- Figure 7.15: Line graph depicting the effect of reconstruction algorithms on objective image noise at each of 13 anatomical sites
- Figure 7.16: Graphical representation of the attenuation values in the right ischiorectal fossa across reconstruction algorithms
- Figure 7.17: Mean attenuation with standard deviation for increasing strengths of ASiR for modified dose CT imaging.
- Figure 7.18: Box and whisker plot demonstrating objective noise values across reconstruction algorithms
- Figure 7.19: Line graph depicting the effect of reconstruction algorithm on objective image noise at each of 13 anatomical sites
- Figure 7.20: Graphical representation of the signal to noise ratio with each reconstruction algorithm
- Figure 7.21: Expanded detail of line graph (Figure 7.16) above depicting the effect of reconstruction algorithm on objective image noise in the fat in the buttock and ischiorectal fossa.

Declaration

This thesis is submitted University College Cork in accordance with the requirements for the degree of Doctor of Philosophy (PhD) in the Faculty of Medicine.

This is to certify that the work I am submitting is my own and has not been submitted for another degree, either at University College Cork or elsewhere. All external references and sources are clearly acknowledged and identified within the contents. I have read and understood the regulations of University College Cork concerning plagiarism.

Parts of this work have appeared in the following peer reviewed publications and presentations:

Peer-reviewed journal publications:

1. O' Neill SB, McLaughlin PD, Crush L, et al. A prospective feasibility study of sub-millisievert abdominopelvic CT using iterative reconstruction in Crohn's disease. *Eur Radiol* 2013; 23:2503-12.
2. Craig O, O' Neill S, O' Neill F, et al. Diagnostic accuracy of computed tomography using lower doses of radiation for patients with Crohn's disease. *Clin Gastroenterol Hepatol* 2012; 10(8):886-92.
3. McLaughlin PD, Murphy K, Twomey M, O' Neill S, et al. Pure iterative reconstruction improves image quality in computed tomography of abdomen and pelvis acquired at substantially reduced radiation doses inpatients with active Crohn's disease. *J Comput Assist Tomogr* 2016; 40(2) ;225-33.
4. O' Neill SB, O' Connor OJ, McWilliams SR, et al. Minimization of radiation exposure due to computed tomography in inflammatory bowel disease. *Clin Res Hepatol Gastroenterol* 2011; 35(2):105-10.

5. McLaughlin PD, O'Connor OJ, O'Neill SB, et al. Minimization of radiation exposure due to computed tomography in inflammatory bowel disease. *ISRN Gastroenterol* 2012; 2012:790279.

Book chapters:

1. McLaughlin P, O'Neill SB, O'Connor OJ, Shanahan F, Maher M. Crohn's disease: Minimizing radiation dose. *Abdominal Imaging* 11/2013; pp671-6. DOI: 10.1007/978-3-642-13327-5_219.

International presentations:

1. O' Neill SB, McWilliams SR, O'Neill F, et al. A quantitative comparison of model-based iterative reconstruction, adaptive statistical iterative reconstruction and filtered back projection for abdominal CT. *Presented at the Radiological Society of North America (RSNA) meeting, Chicago, December 2011.*
2. O' Neill SB, McWilliams SR, Breen M, et al. The effect of statistical iterative image reconstruction on diagnostic quality and noise indices for low dose CT: established the optimum level of iterative reconstruction to apply. *Presented at the Radiological Society of North America (RSNA) meeting, Chicago, December 2011.*
3. O' Neill SB, Breen M, Hayes S, et al. A pictorial review of the use of ultra low dose CT of abdomen and pelvis in patients with Crohn's disease: How low can we go? *Poster presentation at the Radiological Society of North America (RSNA) meeting, Chicago, December 2011.*
4. O'Neill SB, Leong S, McWilliams SR, et al. Is low-dose CT with adaptive statistical iterative reconstruction (ASiR) a feasible alternative diagnostic examination for investigation of patients with Crohn's disease? A prospective study. *Presented at the European Society of Gastrointestinal and Abdominal Radiology (ESGAR) meeting, Venice, June 2011 with abstract published in Insights into Imaging.*

5. O'Neill SB, McWilliams SR, Breen M et al. The effect of statistical image reconstruction on measured Hounsfield Unit densities and noise at various anatomical sites – the experience with 40 patients. *Presented at the European Society of Gastrointestinal and Abdominal Radiology (ESGAR) meeting, Venice, June 2011 with abstract published in Insights into Imaging.*
6. Craig O, O'Neill SB, Maher MM, et al. A prospective trial of low-dose abdominal computed tomography (CT) with iterative reconstruction vs conventional CT in Crohn's disease. *Presented at Digestive Disease Week (DDW), Chicago, May 2011 with abstract published in Gastroenterology.*
7. O'Neill SB, O'Neill F, Bye J, et al. Low-dose CT in initial evaluation of Crohn's disease in the emergency setting? Toward replacing the PFA. *Presented at the European Congress of Radiology (ECR), Edinburgh, March 2012 with abstract published in Insights into Imaging.*
8. O'Neill SB, O'Neill F, Bye J, et al. Low-dose CT in initial evaluation of Crohn's disease in the emergency setting? Toward replacing the PFA. *Presented at the Southern Radiology Society meeting, Cork, June 2012 and awarded the SRS radiology registrars' medal and bursary.*
9. O'Neill SB, McLaughlin PD, Ryan MF, et al. Replacing the emergency department abdominal radiograph with low dose CT in the setting of active Crohn's disease. *Presented at the Radiological Society of North America (RSNA) meeting, Chicago, December 2012.*
10. McLaughlin PD, O'Neill SB, O'Regan K, et al. Low dose abdominopelvic CT in active Crohn's disease: image quality and diagnostic accuracy with model-based iterative reconstruction. *Presented at the Radiological Society of North America (RSNA) meeting, Chicago, December 2012.*
11. O'Neill SB, Crush L, O'Regan KN, et al. Low dose abdominopelvic CT in active Crohn's disease: image quality and diagnostic accuracy with model-based iterative reconstruction. *Presented at the European Congress of Radiology (ECR), Barcelona, March 2013 with abstract published in Insights into Imaging.*

Siobhán O' Neill

January 2016

Acknowledgements

"Limits exist only in the mind"

- Aristotle

I found these words roughly scrawled on the inside cover of my secondary school biology book, a hand-me-down from some cousin or other who was, no doubt, seeking inspiration and focus in their study. They have stuck with me through many years, my motivational mantra when circumstance demands. Early in this research, appreciation of the importance of the concept of limits in the realm radiation dose in medical imaging made limits a more concrete reality and undermined my belief in Aristotle's philosophy. There was a necessity to limit radiation exposure to patients but also a limit to any dose reduction possible. The novel iterative reconstruction algorithms studied in this work have reaffirmed my faith in Aristotle's wisdom, with limits again banished to the mind, and the world of possibilities for pushing the lower boundaries of radiation dose a tangible reality.

Firstly, I would like to thank my supervisor, Professor Michael Maher. From my early days as a medical student, he stood out as an excellent teacher and mentor and I am indebted to him for enticing me into the worlds of clinical and, later, academic radiology. His constant positivity and seemingly unwavering belief in my abilities have inspired me and have made me surprise myself with what I can achieve.

While 'Freddy the Phantom' didn't get much choice in the matter, many patients willingly and generously gave their time and consent to partake in this clinical research project and I am extremely grateful.

Professor Fergus Shanahan was central to conceiving, designing and executing this study. He brought inspiration, drive, common sense and a wealth of experience to the table and made this research possible. Professor Joseph Eustace was also of enormous value to this research, advising us mere mortals on all matters statistical.

Particularly in the past year, Sinéad Kinsella has been my PhD hero, helping me in ways she didn't even know. To her, I am forever grateful.

During the course of this research, the radiation dose team in Cork University Hospital has grown and gone from strength to strength. The support and involvement of my many co-authors, in particular Dr. OJ O'Connor, Dr. Paddy McLaughlin and Dr. Kevin Murphy, is greatly appreciated. Thank you also to Fiona O'Neill, Niamh Moore, Mary-Jane Murphy, AnneMarie McGarrigle and Orla Craig for their individual roles in making this research possible.

The on-going and continued support of GE Healthcare for radiation dose research in Cork is also much appreciated. In particular, Jackie Bye was extremely valuable with her advice and frequent on-site presence.

Also, a special thank you to Marian Bourke for her support and kindness.

Thank you to my parents (Christy and Noreen) and siblings (Michelle and Damien) for their belief in me and constant support and encouragement over many, many years. A special mention also to my niece, Eva, and nephews Seán and Dara, for providing much-needed distraction and entertainment along the way.

For his love, patience, kindness and presence through each and every rough day Jamie Sheehan has my endless gratitude. I'm looking forward to the next and many more chapters with you.

Finally, the financial support of the UCC Medical Alumni Professor Denis O' Sullivan Clinical Research Fellowship helped make this research possible and, as a proud UCC graduate, I am honoured to be associated with this prestigious fellowship.

I am indebted for the support and kindness shown to me by all of the above and the many others not acknowledged here.

Dedication

To my parents, Christy and Noreen,
Thank you both,
for everything.



*"You can never cross the ocean until you have the courage to lose sight
of the shore"*

- Christopher Columbus

Abstract

Prior work of our research group, that quantified the alarming levels of radiation dose to patients with Crohn's disease from medical imaging and the notable shift towards CT imaging making these patients an at risk group, provided context for this work. CT delivers some of the highest doses of ionising radiation in diagnostic radiology. Once a medical imaging examination is deemed justified, there is an onus on the imaging team to endeavour to produce diagnostic quality CT images at the lowest possible radiation dose to that patient. The fundamental limitation with conventional CT raw data reconstruction was the inherent coupling of administered radiation dose with observed image noise – the lower the radiation dose, the noisier the image. The renaissance, rediscovery and refinement of iterative reconstruction removes this limitation allowing either an improvement in image quality without increasing radiation dose or maintenance of image quality at a lower radiation dose compared with traditional image reconstruction.

This thesis is fundamentally an exercise in optimisation in clinical CT practice with the objectives of assessment of iterative reconstruction as a method for improvement of image quality in CT, exploration of the associated potential for radiation dose reduction, and development of a new split dose CT protocol with the aim of achieving and validating diagnostic quality submillisievert CT imaging in patients with Crohn's disease.

In this study, we investigated the interplay of user-selected parameters on radiation dose and image quality in phantoms and cadavers, comparing traditional filtered back projection (FBP) with iterative reconstruction algorithms. This resulted in the development of an optimised, refined and appropriate split dose protocol for CT of the abdomen and pelvis in clinical patients with Crohn's disease allowing contemporaneous acquisition of both modified and conventional dose CT studies. This novel algorithm was then applied to 50 patients with a suspected acute complication of known Crohn's disease and the raw data reconstructed with FBP, adaptive statistical iterative reconstruction (ASiR) and model based iterative reconstruction (MBIR). Conventional dose CT images with FBP reconstruction were used as the reference standard with which the modified dose CT images were compared in terms of radiation dose, diagnostic findings and image quality indices. As there are multiple possible user-selected strengths of ASiR available, these were compared in terms of image quality to determine the optimal strength for this modified dose CT protocol. Modified dose CT images with MBIR were also compared with contemporaneous abdominal radiograph, where performed, in terms of diagnostic yield and radiation dose. Finally, attenuation measurements in organs, tissues, etc. with each reconstruction algorithm were compared to assess for preservation of tissue characterisation capabilities.

In the phantom and cadaveric models, both forms of iterative reconstruction examined (ASiR and MBIR) were superior to FBP across a wide variety of imaging protocols, with MBIR superior to ASiR in all areas other than reconstruction speed. We established that ASiR appears to work to a target

percentage noise reduction whilst MBIR works to a target residual level of absolute noise in the image. Modified dose CT images reconstructed with both ASiR and MBIR were non-inferior to conventional dose CT with FBP in terms of diagnostic findings, despite reduced subjective and objective indices of image quality. Mean dose reductions of 72.9-73.5% were achieved with the modified dose protocol with a mean effective dose of 1.26mSv. MBIR was again demonstrated superior to ASiR in terms of image quality. The overall optimal ASiR strength for the modified dose protocol used in this work is ASiR 80%, as this provides the most favourable balance of peak subjective image quality indices with less objective image noise than the corresponding conventional dose CT images reconstructed with FBP. Despite guidelines to the contrary, abdominal radiographs are still often used in the initial imaging of patients with a suspected complication of Crohn's disease. We confirmed the superiority of modified dose CT with MBIR over abdominal radiographs at comparable doses in detection of Crohn's disease and non-Crohn's disease related findings. Finally, we demonstrated (in phantoms, cadavers and in vivo) that attenuation values do not change significantly across reconstruction algorithms meaning preserved tissue characterisation capabilities with iterative reconstruction.

Both adaptive statistical and model based iterative reconstruction algorithms represent feasible methods of facilitating acquisition diagnostic quality CT images of the abdomen and pelvis in patients with Crohn's disease at markedly reduced radiation doses. Our modified dose CT protocol allows dose savings of up to 73.5% compared with conventional dose CT, meaning submillisievert imaging is possible in many of these patients.



Brief Introduction

Siobhan O' Neill

Iterative Reconstruction as a Novel Method of Radiation Dose Reduction at
Computed Tomography in Patients with Crohn's Disease

Brief introduction:

CT and its role in current imaging

Computed tomography (CT) is an advanced imaging modality that employs ionising radiation and advanced data reconstruction algorithms to achieve cross-sectional imaging with high spatial resolution in patients with a variety of disease entities. CT was introduced into clinical use in 1972 and CT continues to rank as one of the top five medical developments in the last 50 years. Its use has soared over the last four decades and CT is now the imaging modality of choice for a wider range of clinical applications than all other imaging modalities combined, occupying an important and ever-expanding role in the investigation, diagnosis and follow-up of disease.

Dose as a limiting factor to more widespread use

Because of its broad availability, excellence in image quality and suitability for a wide range of clinical indications, CT has become the most widely used cross-sectional imaging modality. In excess of 85 million CT scans are performed annually in the United States alone, a more than twenty fold increase since 1980 [1,2] and use continues to grow worldwide. It enables better surgery, better diagnosis and treatment of cancer, better treatment after injury, better treatment of stroke and better treatment of cardiac conditions [3,4]. **However, CT delivers some of the highest doses of ionising radiation in diagnostic radiology.** While the biological effects of high doses of radiation are well known and documented [5-8], most of what we believed about low-dose ionising radiation came from information extrapolated from atomic bomb survivors, who

received far greater doses of radiation than a patient typically receives from a CT, and was a contentious issue. Comparatively recently, a large and well-designed epidemiologic study has clearly shown that the individual risks from CT radiation, though small, are real [9]. This proof of risk obliges us to redouble our efforts to justify and optimise every scan.

Justification:

For almost all patients, the adverse health consequences of refusing a needed medical procedure such as CT far outweigh any potential radiation-associated risks or other risks that may be associated with the procedure [10]. However, while the diagnostic information gained from CT imaging can be hugely beneficial to the management of patients, if there is a less than robust indication for imaging and the radiologist's report does not impact upon clinical management of the patient, then the potential harm that may ensue for the patient as a result of radiation exposure is difficult to justify. Justification is facilitated by the 'three-As': *awareness* by knowledgeable healthcare professionals who assist the patient in balancing the immediate benefits of medical radiation with its downstream radiation risk, use of *appropriateness* guidelines to ensure that those patients referred for radiological examinations need them, and post-hoc *audit* of imaging use against agreed standards of good practice [11].

Optimisation:

For some patients, CT imaging is justified with good clinical reasons and unavoidable. For most patients, a single, albeit high dose, radiation event is of

low risk to the individual. However, other subgroups such as patients with chronic illnesses [end-stage kidney disease, cystic fibrosis, Crohn's disease] have been demonstrated as 'at risk' for high cumulative exposures to ionising radiation as a result of undergoing serial diagnostic imaging, particularly CT, studies [12-14] over decades of active disease. Optimisation incorporates keeping radiation exposure as low as reasonably achievable (ALARA) for every study, usually by applying various modality and procedure-specific techniques. ALARA requires the use of the lowest radiation dose that will yield appropriate image quality for a particular patient to enable the correct clinical decision – i.e. the dose used in a given examination must be enough to deliver sufficient image quality to answer the clinical question but as low as possible to minimise the risk to the patient. While this principle applies to all medical imaging studies, it is most relevant in 'at risk' groups for high cumulative doses.

CT dose reduction and the maintenance of diagnostic accuracy:

Radiation dose is related to the amount of energy that x-ray photons deliver during a CT scan [15] and is a major determinant of image quality. The application of low-dose CT protocols in clinical practice needs to be tailored to the specific diagnostic task required, so that diagnostic accuracy is maintained. The fundamental limit to image quality of a CT image is noise; image noise is inversely proportional to radiation dose. Noise is caused by variation in attenuation coefficients between individual voxels and affects the visibility of low contrast objects within a CT image. When evaluating for objects with high contrast (such as renal calculi or at CT angiography), diagnostic accuracy is only minimally affected with the use of low dose protocols, whereas it is more

adversely affected when evaluating objects with low contrast (such as hepatic metastases). Reducing radiation dose decreases the number x-ray photons absorbed in each voxel during the imaging process, making the measurement of attenuation coefficient values more imprecise and increasing image noise. By decreasing tube time current product (mAs) or voltage (kV), we deposit less photons in each voxel of tissue ($\text{photons} \propto \text{mAs}$; $\text{photons} \propto \text{kV}^3$), which results in increased statistical variation and more image noise.

Several recent advances in CT scanning techniques have allowed reduction of radiation dose at CT while maintaining diagnostic image quality: (a) advances in CT scanner hardware (higher power x-ray sources, improved detector capability), (b) use of automated tube current modulation (ATCM), (c) modifying CT protocols to optimise the tube voltage based on the diagnostic task and patient habitus, and (d) iterative image reconstruction. While advances in CT hardware continue to expand the boundaries of physical limitations, increases in computing power have opened additional pathways for improving the performance of CT via enhanced data processing methods, including the renaissance of iterative reconstruction [16]. Iterative reconstruction currently represents the most exciting development being implemented in clinical practice for the purpose of radiation dose optimisation in CT [17].

Iterative reconstruction techniques are software-based algorithms that allow either an improvement in image quality without increasing radiation dose or maintenance of image quality at a lower radiation dose compared with traditional image reconstruction [18].

A comprehensive discussion of each of these advances is outside the scope of this work. The focus of this thesis is on the role of iterative reconstruction in the development of optimal imaging protocols aimed at achieving the desired image quality with a reduced dose, though the complimentary dose-saving techniques of ATCM and tube voltage optimisation are also applied to protocol development. We concentrate on the subgroup of patients with Crohn's disease as our research group has demonstrated them an 'at risk' group for high cumulative doses of medical radiation [13] and because CT scans in this population will have a high yield of positive diagnostic findings, important when assessing for diagnostic non-inferiority. We aim to push the lower boundaries of acceptable dose in abdomino-pelvic CT imaging to the submillisievert realm, to achieve a dose comparable to that of a conventional abdominal radiograph.

The work described in the following chapters attempts to: provide a setting and context for the need for iterative reconstruction in current medical imaging practice (chapter 1), to examine the interplay of user selected parameters on radiation dose and image quality factors with both traditional and iterative reconstruction algorithm in an attempt to develop the optimal CT protocol for imaging of patients (chapter 2), to validate the use hybrid iterative reconstruction (adaptive statistical iterative reconstruction, ASiR) with modified dose CT protocols and to determine the optimal strength level to apply (chapters 3 and 4), to validate to use of pure iterative reconstruction (model based iterative reconstruction, MBIR) for modified dose CT protocols (chapter 5), to examine whether low dose CT with MBIR may be a suitable replacement for

plain abdominal radiographs performed at the same radiation dose (chapter 6), and to examine the fidelity of attenuation measurements with both iterative reconstruction algorithms and their suitability for continuing use for tissue characterisation (chapter 7). Initial preliminary imaging studies are performed on anthropomorphic and Catphan phantoms, progressing through to cadavers, and finally imaging of patients.



Chapter 1

Background

Iterative Reconstruction as a Novel Method of Radiation Dose Reduction at
Computed Tomography in Patients with Crohn's Disease

Background:

In order to provide a context for this thesis, this chapter aims to describe the history and principles of CT imaging, out-lining the main issues with this increasingly utilised imaging modality and some of the technological developments that have helped to resolve them. Parallel advances in the fields of x-ray physics and computing have facilitated the introduction of iterative reconstruction into clinical practice. This technology and the current state of knowledge regarding its clinical efficacy and utility are examined, in the context of the peer-reviewed literature. This work focuses in particular on dose reduction in abdominal imaging and on patients with Crohn's disease.

This chapter is divided into the following sections:

- Techniques and principles of computed tomography
- Radiation dose concerns
- Image reconstruction: traditional and novel algorithms
- Radiation dose and image quality trade-off
- Radiation dose metrics and their measurement
- Image quality parameters and their measurement
- Aims of this thesis

TECHNIQUES AND PRINCIPLES OF COMPUTED TOMOGRAPHY

CT history:

The concept of computed tomography was first developed, in 1971, by the British engineer Godfrey Hounsfield [19-20]. Tomography is derived from the Greek words '*tomos*', meaning slice or section, and '*graphia*', meaning describing. CT built on evolving developments in two fields – computing and x-ray imaging. Within months, CT scanners were developed on a commercial scale and introduced into clinical facilities worldwide.

X-rays were discovered in 1895 by Roentgen and within a few years were an established medical tool [21]. By the 1930s, x-ray tomography was developed, enabling visualisation of sections through a body. By the 1960s, several researchers were working independently on cross-sectional imaging with x-rays. Hounsfield was an engineer at Electric and Musical Industries Ltd. (EMI) and his work there culminated in the EMI scanner, a device that acquired data from multiple x-ray transmissions through a subject and utilised computers to reconstruct this image data. This relied on the previously reported work of South African born physicist Allan McLeod Cormack on the mathematical implementation for tomographic reconstruction [22]. By the end of the 1970s, the importance of CT scanning to medicine was clear.

In 1973 EMI was awarded a prestigious Queen's Award for Technological Innovation for the EMI scanner, now called the CT scanner [23]. For their independent but parallel work, Cormack and Hounsfield are considered the

pioneers of medical CT and received the Nobel prize for Medicine in 1979 for their epochal accomplishments during the 1960s and 1970s [22]. In 1981, Hounsfield received a knighthood for his work.

CT technology:

Since its conception, the CT imaging technique has undergone evolution in terms of both hardware and software. A CT scanner consists of a fixed gantry with an aperture through which a mobile bed/table travels. The scanning apparatus is housed in the gantry (see figure 1.1). During image acquisition, a rotating source of x-rays (tube) is used to acquire volumetric images of the subject whilst they 'translate' through the CT scanner (see figure 1.2). Throughout the scan the tube continually rotates around the subject while a detector on the opposite side records the remaining beam intensity (transmitted photons) – how much the subject attenuates the x-rays – at different angles (projections). The data at each detector represent the sum of the attenuation of all tissues through which the beam has passed; this is the CT raw data. Essentially, the detectors measure how much the subject attenuates the incident x-rays. Attenuation is expressed in Hounsfield Units (HU).

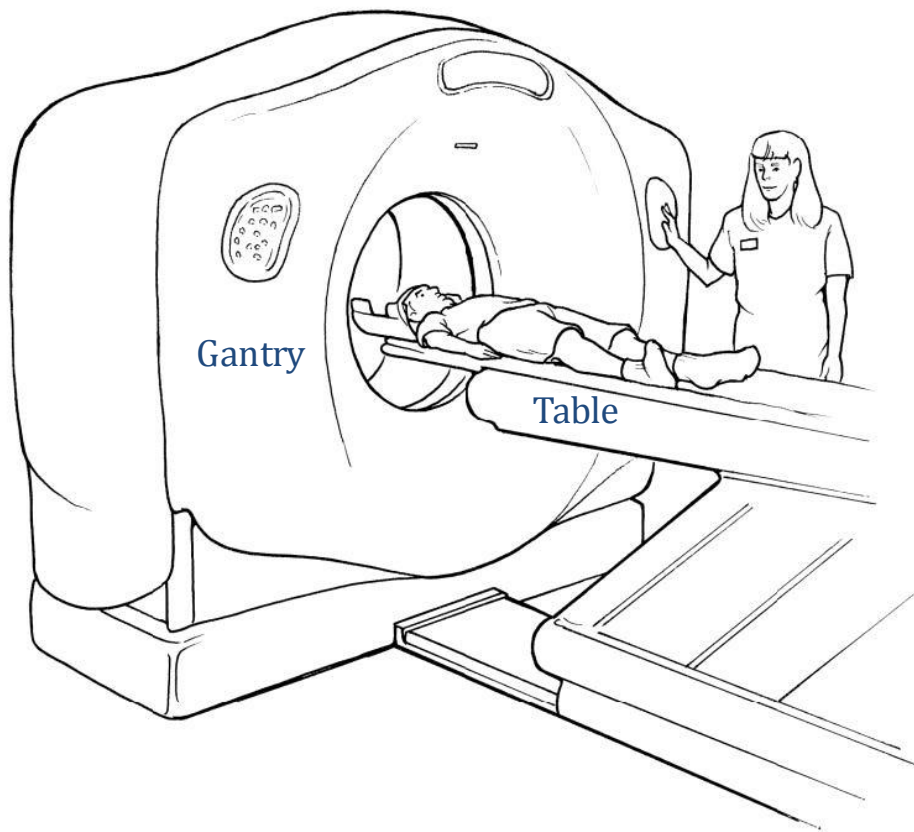


Figure 1.1: CT scanner set-up with a mobile bed/table translating through an aperture in the gantry, which houses the scanning apparatus.

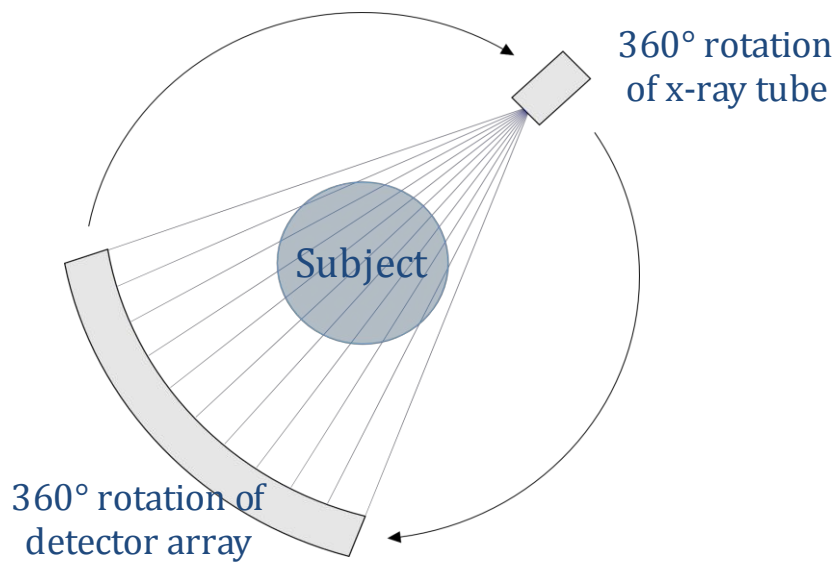


Figure 1.2: Schematic of the x-ray tube and detectors rotating around the subject. The x-rays from the tube are attenuated by the subject and the detectors measure the transmitted photons.

Attenuation:

X-rays are a form of ionising radiation, known to have very high but material-dependent matter penetration capabilities. As an x-ray passes through an object, the number of photons decreases exponentially along the projection path. Photons interact with the constituent tissues and mainly get scattered (Compton effect) or absorbed (photoelectric effect), such that the emerging x-ray beam has a reduced intensity, a phenomenon known as attenuation. At each location, the loss of photons can be characterised by the local attenuation coefficient and this value is energy dependent. CT is based on the fundamental principle that the density of the tissue traversed by the x-ray beam can be measured from calculation of the attenuation coefficient, possible as attenuation in CT is mainly due to electron density (equivalent to density). Materials with a high atomic number will be comparatively much denser due to the photoelectric effect.

Hounsfield units:

The linear attenuation coefficient (i.e. the density) of a tissue is displayed as Hounsfield Units (HU). The Hounsfield Unit is the measure of CT attenuation/density of the imaged substance and is a function of the linear attenuation coefficients of water, air and the substance of interest [24]. The HU scale is a linear transformation of the original linear attenuation coefficient of a tissue into one in which the radiodensity of distilled water at standard temperature and pressure is defined as 0HU, while the radiodensity of air under the same conditions is defined as -1000HU. These two values are independent of the energy from x-rays and, therefore, constitute fixed points on the CT attenuation scale. Other HU values, although correlating with density, cannot be

considered a direct measure of density. In a voxel with an average linear attenuation coefficient μ_x , the corresponding HU values is therefore given by:

$$HU = 1000 \times (\mu_x - \mu_{\text{water}}) / \mu_{\text{water}}$$

Where μ_{water} is the linear attenuation coefficient of water.

CT/Hounsfield numbers are rescaled normalised functions of linear attenuation coefficients and refer to the number assigned to each voxel in the CT image [25-26]. These quantitative measurements of tissue attenuation thus allow a quick and simple method to characterise certain tissue types on CT. It has been reported since the early days of CT imaging that CT number accuracy may be influenced by several factors, including the reconstruction kernel, reconstruction artifacts, beam hardening, spectral energy and scatter, as well as variations in patients size, shape, and position in the scanner [27-30]. Despite this, radiologists rely on Hounsfield unit values to make important clinical decisions, especially with respect to lesion and fluid characterisation. The basis for this practice is that certain recognised constituent tissues have CT numbers that, under ideal conditions, occupy specific ranges of the HU spectrum (see figure 1.3 and table 1.1 below).

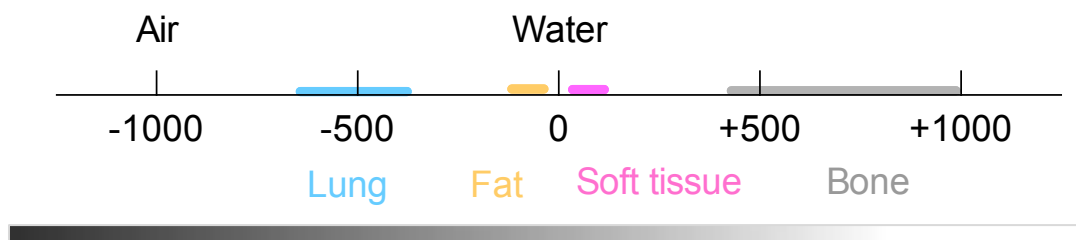


Figure 1.3: The Hounsfield scale of CT numbers outlining some of the main constituent tissues in the body and their attenuation ranges.

Table 1.1: Approximate range of CT numbers (HU) for a selection of common tissues

| | |
|-------------|---------------|
| Bone | +400 -> +1000 |
| Soft tissue | +40 -> +80 |
| Water | 0 |
| Fat | -60 -> -100 |
| Lung | -400 -> -600 |
| Air | -1000 |

CT scanner set-up:

The CT scanner built by EMI in 1971 is referred to as the first-generation CT. With this scanner set-up, there was an x-ray source and a single detector and data acquisition involved moving both the tube and the detector across the scanning plane to acquire a series of transmission measurements. The detector and tube were then rotated by 1° and the process repeated. This approach was extremely time consuming and limited by patient motion during the long x-ray exposure time. CT scanners evolved through successive generations to fifth-generation scanners though, with the advent of multi-detector CT, the third-generation scanner has become the industry standard. The third-generation scanner set-up comprises a large number of small detectors arranged in an arc opposite the source to cover the complete cross-section of the patient (see figure 1.2 above). This allows for continuous data collection through a full 360° rotation.

Multi-detector CT:

Multi-detector CT (MDCT) uses an array of detectors, arranged in both the axial (x-y) and longitudinal (z) planes. Use of multiple detector rows permits the simultaneous acquisition of data from multiple parallel slices, thus reducing

examination time. Current mainstream CT systems allow simultaneous acquisition of 64 to 128 slices, with up to 512-slice systems being available. Beam collimation is a product of the number of detector rows and the detector row width. In a 64-slice system with a detector row width of 0.625mm, the collimation is 64 x 0.625mm resulting in a total coverage of 4cm. MDCT increases scanning speed but also increases resolution in the longitudinal plane, allowing better multi-planar reconstructions and three-dimensional analysis. A disadvantage of MDCT is slightly reduced image quality with increasing number parallel slices due to cone beam artefacts and scattered radiation.

Helical scanning:

Body scanning is predominantly performed in helical mode, that is, the subject moves along the z-axis of the scanner, orthogonal (perpendicular) to the plane of rotation of the x-ray source and detector (x-y axis). The main benefits compared with axial scanning (i.e. the subject is fixed while the x-ray source and detector rotate around it in the x-y plane) include speed and continuity of image data acquisition, benefits which are generally considered to outweigh the marginal reduction in image quality compared with axial mode. Both modes are demonstrated in figure 1.4 below.

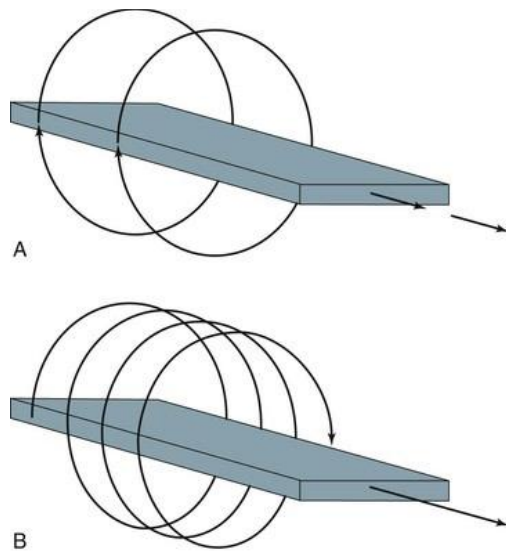


Figure 1.4: (A) Axial and (B) helical mode CT scanning.

Data acquisition:

Acquisition of three-dimensional data is achieved by the reconstruction of contiguous two-dimensional cross sections of the subject. Each two-dimensional image is constructed from a large number of equally spaced x-ray projections, which pass through the subject. The x-y plane effectively constitutes the image acquisition matrix while the z-axis is determined by the thickness of the image detector. The fundamental goal of CT data acquisition and reconstruction is to assign an attenuation value to each volume of information (voxel) of a three-dimensional volume. The image matrix describes multiple (typically 512×512) discrete voxels presented as a two-dimensional set of pixels. The spatial resolution of the images and, therefore, the image quality is an important physical parameter, which is defined by the dimensions of the pixels and their thickness (the voxel thickness). The smaller the pixel, the greater the spatial resolution. Isotropic voxels are important for multi-planar image reconstruction.

Image processing:

The data at each detector represent the sum of the attenuation of all tissues through which the beam has passed; this is the CT raw data. Once the detectors have collected the transmission measurements, they are sent to the computer for processing. Reconstruction algorithms use the raw data to determine attenuation values for each voxel; differences between reconstruction techniques involve determining how this attenuation value is assigned in the final image. During the CT reconstruction process, the attenuation data from a large number of projections (projection domain) are mathematically processed to create an image of the examined volume (image domain). Essentially, back projection involves reversal of the attenuation measurement process, where data from thousands of projections are used to reconstruct an image of the subject. The computer uses reconstruction algorithms, complex mathematical techniques, to reconstruct the CT images in a finite number of steps. There are two major classes of reconstruction algorithms: analytical and iterative. These will be discussed in detail in a later section.

Filters:

As part of the reconstruction process, mathematical filters (reconstruction kernels) are applied to the acquired data. This process aims to achieve appropriate balance between the inherently coupled factors detail resolution and noise for the diagnostic task and to counteract blurring. Since the reconstruction kernel plays a large role in determining spatial resolution, it has a great effect on the amount of noise in the image and, consequently, on the dose needed to achieve a specific level of image noise. Noise is objectively observed as

graininess making soft tissue structures difficult to differentiate. Filters are therefore a compromise between resolution and noise creation. The choice of kernel is made on the basis of clinical need. Different filter algorithms can be selected to enhance particular features within the image data such as a hard/smooth algorithm to enhance bone and lung images or a soft tissue algorithm that provides better soft tissue contrast.

Automated tube current modulation:

The radiation dose administered to the patient is dependent on the number of photons emitted from the x-ray tube and tube current is an important determinant of this. Along the z-axis of the patient, the patient's dimensions change resulting in changes in beam attenuation with more attenuation in thicker regions (such as the bony pelvis) and less attenuation in the mid-abdomen. A constant tube current over the entire scan length may result in over or under-exposure of some regions. Adjustment of the tube current based on regional body anatomy can aid in establishing an appropriate balance between image noise and radiation exposure with improved dose efficiency. Automated tube current modulation is a pre-programmed technology that adjusts the current based on variations in measured attenuation from one anatomic region to the next along the length of the patient from the CT localiser radiograph, seeking to produce approximately equivalent image quality along the length of the patient. This most commonly occurs in a longitudinal format, with modulation along the patient's length (z-axis), though angular modulation (in plane, x-y axis) or a combination of both may also be used.

RADIATION DOSE CONCERNS

CT radiation dose:

Because of its broad availability, excellence in image quality and suitability for a wide range of clinical indications, CT has become the most widely used cross-sectional imaging modality. Driven particularly by advances in multi-detector CT (MDCT) technologies, the number of CT scans performed each year in the United States has reached nearly 81.2 million in 2014 [2]. In Europe, CT accounts for 8.7% of the 660 million x-ray procedures performed annually. In Ireland CT accounts for 5.1% of all x-ray procedures, equating to 66.8 CT examinations per 1000 of population per year [31]. The United Nations Scientific Committee on the Effects of Atomic Radiation (UNSCEAR) 2008 report estimated that 44% of the global collective effective dose from medical exposures arises from CT, with 221 million CT examinations performed annually worldwide [32] (see figure 1.5 below). This corresponds to an annual rate of 207 CT examinations for every 1000 people, though the geographic distribution of much of this dose is skewed.

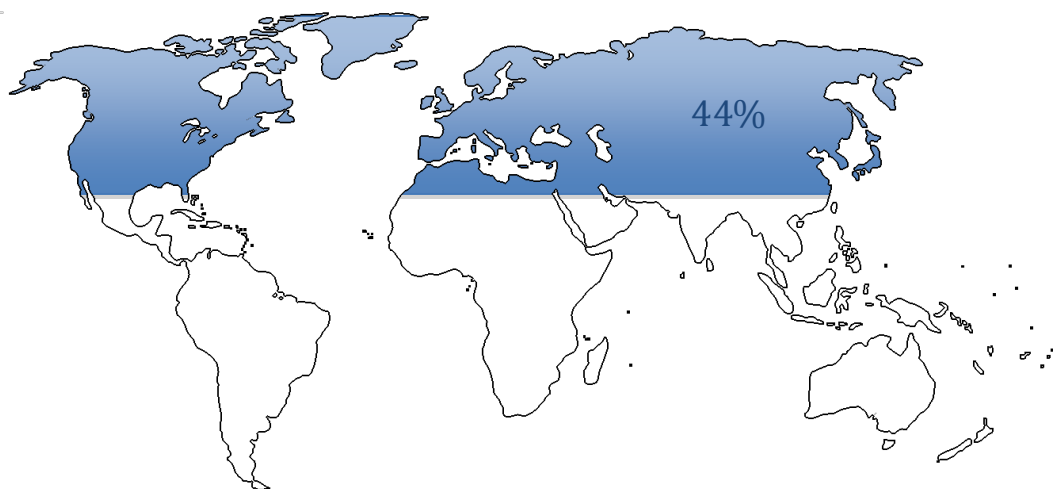


Figure 1.5: The UNSCEAR 2008 report estimated that CT accounts for 44% of the global collective dose from medial exposures.

The main disadvantage of CT is the use of ionising radiation; CT delivers some of the highest doses of ionising radiation in diagnostic radiology (see table 1.2) [33]. The potential radiation risk to the patient population, particularly children, has led to increasing attention from the radiology community in the past few years [9-10, 34-37]. The first suggestion of a link between medical radiation and cancer induction came in 2001, with two articles [7,38]. Brenner provided the first quantitative estimates of radiation risks associated with paediatric CT and Paterson outlines that the use of adult-based settings at paediatric CT were imparting higher than necessary radiation doses to these patients. These articles drew the attention of both the medical and the lay communities and brought recognition to the potential risks of CT.

Table 1.2: Average effective doses of radiograph for various diagnostic radiology procedures [33].

| Examination | Average effective dose (mSv) | Equivalent number of radiographs | Equivalent period of average natural background radiation (days) |
|---|------------------------------|----------------------------------|--|
| PA chest radiograph | 0.02 | 1 | 3 |
| Skull radiograph | 0.1 | 5 | 15 |
| Mammogram | 0.4 | 20 | 61 |
| Pelvic radiograph | 0.6 | 30 | 91 |
| Abdominal radiograph | 0.7 | 35 | 106 |
| Lung perfusion scintigraphy (99mTc-mmA) | 2 | 100 | 304 |
| CT brain | 2 | 100 | 304 |
| Intravenous urography | 3 | 150 | 456 |
| Bone isotope scintigraphy (99mTc-MDP) | 6.3 | 315 | 958 |
| CT chest | 7 | 350 | 1,065 |
| CT of abdomen and pelvis | 8 | 400 | 1,217 |
| Barium enema | 8 | 400 | 1,217 |

Until comparatively recently, the true nature and magnitude of the risk from the low levels of ionising radiation imparted at medical imaging was a controversial issue, with estimates of risk derived from studies of exposed Japanese atomic bomb survivors [39-40]. From these high dose effects, a conservative model of radiation risk, known as the linear no-threshold model, was developed [41]. This model assumes that the effects of high radiation doses can be extrapolated to low doses and that any dose, no matter how small, has the potential to cause harm.

In 2012, when Pearce et al published a landmark paper that proved a causal link between ionising radiation from medical imaging and carcinogenesis [9], the landscape of CT radiation risk changed completely. This comprehensive epidemiologic study of paediatric CT followed-up a cohort of 180,000 patients who had undergone CT imaging (280,000 CT scans) for a typical follow-up period of 10 years (maximum 23 years). During the follow-up period, there were increased incidences of leukaemia and brain tumours with bone marrow doses in excess of 30mGy and brain doses of in excess of 50mGy, respectively. These findings suggest similar risks of these two malignancies per unit radiation dose compared with data from atomic bomb survivors, validating the risk estimates proposed by the linear no-threshold model [41]. It follows that the individual risks from CT radiation, though small, are real.

With the growth of CT, both consumer and provider radiation dose awareness is high and this confirmation has fuelled growing uneasiness worldwide about radiation exposure from all diagnostic imaging, but particularly CT. While the immediate benefit to the individual patient of having a CT examination can be

substantial, there is a relatively high radiation dose associated with CT when compared with other imaging modalities. There is also increasing concern regarding the issue of cumulative radiation dose, particularly among patients with chronic illnesses who have been demonstrated as 'at risk' undergoing serial imaging studies and accumulating high exposures over years, sometimes decades, of active disease [12-14]. In these populations, as with others, the imaging modality that contributes the majority of exposure is computed tomography [3]. In its Publication 102, the international commission on radiological protection (ICRP) emphasised the importance of managing patient dose, particularly from repeated or multiple examinations [42]. Public campaigns such as Image Wisely [43] and Image Gently [44] have been initiated to engage the radiology community, with moves toward establishing local, national and international dose registries [45].

When a CT examination is clinically justified, the ALARA principle (As Low As Reasonably Achievable) is core to optimising the study [46] and is widely adopted in the radiation protection of patients undergoing diagnostic imaging including CT [47-51]. ALARA requires the use of the lowest radiation dose that will yield appropriate image quality for a particular patient to enable the correct clinical decision – i.e. the dose used in a given examination must be enough to deliver sufficient image quality to answer the clinical question but as low as possible to minimise the risk to the patient. Too low a dose may compromise the necessary image quality and lead to either misdiagnosis or even the need to repeat the entire study. Thus, the appropriate dose will vary with the clinical context and, in order to determine this, the clinician will need to define the

clinical question. For example, a lower dose is appropriate to evaluate a patient with Crohn's disease for potential extra-mural complications due to the inherent contrast provided by the peri-enteric and peri-colonic fat, whereas a higher dose would be appropriate if the clinical task were to visualise a small, low contrast lesion in the liver as this could easily be obscured by image noise at a lower dose.

Factors affecting radiation dose:

With conventional CT data reconstruction, image noise is inversely proportional to radiation dose [52]. In CT, factors that affect patient dose and image quality comprise scan parameters, inherent scanner factors and patient attributes. User-controlled parameters that affect radiation dose include tube current (mA), slice scan time (s) and peak tube voltage (kV). These are summarised in table 1.3 below [53]. Patient size plays a large role in the total absorbed dose for the same technique. With smaller patients, the dose can be two to three times higher than for a larger adult when using the same technique. With smaller patients, less kV and mAs are needed to achieve the same image quality so these parameters should be tailored to the individual patient. Different body organs have different sensitivities to radiation (e.g. bowel > liver > bone), meaning that, for the same absorbed dose, there is more risk if the abdomen is scanned versus the ankle. The risk of developing deleterious effects of radiation, such as cancer, decreases with age. Younger patients' organs are more radiosensitive due to the rapid rate of cell division and growth. Also, there is a latent period in the order of 10 years or more between radiation exposure and the clinical onset of cancer, meaning younger patients have a longer time frame in which this has potential to occur

[7,9,34]. Therefore, judicious and optimised use of CT imaging in young patients is critical.

Table 1.3: CT technical parameters and effects on radiation dose [53]

| CT technical parameter | Definition | Effect of CT technical parameter on radiation dose |
|--|--|---|
| X-ray tube current (mA) | The number of x-rays the tube produces | Radiation dose is directly proportional to x-ray tube current; may be chosen by operator or modulated automatically based on CT radiograph |
| X-ray tube rotation time, exposure time (s) | Time to complete one 360° rotation of the CT gantry | Radiation dose is directly proportional x-ray tube rotation time and inversely proportional to rotation speed |
| X-ray tube peak kilovoltage (kVp) | The amount of voltage between and x-ray tube's anode and cathode; it determines the energy of the x-rays being emitted | Radiation dose is proportional to kVp raised to an exponential power ranging from 2.5-3.1 depending on patient size; the higher the energy of the x-ray, the greater the probability of passing through the body and creating a signal at the detector. Importantly, HU values of human tissue relative to water are decreased at increased kVp settings. Thus, although noise is reduced, the contrast to noise ratio may actually decrease for the dose used. |
| Acquired slice thickness | Determines the minimum image width that can be reconstructed; governed by the MDCT detector configuration | A smaller acquisition slice thickness decreases the number of photons used to create the image, so to achieve an image with similar noise as a thicker slice, the radiation dose must increase – i.e. the patient dose must vary in inverse proportion to the slice thickness |
| Noise index (NI) | A user-selected measure of the level of noise they are willing to tolerate in the image | Radiation dose is inversely proportional to square root of NI. Decreasing NI by 5% increases dose by 10.8%, whereas increasing NI by 5% decreases dose by 9.3% |

IMAGE RECONSTRUCTION: TRADITIONAL AND NOVEL ALGORITHMS

Traditional algorithms:

Differences in attenuation within the examined volume determine the CT image contrast [52]. CT image reconstruction refers to the process by which attenuation data from a large number of projections (projection domain) is mathematically processed to create an image of the examined volume (image domain) [52].

Since its introduction into mainstream clinical practice, CT technology has undergone rapid and frequent evolution. Advances in hardware have mainly driven the evolution of CT technology. Important milestones have included the introduction of electron beam CT in the mid-1980s, spiral (helical) CT imaging in 1989, and multi-detector CT in 1998. Novel methods of CT reconstruction currently represent the most exciting developments being implemented in clinical practice for the purpose of image quality improvement and radiation dose optimisation in CT [17].

Conventional image reconstruction is achieved through Filtered Back Projection (FBP), a rapid and robust mathematical procedure that has been in use since the introduction of CT imaging to clinical practice. Filtration of the projection data prior to reconstruction reduces noise and enhances the edges by smoothing, helping to achieve appropriate balance between detail resolution and noise for the diagnostic task [54]. It is a characteristic of filtration that image sharpness and image noise are directly coupled: the sharper the image, the higher the

image noise. Back-projection involves reversal of the attenuation measurement process, where data from thousands of projections are used to reconstruct an image of the subject.

While FBP generates CT images of adequate quality, a limitation is its reliance on assumptions of an ideal system to allow for fast reconstruction [55]. These assumptions, necessary to simplify the mathematics, include the following: the measured signal contains no error due to photon statistics or electronic noise; the x-ray tube focal spot is an infinitely small point; the detector is also formed of points located at the centre of each cell; and the reconstructed voxel is a point with no shape or size [56-57]. All measurements are treated equally and only processed once. This process acts as an estimate and therefore includes inherent errors.

FBP reconstruction fails to account for image noise that results from Poisson statistical variations in photon number across the image plane; practically speaking, this means that there is an inverse relationship between radiation dose and image noise. Noise may propagate and sometimes amplify into patient images, creating streaks and artifacts, which may hide pathology and valuable diagnostic information [57]. While the limitations of FBP are not generally an issue in CT examinations with standard radiation dose levels, they become apparent in low radiation dose acquisitions, when image quality becomes compromised by disproportionately high levels of noise and image artefacts. High image noise interferes with the delineation and low-contrast detectability of a structure, so that certain minimal dose requirements need to be fulfilled to

generate a diagnostic CT data set. The remaining three assumptions of FBP all deal with the geometry of the system optics. While necessary to simplify the mathematics of the system, these assumptions lead to a trade-off in image quality simply due to the fact that they do not give an accurate description of the data acquisition process in the CT system.

Novel algorithms:

Advances in computing power have opened additional pathways for enhanced data processing methods. Iterative reconstruction algorithms (novel software-based algorithms developed to preserve image quality with low-dose CT) are the latest advance in CT technology and comprise two basic formats: (1) statistical iterative reconstruction, based on photon statistics, assuming an ideal system, and (2) model-based iterative reconstruction, that additionally attempts to model the system and the acquisition process, including system optics. Put simply, these iterative reconstruction techniques address the main assumptions of the FBP system listed in the previous section. These iterative algorithms perform in both the image and projection domains (depending on the exact vendor specifications). Optimisation of projection data (raw data directly from the CT scanner) prevents noise and artefacts in the projection domain propagating into the image domain (i.e. after an initial reconstruction) where they might be more difficult to remove [56]. Iterative algorithms are therefore more robust than FBP for dealing with low signal levels in reduced dose CT acquisitions and are promising tools to decrease radiation requirements via noise reduction. **Iterative reconstruction allows either an improvement in image quality without increasing the radiation dose or maintenance of**

image quality at a lower radiation dose compared with traditional FBP image reconstruction [18].

The basic principle of iterative reconstruction consists of three steps repeated iteratively [18] (see figure 1.6 below):

1. Forward projection of the examined object with creation of artificial raw data.
2. Comparison of the artificial raw data with real measured raw data to compute a correction term.
3. Back projection of the correction term onto the volumetric object estimate.

The process is repeated continuously (iteratively), with the difference between the simulated and measured projections decreasing with each subsequent iteration, until: (a) a predefined number of iterations is reached, (b) the update of the current image is minor, or (c) the quality of the final image is satisfactory.

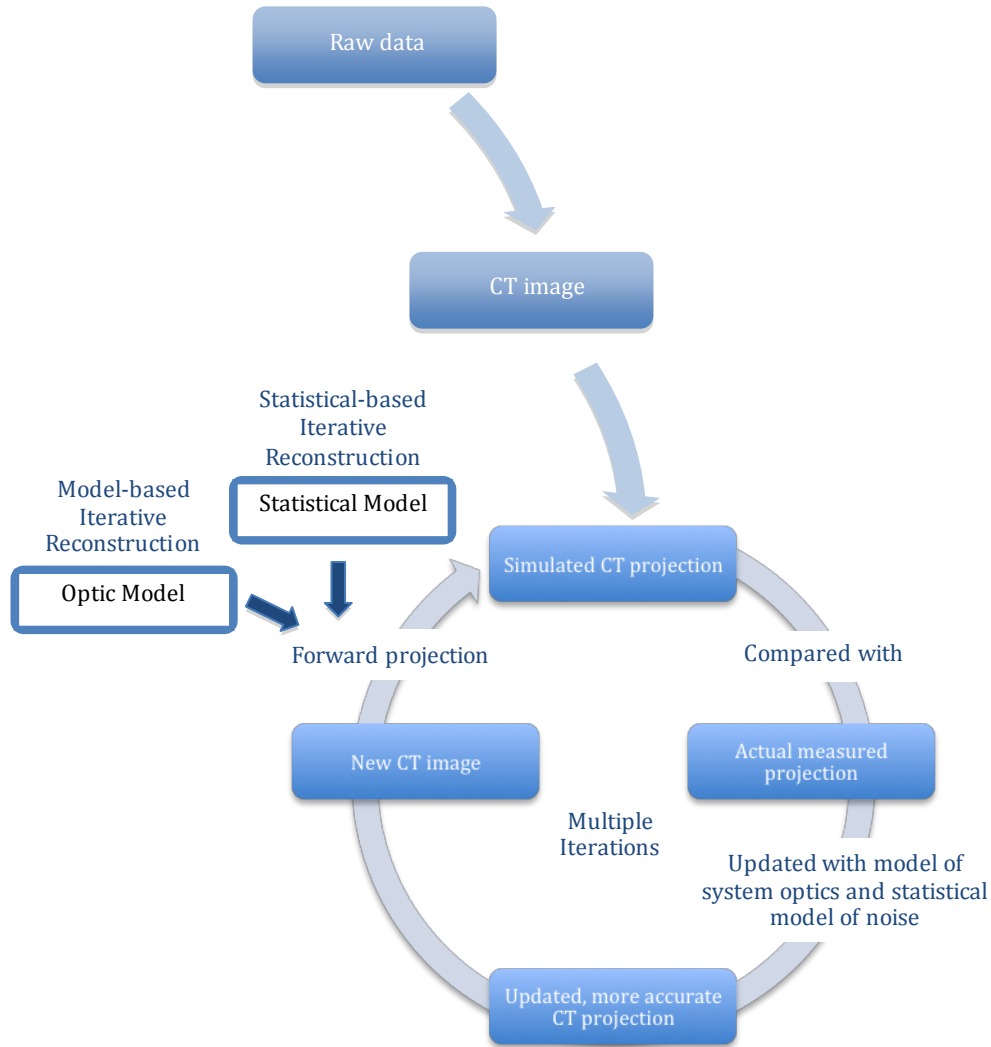


Figure 1.6: Schematic representation of the steps of iterative reconstruction. With each successive iteration, the difference between the simulated and measured projection is reduced. The iterative process is usually discontinued when the predefined image quality criterion is met [18,58].

The iterative renaissance:

This represents somewhat of a renaissance for iterative reconstruction in CT, having been the initially proposed method for data reconstruction in the early days of CT technology in the 1970s, then called algebraic reconstruction technique (ART)[16,59]. However, until recently iterative reconstruction had not been practical for clinical purposes due to its mathematically demanding

properties and the large amount of data in CT imaging and was abandoned in favour of FBP [60]. Instead, it was adopted by nuclear medicine emission tomography imaging modalities (SPECT, PET) because of the smaller data volumes, less data handling and the lower spatial and temporal resolution requirements [16,56,61].

Vendor differences:

Both statistical and model-based iterative reconstruction algorithms have been demonstrated to improve image quality in CT, and allow for considerable radiation dose reduction while maintaining diagnostic image quality [62-67]. This improvement in image quality is mainly achieved through image noise reduction. Though there are many currently available iterative reconstruction algorithms on the market from the major CT manufacturers [summarised in table 1.4], the exact underlying computational algorithms are mostly considered proprietary and are only partly revealed by manufacturers. Published data, however, suggest that there can be substantial differences between algorithms regarding the underlying assumptions of data acquisition, data processing, system geometries and noise characteristics [16,68]. From comparison of the commercially-available algorithms, the use of the projection and image domains is perhaps the main differentiating factor among the vendors' algorithms [69]. However, precise literature comparison between algorithms is difficult as many studies are algorithm or vendor-specific and studies comparing the products of different vendors are scarce as this technology is expensive and institutions tend toward a single vendor [62]. As expectations concerning image quality can substantially differ between institutions, careful attention to specific data

acquisition protocols is required when reviewing literature about iterative reconstruction technology.

Table 1.4: A summary of the currently available iterative reconstruction algorithms [58]

| Vendor, Reconstruction Technique | Algorithm | Iteration Domain | Strength Levels | Reconstruction Time |
|--|-------------|---------------------------|---------------------|---------------------|
| GE Healthcare | | | | |
| Adaptive statistical iterative reconstruction (ASiR) | Statistical | Image and raw-data spaces | 10 levels (10-100%) | 17 frames/s |
| Model-based iterative reconstruction (Veo) | Model based | Image and raw-data spaces | - | 10-90 min |
| Philips Healthcare | | | | |
| iDose | Statistical | Image and raw-data spaces | Levels 1-7 | 5-10 frames/s |
| Iterative model reconstruction (IMR) | Model based | Image and raw-data spaces | Levels L1-L3 | 5 min |
| Siemens Healthcare | | | | |
| Iterative reconstruction in image space (IRIS) | Statistical | Image space | - | 20 frames/s |
| Sinogram-affirmed iterative reconstruction (SAFIRE) | Statistical | Image and raw-data spaces | Levels 1-5 | 20 frames/s |
| Advanced model-based iterative reconstruction (ADMIRE) | Model based | Image and raw-data spaces | Levels 1-5 | 20 frames/s |
| Toshiba | | | | |
| Adaptive iterative dose reconstruction (AIDR 3D) | Statistical | Image and raw-data spaces | Levels 1-3 | 32 frames/s |

When examining the efficacy and impact of different iterative reconstruction algorithms, it is important to remember the wise recommendation of Beister et al [62]:

“The image quality performance of difference products is hard to compared in general since they are scanner-specific and many other system parameters can also have a noteworthy influence on the reconstruction performance. At best, a comparision of complete systems may be possible.”

This work focuses on the iterative reconstruction technology specific to GE Healthcare, namely Adaptive Statistical Iterative Reconstruction (ASiR) and Model Based Iterative Reconstruction (MBIR, Veo™) as these are available in our institution.

Adaptive statistical iterative reconstruction (ASiR):

ASiR is the first hybrid (a combination of both analytical and iterative methods) adaptive statistical iterative reconstruction method introduced by GE Healthcare in 2008. ASiR uses information obtained from the FBP algorithm as a basis (estimate) for image reconstruction, but models the system statistics in the reconstruction process. The measured value of each pixel is converted to a new estimate of the pixel value by matrix algebra. This pixel value is then evalulated and compared with the ideal value that is predicted with noise modelling. Successive iterations of this process are repeated until the estimated and ideal pixel values converge. This algorithm identifies and suppresses the noise in the image [70]. By focusing on quantum and electronic noise in projection space,

ASiR is able to deliver significant dose reduction potential in a computationally efficient manner and greatly improves image results [57]. As with other hybrid techniques, image reconstruction time is fast.

The strength of ASiR is a user selected parameter (in 10% increments) and refers to the ratio of FBP to ASiR in the resultant image (e.g. 30% ASiR refers to a blend of 70% FBP with 30% ASiR in the resultant image). The optimal level of iterative reconstruction depends on the degree of radiation dose reduction used for scanning and the desired spatial resolution and differs among scanning protocols. The higher the percentage of ASiR, the lower the image noise but the longer the reconstruction takes and the more likely the image displays a 'plastic' texture which can degrade image quality to the unfamiliar reader [68]. This can lead to reduced sharpness of organ margins, a smoothed appearance of solid organs, and reduced perception of small objects [18].

ASiR has been the most explored iterative reconstruction technique in different body regions [52]. Abdominal CT images reconstructed with ASiR 30% showed lower image noise, improved diagnostic confidence, and conspicuity of subtle abdominal lesions at 8.4mGy compared with FBP at 16.8mGy [71]. Images at 4.2mGy were acceptable only in patients weighing less than 90kg and with higher ASiR strength (50% or 70%). Overall, there have been improvements in both quantitative and qualitative image quality parameters [72].

Model based iterative reconstruction (MBIR, Veo™):

Veo™, initially introduced as model based iterative reconstruction, is GE Healthcare's second generation iterative reconstruction algorithm. The word 'Veo' is the Spanish for '*I see*', referring to the proposed parallel improvements in image clarity achieved by reduced image noise and increased spatial resolution. The MBIR process is complex and a complete description exceeds the scope of this work; a brief description will follow but the reader is referred to the publications of Hsieh et al, Thibault et al and Yu et al for a more detailed description [56-57, 73]. MBIR is uniquely designed for CT systems, with optimal use of the statistical model, to achieve stable convergence with high resolution detail and low image noise [57].

This algorithm incorporates an extensive three dimensional model of the data acquisition process, including system optics (e.g. geometry of the x-ray source, cone-beam shape, detector characteristics), in addition to the noise statistical model [56]. The simplified assumptions of FBP are disregarded and the system optics model describes how each element of a scanned object is projected onto the detector, more accurately describing the real data acquisition process [56]. A focal spot with known dimensions, as well as an active area of the detector, are taken into account and MBIR assumes a three-dimensional volume of each voxel element. MBIR also models the statistical distribution of the measured data from the physics of the interactions of radiation with matter, as x-rays are produced in the x-ray tube, attenuated through the CT system and the patient, measured at the detector, and transformed into a digital signal. All voxels of the image are updated within one complete iterative cycle. In an iterative manner through

multiple passes over the projection data, the estimate of the solution is determined using MBIR.

MBIR operates to explicitly reduce or eliminate image noise with the goal of obtaining image clarity; it challenges the common trade-off to improve resolution while simultaneously reducing noise significantly and improving contrast [57]. With the newest version of MBIR technology (Veo™ 3.0), there are two further settings that have been introduced in addition to Standard MBIR that can be user-selected depending on the anatomical focus of the CT scan [74]. The first is MBIR with Noise Reduction (NR). This is annotated with a number indicating the available settings for a given protocol – usually NR05 for abdomino-pelvic imaging and NR40 for head and neck imaging. NR05 provides 5% less noise compared to standard and NR40 provides 40% less noise compared to standard. The second setting is MBIR with Resolution Preference (RP). Again, the available settings are annotated to indicate the percentage improvement in resolution compared with standard, usually RP05 for abdomino-pelvic imaging and RP20 for evaluation of the lung parenchyma with thoracic CT imaging. These settings are novel and their capabilities have not been compared in the literature.

The complexity and the magnitude of the extensive modelling process are demanding on computational power and time, meaning image-processing time for MBIR is longer than during FBP and ASiR. Reconstruction times range between 10 and 90 minutes, depending on the number of images in the series – roughly equating to 0.2-0.5 images per second. On a practical level, the potential

delay between data acquisition and the availability of images for interpretation can have clinical implications, for example, for emergent indications or for maintenance of workflow [75].

MBIR has proved to be the most efficient dose reduction technique of all iterative reconstruction techniques and is especially suited to lower radiation doses as it reduces image noise more effectively than other algorithms [52]. MBIR can be expected to have better noise suppression, spatial resolution, conspicuity, artefact suppression and overall image quality than FBP and ASiR, with similar uniformity and beam hardening [74-77]. Several studies, concerning mainly chest and abdominal CT, have shown that MBIR can reduce patient doses more effectively than FBP or first generation iterative reconstruction methods (i.e. ASiR) while preserving or improving image quality [65,75,77-82]. However, at ultra-low dose levels, MBIR may demonstrate insufficient performance levels for low-contrast and small lesion detectability, though this likely relates to a paucity of photon input [81-82].

Image quality performance:

The familiar texture of CT images is in part due to the image quality and radiation dose trade-off with FBP. Use of iterative reconstruction techniques mandates that the established relationship between image noise and dose, spatial resolution and slice thickness needs to be redefined. Based on Poisson statistics, the image noise in conventional FBP reconstruction is approximately proportional to the square root of the radiation dose. This relationship largely

holds through for ASiR, due to linear blending with FBP images, and the image texture remains in the familiar realm unless the highest ASiR strengths are used.

MBIR is designed to keep image noise constant with changing dose levels, by employing a more correct and intricate physical model in its iteration process [74]. However, images reconstructed with MBIR have a noticeably altered appearance compared with FBP images. This results from a shift of the noise power spectrum toward lower spatial frequencies and yields a smoothed image appearance and a decrease in perceived image quality [83]. Familiarity with the appearance of images reconstructed with ASiR and MBIR with regular-dose protocols is recommended before using this technique with low-dose protocols [18].

A brief summary of the benefits and pitfalls of the iterative reconstruction techniques provided by GE healthcare is provided in table 1.5 below [58].

Table 1.5: A summary of the main benefits and pitfalls of ASiR and MBIR [58]

| Reconstruction Technique | Benefits | Pitfalls |
|--------------------------|---|---|
| ASiR | <ul style="list-style-type: none"> – Fast image reconstruction – Allows substantial noise reduction – Different strength levels for image noise influence – Variable implementation complexity | <ul style="list-style-type: none"> – Costly – Vendor specific – Blotchy appearance – Requires education for technicians and image quality familiarisation for radiologists |
| MBIR | <ul style="list-style-type: none"> – Robust noise and artefact reduction – Allows greater dose reduction than ASiR – User-selectable reconstruction settings (NR and RP) – Variable implementation complexity | <ul style="list-style-type: none"> – Costly – Vendor specific – Limited to premium scanners – Long image processing time – Blotchy appearance – Requires education for technicians and image quality familiarisation for radiologists |

For the implementation of iterative reconstruction algorithms into clinical practice, performance evaluation is necessary. Since the introduction of the first iterative reconstruction algorithm (ASiR, GE Healthcare) in 2008, the concept of extracting more information from the acquired signal at CT in the pursuit of low-dose, high-quality images has lured the attention of the radiology community. The promise of noise reduction, image quality improvement, and artefact reduction compared with FBP has resulted in a large number of studies of both phantom and human models to investigate these purported benefits during the period of this thesis. It is not within the scope of this work to describe the details of these studies; however, there follows a table (table 1.6) summarising some key studies that illustrate the performance evaluation of iterative reconstruction algorithms from multiple vendors.

Table 1.6: A brief summary of performance evaluation studies of iterative reconstruction algorithms.

| Time | Author | Algorithm | Key results |
|--------------------|-----------------------------------|--------------|---|
| 2010 - 2011 | Leipsic, | ASiR | – Improved image quality |
| | Prakash, Schindera, Singh [84-87] | | – Noise and dose reductions when compared with FBP |
| 2012 | Protik [88] | ASiR | – 26-30% reduction in image noise |
| | Singh [89] | ASiR | – 46.4% dose reduction for chest CT – 38.2% dose reduction for abdominal CT – Substantially less objective noise with ASiR than with FBP |
| 2013 | Vardhanabhuti [67] | ASiR MBIR | – MBIR produced significant noise reduction with low-dose CT thorax |
| | Ghetti [90] | SAFIRE | – Improved low contrast resolution and less lesion with SAFIRE – Improved image quality with increasing strength of SAFIRE – Preserved CT number accuracy, linearity and spatial resolution. |
| | Vardhanabhuti [66] | ASiR MBIR | – MBIR resulted in a significant noise reduction compared with ASiR and FBP with varying noise index for abdominopelvic CT – Degradation in image quality at higher noise indices with <120kV tube voltage despite improving contrast-to-noise ratio |
| | Metha [91] | IMR | – 60-80% dose reduction, 43-80% low contrast detectability improvement, and 70-83% noise reduction compared with FBP in phantom |
| | Smith [65] | MBIR ASiR | – Paediatric CT – maintained diagnostic quality CT with 46% CTDI _{vol} reduction compared with a standard dose protocol using 30% ASiR |
| 2014 | Goenka [92] | SAFIRE | – Non-inferior diagnostic accuracy of low attenuation lesions in a liver phantom with SAFIRE at 25% exposure reduction – Reduced lesion detection with |

| | | | |
|------|--------------|---------|--|
| | | | exposure reduction below this, particularly smaller lesions |
| | Kim [93] | AIDR 3D | <ul style="list-style-type: none"> – AIDR 3D is effective in both noise reduction and image quality improvements compared with FBP – AIDR 3D's effectiveness may increase as the phantom size increases |
| | Klink [94] | iDose | <ul style="list-style-type: none"> – Significantly improved noise reduction compared with FBP, regardless of the tissue imaged or scan input parameters – At comparable image quality levels, the CTDI_{vol} was reduced by 26-60% |
| | Samei [82] | IRIS | <ul style="list-style-type: none"> – Phantom study demonstrating greater dose reduction compared with FBP, even with thinner slices – Improvement in image quality at constant dose |
| 2015 | Khawaja [95] | IMR | <ul style="list-style-type: none"> – All true lesions were detected on submillisievert abdominal CT with IMR – Objective noise with submillisievert CT with IMR was 8-56% less than that for standard dose with FBP |

RADIATION DOSE METRICS AND THEIR MEASUREMENT

CT dosimetry:

A basic understanding of CT dosimetry is a prerequisite for successful radiation dose optimisation. In order to adequately compare doses between different CT systems, it is necessary to understand how dose is measured and reported. While it would be ideal to measure the actual radiation dose to each patient undergoing a CT scan, such measurements are not possible. Rather, proxies for dose, or 'dose indices' have been established. While these measurements are straightforward and repeatable, it is important to appreciate that these values are estimates based on simplifying assumptions and phantom measurements. As CT

technology continues to advance, so too do the radiation dose metrics that quantify scanner output from multiple acquisitions.

Radiation output for CT is commonly reported in terms of a volume CT dose index ($CTDI_{vol}$) in units of milligray (mGy) to one of two possible phantoms based on the scan field of view. These are a 16cm diameter (head or paediatric body) and a 32cm diameter (body) cylindrical acrylic phantom. $CTDI_{vol}$ is not patient absorbed dose, skin dose or organ dose; it simply describes the radiation that leaves the x-ray tube in the scanner regardless of whether it interacts with the patient. It is a useful metric in comparing protocols across devices and evaluating the effects of parameter settings. Actual patient dose may be over or under-estimated relative to $CTDI_{vol}$.

There are multiple metrics available for characterising radiation output from CT devices (see table 1.7) [96] but most are derived from $CTDI_{vol}$ with its inherent limitations. Transforming this information into an estimate of actual patient dose for every procedure is difficult due to confounding factors such as variability in body habitus, positioning and imaging technique. Most recently, a standards-based approach to this problem developed by the American Association of Physicists in Medicine (AAPM) in the Task Group 204 report is the calculation of SSDE, using a measure of device radiation output ($CTDI_{vol}$) and patient diameter or effective diameter [97]. This converts $CTDI_{vol}$ values for the torso into something more representative of actual patient dose.

Table 1.7: A summary of CT dose descriptors and the CT parameters that affect them [96]

| Definition | How calculated | Unit | Effect on radiation dose | Most affected by |
|---|---|--------|--|---|
| Volume CT dose index (CTDI_{vol}) | | | | |
| A measure of the radiation output from the CT scanner as determined with either a 16 or 32cm PMMA phantom | Weighted average to depict an average value of radiation across the diameter of CT phantom; corrects for pitch factor and other scan parameters | mGy | Linear changes in CTDI _{vol} would result in linear changes of exposure | <ol style="list-style-type: none"> 1. Tube voltage 2. Tube current 3. Pitch 4. Phantom specific |
| Dose length product (DLP) | | | | |
| Indicates the extent of z-axis coverage and CTDI _{vol} | CTDI _{vol} multiplied by scan length (cm) | mGy.cm | Linear changes in DLP would result in linear changes of exposure | <ol style="list-style-type: none"> 1. CTDI_{vol} 2. Scan length 3. Number of acquisitions (radiation events) |
| Effective dose | | | | |
| The theoretical uniform whole-body dose that has the same nominal risk of carcinogenesis as any given non-uniform CT exposure | DLP multiplied by a conversion factor (k) is a common way to estimate mSv or weighted sum of organ equivalent doses using ICRP 60 or ICRP 103 weighting factors [98-99] | mSv | Linear change in millisieverts represents a proportional change in absorbed dose | <ol style="list-style-type: none"> 1. DLP 2. Patient size 3. Relative radiosensitivity of the imaged organs |
| Effective diameter | | | | |
| Reference patient size, i.e. circular water phantom having overall similar attenuation as an actual patient | Estimated by: square root of the product of anterior-posterior and lateral patient diameter of the CT radiograph | cm | Larger patient diameters result in larger exposures when using tube current modulation | Patient size |
| Size-specific dose estimate (SSDE) | | | | |
| A measure of dose that includes individual patient size | CTDI _{vol} multiplied by a correction factor base on patient effective diameter | mGy | Improves accuracy of average patient dose for all sized patients | CT radiographs, patient contour along the z-axis and patient positioning in the gantry |
| Absorbed dose | | | | |
| Amount of ionising radiation (Joule) absorbed by tissue (kilogram) | May be measured or calculated; estimated from SSDE | mGy | Not applicable | <ol style="list-style-type: none"> 1. DLP 2. Patient size 3. Organs scanned* |

*Calculations using Monte Carlo require details of the simulated scanner and may also require patient-specific phantom models

Authors Bankier and Kressel recommend that for research studies in which CT dose levels are evaluated, four dose parameters should be reported: CTDI_{vol}, DLP, effective patient diameter and SSDE [100]. CTDI_{vol} and DLP provide information about the scanner radiation output, effective diameter provides information about the size and dimensions of the study cohort, and SSDE provides an approximation of the dose absorbed by the individual patient for a given scan. Effective dose is useful and recommended when comparing doses across modalities (e.g. CT of abdomen and pelvis with plain abdominal radiograph) [100].

IMAGE QUALITY PARAMETERS AND THEIR MEASUREMENT

Parameters of image quality in CT:

The ALARA principle encompasses the goal of appropriate clinical CT imaging, that is, to produce images of diagnostic quality using the lowest possible radiation exposure for the clinical indication. This implies adequate reproduction of clinically important anatomic structures and pathological processes, such that a diagnosis can be made. The goal is not necessarily to produce technically flawless or aesthetically pleasing images.

Image quality in CT is a result of interaction between many factors. If new dose reduction techniques are implemented, the impact on image quality has to be investigated. The following table (1.8) summarises the fundamental determinants of image quality in CT systems [101].

Table 1.8: The fundamental determinants of image quality in CT systems.

| | |
|--------------------------------|--|
| Low contrast resolution | The ability of the system to reproduce two adjacent objects with similar CT attenuation values as separate structures or to distinguish a low contrast object from its background. With increased image noise, low contrast resolution is primarily decreased [101-102]. |
| Spatial resolution | The ability of an imaging system to resolve image detail and preserve the spatial information in a high contrast object, accurately representing it in the image. Spatial resolution is affected by many factors, including the design of the x-ray tube and detector (object to detector distance, focal spot size, detector size, reconstruction matrix resolution and slice thickness), as well as the reconstruction algorithm |

| | |
|-----------------------|---|
| | [101]. Traditional trade-offs between noise and spatial resolution in CT exist via the reconstruction filter. In FBP, smoother filters can be used to produce images with less noise, but with reduced spatial resolution. With MBIR these factors are uncoupled; noise is reduced while simultaneously improving high contrast spatial resolution. |
| Noise | This is a measure of local statistical fluctuation in CT attenuation values of individual image elements [101]. It is a consequence of a variety of statistical processes that occur in the attenuation and detection of x-rays by a CT system, but the dominant source is the quantum fluctuation in x-rays. An x-ray tube will not emit an exact number of x-rays over a given time period, but rather the number of x-rays will fluctuate about some mean value according to a Poisson distribution. Image noise increases with decreased radiation exposure (mAs, kV) and is also affected by slice thickness and reconstruction algorithm. |
| Image artefact | A systematic discrepancy between CT attenuation values in the reconstructed image and true attenuation coefficients of the examined volume. Artefacts can arise from physics (e.g. beam hardening, photon starvation, partial volume), the patient (e.g. metal and motion artefacts), or the CT system (e.g. ring and distortion artefacts) [103]. |

Optimisation of CT image quality requires reliable methods for evaluation of the resultant images to ensure adequate diagnostic quality [104]. While objective technical examination of new reconstruction processes is essential, the diagnostic process culminates in human interpretation of images so subjective evaluation is important in studies of diagnostic image quality. The use of these image quality parameters is tailored for each chapter of this thesis, depending on

whether applied to cylindrical and anthropometric phantoms, cadaveric models or in vivo in human subjects.

Objective evaluation:

CT attenuation or CT number (HU) are measured by means of a spherical region of interest placed in the tissue of interest. The mean attenuation value within the region of interest is recorded. To ensure as accurate a representation as possible, the ROI is placed in as homogenous an area as possible, away from the edge of the organ or vascular structures within. CT attenuation values are important in clinical practice for diagnosis of disease entities, such as diffuse reduction of liver attenuation representing fatty infiltration (hepatic steatosis), or characterisation of an indeterminate lesion based on the constituent tissues, usually to distinguish a benign adrenal adenoma from other adrenal lesions or to characterise a fatty adnexal lesion as a dermoid tumour.

Noise in CT is typically expressed as the standard deviation (SD) of the CT attenuation value within a region of interest in a uniform section of phantom or tissue, assuming a normal distribution [101]. Examination of the noise power spectrum (NPS) provides information about spatial characteristics (texture) of noise and is assessed in homogenous phantoms using advanced mathematics [105]. While valuable for comparison of noise distributions in different reconstructions, its use is beyond the scope of this thesis.

Signal to noise ratio (SNR) is expressed as signal (attenuation in HU) divided by noise (SD in HU) in the same homogenous ROI: $SNR = HU/SD$ [102]. A high SNR

indicates that true information (i.e. signal) overpowers noise and is indicative of superior image quality.

Contrast to noise ratio (CNR) is an objective assessment of the inter-relationship between contrast and noise where the contrast between two structures is expressed as a function of noise. The CNR between A and B is calculated as follows: $CNR = (HU_A - HU_B)/SD_B$. For analysis of module CTP515 of the Catphan phantom, for example, ROIs are placed in the target of choice and in the background material of the module adjacent to this point, with CNR calculated as the difference in attenuation between the target and background ROIs divided by the standard deviation of the background ROI [106].

Subjective evaluation:

Low-contrast resolution can be subjectively evaluated as the smallest discernible object in an image, with specific difference in contrast relative to the adjacent background or by evaluating how well demonstrated a target or tissue with a specific contrast difference is on a linear scale [101,106]. Low contrast resolution is measured with a Catphan CTP515 module, using a helical CT acquisition viewed with a window setting close to the CT number values of the low contrast targets. Low contrast resolution is usually expressed as the smallest visible target at a specific contrast level, at the scanned CTDI. Low contrast resolution is highly dependent on image noise [101-102].

Spatial resolution (high contrast resolution) is a measure of the ability of the system to resolve image detail [102]. Spatial resolution is usually determined in a phantom with test objects with large differences in CT attenuation to eliminate the interference of image noise. In the Catphan 600 phantom, the CTP528 module is used [106]. This comprises a metal gauge cast in epoxy with a variable number of line pairs cut in each centimetre section. Visual assessment is performed where the reader counts visible line pairs to determine the spatial resolution of the study. Objectively, spatial resolution can be assessed by the modulation transfer function (MTF), which involves complex calculations based on the degree of sharpness observed in the image of a specific test object, typically a high density bead or wire [105-106]. This metric is beyond the scope of this thesis.

Diagnostic acceptability is an indirect measure of diagnostic performance. This utilises visual grading analysis of clinically important anatomical structures at multiple levels in the image volume on an ordinal scale, using criteria based on the European Guidelines on Quality Criteria for Computed Tomography [102]. These criteria list a large number of anatomical structures (e.g. liver parenchyma, intestine, etc.) of which visually sharp reproduction is expected. The underlying theory is that the ability to detect pathology correlates well with accurate reproduction of anatomy [107].

Diagnostic accuracy is a direct measurement of diagnostic performance. It evaluates the ability of the study to resolve normal from abnormal cases and to adequately demonstrate the pathological findings when present. Assessment

involves direct comparison with a reference standard (in many chapters of this work, the conventional dose CT examinations acted as the reference standard for the reduced dose CT examinations). Qualitative results are obtained and the goal is to assess for non-inferiority.

Potential for bias:

It can be argued that subjective evaluation of image quality is less reliable than objective measurements due to the introduction of observer bias by its dependence on human observers [108-111]. However, omission of subjective assessment in studies on diagnostic image quality is impossible. Recognition of the more important sources of potential observer bias is therefore important and careful study design can help minimise/counteract these and enhance reliability of study results.

Adaptation bias occurs when observers, accustomed to a certain image appearance and noise texture, prefer these images to clinically equivalent images with a slightly different appearance. During the introduction of new methods/techniques/equipment that affect image appearances, this bias has potential to cause reduced acceptability to the reader.

Recognition bias occurs when it is intended that observers be blinded to an evaluation variable (e.g. new reconstruction technique) but they nevertheless can, or believe they can, identify which reconstruction they are looking at. Even the slightest deviations from usual image characteristics may be evident to

experienced radiologists, meaning complete blinding of observers is difficult to achieve.

Substantial observer variation highlights that in order to produce representative results, studies on subjective image quality require adequate numbers of both cases and observers. Most studies on radiation dose and image quality include only two observers. It can be assumed that observer diversity, caused by disparate cognitive and visual abilities, will lead to inter-individual differences in interpretation [112]. For most purposes in this work, two observers was felt a sufficient number.

Evaluation scales:

Clinical image quality is typically assessed by applying a visual grading analysis (VGA) using a relatively simple form of ordinal scale. Here, the order of grades is defined but the degree of difference between them is not. Observers are typically asked to grade individual images/studies according to image quality criteria. Each grading step is defined using an absolute description (instead of relative as in ranking scales). Grading steps can be defined to reflect an approximately linear improvement in image quality, allowing some degree of quantification of differences. Images are reviewed separately (not side-by-side) reducing the risk for recognition and adaptation biases.

Grading scales are tailored for the specific study purpose. Ideally, in clinical studies on subjective image quality, the number and size of the steps should reflect clinically relevant differences. The number of steps in the grading scale is

a balance between resolution (small steps) and reproducibility (ease of use). Detection of small differences in image quality requires scales with high resolution. To reflect basic diagnostic requirements, it is important that the scale allows clear delineation between diagnostic (grades 2-5) and non-diagnostic (grade 1) examinations.

Commonly employed grading scales employ five steps:

1. Unacceptable
2. Barely acceptable
3. Adequate
4. More than adequate
5. Excellent

CT optimisation aims to achieve image quality without significant diagnostic limitations using the smallest possible radiation dose (ALARA principle), corresponding to grade 3 in the scale shown. For clinical purposes, it is not usually important to know how poor the non-diagnostic examinations are (i.e. non-diagnostic remains non-diagnostic, however you look at it). However, from a protocol evaluation and planning strategy, the differentiation between barely acceptable and unacceptable is valuable. Likewise, grades 4-5 represent image quality better than what is clinically required, implying usage of unnecessarily high radiation dose that should be reduced. Therefore, further grades at the higher end of the scale are unnecessary clinically but are of value when evaluating protocols.

Research subjects:

While medical physicists assess image quality in CT using technical phantoms, these models are not representative of patient anatomy and such phantoms are not ideal for assessment of image quality. This is particularly true for noise, since noise measurements in a uniform phantom do not account for the complex relationship between anatomical variability and image quality [113]. To investigate novel reconstruction algorithms, the logical sequential progression of subjects for evaluation comprises cylindrical phantoms, anthropometric phantoms, cadaveric models and clinical studies in human subjects, prior to introduction into clinical routine. Detailed description of the phantoms and cadavers used in this work is provided in chapter 2. The human subjects included are described in detail in chapter 3 and briefly thereafter.

In phantoms, repetitive adjustments can be performed under standardised conditions allowing for exact comparison of results. Protocols can be tailored and refined with parallel assessment of the effect on image quality indices. These protocols can be evaluated in human cadaveric subjects to simulate clinical examinations, without adverse consequence of repeated irradiation. This provides a refined, validated, appropriate and safe protocol for application to clinical subjects and helps minimise the required sample size.

Studies on diagnostic image quality should preferentially be designed to be able to detect clinically significant differences. Detection of small intervention effects, such as the effect of different image reconstruction methods on image quality, against a background of relatively large inter-individual variation (i.e. anatomical

differences) requires an adequate number of cases and good matching between cases and controls. Better matching allows fewer cases to be used. Ideally, this involves using identical case and control populations with each case serving as their own control. Using the same case and control populations when evaluating different radiation doses can involve increased radiation exposure to the research subjects. The use of a split dose CT protocol where the total dose of ionising radiation to the patient remains the same but is split between conventional and reduced dose CT examinations is novel but has been used successfully in our institution for other clinical papers [114-115].

AIMS OF THIS THESIS

The main aims of this thesis were:

1. To explore the effects of iterative reconstruction on image quality with variation in CT input parameters (mA, kV, NI)
2. To develop a modified dose CT protocol that would achieve preserved image quality with a significant reduction in radiation dose by using iterative reconstruction
3. To apply this protocol clinically to patients with Crohn's disease to assess for non-inferiority and validate the clinical use of these dose-saving technologies in this 'at risk' population.

The hypotheses under test in this study are:

- That, with iterative reconstruction, development of an optimized modified dose protocol for CT of abdomen and pelvis is technically feasible in phantom and cadaveric models.
- That modified dose CT of abdomen and pelvis with iterative reconstruction has an equivalent diagnostic yield to conventional dose CT with traditional filtered back projection reconstruction in patients with Crohn's disease.
- That CT of abdomen and pelvis acquired at a radiation dose less than or equivalent to plain abdominal radiograph provides superior diagnostic information.

Specific objectives of the individual chapters were as follows:

Chapter 2

- To examine the interplay of user selected parameters on both radiation dose and image quality with traditional filtered back projection and iterative reconstruction algorithms.
- To develop and refine an optimal split dose CT protocol for the imaging of the abdomen and pelvis in patients with Crohn's disease.

Chapter 3

- To validate the use of hybrid iterative reconstruction (adaptive statistical iterative reconstruction, ASiR) with modified dose CT protocols for imaging of the abdomen and pelvis in patients with Crohn's disease.

Chapter 4

- To determine the optimal strength level of ASiR to apply for modified dose CT protocols for imaging of the abdomen and pelvis in patients with Crohn's disease.

Chapter 5

- To validate the use of pure iterative reconstruction (model based iterative reconstruction, MBIR, Veo™) for modified dose CT protocols for imaging of the abdomen and pelvis in patients with Crohn's disease.

Chapter 6

- To examine whether modified dose CT with MBIR may be a suitable replacement for plain abdominal radiographs performed at the same radiation dose as a first line investigation for patients with Crohn's disease.

Chapter 7

- To examine the fidelity of attenuation measurements with both iterative reconstruction algorithms and their use for tissue characterisation.



Chapter 2

Evaluation of Iterative reconstruction in phantom and cadaveric models with varying CT acquisition protocols with eventual development of a modified dose protocol for CT of abdomen and pelvis

Introduction:

To improve diagnostic performance in medical imaging, there is an increasing desire for higher spatial resolution, increased low contrast detectability, greater volume coverage and faster scan acquisition. There is also a demand for reduction in radiation doses [3,9,42]. At a hospital level, further efforts are being made regarding scan justification and optimisation of CT protocols with respect to tube current, tube voltage and pitch to reduce radiation dose and maintain diagnostic information in the images. CT vendors have made efforts to reduce radiation dose while maintaining diagnostic image quality by developing new technologies such as automated tube current modulation and further refinement of post-processing filters.

The most recent development in an effort to improve image quality and reduce radiation dose from CT examinations is the clinical introduction of iterative reconstruction algorithms. When conventional FBP, a fast and efficient algorithm, is used, excessive dose reduction results in increased noise and artefacts that degrade image quality and render images suboptimal for diagnostic interpretation [68, 116-117]. Iterative reconstruction allows either an improvement in image quality without increasing the radiation dose or maintenance of image quality at a lower radiation dose compared with traditional FBP image reconstruction [18].

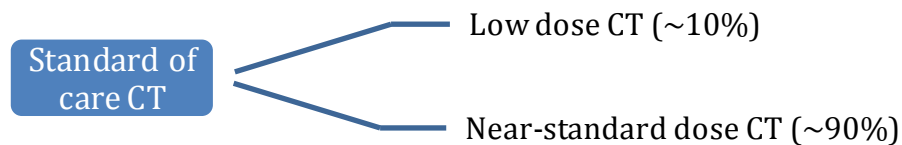
There are many vendor-specific forms of both hybrid and pure iterative reconstruction [75,86,118-120]. Each algorithm uses a unique technical approach for image noise reduction and possesses different applicable strengths

that influence image noise and texture [58]. For this work, we focus on the GE Healthcare products Adaptive Statistical Iterative Reconstruction (ASiR), which is a hybrid algorithm, and Model Based Iterative Reconstruction (MBIR), which is pure iterative reconstruction. With its Veo 3.0 release, MBIR provides two subtypes of reconstruction settings, used depending on the anatomical focus of the examination. These comprise MBIR with Resolution Preference (RP) and Noise Reduction (NR). The recommended settings for abdominal CT imaging are RP05, which delivers a 5% increase in resolution compared with Standard, or NR05, which yields 5% less noise compared with Standard [74]. Both settings cannot be applied together. The vendor recommended strengths of these settings vary depending on the anatomical region being imaged and the focus of the study (e.g. RP05 and RP20 settings are provided for CT imaging of the thorax as parenchymal detail is the focus, whereas NR40 is an option for CT imaging of the head and neck as soft tissue assessment and delineation is more important) [74].

Prior to clinical introduction of iterative reconstruction into diagnostic imaging practice to enable use of modified radiation dose protocols, this technology needs to be validated as fit for purpose. In isolation, a modified dose CT protocol is of limited use – it requires a reference standard to compare it with to ensure non-inferiority in terms of diagnostic sensitivity and acceptability. The ideal scenario is where the patient is imaged twice and acts as their own contemporaneous control but this requires two CT examinations with the associated increased radiation exposure. Previous studies have used matched controls [116,121] and others have used a previous CT for that patient as the comparison examination [65,122-125]. Neither of these options is perfectly

suited for purpose as they involve inter-individual comparison or intra-individual comparison but with temporal heterogeneity in the clinical findings. For patients with Crohn's disease in particular, where diagnostic findings may change significantly over the course of weeks or even days, these reference options are inappropriate for adequate validation.

The solution is development of a split dose CT protocol comprising two contemporaneous CT acquisitions for which the combined radiation dose is equivalent to the standard of care CT of abdomen and pelvis. In CT, too low or too high image quality is inappropriate – while images of insufficient quality are non-diagnostic, image quality better than what is clinically required implies usage of unnecessarily high radiation dose. For most patients and most CT departments, there is scope for further optimisation of the standard of care CT protocol. In pursuit of sub-millisievert CT imaging of the abdomen and pelvis, the aim was to develop a CT protocol for an adequate quality CT of abdomen and pelvis at the lowest possible dose, ideally approximating to that of a conventional abdominal radiograph, with a near-standard dose CT for comparison.



The development, refinement and optimisation of a CT protocol is a complex process with an array of adjustable parameters that interplay in an intricate manner to affect the resultant image quality and radiation dose. These

parameters and their effects are listed in table 1.3. Briefly, to reduce radiation dose, there needs to be a reduction in the number of photons emitted from the x-ray tube and/or the energy of these photons [126]. This can be achieved with a decrease in the tube current or tube voltage or an increase in the tolerated noise index (noise index is a parameter that applies when automated tube current is used at a fixed tube voltage – a pre-selected tolerated level of noise in the image based on the clinical task). With so many variables at play and innumerable potential permutations and combinations, a trial and error approach is warranted to find the balance that yields the optimal modified dose protocol. CT examinations need to be obtained with each of many different combinations of input parameters and the study that yields adequate image quality for the lowest possible dose selected.

The advent of novel reconstruction methods somewhat complicates this process. If new dose reduction techniques are to be implemented, their impact on the image quality has to be assessed. Therefore, in addition to multiple CT acquisitions with varying parameters, each series should be reconstructed with the reference standard reconstruction algorithm (FBP) and with the algorithms under examination (ASiR and MBIR).

Multiple CT acquisitions in human subjects are not possible due to the large cumulative radiation dose that they would accrue. Previous studies have demonstrated the feasibility of using either geometric or anthropomorphic phantoms to optimise clinical protocols [58,76,86,122,127-128]. For this initial work, an anthropomorphic phantom is the appropriate test subject. This allows

objective measurement of attenuation, image noise and signal to noise ratio. Contemporaneous imaging of a Catphan 600 cylindrical phantom with identical protocols makes measurement of contrast resolution, contrast to noise ratio and spatial resolution possible. The next logical progression is to image human cadavers with these identical protocols to validate the findings in the phantom models. Finally, an optimised and validated protocol can then be applied to clinical human subjects.

The aims of this chapter are:

- To demonstrate how user-selected parameters (tube voltage, tube current and noise index) affect radiation dose and thus image quality.
- To compare the effects of each reconstruction protocol on these data sets to establish how iterative reconstruction affects the image and image quality indices.
- To develop an optimised split-dose CT protocol for imaging of clinical patients with Crohn's disease.

Methods:

The Kyoto CTU-41 torso phantom (Kyoto Kagaku, Fushimi-ku, Kyoto, Japan) is a life-size male anthropometric phantom with a height of 100cm and a body weight of 45kg. It is constructed from a combination of urethane base resin and epoxy base resin with synthetic internal organs, bones and soft tissues. Each individual organ has a particular Hounsfield number, which corresponds with that of the matched structure in the human body. The phantom is placed supine on the CT table and centred by means of lateral and antero-posterior CT localiser radiographs, as would a human subject (figures 2.1 and 2.2). The scan length extended from the lung bases to the pubic symphysis as per standard of care CT protocol.



Figure 2.1: Kyoto anthropomorphic phantom positioning on the CT table. The phantom is placed supine and lateral and antero-posterior CT localiser radiographs are obtained.

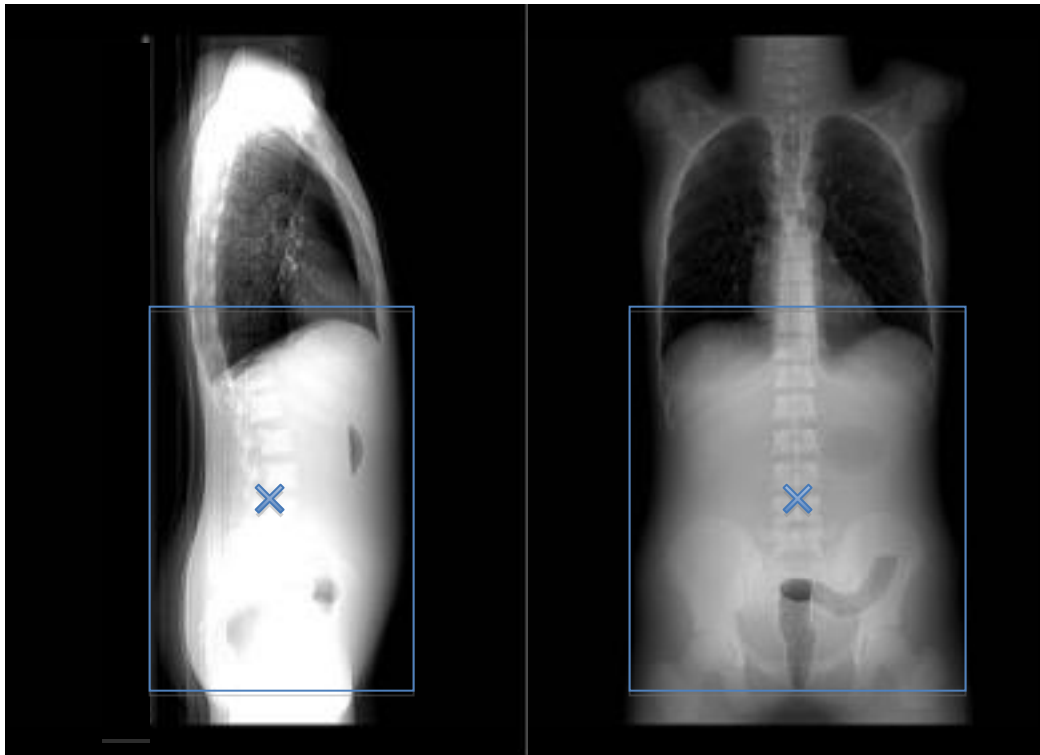


Figure 2.2: Lateral and antero-posterior CT localiser radiographs of the Kyoto phantom. The scan range is planned as it would in a human subject, extending from the lung bases to the pubic symphysis. Care is taken to align the isocentre of the phantom to that of the gantry to optimise the image.

The Catphan 600 phantom (The Phantom Laboratory Inc., Salem, NY) is a cylindrical phantom for measurement of image quality. The phantom, cylindrical in shape, is constructed of PMMA and consists of 5 modules designed to perform various quality tests in tomographic images [106]. The phantom's long axis (z-axis) is placed longitudinally on the CT table and aligned with the scanner's isocentre so the modules are in transverse planes to the phantom z-axis (x-y plane). To ensure the appropriate positioning at the isocentre of the CT gantry, the phantom is placed at the gantry end of the CT table, mounted on its case. Orientation of the alignment dots on the side and top of the phantom with the scanner alignment laser is achieved by a combination of alteration of the

adjustment screws and placement of counterweight. Z-axis alignment is assessed by means of a spirit level. See figures 2.3 and 2.4 below.

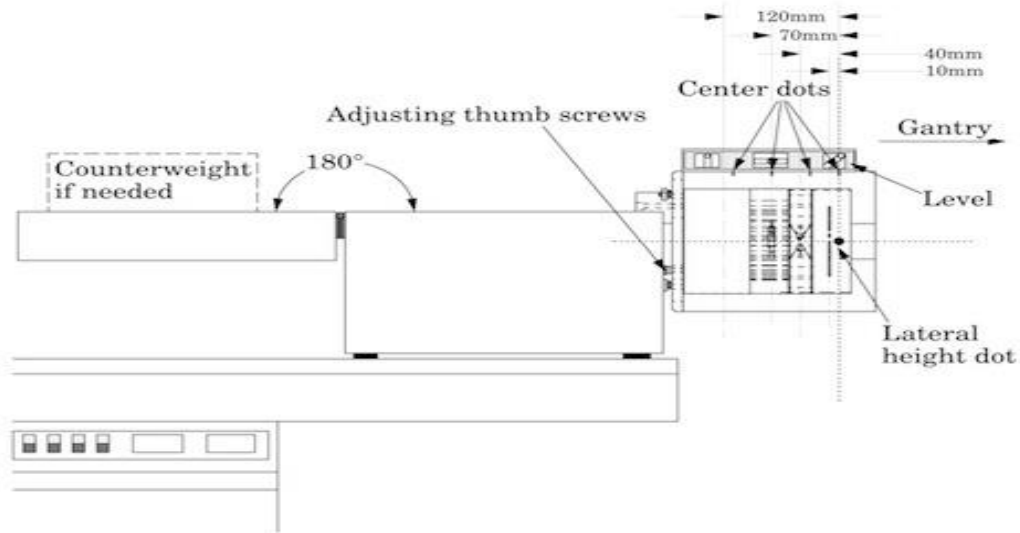


Figure 2.3: Schematic of the set-up of the Catphan 600 phantom on the CT table as per the recommendations of the Phantom Laboratory manual. [106]



Figure 2.4: Photographs of Catphan 600 phantom in position on the CT table. The box is used to support the phantom with the CT gantry laser guides and spirit level used to align the phantom with the gantry isocentre.

Two modules of the Catphan phantom were used for analysis:

- The CTP528 module is used for assessment of spatial resolution (see figure 2.5). This module has a diameter of 150mm and a thickness of 40mm. It contains a 21 line pair per centimetre gauge cut from 2mm thick aluminium sheets and cast into epoxy in a radial pattern. The resolution is determined by the maximum number of line pairs one can visualise out of the 21 line pair gauge, ranging from 1 to 21 line pairs per centimetre [106]. The higher the value the better the resolution.

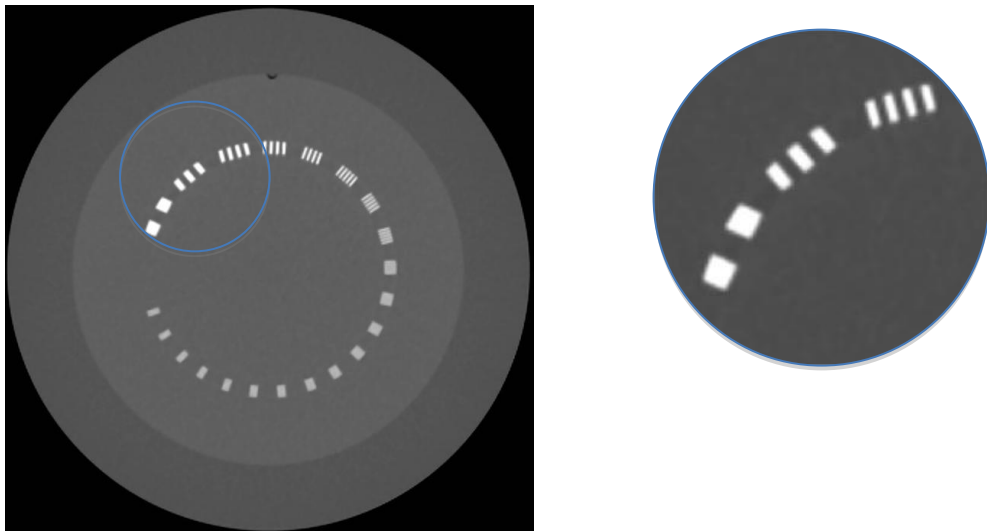


Figure 2.5: CT slice through the CTP528 module of the Catphan 600 phantom with close up detail of the line pairs in single centimetre sections. The maximum number of visualised line pairs per centimetre is taken as a measure of the spatial resolution.

- The CTP515 module is used for low-contrast performance measurements, such as low contrast resolution and contrast to noise ratio (CNR). It consists of a low-contrast module with a thickness of 40mm and a diameter of 150mm (see figure 2.6). The low contrast targets comprise 40mm long cylinders of various diameters aligned with the z-axis of the scanner with in-plane diameters ranging from 2 to 15mm at three contrast levels: 0.3, 0.5 and 1.0% compared with the background material.

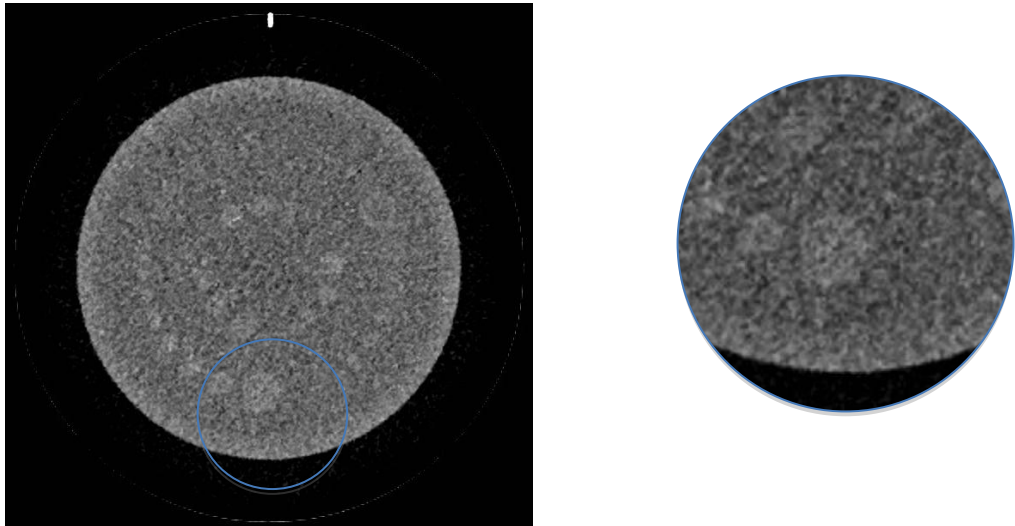


Figure 2.6: CT slice through the CTP515 module of the Catphan 600 phantom with close up detail of the 15mm target with 1.0% contrast. This target and the adjacent background material were used in this study for measurement of low contrast resolution and contrast to noise ratio.

Human cadavers were used in compliance with the Helsinki Declaration and approval was granted for their use by the institutional ethical review board. Five cadavers (3 male, 2 female) were obtained from anatomical bequests to the Department of Anatomy in University College Cork. All were embalmed with using the Thiel methodology [129-130], resulting in well-preserved organs and

tissues. The cadavers were placed supine and headfirst on the CT table in an arms-down position. Appropriate isocentre alignment was achieved by use of lateral and antero-posterior CT localiser scans. The scan length extended from the lung bases to the pubic symphysis as per standard of care CT protocol.

The CT acquisitions for this chapter were performed on a GE Discovery CT750 HU 64 slice CT scanner (GE Healthcare, Milwaukee, Wisconsin, USA) with inbuilt ASiR capability and upgraded with MBIR reconstruction capability. Table 2.1 summarises the standard parameters that were applied to all acquisition protocols.

Table 2.1: Standard scan parameters applied to all CT acquisition protocols

| | |
|-------------------------------------|--|
| Pitch: | 1 |
| Rotation time: | 0.8 sec for all protocols other than 100kV with ATCM acquisitions with variable noise index where 0.5 sec was used |
| Image matrix: | 512 x 512 |
| Field of view: | 36cm for Kyoto phantom and cadavers, 26.5cm for Catphan phantom |
| Acquisition slice thickness: | 0.625mm |

Repeated CT acquisitions were performed on both phantoms and the five cadavers with variation of the user-selected parameters for each protocol. With a fixed tube voltage of 120kV, examinations were performed with tube currents of 400mA, 200mA and 100mA. With a fixed tube current of 225mA, examinations were performed with tube voltages of 140kV, 120kV, 100kV and 80kV. With use of tube current modulation and fixed kV settings of 120kV and 100kV, examinations were performed with noise index setting of 20, 30, 40, 50, 60 and 70. The acquisition protocols are summarised in figure 2.7 below.

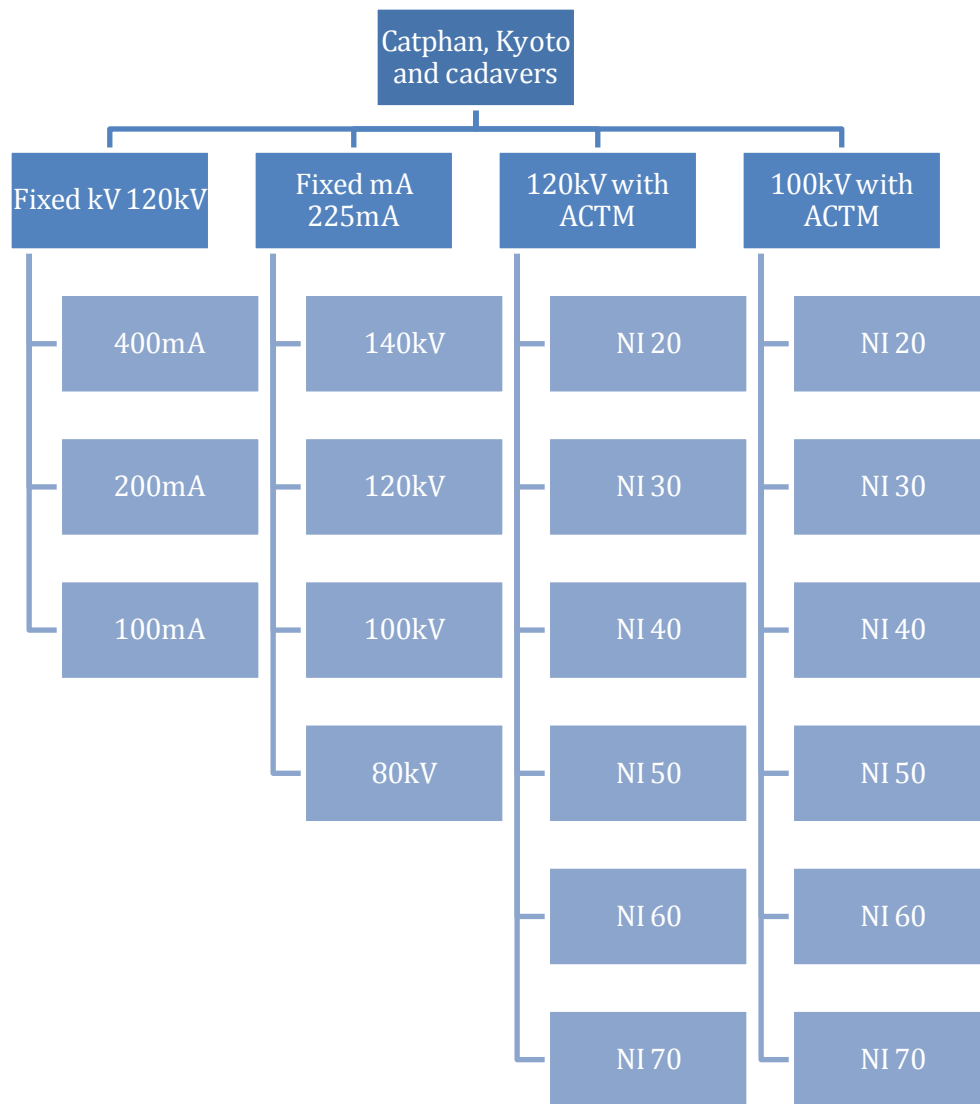


Figure 2.7: Schematic summarising the CT scanning parameters used for each of the CT acquisition protocols. Each of the Kyoto and Catphan phantoms and all five cadavers were scanned with each of 19 separate protocols.

Data reconstruction:

The raw data for each examination were reconstructed with traditional filtered back projection (FBP) to act as the reference standard. Raw data were also reconstructed with each of adaptive statistical iterative reconstruction (ASiR) with a strength of 40% (as per vendor recommendation) and model based iterative reconstruction (MBIR), with each of the two provided MBIR settings for abdomino-pelvic CT (MBIR RP05 for improving spatial resolution and MBIR NR05 for maximal noise reduction). This yielded 4 series for each of 19 scan protocols for each of the Catphan and Kyoto phantoms, as well as five cadavers (532 individual series). For simplicity, in the results section the reconstruction algorithms are labelled as follows: FBP, ASiR 40, MBIR R, MBIR N.

Dose measurements:

The volumetric CT dose index ($CTDI_{vol}$) and dose length product (DLP) values were recorded after each acquisition. SSDE was calculated as per AAPM methodology for the Kyoto phantom and the cadavers by calculating the effective diameter and multiplying the derived conversion factor by the $CTDI_{vol}$ [97]. Effective dose was calculated by multiplying the DLP value by the conversion coefficient for abdomen and pelvis, known as the k factor. The value of this conversion coefficient for a 32cm phantom is 0.015 [131].

Image review:

Images were reviewed on a dedicated advanced image review workstation (Advantage Workstation VolumeShare 2, Version 4.4, GE Medical Systems, Milwaukee, USA). Kyoto phantom and cadaveric images were reviewed in axial

slices with a thickness of 0.625mm on a soft tissue window (window width 40HU, window length 350HU). Catphan phantom images were reviewed in 3mm thick axial slices on a bone window (window width 2000HU, window length 350HU) for the CTP528 (spatial resolution) module and a narrow soft tissue window (window width 100HU, window length 70HU) for the CTP515 (low contrast resolution) module.

Kyoto phantom and cadaveric analysis:

Attenuation and objective noise were measured by placing spherical regions of interest in anatomical tissues/organs at five different anatomical levels within the phantom and cadavers (see figure 2.8). For the anthropomorphic phantom, these locations were chosen to approximate to anatomical levels used in human models in this and future chapters, but with slight deviation due to phantom composition. These comprised the liver parenchyma at the level of the right hemidiaphragm, the liver parenchyma at the level of the porta hepatis, the right renal parenchyma at the level of the renal hilum, the right common iliac artery at the level of the right iliac crest and the right gluteal region at the level of the roof of the right acetabulum (see figure 2.9 below). In human subjects, the sites varied at the level of the renal hilum where the right erector spinae was measured and the right iliac crest where psoas was measured. Care was taken to place the ROIs in as homogenous an area of tissue as possible, away from blood vessels, fat planes and organ edges. Identical spherical regions of interest (diameter 10mm, volume 519mm³) were used and propagated to identical loci on each series by means of a cut and paste function to ensure consistency and repeatability.

The mean attenuation value within the ROI was recorded, as was the standard deviation of this value, which acted as a measure of objective noise [101, 113]. The *signal to noise ratio* (SNR) within each ROI was calculated by dividing the mean attenuation value by its standard deviation [132].

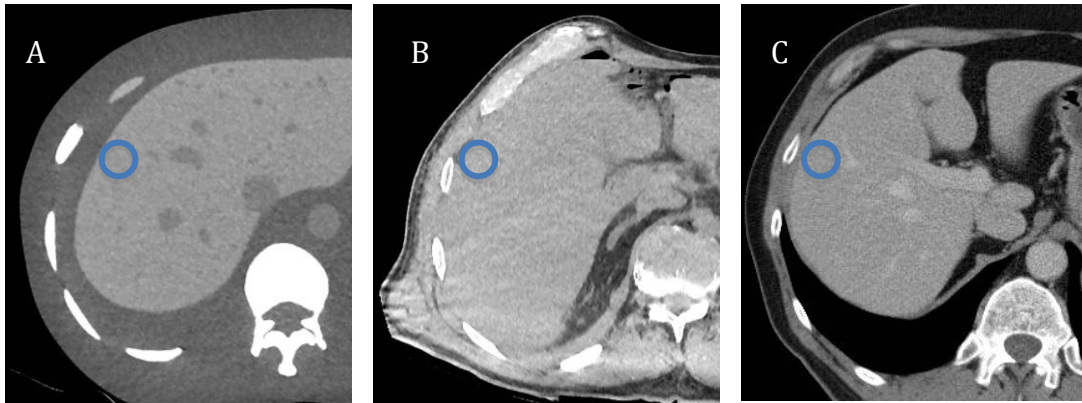
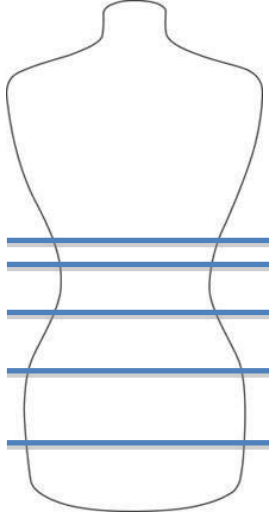


Figure 2.8: Details of individual axial slices from CT of abdomen and pelvis for the anthropomorphic phantom (A), a cadaver (B) and a live human subject (C). Fixed volume spherical regions of interest (ROIs) are placed in the liver parenchyma at the level of the porta hepatis. The value of the pixels within the ROI is indicative of attenuation and the standard deviation of this value is a measure of objective image noise. The ratio of these two values is the signal to noise ratio.

Figures 2.9: The slice levels where ROIs are placed in both phantom (A) and cadaveric (B) models to assess attenuation, objective noise and signal to noise ratio.

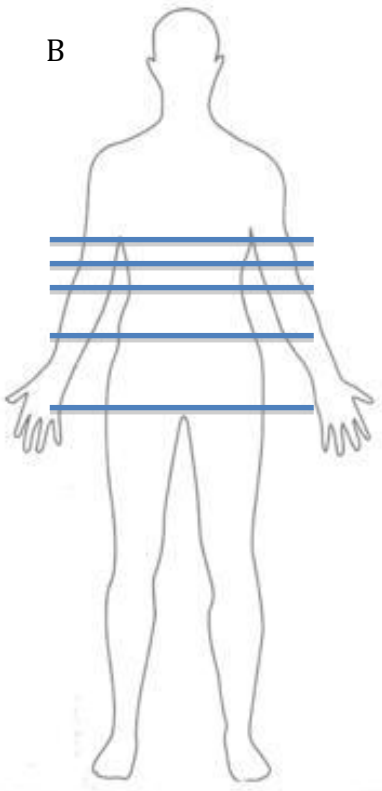
A



Kyoto phantom

- A Liver parenchyma at the level of the right hemidiaphragm
- B Liver parenchyma at the level of the porta hepatis
- C Right renal parenchyma at the level of the renal hilum
- D Right common iliac artery at the level of the right iliac crest
- E Right gluteal region at the level of the roof of the right acetabulum

B



Cadavers

- A Liver parenchyma at the level of the right hemidiaphragm
- B Liver parenchyma at the level of the porta hepatis
- C Right erector spinae muscle belly at the level of the right renal hilum
- D Right psoas muscle belly at the level of the right iliac crest
- E Right gluteus maximus muscle belly at the level of the roof of the right acetabulum

Catphan analysis:

Spatial resolution was calculated from the CTP528 module by counting the number of visible line pairs per centimetre for each study. A score of 0 to 21 was recorded based on the number discernable, where a higher value equates to better image resolution.

Low contrast resolution was subjectively assessed by visual analysis of the CTP515 module by an experienced blinded observer. For this study, to avoid a partial volume effect [133], only the 15.0mm target with a contrast difference of 1.0% (having an attenuation difference with the background of 10HU) was chosen to be analysed – i.e. the largest target with the greatest contrast difference. The visualisation of this target was graded on a 3-point scoring scale: 3 = object clearly visible, 2 = object not clearly visible, 1 = object could not be detected [133]. This analysis was performed on three images of each series and an overall score out of 9 was calculated by summation of these three values.

Contrast to noise ratio was calculated using the same target on the CTP515 module as for contrast resolution. For each series, the CT attenuation values of this target and of the background material of the module adjacent to the target were measured using a spherical region of interest. Their standard deviations were also recorded. The region of interest used to perform the measurements was kept at a fixed volume (diameter 10mm, volume 519mm³) and placed at identical loci on each series, again by means of a cut and paste function. The contrast to noise ratio is calculated as follows: $CNR = (HU_T - HU_B) / SD_B$, where HU_T

is the mean attenuation of the low contrast target and HU_B and SD_B are the mean attenuation and standard deviation values of the background region of interest [134]. A CNR was calculated on three images of each series and, from these three measurements, a mean CNR was calculated for each series [135].

Statistical analysis:

Data compilation and statistical analyses were performed using Microsoft Excel (Microsoft Corporation, Redmond, WA) and GraphPad Prism version 6.0 (GraphPad Software Incorporated, San Diego, CA). Descriptive statistics are provided in terms of means with standard deviations and medians with interquartile ranges (IQR) for parametric and non-parametric values. Variables were compared with paired t-tests and repeated measures ANOVA (with Tukey's and Dunnett's multiple comparison tests if ANOVA showed a significant difference) if parametric. If non-parametric, Wilcoxon matched pairs tests and Friedman tests (with Dunn's multiple comparison test) were used. Pearson and Spearman correlations were used for parametric and non-parametric variables, respectively. The criterion for significance was taken as $P < 0.05$.

Results:

Radiation dose:

The mean radiation dose in terms of CTDI_{vol}, DLP, SSDE and effective dose for the anthropomorphic phantom scanned with each protocol are expressed in table 2.2 below.

Table 2.2: Mean radiation doses for the anthropomorphic phantom with each CT protocol

| | | CTDI _{vol} (mGy) | DLP (mGy.cm) | SSDE (mGy) | Effective dose (mSv) |
|--------------------------------|-------|------------------------------|-----------------|------------|-------------------------|
| 120kV | 400mA | 25.32 | 1037.54 | 39.50 | 15.56 |
| | 200mA | 12.68 | 560.03 | 19.78 | 8.4 |
| | 100mA | 6.34 | 279.92 | 9.89 | 4.2 |
| 225mA | 140kV | 20.33 | 898.02 | 31.71 | 13.47 |
| | 120kV | 14.26 | 630.03 | 22.25 | 9.45 |
| | 100kV | 8.99 | 397.05 | 14.02 | 5.96 |
| | 80kV | 4.8 | 211.9 | 7.49 | 3.18 |
| 120kV with ATCM | NI 20 | 19.81 | 873.67 | 30.90 | 13.1 |
| | NI 30 | 9.6 | 423.45 | 14.98 | 6.35 |
| | NI 40 | 5.47 | 241.32 | 8.53 | 3.62 |
| | NI 50 | 3.48 | 153.61 | 5.43 | 2.3 |
| | NI 60 | 2.42 | 106.65 | 3.78 | 1.6 |
| | NI 70 | 1.77 | 77.86 | 2.76 | 1.17 |
| | | | | | |
| 100kV with ATCM | NI 20 | 8.72 | 384.76 | 13.60 | 5.77 |
| | NI 30 | 8.3 | 366.36 | 12.95 | 5.5 |
| | NI 40 | 5.66 | 249.99 | 8.83 | 3.75 |
| | NI 50 | 3.56 | 157.22 | 5.55 | 2.36 |
| | NI 60 | 2.52 | 111.13 | 3.93 | 1.67 |
| | NI 70 | 1.83 | 80.74 | 2.85 | 1.21 |
| | | | | | |

As expected, with a decrease in the number of photons from the x-ray tube, the radiation dose incurred decreased. This is demonstrated graphically in figure

2.10. Identical trends in dose reduction were observed across the protocols, regardless of which dose metric is utilised. The doses for the cadavers mirrored those for the anthropomorphic phantom, following a similar trend in terms of dose reduction.

With a fixed tube voltage, doubling the tube current doubles the radiation dose confirming that these two values are in direct proportion. Changing tube voltage with a fixed tube current is an effective means of affecting the overall radiation dose from the CT acquisition. For example, decreasing the tube voltage from 120kV to 100kV leads to a 37% reduction in radiation dose and from 120kV to 80kV yields a 66% dose reduction. The relationship with radiation dose reduction with a fixed tube voltage and modulated tube current demonstrates an overall exponential decrease with increasing noise index.

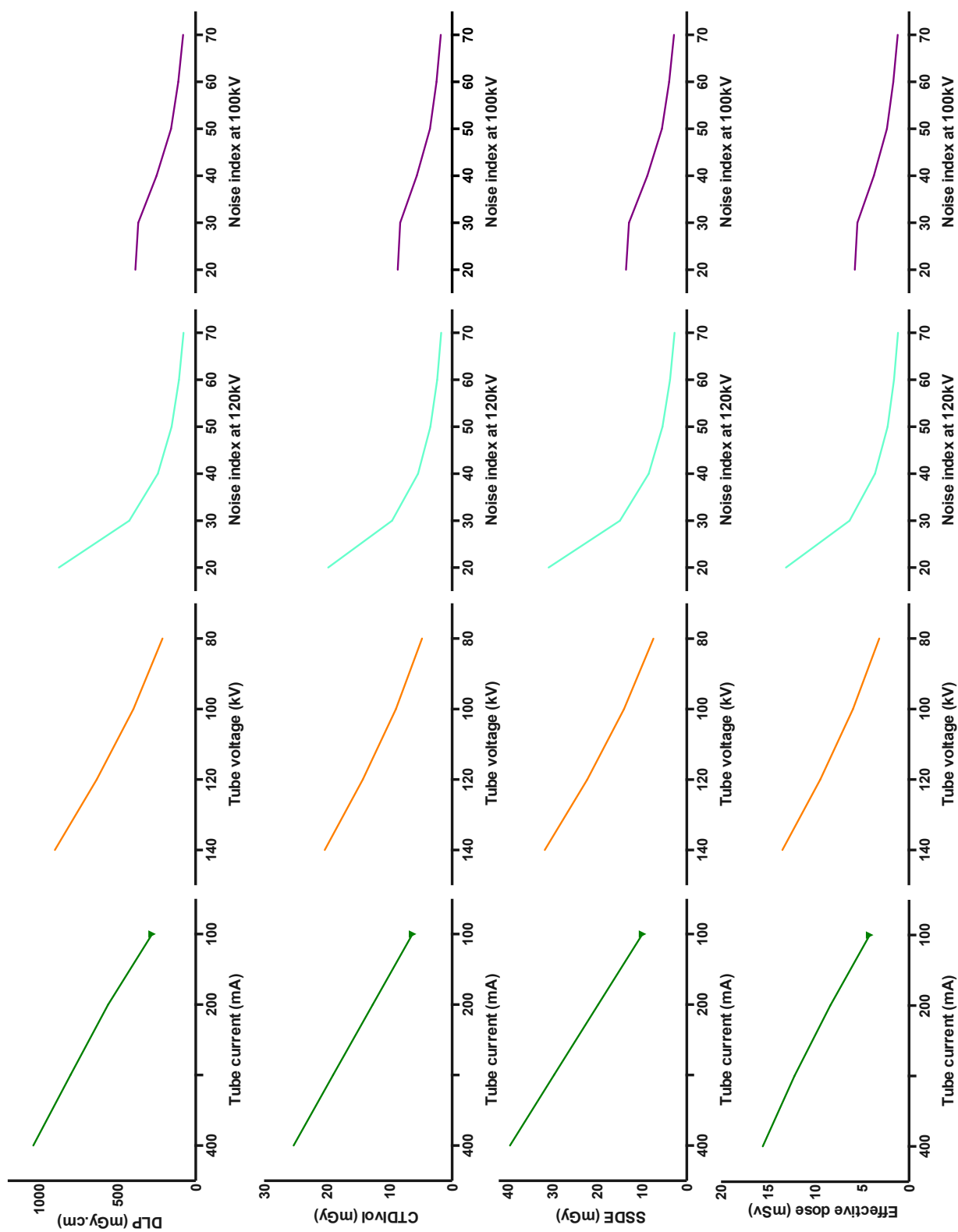


Figure 2.10: Variations of radiation dose in terms of DLP, CTDI_{vol}, SSDE and effective dose with tube current, tube voltage and noise index.

Image quality measurements (i.e. what ASiR and MBIR actually do):

Hounsfield units, the unit of CT density, were measured at five distinct anatomical locations on both the anthropomorphic phantom and the cadavers on all studies. The mean attenuation from a composite of these locations for the anthropomorphic phantom with each reconstruction algorithm is demonstrated in figure 2.11 below. There is no significant correlation between radiation dose and measured attenuation values ($P>0.05$ for all comparisons).

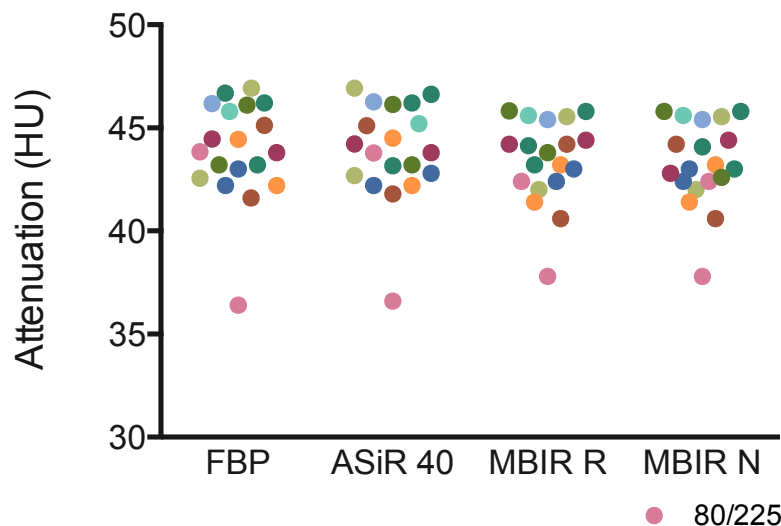


Figure 2.11: Scatter graph demonstrating the mean attenuation from a composite of 5 anatomical sites in the anthropomorphic phantom with each reconstruction algorithm. Each dot represents the mean attenuation from a different acquisition protocol. Note that the 80kV/225mA protocol (pink dot) is an outlier.

Comparison across scanning protocols:

When the mean attenuation values for the protocols were compared with one another, a statistically significant ($P=0.0014$) difference was observed between some protocols. This was most evident with the 80kV with 225mA protocol when compared with the others – well demonstrated on figure 2.11 above as an

outlier. If this protocol was excluded, statistically significant differences were observed between some protocols but the magnitude of each was <5HU so did not prove clinically significant - for the CT number accuracy of water, the AAPM Task Group 66 has defined a tolerance of $\pm 5\text{HU}$ [136].

Comparison across reconstruction algorithms:

Repeated measures ANOVA testing with Tukey's multiple comparisons test demonstrated a statistically significant difference between measured Hounsfield units across reconstruction protocols ($p=0.0086$) but this difference is <1HU so, again, is not of clinical significance. This indicates that fidelity in HU values is preserved with iterative reconstruction. For the cadaveric models, no statistically significant difference was observed in attenuation values between scanning protocols or reconstruction algorithms ($P>0.05$ for both).

Objective noise

The relationship between objective image noise and reconstruction algorithm for each scanning protocol is demonstrated in figure 2.12. Due to a lack of significant differences between objective image noise measurements between the anthropomorphic phantom and the cadavers, for simplicity and to avoid duplication the data were merged and those presented below are a composite of both.

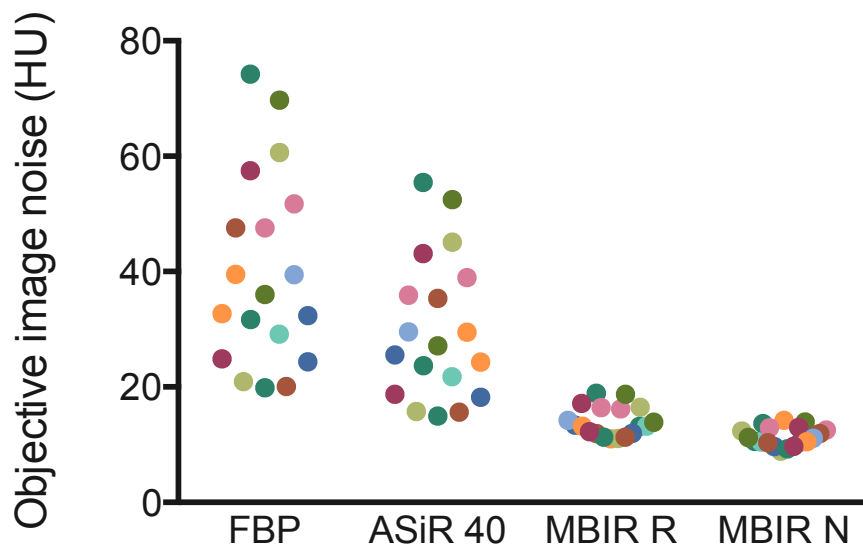


Figure 2.12: Scatter graph demonstrating the mean objective image noise from a composite of 5 anatomical sites in the anthropomorphic phantom and cadavers with each reconstruction algorithm. Each dot represents the mean objective noise from a different acquisition protocol.

Objective noise was observed to decrease in magnitude with increasing radiation dose for conventional FBP reconstruction (Pearson coefficient = -0.84, $P < 0.0001$), regardless of dose metric examined. This accounts for the wide range of observed image noise levels with FBP as a wide range of doses was used. A similar relationship exists for ASiR 40 with Pearson correlations of -0.84 for each dose metric ($P < 0.0001$) but the mean noise with ASiR 40 is less than FBP for all protocols ($P < 0.0001$). With both subtypes of MBIR reconstruction, there were also strong relationships with increasing radiation dose and a reduction in objective image noise (Pearson coefficients of -0.73 and -0.78 for MBIR R and MBIR N, respectively with $P < 0.0005$).

Observing the MBIR N and MBIR R columns in figure 2.12 demonstrates that MBIR reduces image noise to a particular threshold noise level within the image. The mean image noise with MBIR N (11.41 ± 1.633 HU, range 8.9-14.22 HU) was

significantly less than observed with MBIR R (13.99 ± 2.566 HU, range 11-18.88 HU) reflecting the proposed superior noise reduction properties of this reconstruction algorithm ($P < 0.0001$).

Noise reduction and % noise reduction:

The magnitude of noise reduction in terms of Hounsfield units is demonstrated in figure 2.13 (A and B). This uses FBP as the standard against which reduction in noise is measured (noise reduction = $\text{noise}_{\text{FBP}} - \text{noise}_{\text{Recon}}$, where $\text{noise}_{\text{Recon}}$ is the objective noise in the reconstruction algorithm under examination).

Percentage noise reduction is calculated as follows: % noise reduction = $(\text{noise reduction}_{\text{Recon}} / \text{noise}_{\text{FBP}}) \times 100$.

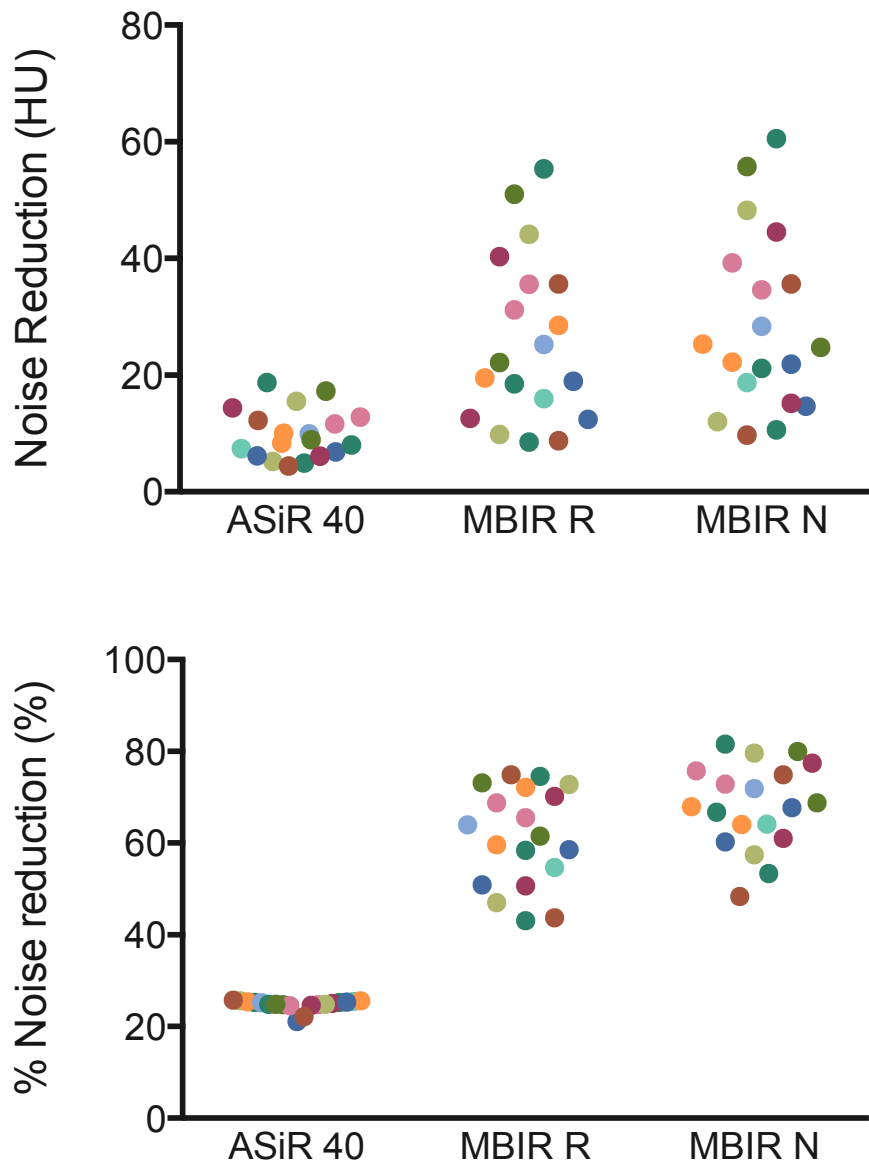


Figure 2.13 (A and B): Scatter graphs demonstrating the absolute and percentage objective image noise reduction with each reconstruction algorithm when FBP reconstruction is used as the reference for comparison. Each dot represents the mean absolute (A) and percentage (B) objective noise reduction from a different acquisition protocol.

Absolute noise reduction demonstrates a very strong inverse relationship with radiation dose for ASiR 40 (Pearson coefficient = -0.84), MBIR R (Pearson coefficient = -0.84) and MBIR N (Pearson coefficient = -0.83), with $P < 0.0001$ for each. The mean magnitude of noise reduction with ASiR is 9.947 ± 4.27 HU (range 4.44-18.76 HU), equating to a mean reduction of 24.74% (range 21.08-25.71%).

With both the R and N MBIR subtypes there was a greater magnitude but wider spread in the absolute reduction in noise in terms of Hounsfield Units (26.01 ± 14.39 HU, range 8.56-55.34 and 28.59 ± 15.26 HU, range 9.7-60.56, respectively) with MBIR N superior to MBIR R in terms of noise reduction ($P < 0.0001$).

MBIR N achieved a significantly superior mean percentage noise reduction of 68.08% compared with 61.27% with MBIR R ($P < 0.0001$). The percentage noise reduction with both MBIR subtypes correlated very strongly with the radiation dose, regardless of metric used (Pearson coefficients = -0.94 for MBIR R and -0.95 for MBIR N, $P < 0.0001$) indicating that the lower the radiation dose administered, the larger the percentage noise reduction achieved by MBIR. The relationship with ASiR and percentage noise reduction was weaker (Pearson correlation coefficient = -0.37, $P < 0.0001$).

Signal to noise ratio:

The signal to noise ratio (SNR) examines the interplay of mean attenuation values and the level of image noise and is an index of overall image quality. $SNR = \text{mean attenuation/objective noise}$. The SNR across all protocols is demonstrated in figure 2.14. MBIR N demonstrates the best SNR of all the reconstruction algorithms (mean SNR = 3.87, $P < 0.0001$), with MBIR R and ASiR 40 both performing significantly better than FBP ($P < 0.0001$ for both). For all dose metrics, signal to noise ratio correlates very strongly with radiation dose for FBP (Pearson coefficient 0.95) and ASiR (Pearson coefficient 0.94) ($P < 0.0001$ for all comparisons). There is also a strong correlation of SNR and dose with

MBIR R and N with correlation coefficients of 0.71 and 0.74, respectively ($P=0.0006$ and 0.0003 , respectively).

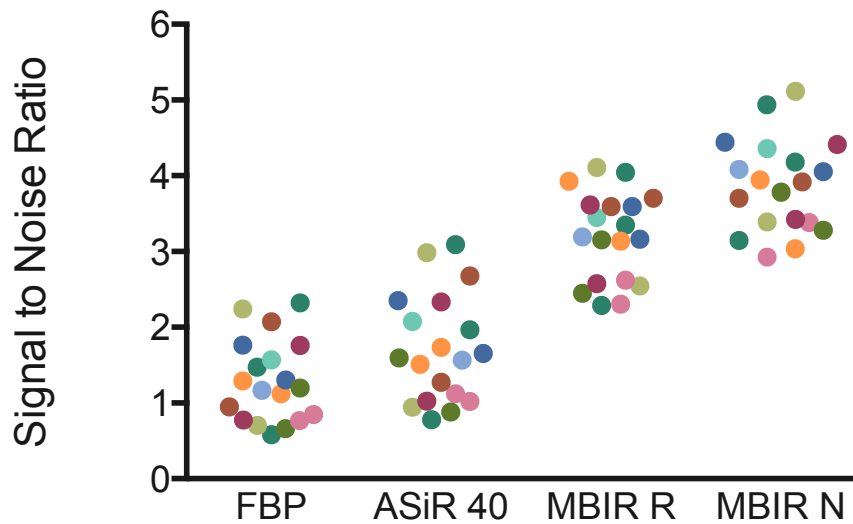


Figure 2.14: Scatter graph demonstrating the mean signal to noise ratio with each reconstruction algorithm. Each dot represents the mean signal to noise ratio from a different acquisition protocol.

Contrast resolution:

Contrast resolution was measured from the Catphan CTP515 module on a scale from 1-3, depending on target visualisation. The summation of three iterations of this process on three separate slices yielded a minimum possible score of 3 and a maximum of 9 [133]. The contrast resolution scores for each reconstruction algorithm are demonstrated in figure 2.15 below. Subjectively, the best contrast resolution was observed with MBIR N (median 7, IQR 3-9). MBIR R had a median value of 6 (IQR 3-9), which was not significantly different to MBIR N ($p=0.1719$) suggesting equivalence in terms of contrast resolution. MBIR was significantly superior to ASiR 40 for contrast resolution. There was no statistically significant difference between contrast resolution for FBP and ASiR 40 ($P=0.7813$). For FBP

and ASiR 40, the contrast resolution score correlates strongly with dose (Spearman coefficients 0.777 and 0.8607, respectively with $P < 0.0001$). There are moderate correlations of 0.4763 and 0.5794 ($p < 0.05$) for MBIR R and N, respectively, with contrast resolution.

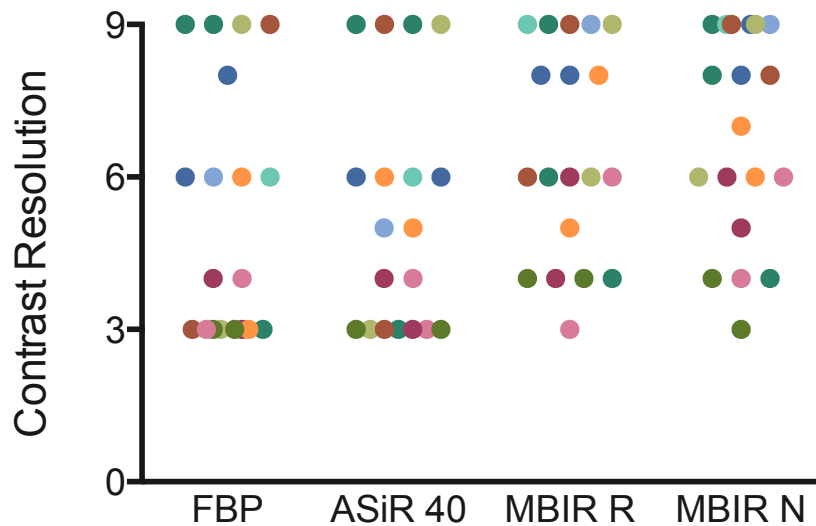


Figure 2.15: Scatter graph demonstrating the median contrast resolution scores across the reconstruction protocols. Each dot represents the median contrast resolution score from a different acquisition protocol.

Contrast to noise ratio:

Contrast to noise ratio (CNR) for each CT protocol with each reconstruction algorithm is demonstrated in figure 2.16 below. The mean contrast to noise ratio was best with MBIR N (CNR = 1.088, range 0.8083-1.428, $p < 0.0001$). The mean contrast to noise ratios for MBIR R, ASiR 40 and FBP were 0.8601, 0.555 and 0.4103, respectively ($P < 0.0001$). For all comparisons, CNR correlated strongly or very strongly with radiation dose ($P < 0.005$ for all comparisons) with Pearson coefficients of 0.8825, 0.8676, 0.7196 and 0.6283 for FBP, ASiR 40, MBIR R and MBIR N, respectively.

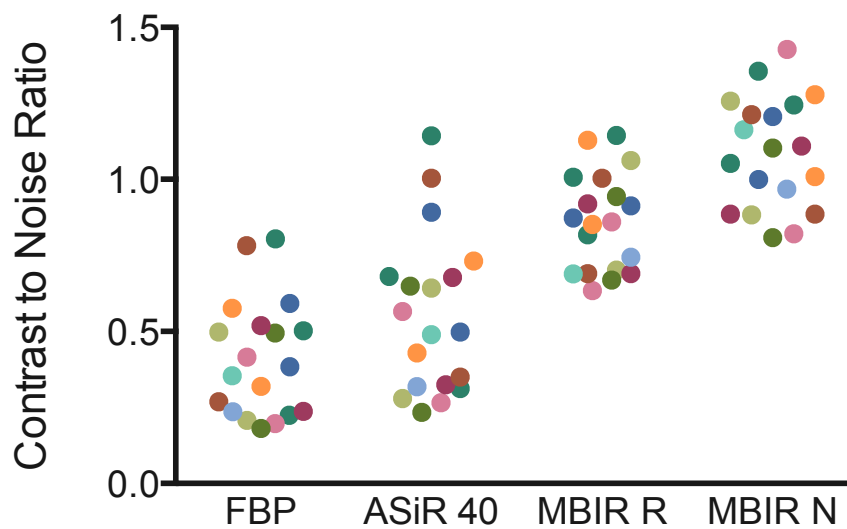


Figure 2.16: Scatter graph demonstrating the median contrast to noise ratio across the reconstruction protocols. Each dot represents the median contrast to noise ratio from a different acquisition protocol.

Spatial resolution:

For each CT protocol, the relationship between spatial resolution and reconstruction algorithm is demonstrated in figure 2.17 below. Spatial resolution is scored on a scale from 0 to 21 in terms of the number of line pairs per centimeter visible on Catphan module CTP528. The typical spatial resolution expected from CT imaging is circa 7 lp/cm. The median spatial resolution with MBIR R and N is 8 lp/cm (range 6-8 lp/cm) with no significant difference between the two algorithms ($p > 0.05$). FBP and ASiR 40 are inferior in terms of spatial resolution ($p < 0.0001$), both with median values of 7 lp/cm (range 6-7 lp/cm). For all reconstruction algorithms, there is a very strong and significant correlation between radiation dose and spatial resolution with Spearman coefficients of 0.81-0.86 ($P < 0.0001$).

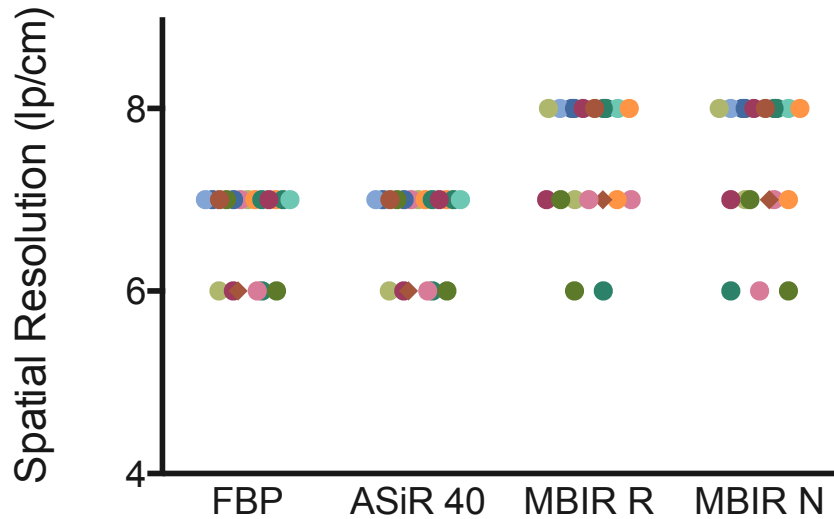


Figure 2.17: Scatter graph demonstrating the median spatial resolution scores across the reconstruction protocols. Each dot represents the median spatial resolution score from a different acquisition protocol.

Effect of radiation dose on image quality:

The impact of increasing radiation dose on the image quality indices across the four reconstruction algorithms examined is summarized in table 2.3. This demonstrates the presence and strength of dose related correlations with each image quality parameter.

Table 2.3: How radiation dose correlates with image quality indices across the four reconstruction algorithms.

| | FBP | ASiR 40 | MBIR R | MBIR N |
|---|-------------|-------------|-------------|-------------|
| Attenuation | - | - | - | - |
| Objective noise | *** inverse | *** inverse | *** inverse | *** inverse |
| Noise reduction | n/a | *** inverse | *** inverse | *** inverse |
| % Noise reduction | n/a | * inverse | *** inverse | *** inverse |
| Signal to noise ratio | *** | *** | *** | *** |
| Contrast resolution | *** | *** | * | * |
| Contrast to noise ratio | *** | *** | ** | ** |
| Spatial resolution | *** | *** | *** | *** |
| Correlation coefficients are in terms of Pearson for parametric and Spearman for non-parametric variables | | | | |
| Strength of correlation: | | | | |
| - = Absence of a significant correlation | | | | |
| * = Weak correlation | | | | |
| ** = Moderate correlation | | | | |
| *** = Strong correlation | | | | |

Discussion:

To simultaneously improve image quality and reduce radiation doses from CT examinations, CT manufacturers have introduced iterative reconstruction algorithms. The results from this study indicate that large reductions in CT dose with maintained diagnostic performance are possible when using iterative reconstruction.

In producing a CT image, both tube current and voltage must be carefully chosen to ensure sufficient delivery of x-rays to achieve acceptable image quality at a radiation dose that is as low as reasonably achievable. When x-rays leave the tube and pass through an object, the beam intensity is reduced (i.e. attenuated). CT images are a display of the amount of attenuation that has occurred when the x-ray beam penetrates the body and image quality is dependent upon recording sufficient x-ray events by the detector. Reduction in radiation dose while maintaining image quality is a primary focus of diagnostic imaging.

We examined the interplay of user selected input parameters with radiation dose:

- Firstly, we investigated the theoretic relationships between tube current and voltage and radiation dose, namely that radiation dose is directly proportional to tube current [50,116,122] and that radiation dose is proportional to tube voltage raised to an exponential power ranging from 2.5-3.1. Radiation dose (regardless of dose metric used) is proven directly proportional to tube current with a Pearson correlation coefficient of 1

($P=0.0005$). Radiation dose is proven proportional to tube voltage to an exponential power of 2.5 with a Pearson coefficient of 0.99 ($P=0.0008$).

- Secondly, we investigated the effect of automated tube current modulation on radiation dose at two different fixed kV settings. The relationship between noise index and radiation dose at each tube voltage level is very strongly inverse (Pearson coefficients of -0.89 and -0.98 for 120kV and 100kV, respectively) with an increase in noise index yielding a corresponding reduction radiation dose.

The dose relationships observed in the anthropomorphic phantom with each change in input parameter were not significantly different from the relationships observed with the cadaveric data ($p<0.05$ for all comparisons). In light of this, for simplicity, just the phantom dose data is presented.

We then examined the interplay of image quality with reconstruction protocol for each of the CT acquisition protocols in both phantom and cadaveric models.

With traditional filtered back projection, the noise-dose trade-off is well established and is the major barrier to radiation dose reduction. In parallel with reducing dose, there is a fall-off in signal to noise ratio, contrast resolution, contrast to noise ratio, spatial resolution and diagnostic acceptability. The lower the dose, the less diagnostic the image. Due to the proprietary nature of much of the information regarding how vendor-specific iterative reconstruction algorithms work, information regarding the precise image quality targets that

these algorithms work to is not readily available. We therefore try to establish, on a practical level, what these algorithms achieve and estimate these targets.

The main effect of ASiR 40 on the image is reduction of image noise at lower radiation doses. More specifically, ASiR 40 achieves a mean noise reduction of 24.74% when compared with FBP. This value demonstrates a very narrow interquartile range of 24.73-25.39% suggesting the main effect of ASiR 40 to be an attempt at reduction of image noise by 25%, regardless of the acquisition protocol used.

By comparison, when MBIR R and N are applied to each dataset, the objective noise level within the images is centred on 14HU and 11.4HU, respectively with narrow standard deviation ranges (2.57HU and 1.63HU, respectively). This suggests that the aim of the MBIR reconstruction algorithms is to reduce the level of noise in the image to a predetermined noise threshold, regardless of the acquisition protocol used. This accounts for the longer reconstruction times required for noisier and lower dose datasets as more iterations may need to be performed when compared with conventional dose images.

Despite being superior to FBP regarding objective image noise, in terms of subjectively assessed image quality indices such as contrast and spatial resolution, ASiR was not significantly superior to FBP though both subtypes of MBIR were. At a minimum, ASiR was demonstrated non-inferior to FBP for these indices and the noise-spatial resolution trade-off experienced with FBP is not evident. The contrast to noise and signal to noise ratios both demonstrated ASiR

superior to FBP, suggesting that the subjective analyses may have been subject to bias despite blinding. Adaptation bias (where observers are accustomed to a certain image appearance and, so, prefer it to images with a slightly altered appearance) has been described in research regarding the introduction of ASiR and has been observed to reduce acceptability of the image due to the unfamiliar plastic appearance [71,88]. Overall, ASiR is superior to FBP in terms of image quality indices at equivalent radiation doses in phantom and cadaveric models.

MBIR R and MBIR N are superior to both ASiR and FBP in terms of objective noise levels, noise reduction and signal and contrast to noise ratios. Scores for the subjective indices contrast and spatial resolution were superior also with the MBIR algorithms suggesting that the images were more familiar in texture and less prone to any adaptation bias. Similar to with ASiR, the noise-spatial resolution trade-off that exists with FBP does not apply with MBIR. Overall, MBIR is superior to FBP and ASiR in terms of image quality indices at equivalent radiation doses in phantom and cadaveric models. Because images reconstructed with MBIR have the lowest image noise irrespective of the scanning protocol, these algorithms provide an opportunity to perform ultra-low dose CT examinations [75].

Even with blinding of readers to radiation dose and reconstruction algorithm, there is potential for recognition bias to occur (when it is intended that observers be blinded to an evaluation variable (e.g. new reconstruction technique) but they nevertheless can, or believe they can, identify which reconstruction they are looking at). The altered texture of the image may alert

the reader to the use of iterative reconstruction but consistency between the subjective and objective measurements for MBIR image assessments suggest that this bias was not a major contributing factor.

The MBIR R and MBIR N subtypes are purported by the vendor to preferentially improve spatial resolution and image noise, respectively. Both subtypes were demonstrated equivalent in terms of spatial resolution when the CTP528 module was examined - MBIR N was demonstrated non-inferior to MBIR R. In terms of image noise, however, MBIR N was superior to MBIR R in terms of a lower level of objective image noise and superior levels of absolute and percentage noise reduction and greater signal to noise and contrast to noise ratios.

The improved image quality with the iterative reconstruction algorithms examined confirms their utility for application to reduction of radiation dose at CT with preservation of image quality. Importantly, attenuation values in tissues of interest are preserved across the reconstruction algorithms without any clinically-significant difference (all $<5\text{HU}$). The protocol acquired with 80kV (fixed current of 225mA) did demonstrate lower mean attenuation values than the others but this finding was uniform across all reconstruction algorithms – i.e. the protocol behaves the same with FBP as it does with ASiR or MBIR in terms of attenuation, despite values being lower than the other acquisition protocols. The amount of attenuation that occurs when an x-ray beam penetrates the body is measured by linear attenuation coefficients. It is well known that the selection of tube voltage has a direct effect on linear attenuation coefficient values, from which the Hounsfield units are extrapolated [126]. Lower kV values experience

increased beam attenuation (due to more photoelectric effect and Compton scatter), i.e. less of the beam penetrates the body (tissue) affecting the CT attenuation value directly. While not as evident with the reduction of tube voltage from 120kV to 100kV, this change in attenuation value with tube voltage is expected and, importantly, attenuation values at a particular voltage remain consistent across reconstruction algorithms. The 80kV protocol was included for completeness but our practice does not include tube voltages of <100kV for routine CT examinations of the abdomen.

This study has some limitations. Firstly, the phantom (torso only with no limbs, weight 45kg) was limited to representation of a small to average sized adult, excluding various body sizes. Equally, none of the cadavers was obese (mean effective diameter of 30.16cm). However, given the similarity of the two datasets, the anthropomorphic phantom represents a good model for humans of similar size. Secondly, because of the large number of datasets derived from this study and the potential for recall bias of phantom anatomy, no subjective assessments of the images were performed for noise, texture, artefacts and diagnostic acceptability. For the cadavers, due to post mortem changes such as fluid accumulation and gas dissociation, as well as the absence of intravenous contrast medium, subjective assessment was also not performed. Both of these limitations are addressed in the following chapters when these protocols are applied to clinical patients.

Protocol selection:

The following section deals with selection of which CT protocols to combine to form the split dose CT of abdomen and pelvis protocol to apply to clinical subjects.

The standard of care protocol in our institution for CT of abdomen and pelvis had a tube voltage of 120kV, a tube current of 225-300mA (dependent on patient size) and a tube rotation time of 0.5-0.8sec. When the anthropomorphic phantom was scanned with these parameters, and reconstructed with FBP, the following radiation dose and image quality results were obtained (table 2.4):

Table 2.4: Radiation dose and image quality parameters for 'standard-of-care' CT of abdomen and pelvis (120kVp, time-current product of 180mAs)

| | |
|-------------------------|--------------|
| Tube voltage | 120kV |
| Tube current | 225mA |
| CTDI _{vol} | 14.26mGy |
| DLP | 630.03mGy.cm |
| SSDE | 14.02 mGy |
| Effective dose | 9.45mSv |
| Attenuation | 43HU |
| Objective noise | 24.36HU |
| Signal to noise ratio | 1.77 |
| Contrast resolution | 8 |
| Contrast to noise ratio | 0.59 |
| Spatial resolution | 7 lp/cm |

Use of automated tube current modulation was not routine in this institution until the introduction of ASiR (both were introduced simultaneously with the purchase of a new CT scanner in 2009) and did not form part of the standard CT protocol. Given that this protocol provided the level of image quality radiologists

were used to looking at, we used this as the gold standard by which to compare all other protocols in terms of image quality indices. However, routine use of ATCM would have reduced the radiation dose incurred from the examination. We acknowledge that the radiation dose from the protocol is in excess of what would have been standard of care had we this technology in place – ATCM can achieve a radiation dose reduction of up to 40-50% for CT of abdomen and pelvis [69,118]. Therefore, when formulating a split-dose protocol, the aim was for the combined tolerated radiation dose of both acquisitions to approximate to 50-60% of the standard of care dose. For reference, the current average radiation dose for a CT of abdomen and pelvis in Europe is 11.3mSv and in Ireland is 8.4mSv [31], with 7.82mSv being the mean radiation dose from standard of care CT of abdomen and pelvis in our institution (mean annual value from the dose-monitoring software DoseWatch GE Healthcare).

The complete dataset of the radiation dose and image quality measurements for all the CT protocols was examined by a multi-disciplinary team comprised of radiologists with a special interest in radiation dose, CT specialist radiographers, medical physicists, vendor CT advanced applications specialist, and a consultant gastroenterologist. From this review, two CT protocols were selected as the most appropriate to form the split dose CT protocol (see table 2.5).

Table 2.5: Summary of the input parameters, radiation dose and image quality of the selected protocols

| | Conventional dose protocol | Modified dose protocol | Standard of care protocol |
|-----------------------------|----------------------------|------------------------|---------------------------|
| Input parameters | | | |
| kV | 120 | 100 | 120 |
| mA | ATCM | ATCM | 225 |
| <i>Min</i> | 20mA | 20mA | n/a |
| <i>Max</i> | 350mA | 350mA | n/a |
| Noise index | 30 | 70 | n/a |
| Rotation time | 0.8sec | 0.5sec | 0.8sec |
| Pitch | 1 | 1 | 1 |
| Slice acquisition thickness | 0.625mm | 0.625mm | 0.625mm |
| Radiation dose | | | |
| CTDI _{vol} | 5.47 | 1.83 | 14.26mGy |
| DLP | 241.32 | 80.74 | 630.03mGy.cm |
| SSDE | 8.53 | 2.85 | 14.02 mGy |
| Effective dose | 3.62 | 1.21 | 9.45mSv |
| Image quality | | | |
| | <i>(With ASIR 40)</i> | <i>(With ASiR 40)</i> | <i>(With FBP)</i> |
| Attenuation | 46.26 | 43.16 | 43 |
| Objective noise | 29.54 | 55.46 | 24.36 |
| Signal to noise ratio | 1.57 | 0.78 | 1.77 |
| Contrast resolution | 5 | 3 | 8 |
| Contrast to noise ratio | 0.32 | 0.311 | 0.59 |
| Spatial resolution | 7 | 6 | 7 |

The following are some points about protocol selection:

- Reducing tube voltage is an appropriate way to achieve a large overall dose reduction, if all other parameters are kept unchanged. We chose 120kV for the conventional protocol but reduced the tube voltage to 100kV to achieve large dose savings for the modified dose protocol.
- Both chosen protocols utilize automated tube current modulation. This is felt preferable in abdomino-pelvic imaging due to differing densities

along the z-axis of the scan length requiring different levels of dose to adequately image the structures of interest. ATCM has been demonstrated useful in reducing dose overall for abdominal and pelvic imaging by concentrating the dose on where its needed and reducing it elsewhere [18,137] and is recommended to be used as standard, where possible, for abdomino-pelvic imaging [138].

- The patients in our clinical cohort are patients with a known and confirmed diagnosis of Crohn's disease. Here, examination for active large and small bowel disease, inflammatory complications and extramural disease are the main focus of investigation. Detection of subtle indeterminate lesions is not the focus of the examination so the tolerated level of low contrast resolution and contrast noise ratio were lower than would be accepted for, say, a patient with a known malignancy. Tolerating lower levels of contrast resolution translates into a significant reduction in radiation dose.

Conclusions:

The results of this study lead to three main conclusions:

1. Significant changes in the imparted radiation dose can be achieved in CT imaging by adjustment of user-selected parameters such as tube voltage, tube current and noise index, when automated tube current modulation is used. Knowledge of the interplay of these parameters and the magnitude of dose reduction achieved per unit change in each is crucial when planning CT protocols.

2. Iterative reconstruction, in both its forms, is uniformly superior to FBP in terms of image noise and image quality indices across a wide variety of imaging protocols in both phantom and cadaveric models. Within the iterative algorithms, MBIR is superior to ASiR for all indices, with MBIR N05 demonstrating the best results in terms of image noise and noise reduction. MBIR NR05 is non-inferior to MBIR RP05 with regard to spatial resolution. The one area where ASiR is superior to MBIR is in terms of speed – reconstructions with ASiR take in the order of a few minutes whereas MBIR reconstruction can take up to 90 minutes, depending of the number of images and the level of image noise. Also, MBIR technology is not currently available for routine clinical use and remains a research tool. ASiR, however, is licensed for clinical use and has, since its introduction, become the standard method of CT data reconstruction for standard dose CT imaging.
3. Despite vendor-specific methods being proprietary, it would appear that ASiR works to a target percentage noise reduction whilst MBIR works to a target residual level of absolute objective noise in the image. Knowledge of the image quality targets of each of these reconstruction algorithms is also of utmost importance in maximizing the dose reductions achievable with protocol development.

This chapter has demonstrated the utility of iterative reconstruction for preserving image quality with reduced dose imaging. It has also yielded an

optimized, refined and appropriate split dose protocol for CT of abdomen and pelvis to use in clinical patients with Crohn's disease in the following chapters.



Chapter 3

A prospective feasibility study of sub-millisievert
abdominopelvic CT using adaptive statistical iterative
reconstruction in Crohn's disease

Iterative Reconstruction as a Novel Method of Radiation Dose Reduction
at Computed Tomography in Patients with Crohn's Disease

Introduction:

This chapter will begin with a brief description of Crohn's disease and its manifestations, focusing particularly on the role of imaging and the risk for high levels of cumulative radiation exposure in this population.

Crohn's disease

Crohn's disease is an inflammatory condition of unknown aetiology that can affect any portion of the gastrointestinal tract from the mouth to the perianal area. This condition was first described by Crohn, Ginzburg and Oppenheimer in 1932 but it was not clinically, histologically or radiographically distinguished from ulcerative colitis until 1959 [139-140]. Untreated, Crohn's disease is characterised by transmural inflammation that produces mucosal as well as deep ulceration, wall thickening, both reversible inflammatory and irreversible fibrotic strictures, and a tendency toward the formation of abscesses and fistulae. The classical involvement of discontinuous segments of intestine (thus, skip lesions) helps differentiate Crohn's disease from ulcerative colitis. Histologically, non-necrotising granulomata composed of epithelioid histiocytes are the signature of Crohn's disease.

Crohn's disease is more common in white individuals living in Western industrial nations and the prevalence ranges from 0.7 to 56 cases per 100,000 persons [141]. The incidence and prevalence of Crohn's disease are steadily increasing. Although the condition can occur at any age, there are 2 peaks of incidence – the first in early adulthood (range, teens-20s) and the second in the 60-70 year age group [141]. Males and females are affected, but there is a slight female

predilection for the disease. The diagnosis of Crohn's disease is based on a combination of typical clinical, radiologic and pathological features.

Crohn's disease is a chronic disease with periods of active inflammation and remission. There are four broad stages of the disease that can be classified by the preponderance of findings: active inflammation, fibrostenotic stage, fistulising/perforating stage, and reparative/regenerative stage. These stages may coexist at the same time in an individual patient and not every patient will experience all stages of disease.

There is a spectrum of clinical presentations as a result of the variability of organ distribution. Crohn's disease can occur at any point along the gastrointestinal tract; it most commonly involves the small bowel and less commonly the colon or stomach. The transmural nature of the gastrointestinal involvement results in both intra and extraluminal manifestations and complications. Presenting symptoms include abdominal pain and diarrhoea, and disease may be complicated by intestinal fistulas, intramural abscesses, and bowel obstruction. Extraintestinal manifestations are common and include ocular manifestations (uveitis, recurrent iritis, and episcleritis), dermal manifestations (erythema nodosum, pyoderma gangrenosum, and Sweet syndrome), primary sclerosing cholangitis and inflammatory seronegative arthropathies.

Crohn's disease confers an increased risk of small bowel adenocarcinoma and lymphoma. Factors associated with increased cancer risk include early age of onset, greater than 10 years of active disease, male gender, fistulous disease,

surgically bypassed loops, and the use of monoclonal antibody therapy [141]. With potential for cancer symptoms to be misinterpreted as Crohn's disease symptomatology, cancer diagnosis is often delayed.

In recent decades, the use of diagnostic imaging in the investigation and management of patients with Crohn's disease has expanded. Imaging now plays a vital role in aiding and expediting the initial diagnosis of Crohn's disease and computed tomography is often the first dedicated investigation in patients who present with a suggestive symptom complex, avoiding the need for endoscopy to be performed in the setting of active bowel inflammation. In patients with an established diagnosis of Crohn's disease, imaging is used to quantify the disease burden and extent and characterise visceral involvement [13,142-143]. Imaging has further roles to play in the detection of both luminal and extraluminal complications of Crohn's disease and in the assessment of the response to treatment.

CT is a valuable modality in assessment of patients with Crohn's disease. This widely available imaging modality has a high sensitivity and specificity for detection of luminal and extraluminal disease and complications [144] yielding images with high temporal and spatial resolution, with a short acquisition time compared to conventional enterography and MRI [145]. The indications for CT scanning in Crohn's disease continue to expand with improvements in CT hardware and software, as well as with refinements in CT technique such as CT enterography [143]. Indeed, the most significant change to the imaging pathway

for patients with Crohn's disease between the 2006 and 2010 European consensus statements is the increased prominence of CT enterography.

Radiation dose in Crohn's disease:

Unfortunately, the increased exposure to ionising radiation of patients with Crohn's disease, largely as a consequence of the wider use of CT scanning, has become a significant cause for concern, attracting much interest in scientific and media publications [13,146].

As stated previously, patients with Crohn's disease often require diagnostic imaging with CT, be it at time of initial diagnosis, for monitoring of therapeutic response, or in the setting of peri-operative evaluation [13, 142-143]. The epidemiology and pathophysiology of Crohn's disease often mean an early age at diagnosis and an, often, protracted course of active disease. These patients can be subject to serial imaging over prolonged periods of follow-up with, sometimes, decades of active disease, thus incurring a substantial burden of cumulative exposure to ionising radiation. In many cases, patients who are diagnosed with Crohn's disease as children or young adults are likely to receive high lifetime cumulative radiation exposures [7,8,13]. From a CT examination, a child will receive greater organ doses than an adult. This is compounded by the heightened radiosensitivity of organs in children due to the increased vulnerability of rapidly dividing cells [7,9]. The increased susceptibility to the effects of radiation are also in part due to a longer post irradiation life

expectancy for children providing an interval for long lead times of neoplastic disease.

The risks associated with high cumulative exposures to medical ionising radiation have been discussed in detail in chapter 1. With the shift from the linear no threshold model extrapolated from atomic bomb survivors to Pearce's landmark paper which established the causal link between medical radiation and cancer, how we look at radiation dose in medical imaging has changed [9]. Protracted exposure to low-level ionising radiation, including that for diagnostic use, could potentially be implicated in the induction of malignancies [7-8]. It has been estimated that, each year in the United States, diagnostic imaging results in 5500 deaths due to radiation-induced cancers [6,147]. Crohn's disease predisposes to an increased lifetime risk of developing small bowel lymphoma and other intestinal malignancies. This existing risk is compounded in patients with more severe disease and by the use of immunomodulatory drugs (6-mercaptopurine, azathioprine or methotrexate) for disease management. The potential synergistic carcinogenic effects of significant cumulative radiation exposures resultant from diagnostic imaging are of particular concern in these patients [148-149].

A large 15-year retrospective review by our research group of all abdominal imaging in a cohort of patients with Crohn's disease attending a tertiary referral centre for the condition (Cork University Hospital) was performed in 2008 by Desmond et al [13]. This study reported subgroups of patients with Crohn's disease who were 'at risk' for increased exposures to ionizing radiation as a

consequence of diagnostic imaging. The subgroups who were at greater risk of high cumulative radiation exposure included patients in whom the diagnosis of Crohn's disease was made at less than 17 years of age, those with more severe disease, particularly those requiring treatment with steroids or infliximab, and those patients who required surgical intervention for disease/complication management [13]. A trend toward increased average cumulative effective dosages per patient during the period of follow-up was reported, from 7.9mSv in the initial 5-year period to 25mSv in the final 5-year period [13]. This escalation was mainly attributed to increased use of CT, without a corresponding drop in the use of plain radiographs of abdomen. Though CT scans comprised just 19.7% of the imaging studies performed during this period, they accounted for 84.7% of the diagnostic radiation exposure [13]. A cumulative effective radiation dose in excess of 75mSv, the effective dose equivalent of 3,750 standard chest radiographs, was noted in almost 16% of patients [13, 150].

Cumulative exposure to low-level ionising radiation of this magnitude has previously been estimated to increase mortality due to cancer by 7.3% [6] and certainly, in light of the findings of Pearce et al, such levels of exposure are indeed worrying [9]. Thus care needs to be taken in imaging of all Crohn's disease patients, particularly in those where the initial diagnosis was made as a child. Future CT scans should be limited to situations where there is a definite justified clinical indication, with every scan optimised to provide a diagnostic CT image at the lowest possible radiation dose.

Current optimisation strategies in imaging of Crohn's disease:

Optimisation of radiation dose is not a singular process, rather a combination of multiple strategies. The best way of protecting patients from the potentially detrimental effects of ionising radiation is to limit their exposure to ionising radiation in every available way. This includes: (1) limiting the use of CT scanning to those clinical scenarios where the examination is unequivocally indicated and likely to change patient management; (2) the use, where feasible, of alternative modalities such as ultrasonography and magnetic resonance (MR) imaging which do not result in exposure to ionising radiation; and (3) when CT is indicated, the use of reduced dose CT protocols which utilise all available CT technology developed for radiation dose optimisation ensuring that a diagnostic quality CT study is acquired at the lower possible radiation exposure.

Current work

The preceding chapter investigated the interplay of user-selected parameters on radiation dose and image quality across reconstruction algorithms and culminated in the design of a split dose CT protocol. This chapter forms the basis for those that follow, focusing on the validation of Adaptive Statistical Iterative Reconstruction (ASiR) as a reconstruction algorithm for reduced dose CT raw data to yield diagnostically acceptable images in clinical patients with Crohn's disease. Its suitability as a technique is assessed by examining the diagnostic accuracy and image quality of reduced dose CT using both subjective and objective measures. A conventional dose CT examination acquired contemporaneously is used as the reference standard throughout.

The following hypotheses were tested:

1. ASiR reconstruction of modified dose CT raw data provides images of comparable diagnostic accuracy compared with conventional dose CT for both CT findings related to Crohn's disease and incidental findings.
2. Modified dose CT images with ASiR are acceptable for diagnostic use in terms of subjective image quality indices.
3. ASiR allows tolerable/acceptable levels of image noise and artefact in modified dose CT images.
4. Significant radiation dose savings can be achieved by using ASiR to reconstruct CT raw data.

Methods:

Ethical considerations:

Institutional review board approval was sought and granted for this prospective study. The study was formally registered with the Clinical Trials Registry (clinicaltrials.gov) with the identifier NCT 01244386.

Study population:

Consecutive patients with a known histological diagnosis of Crohn's disease requiring a clinically indicated CT examination of the abdomen and pelvis to assess for suspected activity or acute complications of Crohn's disease between April 2010 and March 2011 were included. Paediatric patients (<16 years old) and those patients without histological confirmation of Crohn's disease were excluded. Also excluded were patients with mild disease without a suspected acute complication and those patients considered clinically unstable. All patients were referred from a specialty tertiary referral outpatient inflammatory bowel disease clinic. Full, informed written consent was obtained from all included patients prior to CT and there were no refusals. Disease severity was assessed using the Harvey-Bradshaw index [151]. The weight (kg) and height (m) of each participant was measured immediately prior to scan using a calibrated digital device (Seca electronic measuring station Model 763, Seca Medical, Hamberg, Germany) and Body Mass Index (BMI) calculated using the formula $\text{weight}/(\text{height})^2$ and with the unit kg/m^2 . Laboratory tests included C-reactive protein (CRP) as standard of care. Patient characteristics are summarised in table 3.1.

Table 3.1. Patient demographics and clinical characteristics

| | | |
|---|---------------------------------|--------------------|
| Sex (n) | Male | 19 |
| | Female | 31 |
| Age (y), median (IQR) | | 34 (26-46) |
| Disease duration (y), mean (SD) | | 12.5 (9.6) |
| Tobacco use (n) | Smokers | 8 |
| | Former smokers | 5 |
| | Non-smokers | 33 |
| BMI, mean (SD) | | 24.6 (4.8) |
| Disease severity (Harvey Bradshaw Index) | Remission | 9 |
| | Mild disease | 16 |
| | Moderate disease | 22 |
| | Severe disease | 0 |
| Medications | Purine analogues | 11 |
| | Biological agents (anti-TNFs) | 11 |
| | Purine analogues and biologics | 2 |
| Steroids | Prednisolone | 2 |
| | Budesonide | 3 |
| No active treatment | | 21 |
| C-reactive protein (mg/L), median (IQR) | | 11.5 (2.5-27.4) |
| Clinical question asked (n) | Disease complication | 37 |
| | Disease extent and distribution | 36 |
| | Other | 3 |

Indication for imaging:

For each patient, the indication for imaging was recorded with a specific clinical question from the referring clinician to be addressed by the CT examination. Categories of question/indication included: (1) confirmation or exclusion of a complication of Crohn's disease such as perforation, abscess, new fistula or stricture; (2) assessment of disease activity and distribution; and (3) suspected non-Crohn's related pathology.

Harvey Bradshaw Index:

The Harvey-Bradshaw Index was devised in 1980 to quantify Crohn's disease activity as a simpler version of the Crohn's Disease Activity Index for data collection purposes [151]. It consists of only clinical parameters. The first three items are scored on the previous day [table 3.2].

Table 3.2: Harvey Bradshaw Index of Crohn's disease activity [151]

| | | |
|--------------------------------------|----------------------|---|
| General well-being | Very well | 0 |
| | Slightly below par | 1 |
| | Poor | 2 |
| | Very poor | 3 |
| | Terrible | 4 |
| Abdominal pain | None | 0 |
| | Mild | 1 |
| | Moderate | 2 |
| | Severe | 3 |
| Number of liquid/soft stools per day | | — |
| Abdominal mass | None | 0 |
| | Dubious | 1 |
| | Definite | 2 |
| | Definite and tender | 3 |
| Complications | None | 0 |
| | Arthralgia | 1 |
| | Uveitis | 1 |
| | Erythema nodosum | 1 |
| | Aphthous ulcers | 1 |
| | Pyoderma gangrenosum | 1 |
| | Anal fissure | 1 |
| | New fistula | 1 |
| | Abscess | 1 |
| Remission | <5 | |
| Mild disease | 5-7 | |
| Moderate disease | 8-16 | |
| Severe disease | >16 | |

Study population size:

The clinical intent of this research was to determine if modified dose CT scanning could be used in place of conventional dose CT without missing any clinically significant lesions in the acute setting. Because this was a comparative assessment of 2 diagnostic strategies performed on the same day with the same CT scanner, whereby each patient acted as his/her own control, rather than an interventional study with a primary end point, the use of a power calculation to determine sample size did not apply. Instead, a precision estimate was performed by a statistical advisor. This relies on factors such as prevalence, overall population size and the desired confidence interval to determine the size of the study population required. Based on these factors, a sample size of 50 patients was deemed appropriate.

CT technique:

CT images were obtained using a General Electric Lightspeed VCT-XTe 64-slice multi-detector CT scanner (GE Healthcare, Milwaukee, USA) following the administration of oral and IV contrast media, unless contraindicated due to known allergy or renal impairment. Patients were fasted for at least 3 hours prior to CT. Oral contrast medium was ingested over the 90 minutes prior to scan to achieve positive contrast in the bowel. This consisted of 1.5 litres of Gastrografin (Bracco Diagnostics Inc., Princeton, USA in solution with water to give a 2% dilution). Non-ionic intravenous contrast medium (iohexol, Omnipaque 300, GE Healthcare, Mississauga, USA) was used with 100ml administered via a power injector (Stellant, Medrad, Warrendale, PA) at a flow rate of 2.5ml/s.

Automatic bolus tracking software (SmartPrep, GE Healthcare, Waukesha, USA) was used to trigger CT initiation at the appropriate time interval following intravenous contrast injection. A circular region of interest (ROI) was placed in the abdominal aorta with serial scanning of this region following contrast injection to monitor for and identify peak arterial vascular enhancement. After a threshold of 100HU was reached within this ROI, the CT data acquisition was manually triggered after an inbuilt 45 second delay to achieve portal venous phase imaging. Scanning was performed on arrested inspiration to minimise motion artefact.

A split radiation dose CT protocol was designed for this study (please see chapter 2). Each patient underwent two separate CT examinations in rapid succession whilst on the CT scanning table. The net radiation dose from the sum of both of these studies was designed to be equivalent to or less than the radiation dose imparted from a standard departmental CT of abdomen and pelvis, proportional to patient size. The conventional dose CT protocol represented the control arm of the study and the modified dose protocol the study arm.

The modified dose CT protocol was designed to administer an effective radiation dose of approximating to 10-20% of the standard departmental CT, aiming for an effective dose in the 1mSv range when possible. A tube voltage of 100kV and a fixed tolerated noise index of 70% were used. A gantry rotation time of 0.5sec was used.

The conventional dose CT protocol was designed to affect a radiation exposure of 80-90% of that of a standard departmental CT of abdomen and pelvis. A tube voltage of 120kV was used with a fixed tolerated noise index of 38%. A gantry rotation time of 0.8sec was used.

An identical scan range was used for both study protocols, planned from the same CT localiser radiographs (antero-posterior and lateral) and extending from the lung bases to the pubic symphysis aligning the isocentre of the patient to that of the CT gantry. For both protocols z-axis Automated Tube Current Modulation (ATCM) was employed to aid dose savings, with resultant variable mA dependent on patient composition and employed minimum and maximum tube current thresholds of 20 and 350mA, respectively. The modified dose CT was acquired first and the conventional dose CT acquired 6.2 seconds later. Data were acquired in 0.625mm slices.

CT image reconstruction:

For clinical purposes, the conventional dose CT data were immediately reconstructed with filtered back projection (FBP) in the manner of standard departmental CT scans. These images were reviewed and reported on as normal by non study-involved radiologists with a report issued to the clinical team to aid diagnosis and management within the usual time frame. The modified dose CT images were for research purposes only and did not contribute to the clinical report issued. For study purposes, the conventional and modified dose CT raw data sets were both reconstructed with ASIR 40%, thus ensuring dose was the only variable under examination for this study.

Image review:

Reconstructed CT data sets were reviewed in a Digital Imaging and Communications in Medicine (DICOM) format on imaging workstations (Advantage Workstation VolumeShare 2, Version 4.4, GE Medical Systems, Milwaukee, USA). Two radiologists, each with 14 years experience, performed image review independently and a radiologist with 1 year of experience recorded the findings. To minimise the effects of recall bias, all datasets were anonymised and studies identified merely by a random four-digit number. Reviewers were aware that the patient had a history of Crohn's disease but blinded to the medical history and clinical query posed. Previous imaging studies were not available for comparison. The reconstruction algorithm used for each reconstructed series was displayed. Images were reviewed in a random patient order with a delay period 5 months instituted between review of modified and conventional dose CT images to minimise recall bias. In all cases, the modified dose CT images were reviewed first. CT data were reconstructed into axial slices of 3mm thickness only and images were reviewed using soft tissue windows (window width, 400HU; window level, 40HU).

Estimation of radiation dose

As recommended by Bankier, in line with current recommendations CT doses for conventional and modified dose CT protocols are reported in terms of volume CT dose index ($CTDI_{vol}$), Dose Length Product (DLP), effective diameter, Size-Specific Dose Estimate (SSDE) and effective dose [100]. The radiation exposures

resultant from the CT scanned projection radiographs were excluded from analysis.

CTDI_{vol}: this parameter is obtained directly from the CT dose report and measured in milligray (mGy). For all CT scans in this study, a 32cm phantom was used for CT scanner calibration.

DLP: this parameter is obtained directly from the CT dose report also. This is the product of scan length and CTDI_{vol} and is measured in milligray.centimetres (mGy.cm). This is also measured in terms of a 32cm phantom for this study.

Effective diameter: the effective diameter of a patient represents the diameter of the patient at a given location along the z-axis of the patient, assuming the patient has a circular cross-section. As some body parts approximate a circle and many do not, the effective diameter is the diameter of a circle whose area is the same as that of the patient cross section. The lateral and antero-posterior skin-to-skin dimensions (D_{LAT} , D_{AP}) of the patient at the mid point of the CT scanned projection radiograph (midslice level) are measured using electronic callipers on the image viewing workstation (see figure 3.1 below). The effective diameter is calculated using the formula: $\sqrt{(D_{LAT} \times D_{AP})}$ and is expressed in centimetres (cm).

SSDE: this is a patient dose estimate that takes into consideration corrections based on the size of the patient, using linear dimensions measured on the patient images (see figure 3.1 below). The effective diameter is compared with reference tables and a specific correction factor is obtained [97]. The SSDE is calculated by

multiplying the $CTDI_{vol}$ by the correction factors as per the American Association of Physicists in Medicine (AAPM) and is expressed in milligray (mGy).

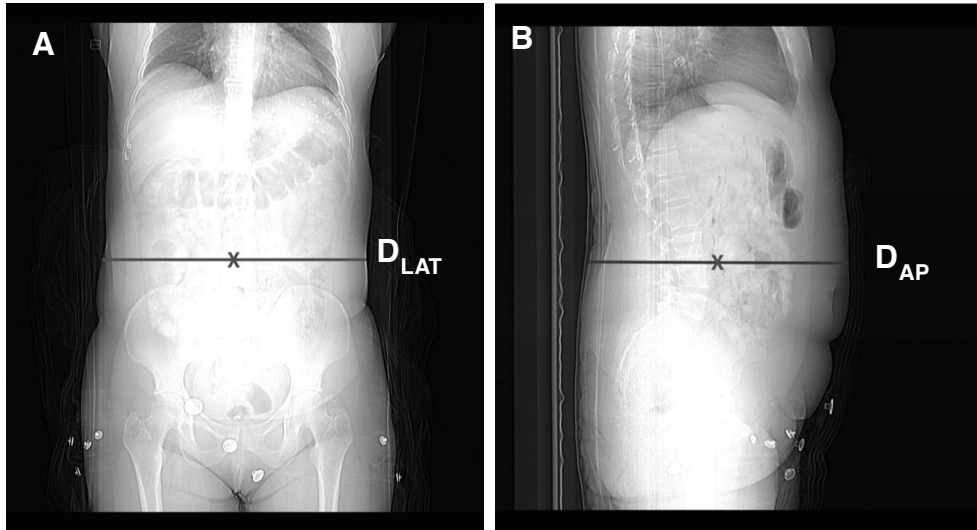


Figure 3.1: Measurement of patient diameters. A-B: measurement of lateral (D_{LAT}) and antero-posterior (D_{AP}) skin-to-skin diameters at the midslice level on the CT localiser images. The X indicates the midpoint of the midslice diameter.

Effective dose: the Imaging Performance and Assessment of CT (ImPACT, version 0.99x, ImPACT Group, London, England) calculator was used to calculate effective dose. The following data were entered into the calculator: scanner type, location and range of scanning on a phantom, kilovoltage, mean tube current, gantry rotation time, slice thickness, collimation and pitch. The software then provides an effective dose readout, displayed in millisieverts (mSv). This approach is valid for an adult of 70Kg and is used by many practitioners for estimation of radiation dose [152]. While this method may underestimate the effective dose for those weighing less than 70kg and overestimate it for those weighing greater than 70kg [152], as we were primarily interested in the

percentage dose reduction, we postulated that when dose was over or underestimated, both protocols for that individual would be affected in equal proportion and the percentage dose reduction would therefore be accurate.

CT calibration for dose measurement:

CTDI_{vol} and DLP tolerances were verified using a standard 32cm perspex phantom and a 10cm ionisation chamber with a Victoreen NERO mAx unit (Fluke Biomedical, OH). The 32cm phantom was imaged at tube currents of 40mA and 50mA with a 32cm field of view. Radiation measurements were taken with the pencil chamber inserted at central and peripheral locations. Three measurements at each location were averaged and used to calculate corresponding CTDI values which were subsequently converted to a weighted CTDI. The displayed CTDI values on the CT console were recorded and the percentage error calculated using ionisation chamber measures. Calibration of the CT unit was performed once per week in accordance with the manufacturer's instruction.

Diagnostic accuracy

Diagnostic findings for both the modified and conventional dose CT protocols were assessed separately. The presence and nature of previous surgery was documented. Crohn's disease related findings such as the presence, extent, severity and complications of active inflammation and/or strictures of the small and large intestine were recorded. Changes in the peri-enteric tissues substantiating the presence of active inflammation or indicative of transmural disease were also recorded. Extraintestinal manifestations of Crohn's disease and any non-Crohn's disease related findings were also noted.

Crohn's disease activity was graded and scored radiologically according to the presence and severity of morphologic changes in both the large and small bowel, changes suggestive of active inflammation and penetrating disease, and the present or absence of acute complications such as acute obstruction, ileus or visceral perforation [table 3.3]. This is a modified version of a scoring system grading severity of radiological Crohn's disease activity that has been validated by our research group [153] and is a summation of the presence and severity of findings in the small bowel, large bowel, mesentery and peri-enteric/peri-colonic tissues. In addition, a designation of A+ or A- was assigned to patients with or without acute complications (obstruction, ileus, perforation), respectively. Utilising this Crohn's disease activity score, disease severity was categorised into grade 0 (0/12), grade I (1-4/12), grade II (5-8) and grade III (9-12/12).

Table 3.3: Crohn's disease activity score [153]

| | | |
|---------------------|---|----|
| Small bowel disease | Normal small bowel | 0 |
| | Wall thickening >3mm | 1 |
| | Stricture(s) without obstruction | 2 |
| | Stricture(s) with obstruction | 3 |
| Large bowel disease | Normal large bowel | 0 |
| | Wall thickening >3mm | 1 |
| | Stricture(s) without obstruction | 2 |
| | Stricture(s) with obstruction | 3 |
| Inflammation | No inflammatory change | 0 |
| | Mesenteric hypervascularity | +1 |
| | Mesenteric fat stranding | +1 |
| | Mesenteric lymphadenopathy | +1 |
| Penetration | No penetrating disease | 0 |
| | Fistulating disease | 1 |
| | Phlegmon | 2 |
| | Abscess | 3 |
| Acute complications | Acute obstruction, ileus, perforation, etc. | A+ |

Image quality – subjective

Parameters for the assessment of image quality were selected based on previous studies using the European Guidelines on Quality Criteria for CT document [71,102,119]. One senior reader, having used these methods previously [154-156], trained the other reader prior to commencing analysis using a training set of five standard CTs. Anatomical sites for measurement of image quality indices were chosen to be reproducible and comparable for assessment across reconstructed series. Image quality was assessed in terms of diagnostic acceptability, subjective image noise, presence and severity of streak artefact and contrast resolution.

Diagnostic acceptability was assessed by means of a 5-point visual grading scale with 1 = unacceptable, 2 = barely acceptable, 3 = adequate, 4 = more than adequate, 5 = excellent. Five different structures were assessed subjectively with this method: the solid organs, large bowel, small bowel, peri-colonic fat and peri-enteric fat. Superior scores were awarded for clear depiction of these structures with lesser scores when images were degraded from noise or artefacts. The median score from all 5 levels was taken as an overall score of diagnostic acceptability.

Subjective image noise was assessed by means of a 5-point inverse visual grading scale with 5 = unacceptable, 4 = barely acceptable, 3 = adequate, 2 = more than

adequate, 1 = excellent. Assessment was made at 5 anatomical levels (the right hemidiaphragm, the porta hepatis, the right renal hilum, the right iliac crest, the right acetabulum). Images were assessed for graininess or mottle affecting depiction of small anatomic structures such as blood vessels and tissue interfaces. Lesser scores were awarded for a lack of appreciable graininess or mottle with greater scores when graininess interfered with structure depiction.

Streak artefact was scored on a 3-point visual grading scale at the same 5 anatomical levels, with 0 = absent, 1 = present but not interfering with image interpretation, 2 = present and interfering with image interpretation.

Contrast resolution was assessed at three locations (liver, spleen, buttock musculature) on a 5-point visual grading scale with 1 = unacceptable, 2 = barely acceptable, 3 = adequate, 4 = more than adequate, 5 = excellent. The depiction of contrast between the abdominal soft tissues was rated with superior scores awarded for clear fat planes and crisp organ margins and lesser scores when these structures were less well visualised.

Image quality – objective

Spherical regions of interest (ROI) of standard size (diameter, 10mm; volume, 519mm³) were drawn in 5 individual anatomical regions: liver parenchyma at the right hemi-diaphragm, liver parenchyma at the porta hepatis, erector spinae at the right renal hilum, psoas at the iliac crest, and gluteus maximus at the roof of the acetabulum. In each structure, the ROI were placed in as homogeneous an area of tissue as possible (away from blood vessels, fat planes etc.) so that the

attenuation value within was representative of the underlying tissue. Objective CT noise was measured as the standard deviation of the pixel values within these ROIs. The signal to noise ratio (SNR) within each ROI was calculated by dividing the mean attenuation value by its standard deviation.

Statistical analysis

Data compilation and statistical analyses were performed using Microsoft Excel (Microsoft Corporation, Redmond, WA) and GraphPad Prism version 6.0 (GraphPad Software Incorporated, San Diego, CA). Descriptive statistics are provided in terms of means with standard deviations and medians with interquartile ranges (IQR) for parametric and non-parametric values. Variables were compared with paired t-tests and repeated measures ANOVA (with Tukey's and Dunnett's multiple comparison tests if ANOVA showed a significant difference) if parametric. If non-parametric, Wilcoxon matched pairs tests and Friedman tests (with Dunn's multiple comparison test) were used. Pearson and Spearman correlations were used for parametric and non-parametric variables, respectively. For cases where testing for inter-observer concordance was required, the Cohen's κ test was used. The criterion for significance was taken as $P < 0.05$.

Results:

Radiation dose

For all four of the dose parameters measured (CTDI_{vol}, DLP, SSDE and effective dose), the mean dose was significantly lower for the modified dose protocol than for the conventional dose acquisition ($P < 0.0001$ for all comparisons). Depending on the dose metric used, the mean reduction in dose with the modified dose protocol was 67.6-73.5%. The effective dose of the conventional dose CT acquisitions ranged from 2-17mSv, with a mean of 4.8mSv whereas the mean dose for the modified dose protocol was 1.3mSv with a range of 0.46-4.7mSv. These findings are summarised in table 3.4.

Table 3.4: A summary of radiation dose from modified and conventional dose CT protocols and the absolute and percentage dose reductions achieved

| | Conventional dose | Modified dose | Absolute reduction | % Reduction |
|---------------------------|-------------------|---------------|--------------------|-------------|
| CTDI _{vol} (mGy) | 6.26±3.83 | 2.03±1.35 | 4.23 | 67.6% |
| DLP (mGy.cm) | 299.42±196.06 | 87.53±60.98 | 211.89 | 70.8% |
| Effective diameter (cm) | 27.79±4.12 | 27.79±4.12 | - | - |
| SSDE (mGy) | 7.81±3.08 | 2.51±1.12 | 5.3 | 67.8% |
| Effective dose (mSv) | 4.77±3.23 | 1.26±0.9 | 3.51 | 73.5% |

Data are presented as means with standard deviations

$P < 0.0001$ for all comparisons

Patient body mass index had a bearing on incurred radiation dose. BMI correlates very strongly with all four of the measured dose metrics for both modified and conventional dose protocols with Pearson correlation coefficients of between 0.84-0.87 ($P < 0.0001$). BMI also correlated strongly with effective diameter (Pearson coefficient 0.88, $P < 0.0001$). Effective diameter demonstrated

a very strong correlation with each dose metric with Pearson correlation coefficients of between 0.87-0.9 ($P<0.0001$).

The mean radiation doses for patients with a BMI $<25 \text{ kg/m}^2$ ($n=32$) and a BMI $\geq 25 \text{ kg/m}^2$ ($n=18$) are summarised in table 3.5 and figure 3.2 below. There were statistically significant differences in the percentage dose reduction in terms of CTDI and DLP achieved between BMI groups with less dose reduction observed in the BMI $\geq 25 \text{ kg/m}^2$ group but the maximum mean difference was 2.2%, which is unlikely to be of clinical significance. There was no statistically significant difference observed in the percentage effective dose reduction between the two BMI groups ($P=0.4023$).

Table 3.5: A summary of radiation dose from modified and conventional dose CT protocols for patients categorised by BMI $<25 \text{ kg/m}^2$ or BMI $\geq 25 \text{ kg/m}^2$

| | Conventional dose | | Modified dose | |
|---------------------------|--------------------|---------------------|-------------------|--------------------|
| | BMI < 25 | BMI ≥ 25 | BMI < 25 | BMI ≥ 25 |
| CTDI _{vol} (mGy) | 4.33 \pm 0.83 | 9.68 \pm 4.65 | 1.36 \pm 0.35 | 3.22 \pm 1.64 |
| DLP (mGy.cm) | 202.36 \pm 41.27 | 471.96 \pm 241.73 | 57.65 \pm 15.35 | 140.65 \pm 74.98 |
| Effective diameter (cm) | 25.58 \pm 2.49 | 31.7 \pm 3.51 | 25.58 \pm 2.49 | 31.7 \pm 3.51 |
| SSDE (mGy) | 6.22 \pm 0.75 | 10.64 \pm 3.61 | 1.94 \pm 0.36 | 3.54 \pm 1.29 |
| Effective dose (mSv) | 3.18 \pm 0.62 | 7.59 \pm 1.64 | 0.82 \pm 0.23 | 2.03 \pm 1.13 |

Data are presented as means with standard deviations
 $P<0.0001$ for all comparisons

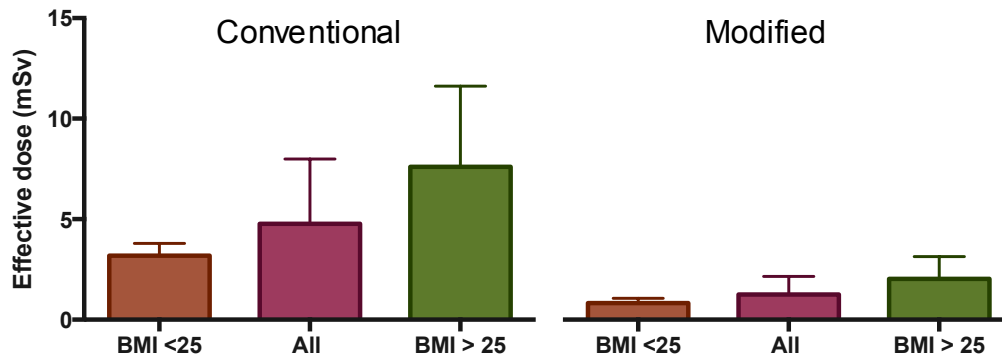


Figure 3.2: Column bar graph summarising the effective doses overall and for the BMI subgroups with both conventional and modified dose CT protocols. The box represents the mean dose and the whiskers the standard deviation. The mean radiation doses are significantly less with the modified dose protocol when compared with the conventional dose protocol, both overall and for both BMI subgroups.

Diagnostic accuracy:

Diagnostic accuracy was quantified in terms of the Crohn's disease and non-Crohn's disease related findings demonstrated on CT with the conventional dose acquisition acting as the reference standard. Inter-observer agreement between the two readers was excellent when findings on the conventional and modified dose CT acquisitions were compared with kappa (κ) values of 0.815 and 0.929 respectively ($P < 0.001$ for both). Lesions detected on the conventional dose images reconstructed with ASiR 40% (reference) were as follows (table 3.6):

Table 3.6: Lesions detected on conventional dose CT

| | CT lesion | Number (n) |
|-----------------------------|--|------------|
| Crohn's disease related | Bowel strictures | 16 |
| | Fistulae | 4 |
| | Abscesses | 4 |
| | Localised bowel perforations | 3 |
| | Inflammatory masses | 1 |
| Non-Crohn's disease related | Cervical tumour | 1 |
| | Focal liver lesions | 2 |
| | Hepatic steatosis | 3 |
| | Cholelithiasis | 1 |
| | Porcelain gallbladder | 1 |
| | Low-density pancreatic lesion | 1 |
| | Duodenal diverticula | 2 |
| | Renal cysts | 7 |
| | Renal calculi | 1 |
| | Abdominal wall herniae | 2 |
| | Inguinal lymphadenopathy | 3 |
| | Ovarian cysts | 7 |
| | Fibroid uterus | 1 |
| | Perforated intrauterine contraceptive device | 1 |
| | Heterotopic bone formation | 1 |

When diagnostic findings detected on the modified dose CT were compared with the reference conventional dose CT, there was excellent agreement for both readers (MMM – $\kappa=0.813$, $p<0.001$; MFR – $\kappa=0.858$, $p<0.001$). The following diagnostic discrepancies were found: two patients had a stricture described on the conventional CT but bowel thickening without stricture was described on the modified dose CT. In one patient, a stricture described as obstructing on the conventional images was described as non-obstructing on the modified dose images. In three further patients, considered to have uncomplicated bowel wall

thickening on the conventional CT images, the presence of a non-obstructing stricture was recorded on the modified dose CT images. Overall, the sensitivity for stricture detection was 87.5% and the specificity for strictures was 91.97% for the modified dose CT with ASiR, with a positive predictive value of 82.3%. There were no discrepancies between the major findings of fistulae, abscesses or acute perforations, with both sensitivities and specificities of 100% for the modified dose protocol with ASiR each of these findings.

Figures 3.3-3.7 below demonstrate both modified and conventional dose CT images of Crohn's disease related findings. An incidental case of cervical cancer is also demonstrated in figure 3.8.

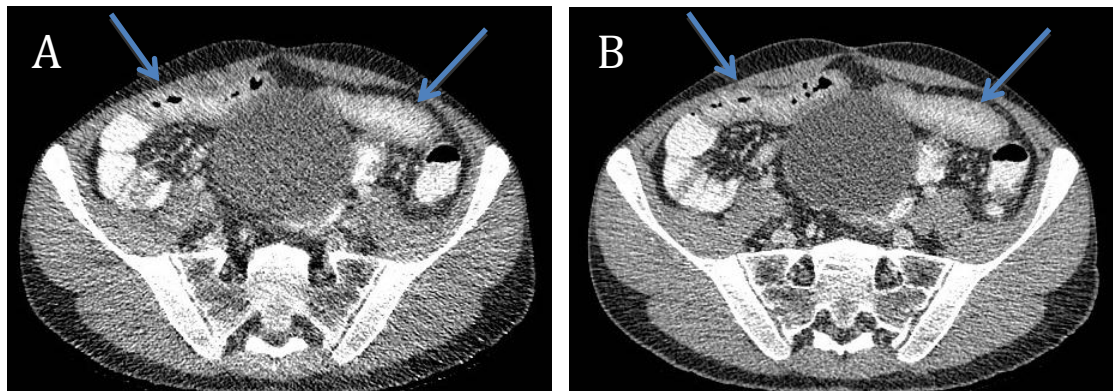


Figure 3.3: Modified (A) and conventional (B) dose axial CT reconstructions of the abdomen and pelvis of a 34 year old man with a BMI of 19.9kg/m² demonstrating small bowel thickening with adjacent mesenteric fat stranding and hypervascularity indicative of acute enteritis (blue arrows). The modified dose CT was acquired with an effective dose of 0.62mSv with the conventional at 2.6mSv.

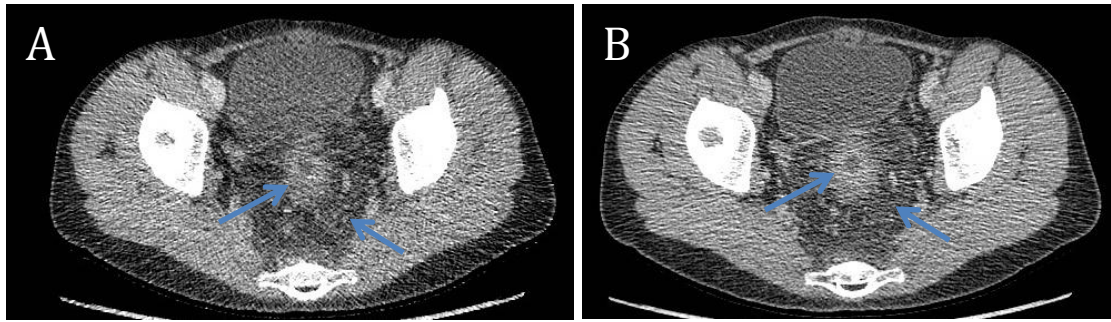


Figure 3.4: Modified (A) and conventional (B) dose axial CT reconstructions of the abdomen and pelvis of a 17 year old man with a BMI of 17.4kg/m^2 demonstrating rectal wall thickening thickening with adjacent peri-rectal fat stranding and hypervascularity indicative of acute proctitis (blue arrows). The modified dose CT was acquired with an effective dose of 0.48mSv with the conventional at 2.5mSv .

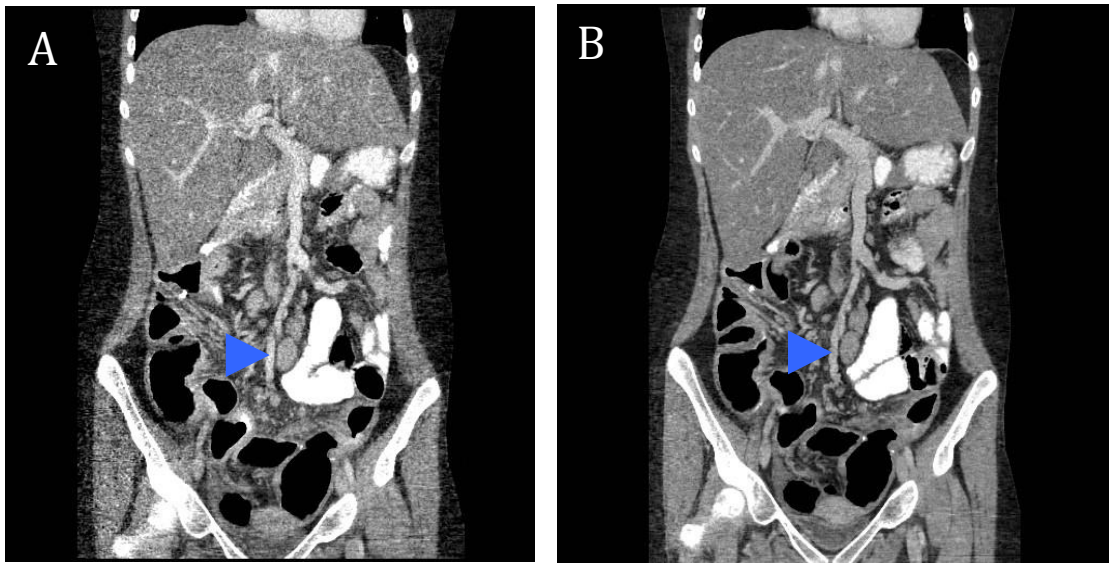


Figure 3.5: Modified (A) and conventional (B) dose coronal CT reconstructions of the abdomen and pelvis of a 20 year old woman with a BMI of 21.2kg/m^2 depicting bulky lymphadenopathy in the small bowel mesentery (blue arrow heads). The modified dose CT was acquired with an effective dose of 0.69mSv with the conventional at 3.1mSv .

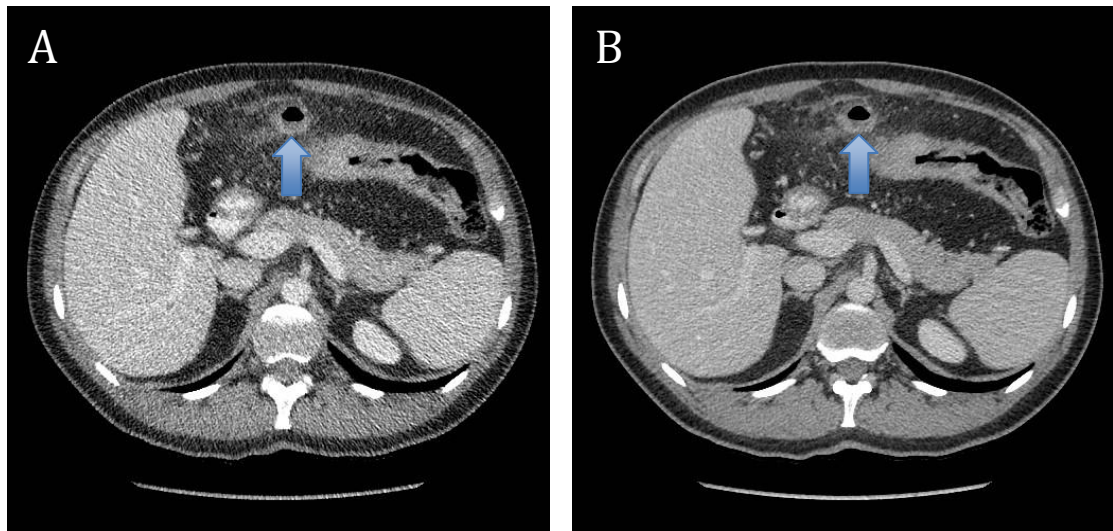


Figure 3.6: Modified (A) and conventional (B) dose axial CT reconstructions of the upper abdomen with blue arrows demonstrating a pericolic abscess in a 46-year old man with a BMI of 26.8kg/m². The effective doses of the modified and conventional dose acquisitions are 1.5mSv and 5mSv, respectively.

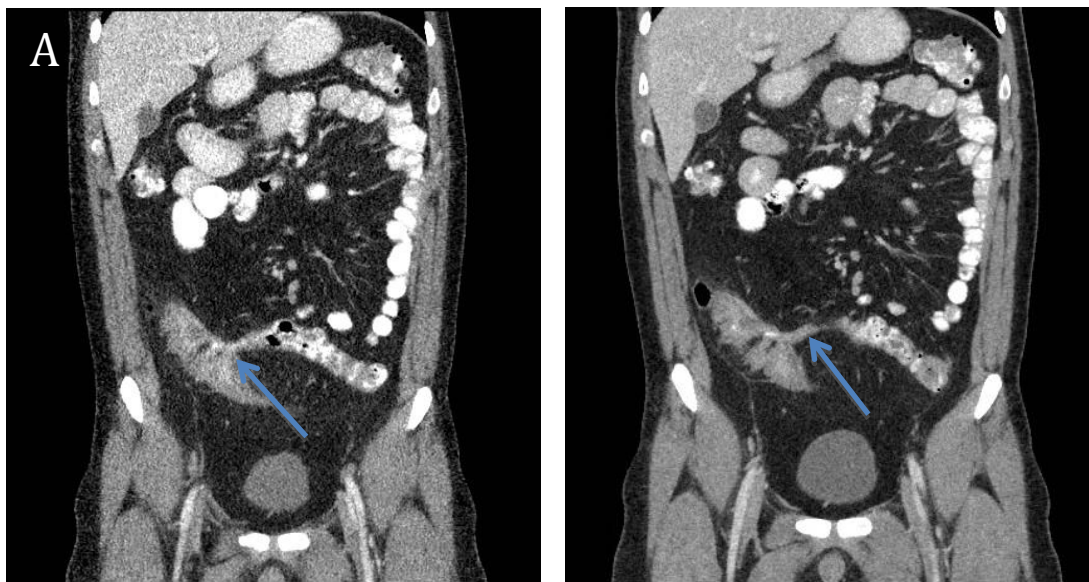


Figure 3.7: Modified (A) and conventional (B) dose coronal CT reconstructions of the abdomen and pelvis with blue arrows demonstrating an enterocolic fistula in a 31 year old man with a BMI of 26.9kg/m². The effective doses of the modified and conventional dose acquisitions are 1.6mSv and 6.5mSv, respectively.

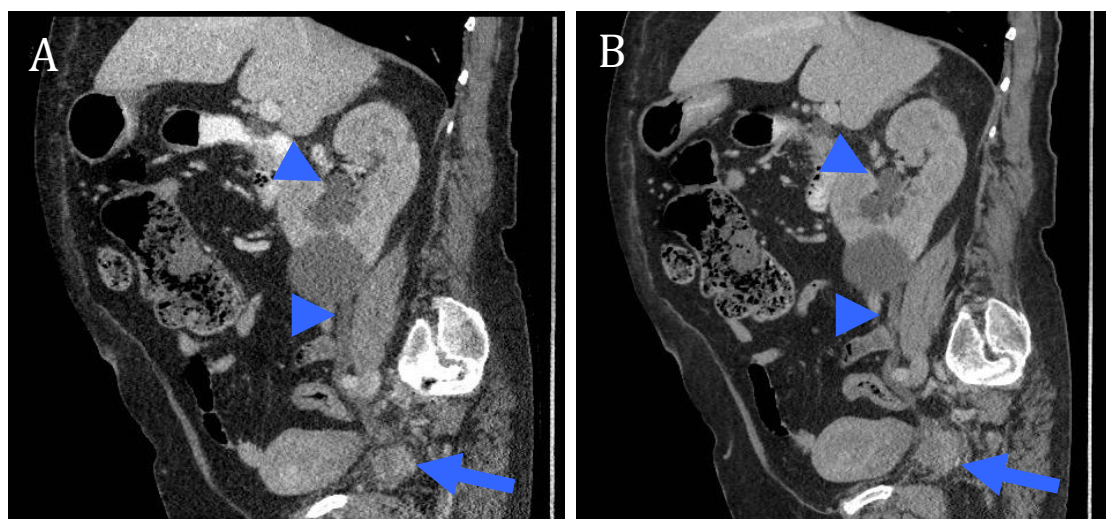


Figure 3.8: Modified (A) and conventional (B) dose sagittal CT reconstructions of the abdomen and pelvis demonstrating a tumour of the cervix (blue arrow) in a 73 year old woman with a BMI of 31.4kg/m². The arrow heads indicate associated hydroureter and hydronephrosis secondary to the tumour. The effective doses of the modified and conventional dose acquisitions are 4.4mSv and 17mSv, respectively.

Incidental findings of two ovarian cysts, one renal cyst and one hepatic cyst were described on the conventional dose CT images but not on the modified dose images. All were sub-centimetre in maximal dimension and benign-appearing, simple cysts. In terms of Royal College of Radiologists (RCR) grading of diagnostic discrepancies, all were felt to be RADPEER 2a – an understandable miss, unlikely to be clinically significant [157]. The sensitivity for incidental findings on modified dose CT with ASiR was 88.2% with a specificity of 100%.

The detection rate of the modified dose CT protocol within this sample for a major complication that would have altered clinical management was 100%. Although the modified dose CT images were not included in the prospective

diagnostic interpretation at time of scanning and did not impact on the clinical management of patients, retrospective evaluation demonstrated that, in all cases, the referring gastroenterologist considered that the modified dose CT report to adequately answer the clinical question posed.

The Crohn's disease activity score was calculated for each study based on the presence of a combination of mural findings and complications of Crohn's disease and the maximum possible score was 12. Both the conventional and modified dose protocols had a median score of 4 ($P=0.0014$) with strong correlation between the two protocols (Spearman coefficient 0.83, $P<0.0001$).

Any differences in Crohn's disease activity scores between protocols were predominantly due to underestimation of secondary inflammatory changes such as fat stranding, mesenteric hypervascularity and mesenteric lymphadenopathy on the modified dose study. For the conventional dose studies, 6 patients were assigned a '+' annotation denoting acute complications compared with 5 patients for the modified dose studies:

Table 3.7: Crohn's disease activity score – acute complications in patients assigned a '+' annotation

| | Conventional dose CT | Modified dose CT |
|---|-------------------------|---------------------|
| Bowel strictures causing obstruction | 2 | 1* |
| Localised bowel perforations with abscess formation | 4 | 4 |

* In one patient, a stricture described as obstructing on the conventional dose CT images was described as non-obstructing on the modified dose CT images.

The clinical score of Crohn's disease activity (Harvey-Bradshaw index) correlated poorly with the radiological Crohn's disease activity score regardless of the protocol used, although this was not statistically significant: MDCT (Spearman coefficient 0.13, $P=0.4$ for modified dose protocol; Spearman coefficient 0.09, $P=0.09$ for conventional dose protocol).

Image quality – subjective

All conventional dose CT images were reported as having above average to excellent contrast resolution and diagnostic acceptability, with minimal or no appreciable subjective image noise when reconstructed with ASIR 40%. Each of these subjective indices of image quality was significantly inferior on the modified dose CT images compared with the conventional dose images ($P<0.0001$).

Diagnostic acceptability findings for the five anatomical structures assessed as well as the overall median score are summarised in figure 3.9 below. With regard to diagnostic acceptability, the most frequent overall rating for conventional dose CT was 5 (excellent) in 43/50 CT scans. The most frequent overall rating for modified dose CT images was 4 (more than adequate) in 24/50 scans. For conventional dose CT, no scan was rated below 4. For the modified dose CT acquisitions, 1/50 was rated as 5 (excellent) and 16/50 and 7/50 scans were rated as 3 (adequate) and 2 (barely adequate), respectively. None were rated as 1 (unacceptable). When individual structures for assessment of diagnostic acceptability were examined, the diagnostic acceptability of the solid organs was deemed suboptimal in 13 patients with scores of 2 (barely acceptable).

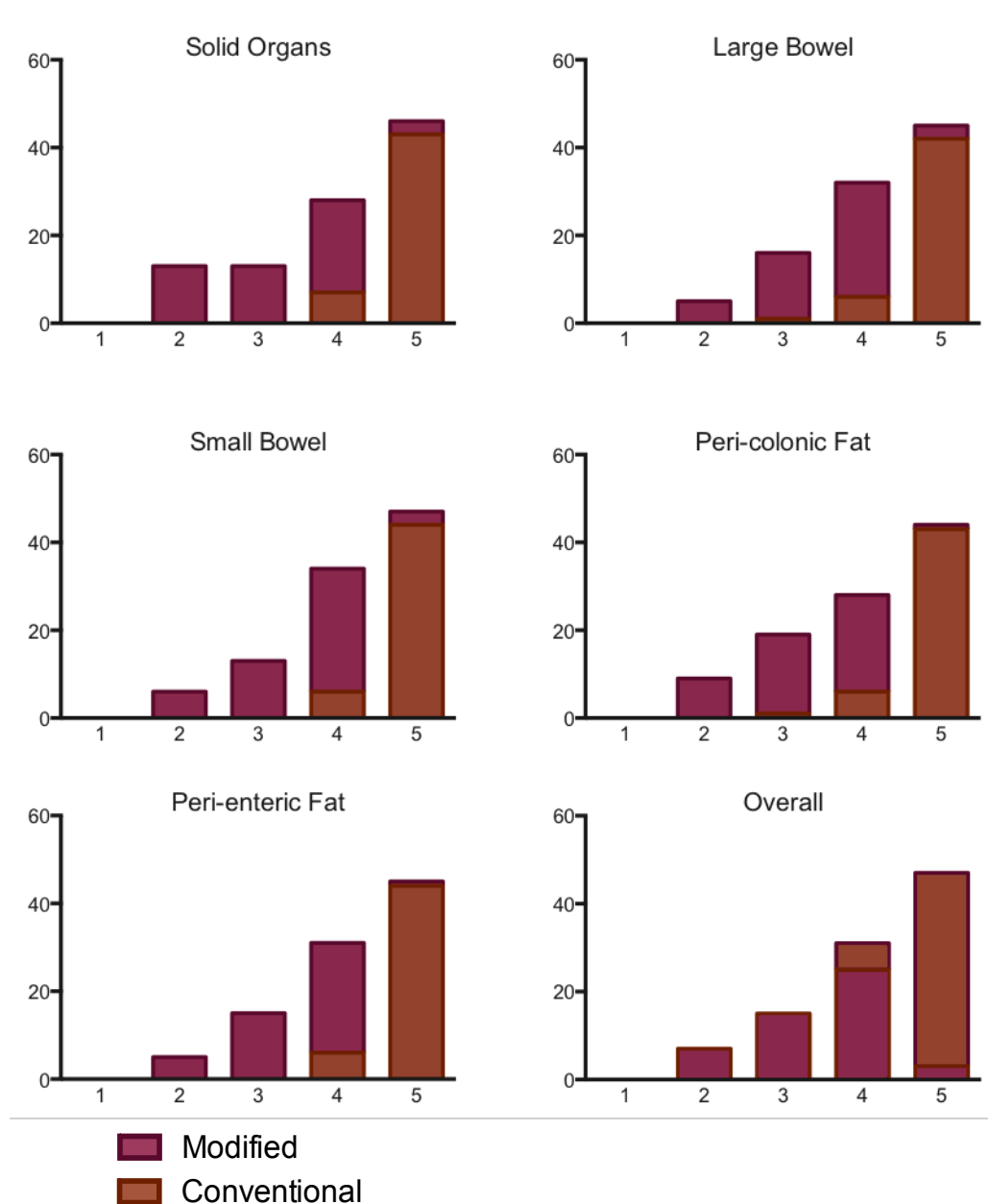


Figure 3.9: Diagnostic acceptability of conventional and modified dose CT images subjectively determined at anatomical structures such as the solid organs, large bowel, small bowel, peri-colonic fat, peri-enteric fat and the median overall value.

Figure 3.10 summarises the distribution and impact of streak artefact for both CT protocols. 49/50 patients had streak artefact present at one or more levels on both modified and conventional dose CT images. Much of this artefact was visualised over the posterior abdominal wall and remote from the bowel, therefore did not interfere with diagnosis. Streak artefact was worse on the

modified dose images compared with the conventional dose images, particularly at the level of the acetabulum where 6 of the modified and 1 of the conventional dose examinations were rated as 2 (artefact present and interfering with image interpretation).

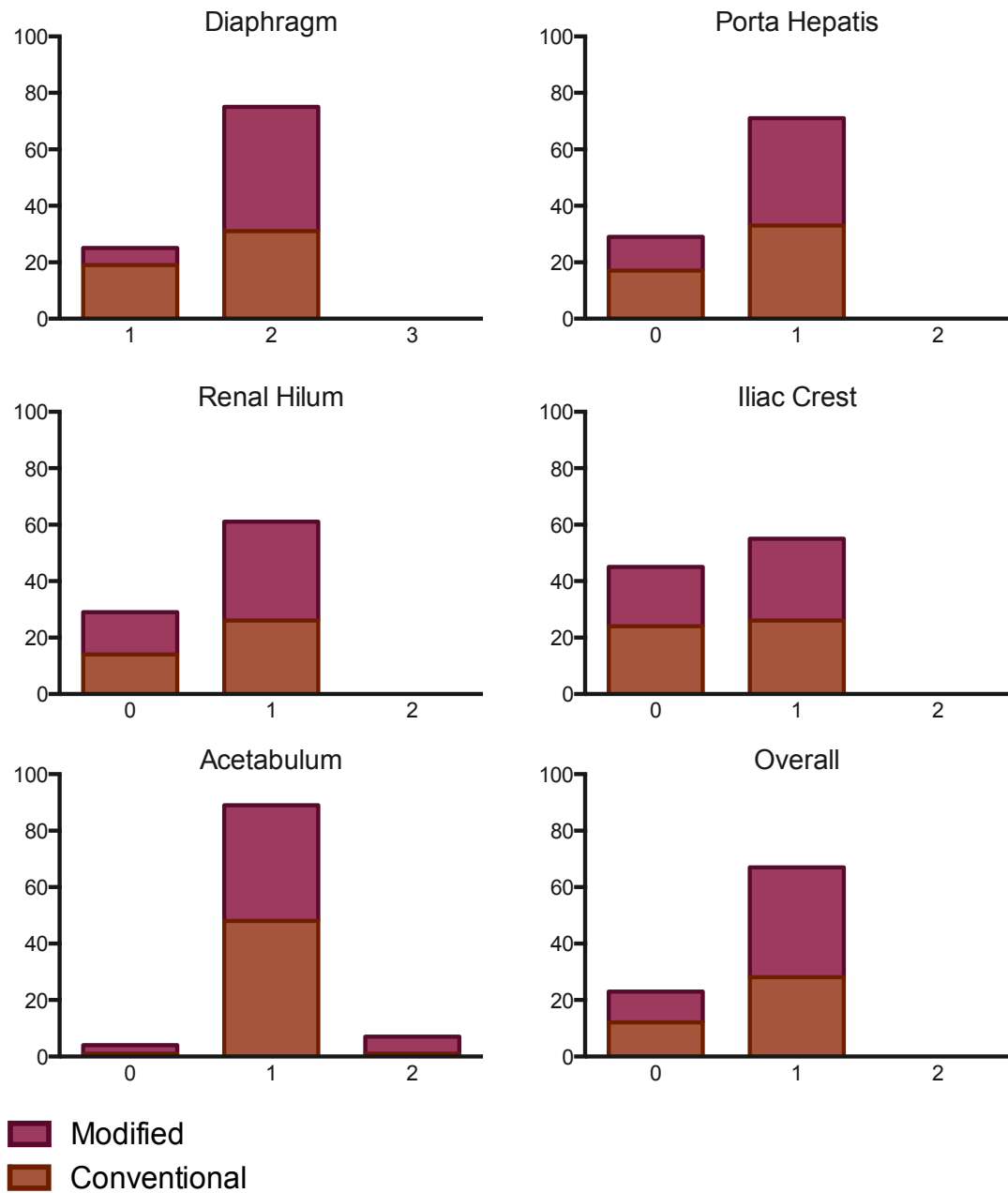


Figure 3.10: Distribution and severity of streak artefact at the level of the diaphragm, porta hepatis, right renal hilum, right iliac crest and right acetabulum. When present, streak artefact can obscure important anatomical and pathological findings if of sufficient severity.

Subjective noise was significantly worse on the modified dose images compared with conventional dose ($p<0.001$) as demonstrated in figure 3.11. However, despite this only 4 patients out of 50 were assigned a subjective noise score of 5 (unacceptable) for one or more anatomical levels. For overall subjective image noise (median of all levels), only 1 patient had a score of 5. Subjective image noise was least at the level of the iliac crest for both modified and conventional protocols.

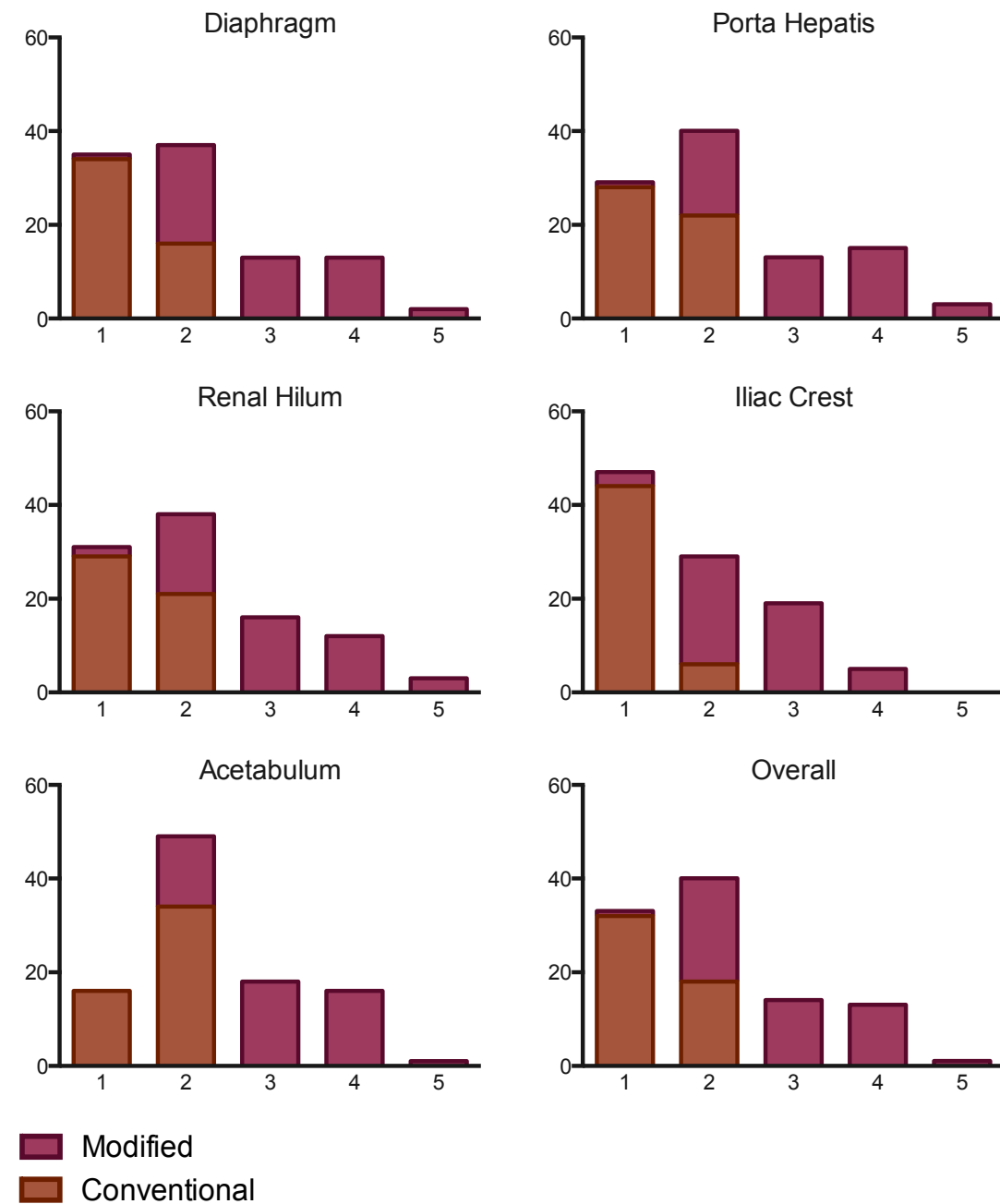


Figure 3.11: Subjective image noise affecting conventional and modified dose CT images subjectively determined at the level of the diaphragm, porta hepatis, right renal hilum, right iliac crest and right acetabulum.

When compared with the conventional dose protocol images, there was inferior contrast resolution on the modified dose acquisitions for all patients, with the images of 9 patients deemed suboptimal for evaluation of the liver and spleen

and of 7 patients deemed suboptimal for evaluation of the gluteal muscles. Findings are summarised in figure 3.12 below.

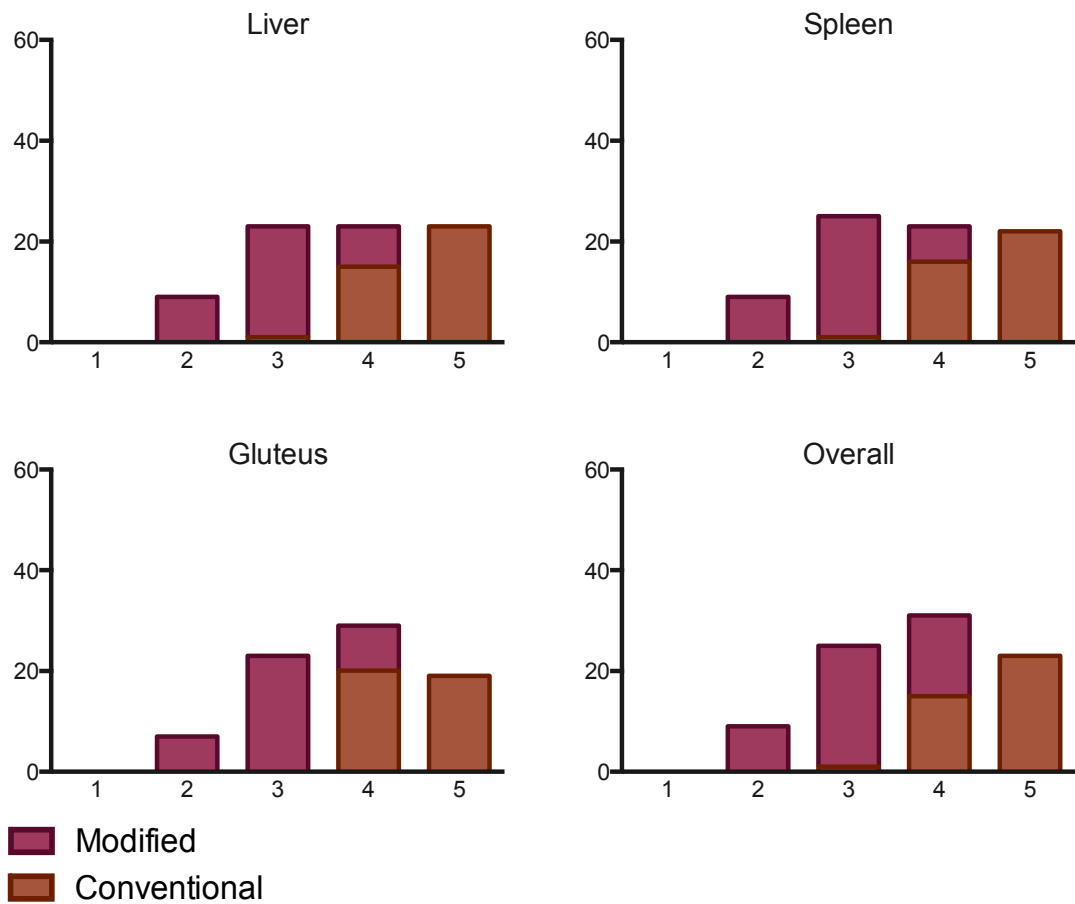


Figure 3.12: Contrast resolution subjectively determined at the levels of the liver, spleen and gluteus musculature on both conventional and modified dose CT images.

Image quality – objective

Overall objective noise was greater for the modified dose CT acquisition than the conventional dose study ($P < 0.0001$, mean absolute difference of 21.42HU). This is demonstrated in figure 3.13 below. At each level, quantitatively measured objective image noise (defined as the standard deviation of the Hounsfield value within a region of interest) was significantly higher for the modified dose versus

the conventional dose CT images ($p < 0.0001$ for all comparisons on paired t-tests) with a mean increase in noise for the modified dose acquisition of 15.14-27.5HU dependent on level – see figure 3.14. The signal to noise ratio, a quantitative measurement of image quality, was significantly higher for studies acquired using the conventional dose protocol (mean SNR 2.74 ± 1.27) than the modified dose protocol (mean SNR 1.69 ± 0.75) overall and at each level ($P < 0.0001$). This is graphically depicted in figure 3.15.

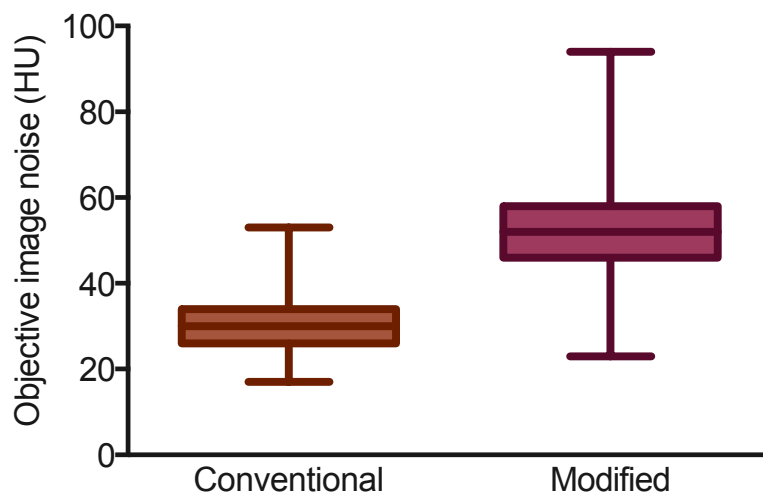


Figure 3.13: Boxplot of the overall objective noise (standard deviation of the measured attenuation in Hounsfield units) for conventional and modified dose CT protocols. The whiskers demonstrate the maximum and minimum measured values for each protocol and line bisecting the box represents the mean.

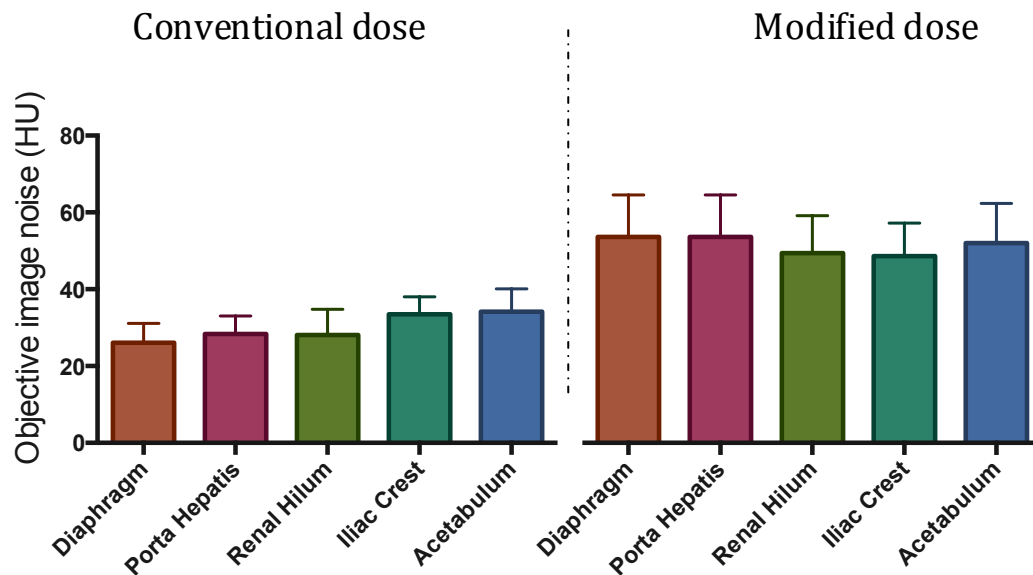


Figure 3.14: Column bar graphs depicting the mean objective noise with standard deviation at 5 distinct anatomical levels for conventional and modified dose CT protocols.

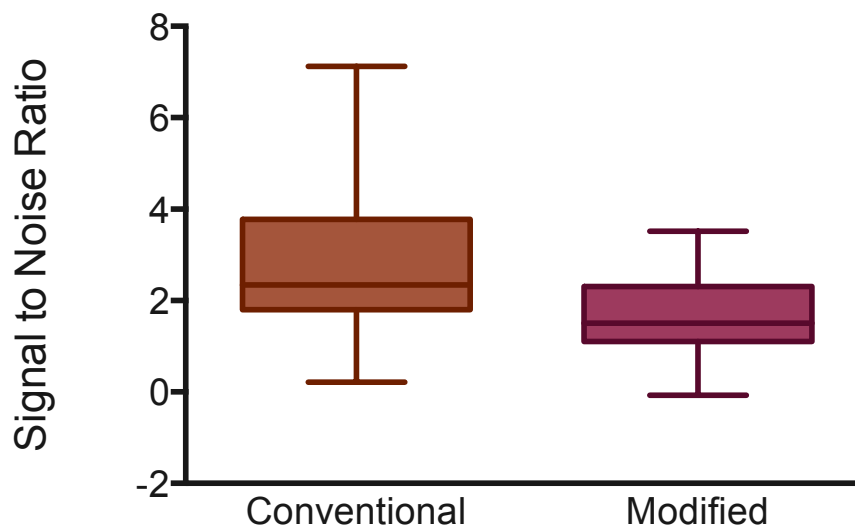


Figure 3.15: Boxplot of the overall signal to noise ratio (mean attenuation in a region of interest divided by its standard deviation) for conventional and modified dose CT protocols. The whiskers demonstrate the maximum and minimum measured values for each protocol and line bisecting the box represents the mean.

Discussion:

Concerns regarding radiation exposure from CT have received considerable attention in the medical literature and news media. We were among the first institutions to intensively study subgroups of patients with Crohn's disease and quantify increasing cumulative radiation exposures from ionising radiation, particularly from CT [13]. A study of 409 patients with Crohn's disease and over 4,000 imaging investigations over a 15 year period also showed that escalating CT use was not associated with reduced reliance on radiography. Further study confirmed that findings at conventional radiography did not affect CT referral practices and, arguably, represented wasted radiation exposure. As part of our response, we developed a modified dose CT technique aimed at imparting radiation doses approximating those of conventional radiography, which could potentially address both issues of dose and unnecessary radiography. The questions we posed were: is sub-millisievert CT possible with iterative reconstruction, and, if so, is it diagnostically valuable?

The current work answered both questions in the affirmative. An important strength of this study is that the modified and conventional dose CT acquisitions were contemporaneous, allowing truly direct comparison of image quality, diagnostic acceptability and diagnostic yield, unlike papers in which conventional and modified CT protocols were chronologically separated [65,70,123-125]. Ethical approval for acquisition of two CT data sets in each patient was justified because the cumulative radiation exposure was less than or equivalent to that of our standard departmental CT of abdomen and pelvis –

mean combined dose of modified and conventional dose protocols = $6.03 \pm 4.12 \text{ mSv}$ versus mean standard of care dose (mean of 3,538 CT of abdomen and pelvis examinations from GE DoseWatch dose-tracking software) = 7.84 mSv . It is also vital that clinically significant findings were not missed on the modified dose series; a split dose technique minimised this chance.

Radiation dose

Overall, modified dose CT resulted in 73.5% ($4.8 \pm 3.2 \text{ mSv}$) radiation dose reduction, with administered doses approaching that of 2 conventional abdominal radiographs. Stratification for BMI demonstrated that diagnostically acceptable images can be acquired in normal or underweight patients ($\text{BMI} < 25 \text{ kg/m}^2$) at a mean effective dose of $0.8 \pm 0.2 \text{ mSv}$, approximating the effective dose of a single abdominal radiograph. While the effective dose for diagnostic imaging with modified dose CT in overweight or obese patients ($\text{BMI} \geq 25 \text{ kg/m}^2$) was $2 \pm 1.1 \text{ mSv}$ (equivalent of 2-3 radiographs), this still represents a 73.3% reduction compared with conventional dose CT. In our experience, suboptimal image quality is often encountered at conventional abdominal radiography in obese patients and additional radiographs (≥ 2 films) are frequently required.

Our standard departmental CT of abdomen and pelvis has an effective dose of 7.84 mSv , which is modest compared with international reference doses. The national average for Ireland is 8.4 mSv and for Europe (average of 36 countries) is 11.3 mSv [31]. The conventional dose data sets in this study were acquired at 80-90% of standard dose. The dose reduction achieved with the modified dose

protocol, therefore, is more accurately calculated against the total radiation exposure (sum of modified and conventional protocol doses), which would equate to a $79.3 \pm 2\%$ overall reduction. Published studies to date, utilising iterative reconstruction for CT of abdomen and pelvis, have yielded maximum dose reductions of 50-56% using phantoms and 50% clinically [70-72,119,158-159].

Diagnostic accuracy

The value of CT in this cohort is demonstrated by detecting, among others, 4 abscesses, an incidental tumour of the cervix and an indeterminate pancreatic lesion. While the number of such lesions was modest, their accurate detection by modified dose CT changed management; furthermore, the accurate exclusion of such lesions in the remaining patients facilitated safe consideration for immunosuppressive therapy. Although subjective and objective measures of image quality were reduced with the modified dose protocol, images were diagnostically acceptable. Previous studies have demonstrated dose reductions of 33% and 50% in unselected patients undergoing abdominopelvic CT and CT colonography, respectively [72,159]. Our mean dose reduction was 73.5% and now approaches that of an abdominal radiograph.

Subjectively, we found that modified dose images reconstructed with ASiR had an impasto appearance, characterised by dough-like image textures quite unlike those of conventional dose. Indices of image quality for modified dose CT were consistently below those of conventional dose which may reflect reviewers' perceptions that images visually 'differed' from those routinely encountered –

recognition bias. This altered image texture was less obvious with the conventional dose CT images, in agreement with other literature examining ASiR [119]. Even though diagnostic acceptability was deemed suboptimal on 7 modified dose studies, diagnostic findings and CDAS remained equivalent to the conventional dose counterpart. Clinically significant findings such as perforations, abscesses, and fistulae were detected on modified dose images despite increased subjective noise and suboptimal contrast resolution.

Stricture assessment was associated with discrepancies. Two strictures were reported on the conventional dose study alone; however three strictures were reported on the modified dose CT alone. These discrepancies reflect that assessment for strictures is a limitation of CT in patients with Crohn's disease, irrespective of dose. CT enterography better depicts mural stratification and allows more confident identification of diseased segments. Sequential or cine imaging with barium or MR enterography allows more accurate differentiation between transient peristalsis and fixed strictures. Peristalsis may explain discrepancies at stricture assessment between modified and conventional dose CT images.

Contrast resolution and diagnostic acceptability were deemed suboptimal in 26% of modified dose studies, which appears to limit solid organ assessment. Reduced detection of sub-centimetre hepatic, renal and ovarian cysts on modified dose images is unlikely to be of major clinical significance in patients with Crohn's disease (RADPEER discrepancy score 2a), who are generally young and lack solid organ involvement [157]. It is our opinion that this is an

acceptable limitation of this modified dose protocol that is justified by substantial reductions in radiation exposure provided modified dose acquisitions do not obscure acute complications of Crohn's disease. Adequate assessment for solid organ pathology requires ultrasound, conventional dose CT or MRI and should be stated by the radiologist reporting the modified dose study.

Limitations

The present study has limitations. Ours was a prospective clinical trial of modified dose CT versus conventional dose CT, both reconstructed with ASiR and performed contemporaneously on the same scanner in patients with active Crohn's disease. It is noteworthy that a clinical trial necessarily introduces artifice. Blending iterative reconstruction with FBP also changes image texture and a gradual transition may be necessary for radiologists to become accustomed to appearances. Altered image texture and increased noise meant that it was almost impossible to randomise the review of modified and conventional dose CT images. To overcome this impossibility of complete blinding because of the obvious difference in appearance of modified versus conventional images and to avoid recall bias regarding diagnostic findings or lesion conspicuity, the modified dose images were reviewed first and the conventional dose images 5 months later. Furthermore, the CT images were interpreted in isolation without bias from previous reports or imaging studies. This created a disadvantage compared with clinical practice for the radiologists reading both types of images, who would normally have access to clinical history, all previous radiological data and participation in a multidisciplinary team

meeting. This may have influenced the high rate of reporting of non-obstructing strictures.

Many authors agree that extraluminal complications are best visualized with CT of abdomen and pelvis with positive oral contrast. Furthermore, routine abdominal CT with positive oral contrast in this setting has compared well with MR enterography in the assessment of inflammatory changes in the bowel wall. The most notable change in the European consensus guidelines on the investigation of Crohn's disease between 2006 and 2010 was the elevation of CT and MR enterography to the investigation with the highest diagnostic accuracy for the detection of intestinal involvement and penetrating lesions in CD [142-143]. Following on from Desmond's paper in 2008 [13], this prospective clinical study was planned and subjects recruited well in advance of the publication of these guidelines, with first CT acquisitions commencing in April 2010. Therefore, we examined CT with positive oral contrast rather than CT enterography as per the older guidelines and our results may not apply beyond the practice of CT with positive oral contrast for the detection of acute extramural complications of Crohn's disease. The 2010 guidelines, however, do indicate the continuing role of CT with positive oral contrast for the detection of acute extramural complications in known Crohn's disease. CT was tailored to detect suspected acute complications of Crohn's disease including bowel wall thickening, obstruction, abscesses and perforation.

In response to the change in recommendations, however, our group did institute and carry out a study of CT enterography using the same study model (i.e. split

dose CT protocol) in patients with Crohn's disease [115]. With CT enterography, the ingestion of large amounts of neutral or negative oral contrast achieves greater luminal distension and improved mucosal enhancement, allowing better detection of mucosal abnormalities than standard CT. However, CT enterography is not without some caveats; the ingestion of a large volume of contrast and that fact that some neutral contrast agents cause diarrhoea means that it is less well tolerated in the acute setting.

At a mean effective dose of 4.77mSv, the conventional dose protocol may be considered low dose in many institutions. If effective doses for standard of care CT far exceed 5mSv in one's institution, this paper likely underestimates the reduction in image quality between conventional and modified dose CT which one could expect, but similarly underestimates the percentage dose reduction achievable.

All patients included in our study belong to a defined subset with a confirmed diagnosis of Crohn's disease and a suspected acute complication requiring CT evaluation. While the modified dose CT protocol would appear appropriate in this population, results should not be loosely extrapolated for de novo diagnosis of Crohn's disease or other gastroenterological pathologies without further study. Furthermore, current iterative reconstruction algorithms are suboptimal for adequate image quality of the solid organs such as the liver at the very low doses at which the modified dose images in the current study were acquired.

Finally, there are 10 possible user-selected strengths of ASiR that can be applied to CT raw data and here we evaluated just one (ASiR 40%) as per vendor recommendation. A complete assessment of the effects of varying the percentage of ASiR on image quality will be provided in chapter 4.

Conclusion:

In conclusion, this study demonstrates that diagnostic sub-millisievert CT of abdomen and pelvis is feasible in patients with Crohn's disease with normal or reduced BMI, i.e. 64% of our cohort. The average effective dose of the modified dose CT protocol was 1.26mSv. This dose is equivalent to just under two abdominal radiographs, yet the resultant images are capable of accurately detecting acute complications of Crohn's disease and quantifying the CDAS, despite reduced subjective and objective indices of image quality. Application of this modified dose CT protocol in other areas of clinical practice will require a tailored approach and careful validation.

We propose that where CT is clinically indicated in the assessment for suspected extraluminal complications of known active Crohn's disease, modified dose CT with iterative reconstruction can be used to substantially reduce radiation dose while accurately addressing the clinical query.



CHAPTER 4:

Determining the optimal strength of adaptive statistical iterative reconstruction to apply to a modified dose CT protocol in patients with Crohn's disease

Introduction:

In chapter 2 we examined the effects of Adaptive Statistical Iterative Reconstruction (ASiR) on a wide variety of CT protocols and developed an optimised split dose CT protocol for clinical imaging of patients with Crohn's disease. In chapter 3 we validated the use of ASiR with this split dose CT protocol, demonstrating that acquisition of diagnostic quality CT images with a 73.5% reduction in radiation dose is possible. Here we aim to determine the optimum strength of ASiR to apply to modified dose CT images acquired using this protocol.

Adaptive statistical iterative reconstruction is a noise-efficient reconstruction algorithm that allows computationally fast reconstruction of raw data while limiting image noise compared with the standard filtered back projection technique [52]. Iterative reconstruction algorithms work as follows. The algorithm begins by hypothesizing the tissue attenuation values – these can be all zeros, random values, or initialized to FBP results. Then, given a particular source location, the algorithm simulates an X-ray beam emanating from the X-ray tube, propagating through the body, and impinging on the detector array. This simulated value is then compared to the actual value obtained by the CT scanner and any discrepancy is used to update the solution to the system of equations of estimated tissue attenuation values. The process repeats until the simulated projections are sufficiently close to the actual projections.

Hybrid reconstruction algorithms use analytical reconstruction (FBP) to create an initial image and iterative algorithms iteratively reduce the noise in the resulting image until specific criteria are reached (such as a sufficiently high signal-to-noise ratio or a nominal reduction in image noise) [52]. As unwanted and unfamiliar image textures may be introduced with iterative reconstruction, the user can 'blend' these two images (simulated and FBP) to produce one that has sufficiently reduced noise, yet retains the desirable textures of conventional reconstructions. The scanner allows the user to select strength of ASiR setting from 0% to 100% in 10% increments. These 'blend levels' provide a varying degree of noise (pixel standard deviation) removal from the images. Selection of 10% ASiR implies that the resulting image will have 10% ASiR blended with 90% FBP and will have higher noise compared to application of ASiR 90% which comprises 90% ASiR blended with just 10% FBP data. These algorithms are designed to reduce artifacts and decrease noise, while preserving the noise power spectrum [160]. Currently, a contribution of 40% by IR is recommended for routine dose CT of abdomen and pelvis. We hypothesise that the ideal strength of ASiR to apply varies with the radiation dose of the CT acquisition as this is inversely related to objective image noise.

The purpose of this study is to determine the strength of ASiR that yields maximally diagnostic images with optimal image quality parameters for this modified dose (sub-millisievert) CT of the abdomen and pelvis.

Methods:

This is a secondary analysis of CT data acquired for the validation of adaptive statistical iterative reconstruction in achieving diagnostic quality CT at markedly reduced radiation doses. Concise methods have been published elsewhere [161-162] and are described in detail in chapter 3.

Briefly, 50 consenting patients, who required a CT of abdomen and pelvis for clinical indications, underwent both conventional dose and modified dose CT of abdomen and pelvis on a 64-slice CT scanner (GE Lightspeed VCT-XTe) as part of an IRB-approved research protocol [ClinicalTrials.gov Identifier NCT 01244386]. The conventional dose protocol comprised CT of abdomen and pelvis acquired at approximately 90% of the radiation dose of the standard departmental CT of abdomen and pelvis protocol (tube voltage 120kV, noise index 38%, gantry rotation time 0.8s). The modified dose protocol comprised CT of abdomen and pelvis acquired at approximately 10% of the radiation dose of standard departmental CT of abdomen and pelvis (tube voltage 100kV, noise index 70%, gantry rotation time 0.5s). All patients were imaged in the portal venous phase of intravenous contrast with the low dose protocol first, followed by the conventional dose protocol 6.2s later. For both protocols z-axis automated tube current modulation resulted in a variable tube current, with minimum and maximum tube current thresholds of 20 and 350mA respectively.

Of these 50 patients, 40 patients had raw data appropriately saved for retrospective reconstruction with adaptive statistical iterative reconstruction. Unfortunately, due to issues with the format in which the CT raw data were

saved to external hard-drives after the acquisition process, the raw data of 10 patients were not in a form suitable for retrospective reconstruction with ASiR. The modified dose image raw data (of 40 patients) were retrospectively reconstructed with filtered back projection (0% ASiR) then with escalating increments of ASiR 10% up to ASiR 100% yielding a total of 11 modified dose series (0%, 10%, 20%, 30%, 40%, 50%, 60%, 70%, 80%, 90%, 100%). The percent of ASiR refers to a blend of that level of iterative reconstruction with the remainder being filtered back projection.

The corresponding conventional dose raw data were reconstructed in standard fashion with FBP and with ASiR 40%. The reconstructed series are summarised in figure 4.1 below.

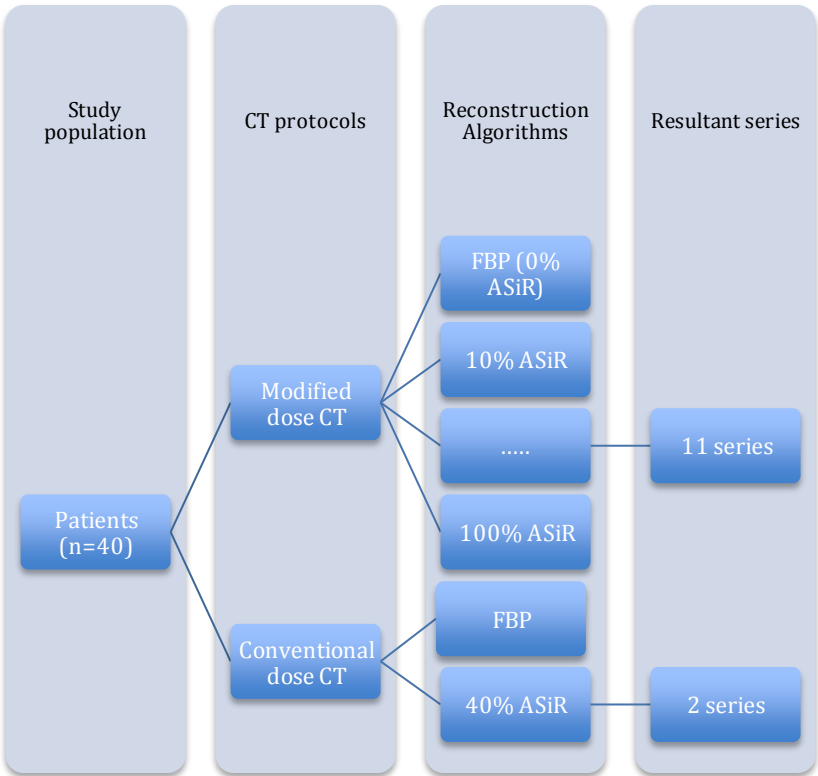


Figure 4.1: Schematic summarizing the reconstructed series yielded from the conventional and modified dose CT raw data. There are a total of 11 modified dose and 2 conventional dose image data sets for comparison.

Image review:

Resultant series were reviewed in a Digital Imaging and Communications in Medicine (DICOM) format on a dedicated workstation (Advantage Workstation VolumeShare 2, Version 4.4, GE Medical Systems, Milwaukee, USA). Blinded data sets were analysed side by side for direct comparison between reconstruction algorithms [see figures 4.2 and 4.3 below]. Datasets were reconstructed to a slice thickness of 3mm in the axial plane and viewed on soft-tissue windows (window width, 400HU; window level, +40HU). Each series was graded by two radiologists in consensus, using previously described and validated qualitative image quality indices. These were the same radiologists as used in chapter 3 as these images are reconstructed from the same CT raw data.

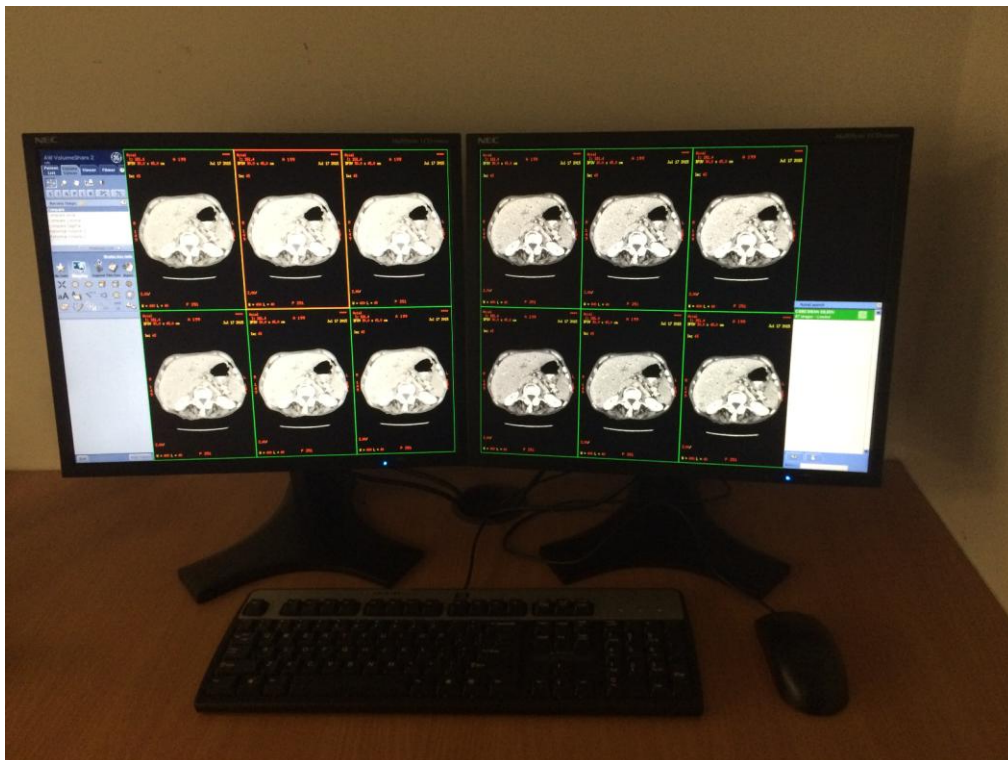


Figure 4.2: Advantage Workstation – an advanced image processing and viewing station used for image review.

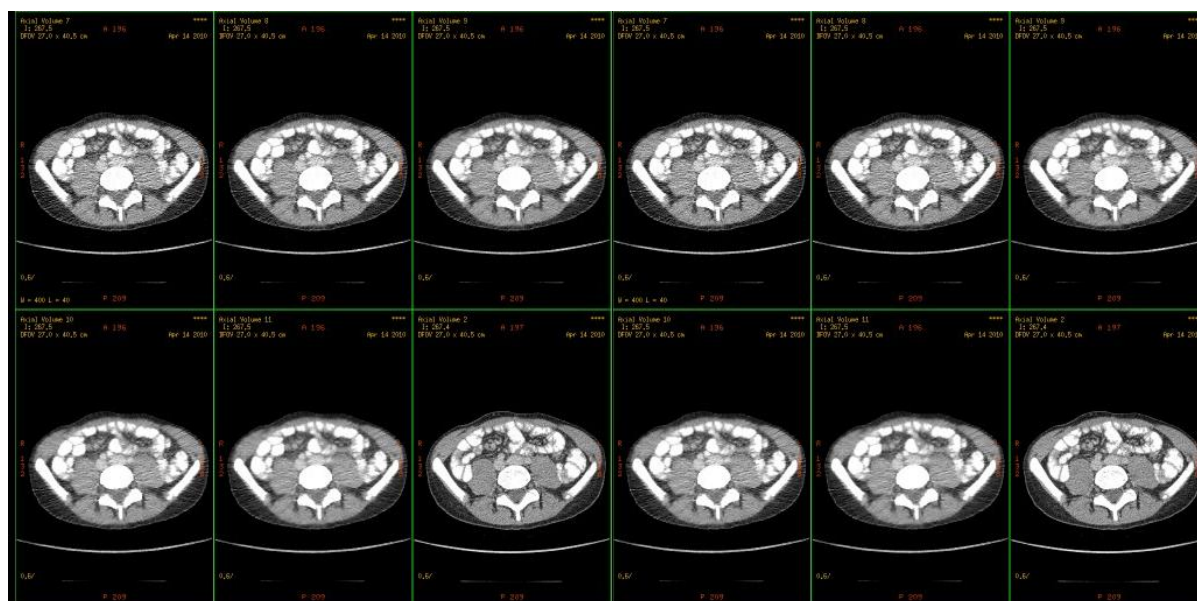


Figure 4.3: Screenshot of the image review set-up on the Advantage Workstation for assessment of image quality indices.

Diagnostic accuracy:

Evaluation for diagnostic accuracy of each reconstructed series was not performed. In chapter 3 we validated the use of ASiR for reconstruction of modified dose CT raw data and demonstrated non-inferiority when compared with conventional dose CT raw data reconstructed with FBP in terms of diagnostic findings. These findings were based on an intermediate percentage of ASiR (i.e. ASiR 40%). It was considered neither practicable nor valuable to subjectively analyse each series for diagnostic findings due to inherent and unavoidable recall bias and the subtly of changes expected between small incremental differences in the ASiR contribution to the hybrid reconstruction algorithm.

Image quality - subjective:

Image quality was assessed in terms of diagnostic acceptability, subjective image noise, the presence of streak artifact, and contrast resolution. The 5-point grading systems described in chapters 2 and 3 were felt too crude for differentiation of subtle image quality variations between the reconstructed series and therefore a more refined 10-point scale was introduced for diagnostic acceptability, subjective image noise and contrast resolution.

Diagnostic acceptability was assessed by means of a 10-point visual grading scale with 1 = unacceptable, 5 = adequate, 10 = excellent. Five different structures were assessed subjectively with this method: the solid organs, large bowel, small bowel, peri-colonic fat and peri-enteric fat. Superior scores were awarded for clear depiction of these structures with lesser scores when images were degraded from noise or artefacts. The median score from all 5 levels was taken as an overall score of diagnostic acceptability.

Subjective image noise was assessed by means of an inverse 10-point visual grading scale with 10 = unacceptable, 5 = adequate, 1 = excellent. Assessment was made at 5 anatomical levels (the right hemidiaphragm, the porta hepatis, the right renal hilum, the right iliac crest, the right acetabulum). Images were assessed for graininess or mottle affecting depiction of small anatomic structures such as blood vessels and tissue interfaces. Lesser scores were awarded for a lack of appreciable graininess or mottle with greater scores when graininess interfered with structure depiction.

Streak artefact was scored on a 3-point visual grading scale at the same 5 anatomical levels, with 0 = absent, 1 = present but not interfering with image interpretation, 2 = present and interfering with image interpretation.

Contrast resolution was assessed at three locations (liver, spleen, buttock musculature) on a 10-point visual grading scale with 1 = unacceptable, 5 = adequate, 10 = excellent. The depiction of contrast between the abdominal soft tissues was rated with superior scores awarded for clear fat planes and crisp organ margins, and lesser scores when these structures were less well visualised.

Image quality – objective

Spherical regions of interest (ROI) of standard size (diameter, 10mm; volume, 519mm³) were drawn in 5 individual anatomical regions: liver parenchyma at the right hemi-diaphragm, liver parenchyma at the porta hepatis, erector spinae at the right renal hilum, psoas at the iliac crest, and gluteus maximus at the roof of the acetabulum. In each structure, the ROI were placed in as homogeneous an area of tissue as possible (away from blood vessels, fat planes etc.) so that the attenuation value within was representative of the underlying tissue. Using a propagation feature on the image review software, the ROI was placed at an identical location on each series, possible as all series were reconstructed from the same data set.

The mean attenuation value of the pixels within the ROI was recorded. Objective CT noise was measured as the standard deviation of the pixel values within these

ROIs. This yielded a total of 400 data-points. Signal to noise ratio (SNR) within each ROI was calculated by dividing the mean attenuation in Hounsfield Units within the ROI by its standard deviation and served as an objective measure of image quality.

Statistical analysis:

Data compilation and statistical analyses were performed using Microsoft Excel (Microsoft Corporation, Redmond, WA) and GraphPad Prism version 6.0 (GraphPad Software Incorporated, San Diego, CA). Descriptive statistics were used to summarise data including mean with standard deviations for parametric data and medians with interquartile ranges for non-parametric data. Paired t tests and Wilcoxon signed rank tests were used for pair comparison. For comparisons between the reconstruction algorithms used, Repeated Measures ANOVA with post hoc Dunnett's multiple comparisons test and Friedman test with post hoc Dunn's multiple comparisons test were used for parametric and non-parametric data, respectively. Pearson and Spearman correlation coefficients were used to express correlations. The criterion for significance was $p < 0.05$.

Results:

The study population is described in table 4.1 below. The mean effective dose from the modified dose protocol was $1.26 \pm 0.8 \text{ mSv}$, representing a 73.2% reduction from conventional dose study ($4.7 \pm 2.9 \text{ mSv}$) ($p < 0.0001$).

Table 4.1: Patient demographics and clinical characteristics

| | | |
|----------------------------|---|----|
| Sex, n | Male | 15 |
| | Female | 25 |
| Age, mean \pm SD (range) | 37 \pm 13.4 years (17-69 years) | |
| BMI, mean \pm SD (range) | 24.4 \pm 4.9 kg/m ² (16.9-38.8 kg/m ²) | |
| Effective diameter | 27.9 \pm 4 cm (19-36 cm) | |

Subjective image quality:

The changes in the subjective quality indices of diagnostic acceptability, contrast resolution and streak artifact with increasing strength of ASiR are summarized in figures 4.4 (A-C) below.

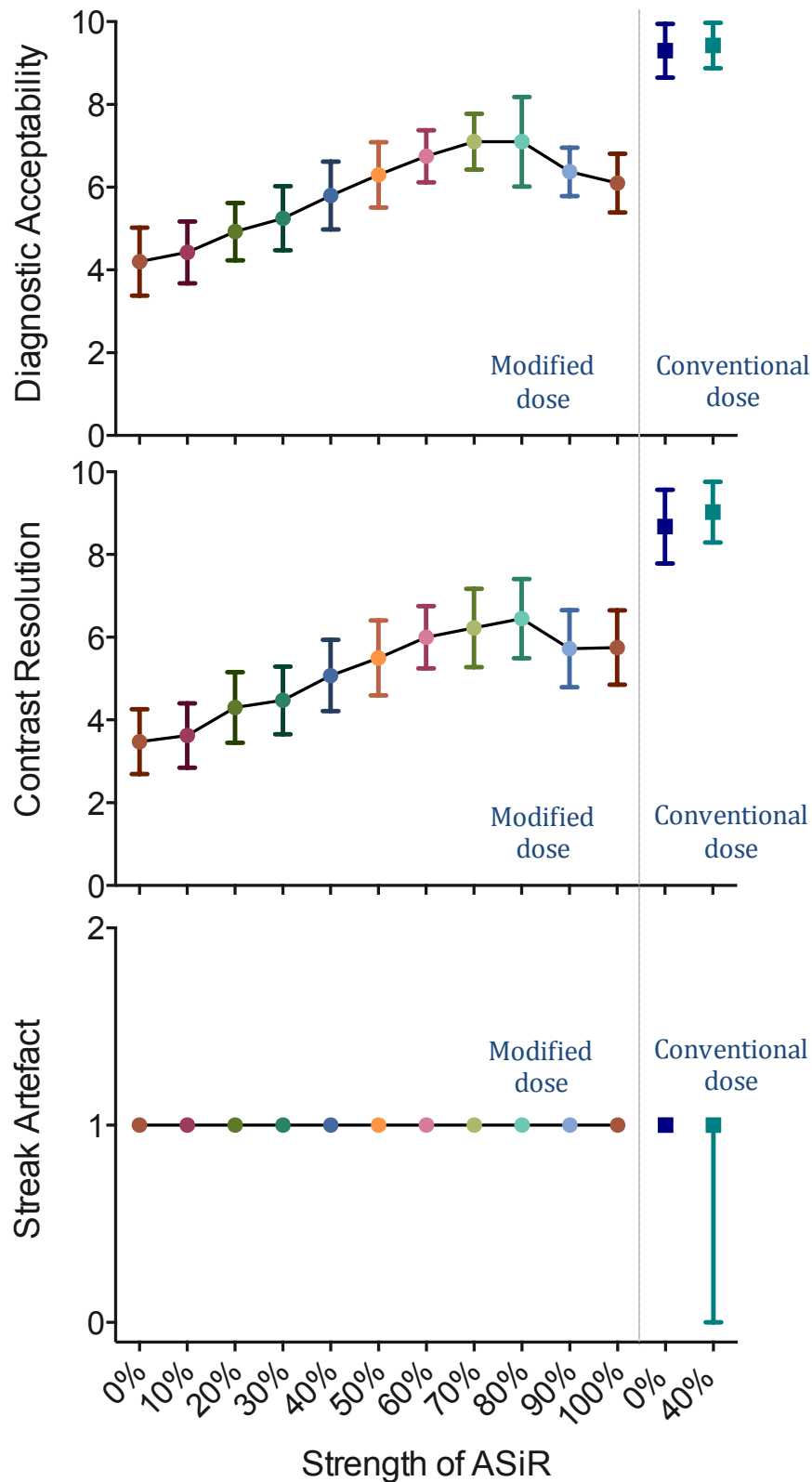


Figure 4.4: The mean subjective diagnostic acceptability (A) and contrast resolution (B) scores (symbols) with standard deviations (error bars) and median scores (symbols) and inter-quartile ranges (bars) for streak artefact (C) with increasing strengths of ASiR for modified dose CT imaging. Values for conventional dose FBP (ASiR 0%) and ASiR 40% are demonstrated for reference.

With increasing strength of ASiR, diagnostic acceptability increases steadily to a peak at 80% ASiR, with a decline in diagnostic acceptability with increasing ASiR strength beyond this. Similarly, contrast resolution also increases steadily to peak at 80% ASiR with a small decline thereafter. The median score for streak artifact across strengths of ASiR for modified dose imaging is constant at a score of 1 (present but not interfering with image interpretation). A similar score is observed for the conventional dose FBP and ASiR 40% datasets, though the 25th percentile for conventional dose ASiR 40% drops to 0. The subjective quality indices of diagnostic acceptability and contrast resolution were uniformly inferior for the modified dose studies when compared with conventional dose, regardless of the strength of ASiR used ($P<0.0001$). The image quality in terms of the presence and severity of streak artifact was equivalent or inferior to conventional dose images for all ASiR strengths ($P<0.0001$). In all cases, these image quality indices were superior for the conventional dose images reconstructed with ASiR 40% when compared with conventional dose images reconstructed with FBP ($P<0.0001$).

Subjective image noise:

With increasing strength of ASiR, there is a decrease in subjective noise in the modified dose image datasets (Spearman coefficient -0.98, $P<0.0001$) (see figure 4.5 below). Similarly, for the conventional dose series subjective noise was greater in the FBP dataset than with ASiR 40% ($P<0.0001$). Subjective noise was predominantly less evident in the conventional dose CT images reconstructed with FBP than in the modified dose datasets. However, subjective image noise

scores for modified dose images with the higher percentage ASiR hybrid blends ($\geq 80\%$ ASiR) were equivalent or superior to the conventional dose FBP images at one or more anatomical level in 24 (60%) patients. Friedman’s test, however, demonstrated a statistically significant difference between subjective noise with these higher ASiR strength modified dose reconstructions and conventional dose with FBP and ASiR 40% ($P < 0.0001$) in terms of subjective noise.

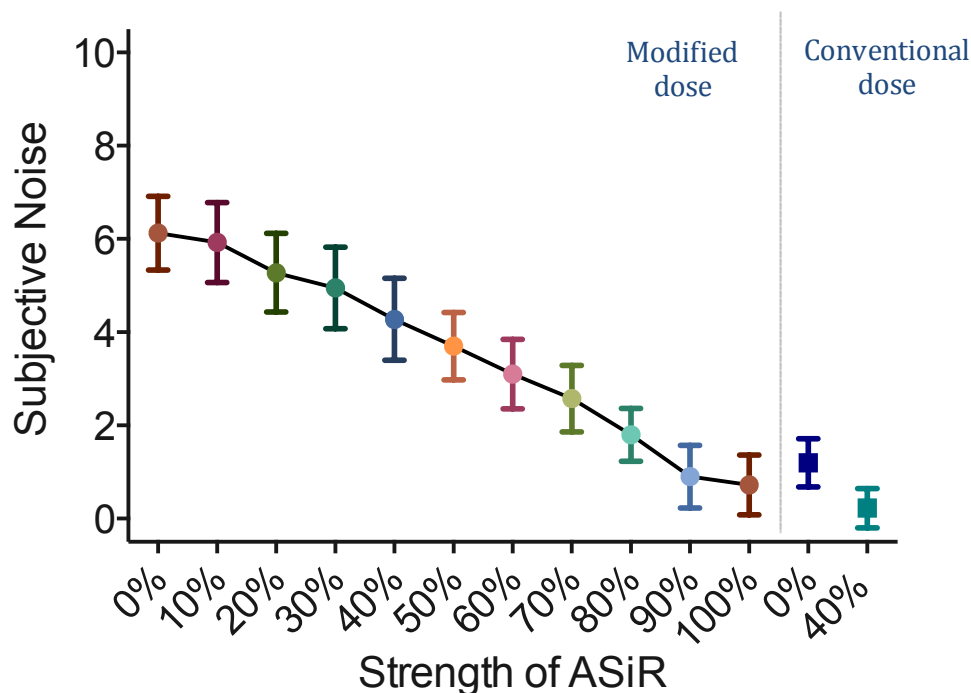


Figure 4.5: The mean subjective image noise scores (symbols) with standard deviations (error bars) for increasing strengths of ASiR for modified dose CT imaging with conventional dose FBP (ASiR 0%) and ASiR 40% demonstrated for reference.

The reduction in subjective noise was calculated using the modified dose CT dataset reconstructed with FBP as reference (i.e. absolute noise reduction = mean objective noise with FBP – mean objective noise with of algorithm in question). With each increasing increment, the mean absolute reduction in subjective noise score is 0.6 (range 0.175-0.775). The absolute reduction in

subjective noise score correlates very strongly with the strength of ASiR (Spearman coefficients 0.98-0.99, $P<0.0001$). There was a similarly strong correlation of the percentage noise reduction (percentage noise reduction = absolute noise reduction/mean objective noise with FBP $\times 100$) with the strength of ASiR (Pearson coefficients 0.95-0.99, $P<0.0001$). These findings are summarized in figure 4.6 (A-B) below.

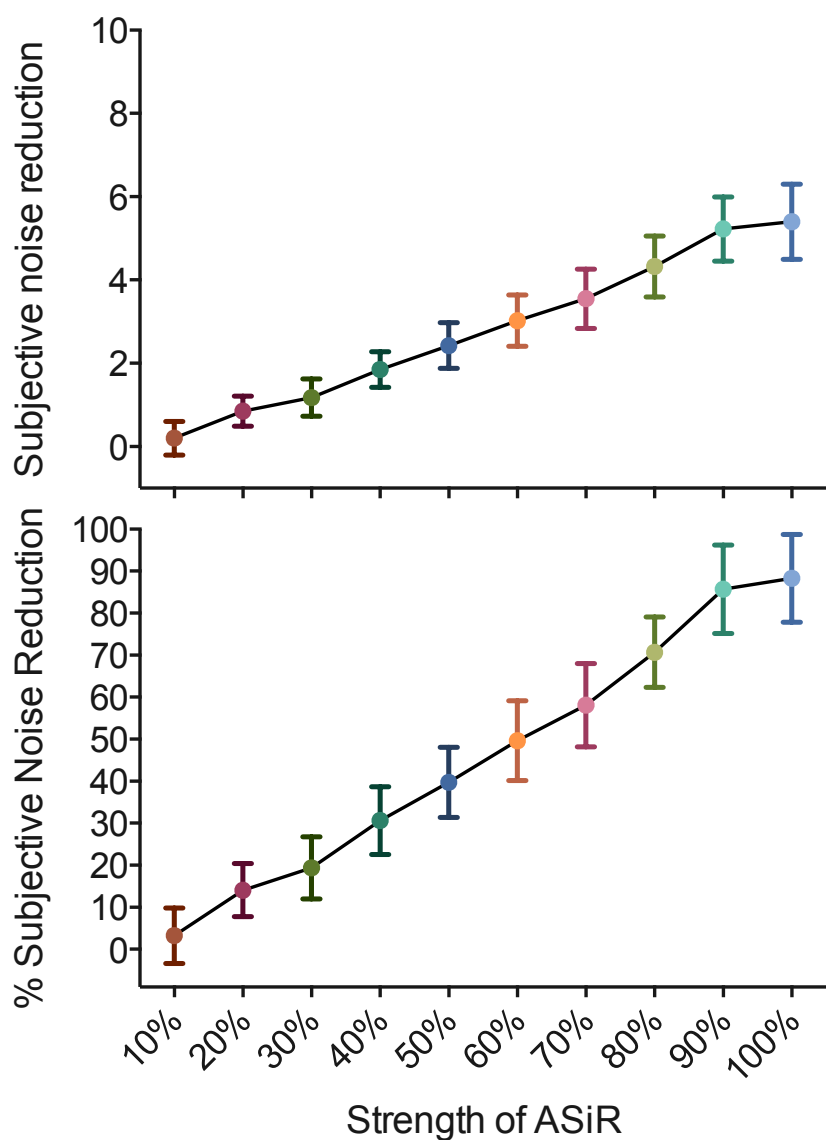


Figure 4.6: The mean absolute and percentage reduction in subjective image noise scores (symbols) with standard deviations (error bars) for increasing strengths of ASiR for modified dose CT imaging. To calculate reduction, the modified dose CT dataset reconstructed with FBP was used.

Objective image noise:

With increasing strength of ASiR, there is a reduction in objective noise in the modified dose CT images. There is a very strong correlation with a Pearson coefficient of -0.99 ($P < 0.0001$). There is also a reduction in the magnitude of the standard deviation of the objective noise with increasing ASiR strength (Pearson coefficient -0.99, $P < 0.0001$). This is illustrated in figure 4.7 by a downward sloping graph with narrowing of the error bars. Similarly, for the conventional dose CT reconstructions, objective noise was significantly less with ASiR 40% than with FBP reconstruction ($P < 0.0001$) with an associated narrowing of the standard deviation of noise levels.

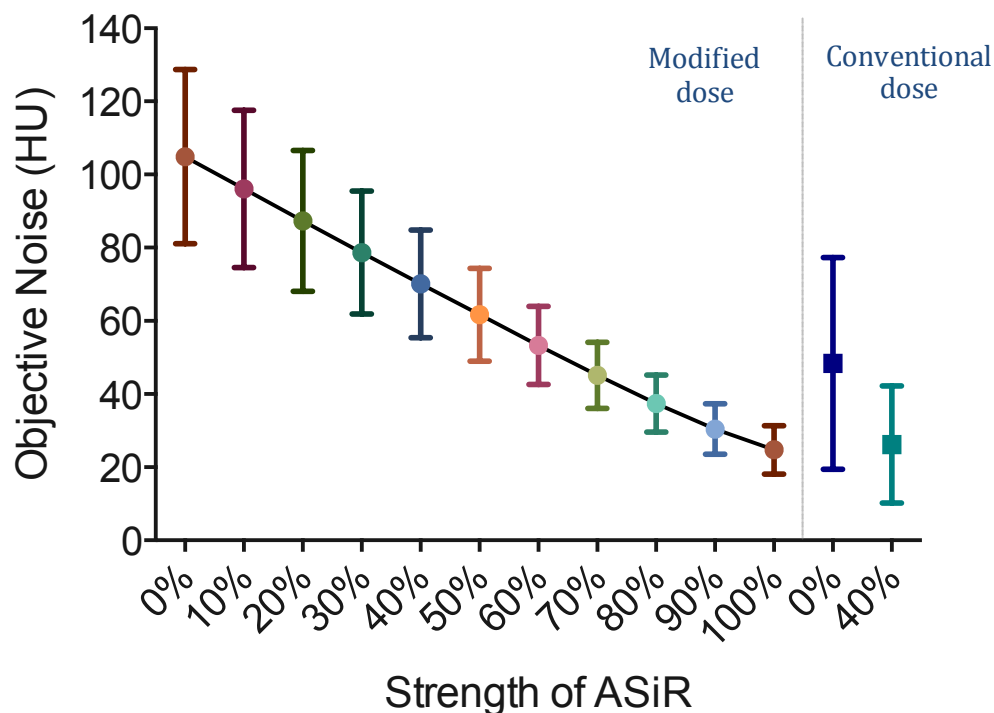


Figure 4.7: The mean objective image noise scores (symbols) with standard deviations (error bars) for increasing strengths of ASiR for modified dose CT imaging with conventional dose FBP (ASiR 0%) and ASiR 40% demonstrated for reference.

Objective image noise for FBP reconstruction of conventional dose images was less than that for the modified dose CT data reconstructed with ASiR 0-60% ($P<0.0001$). The mean objective image noise for modified dose CT reconstructed with ASiR 70-100% was less than that for the conventional dose CT image reconstructed with FBP. While there were statistically significant differences between the means for ASiR 80% and above, there was no statistically significant difference between the mean objective noise for modified dose CT with ASiR 70% and conventional dose CT with FBP ($P=0.07$). Similarly, the mean objective image noise for modified dose CT with ASiR 100% was less than that for the conventional dose CT image reconstructed with ASiR 40% but on paired t testing, this difference was demonstrated not to be statistically significant ($P=0.1235$).

There was a proportional increase in both absolute and percentage objective noise reduction with increasing strength of ASiR with perfect Pearson correlation coefficients of 1.0 and 1.0, respectively and $P<0.0001$. These relationships are graphically demonstrated in figure 4.8 below.

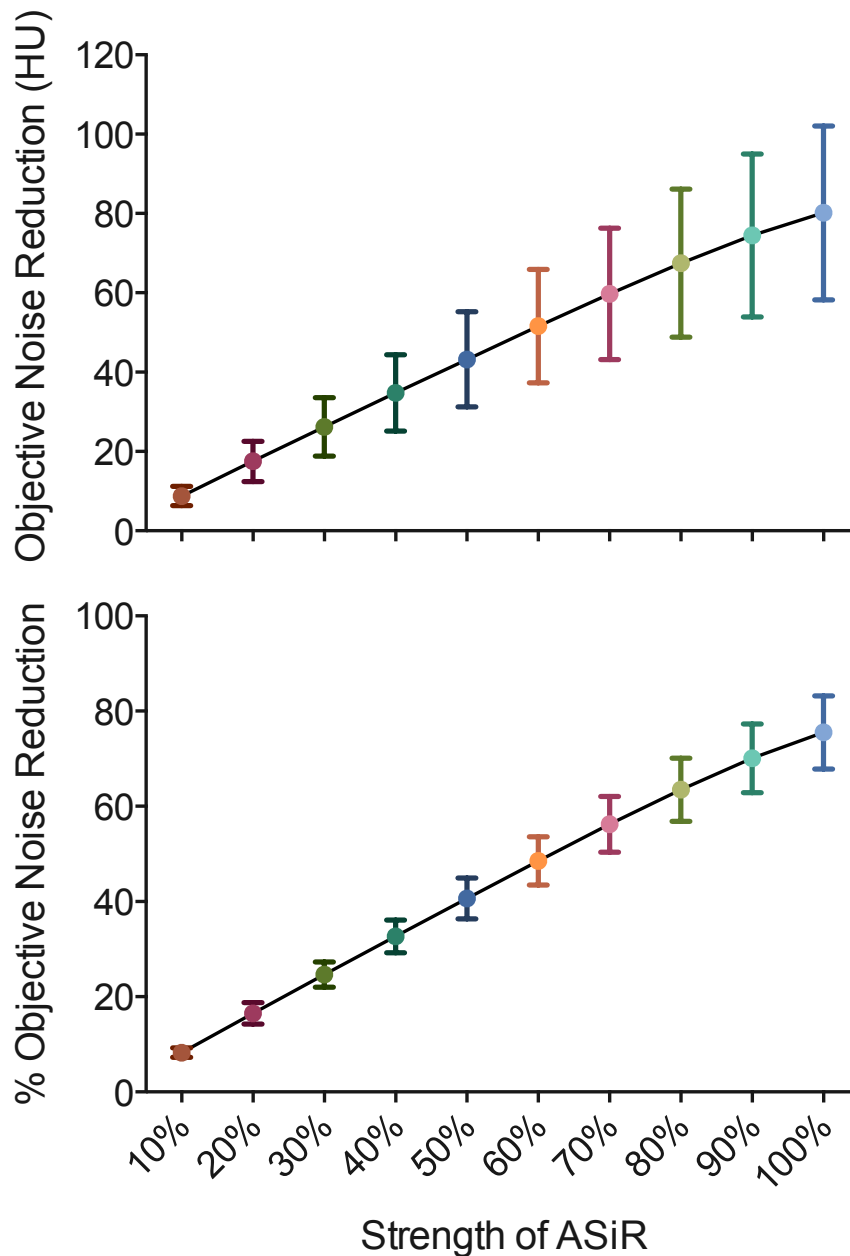


Figure 4.8: The mean absolute and percentage reduction in objective image noise scores (symbols) with standard deviations (error bars) for increasing strengths of ASiR for modified dose CT imaging. To calculate reduction, the modified dose CT dataset reconstructed with FBP was used.

The magnitude of objective noise reduction between FBP and ASiR 40% was examined for both dose protocols and compared. 40% ASiR yielded a 34.76HU (32.7%) reduction in objective noise for the modified dose protocol compared with a 21.5HU (46.1%) reduction for the conventional dose protocol.

Relationship of subjective and objective noise with increasing ASiR strength:

There is a very strong correlation between objective and subjective noise scores with each ASiR strength for images acquired with the modified dose protocol with a Pearson coefficient of 0.85 ($P < 0.0001$).

Attenuation:

Tissue attenuation values were measured at 5 distinct anatomical levels as the mean value of the pixels within a region of interest. With escalating strength of ASiR, the mean attenuation at each of the anatomical sites did not change significantly indicating preserved fidelity of attenuation measurements for tissue characterization. Figure 4.9 below demonstrates the relationship of attenuation with ASiR strength.

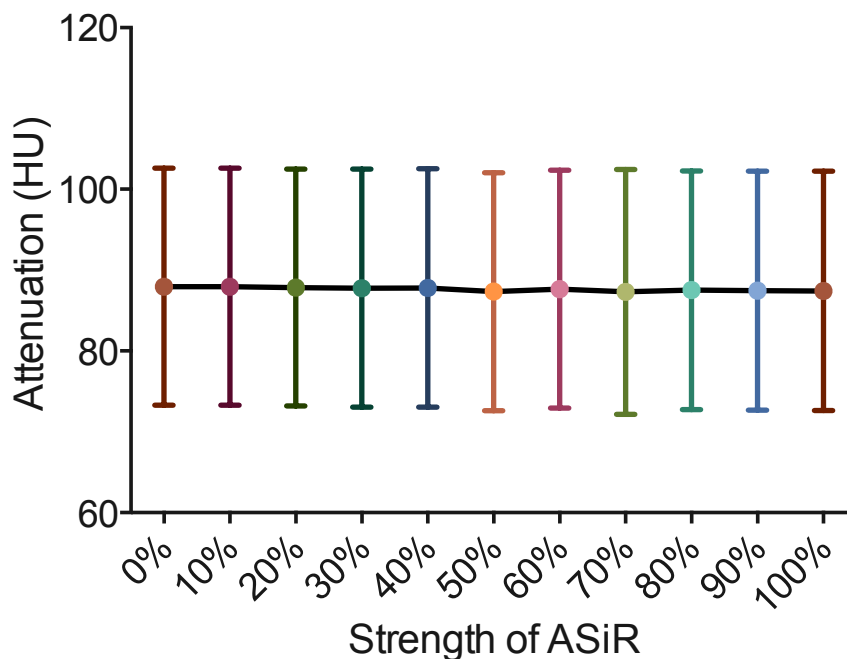


Figure 4.9: The mean attenuation values (symbols) with standard deviations (error bars) for increasing strengths of ASiR for modified dose CT imaging. Attenuation measurements were acquired at anatomically identical sites via a region of interest propagation feature, possible as all series are reconstructed from an identical CT raw dataset. There is no significant change in attenuation with change in ASiR strength.

Signal to noise ratio (SNR) is calculated by dividing the mean attenuation in a region of interest by its standard deviation (objective noise). The higher the SNR, the better the image quality. Figure 4.10 demonstrates that with increasing strength of ASiR, SNR also increases with a very strong correlation (Pearson coefficient 0.91, $P < 0.0001$). The SNR for the modified dose series reconstructed with $\geq 70\%$ ASiR are superior to those for the conventional dose series with FBP reconstruction. Similarly, the modified dose series reconstructed with ASiR 100% has a greater SNR than the conventional dose acquisition with ASiR 40%.

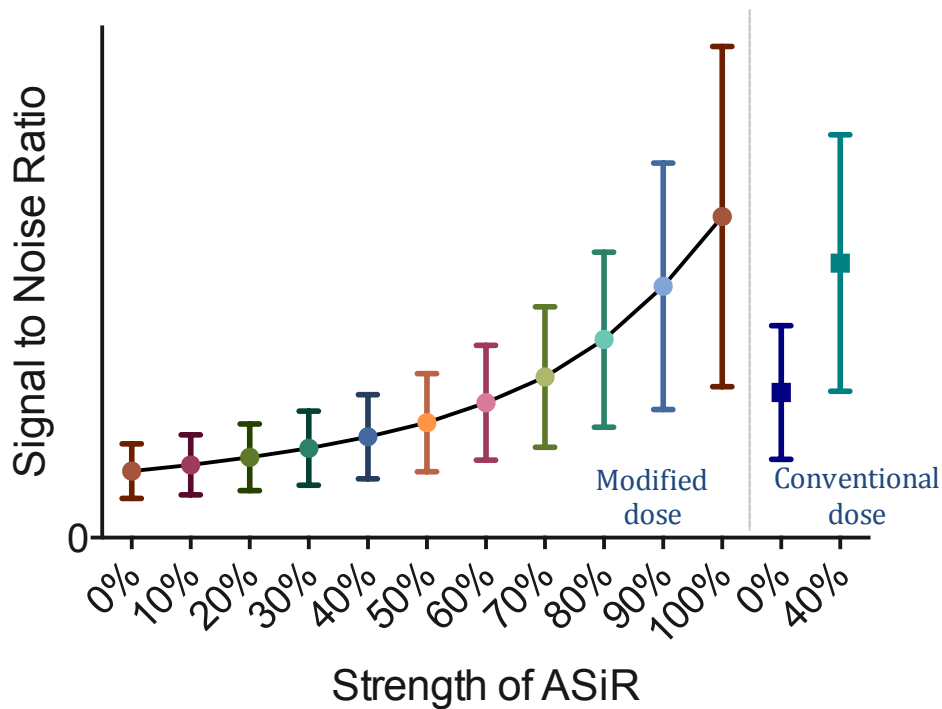
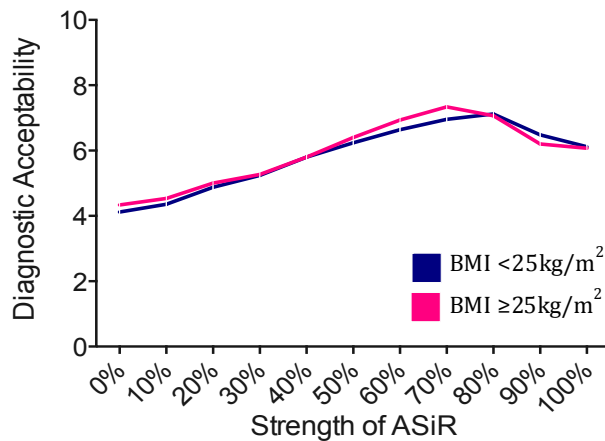


Figure 4.10: The signal to noise ratio (symbols) with standard deviations (error bars) for increasing strengths of ASiR for modified dose CT imaging with conventional dose FBP (ASiR 0%) and ASiR 40% demonstrated for reference. With increasing ASiR strength, signal to noise ratio also increases.

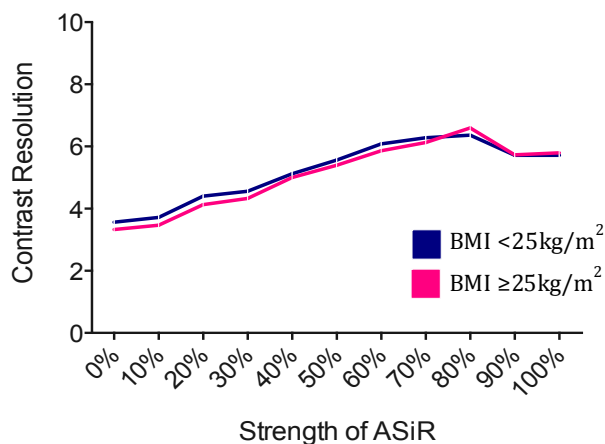
Impact of patient body mass index (BMI):

Figures 4.11 (A-E) below summarise the impact of BMI grouping on image quality indices of diagnostic acceptability, contrast resolution, streak artifact, subjective image noise and objective image noise.



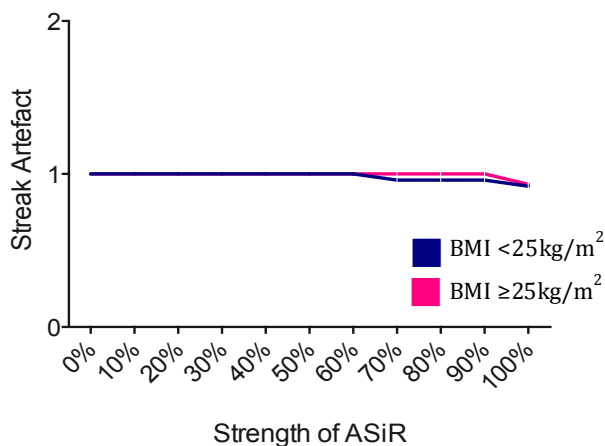
A – Diagnostic acceptability:

Notably, the peak diagnostic acceptability for BMI < 25 kg/m² was with ASiR 80% and for BMI ≥ 25 kg/m² was with ASiR 70% (P<0.0001).



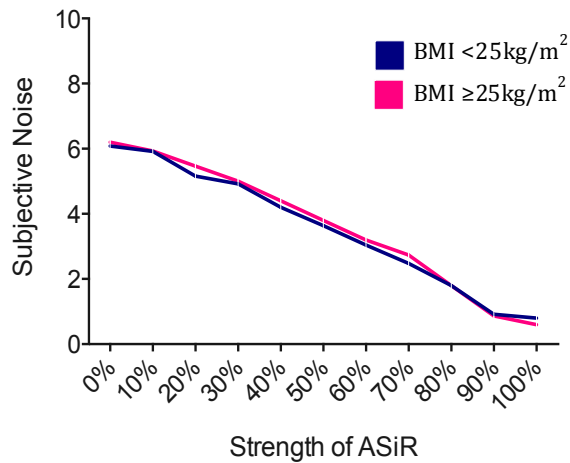
B – Contrast resolution:

The best contrast resolution, regardless of BMI subgroup, was observed with ASiR 80%.



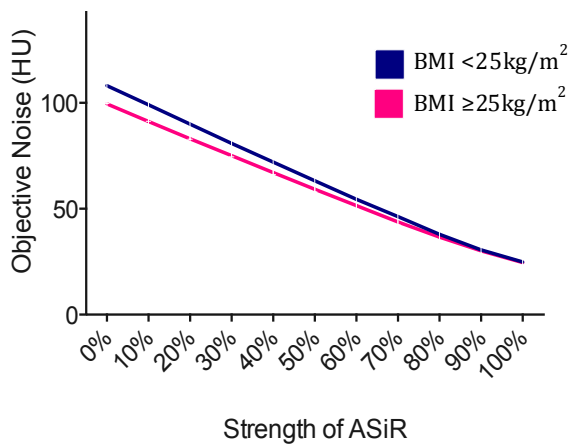
C – Streak artifact:

There was no significant difference in streak artifact between BMI subgroups.



D – Subjective noise:

There was no significant difference in subjective image noise between BMI subgroups.



E – Objective noise:

There was a significant reduction in the difference in objective noise levels between BMI groups with increasing strength of ASiR (Pearson correlation - 1.0, $P < 0.0001$).

Overall optimal strength of ASiR for this modified dose CT protocol:

The reconstruction algorithm that yielded the most favourable combination of image quality indices overall this modified dose imaging protocol was 80% ASiR. This allowed a 63.5% reduction in objective image noise ($P < 0.0001$), a 66.4% improvement in signal to noise ratio ($P < 0.0001$), a 70.6% reduction in subjective image noise ($P < 0.0001$), no significant difference in streak artifact and peak diagnostic acceptability and contrast resolution scores when compared with FBP.

Discussion:

Iterative reconstruction selectively identifies and reduces image noise while maintaining image contrast resolution. This allows either (a) improvement in image quality without increasing the radiation dose, or (b) maintenance of image quality at a lower radiation dose compared with traditional FBP image reconstruction [18,62,68].

With 11 different user-defined increments of ASiR available for hybrid reconstruction, selection of the appropriate algorithm strength is difficult. Based on vendor recommendations, we selected ASiR 40% for validation of ASiR in chapter 3. In that study we demonstrated that, with 73.5% reduction in CT radiation dose, ASiR 40% enabled CT images to be obtained with preserved diagnostic ability with no major discrepancies in terms of significant pathological and incidental findings when compared with conventional dose CT, albeit with uniformly inferior subjective image quality indices. This value was recommended based on vendor experience with conventional dose CT studies and was not specific for modified dose CT protocols. Indeed, at time of study planning there was no available recommended ASiR level for modified dose CT images. With a paucity of literature examining the effects of incremental increase in ASiR on image quality indices, we sought to determine the optimal percentage ASiR to employ for evaluation of modified dose CT images.

In this prospective study of 40 patients, the effect of ASiR on radiation dose reduction was evaluated and image quality compared with ASiR strength. The present study demonstrates that modified dose CT raw data reconstructed with

ASiR, regardless of percentage, provide images that are uniformly superior to those reconstructed with FBP in terms of both subjective and objective image quality indices. Modified dose CT with ASiR with a high percentage ASiR in the hybrid blend (>70%) is equivalent or superior to conventional dose CT with FBP reconstruction in terms of both subjective and objective image noise measures. Importantly, objective diagnostic information including the attenuation values of various anatomical structures was retained across the various strengths of ASiR applied when compared with FBP.

The noise reduction with each ASiR increment was of 5.4-8.3% (5.7-8.8HU), using FBP (0% ASiR) as the reference. The maximum noise reduction with ASiR was 75.5% with 100% ASiR, with lowest subjective image noise scores also observed at this level. However, the diagnostic acceptability and contrast resolution scores did not mirror this peak with maximum scores for both of these parameters observed with ASiR 80%. When stratified for BMI < or \geq 25kg/m², the peak for diagnostic acceptability for BMI \geq 25kg/m² remained at 70% but all others had peak values at 80% ASiR. We conclude, therefore, that the overall optimal ASiR strength to use with this modified dose protocol is ASiR 80% as this provides the optimal balance of peak subjective image quality indices with greatly reduced objective image noise.

With ASiR levels of 20% or below, diagnostic acceptability and contrast resolution scores of <5 (5 = adequate) were observed suggesting the images to be inadequate for diagnosis. Image quality indices in each of these cases were invariably equivalent or superior to the corresponding modified dose FBP

images. It can be concluded that reconstruction with such low ASiR strengths should be avoided with modified dose CT raw data in this dose range as the low level of ASiR employed is insufficient to overcome the excessive noise in the modified dose images. Equally though, FBP (ASiR 0%) reconstruction of modified dose raw data yields inadequate images and is not recommended.

This study has some limitations. Here we examine a data set at a single modified dose level and determine the optimal percentage ASiR to reconstruct with. We also compare a single ASiR setting (40%) for conventional dose CT with FBP. Findings cannot be extrapolated to CT raw data acquired at conventional or ultra low doses, as the optimal percentage is likely to differ. Conventional dose CT with FBP is the standard against which images are assessed. If this protocol is sufficiently optimized in terms of image quality, then reconstruction of these raw data with ASiR may not be demonstrably superior to FBP as maximal image quality scores have been achieved. Thus, when ASiR is applied to fully optimized conventional dose images, an appreciable diagnostic benefit is unlikely to be present. Conversely, with ultra low dose CT imaging, the image raw data may be so noisy as to require a higher strength of ASiR to achieve optimal image quality. At its most extreme, if CT radiation dose is so low as to cause a paucity of photons, adequate image quality will not be achieved regardless of the strength of ASiR applied, as there simply are not enough data projections to form a high quality image. Image quality depends not only on the strength of iterative reconstruction used, but also on the inherent image noise prior to the application of iterative reconstruction. Selection of the optimal strength of iterative reconstruction to use depends on the degree of radiation dose reduction, the

maximum tolerable noise level in the resultant image, and the desired spatial resolution and these factors differ among scanning protocols.

In this study we examine abdomino-pelvic CT and findings cannot be applied to other body regions such as head, neck and thorax. Separate evaluation of the optimal strength of ASiR, for dose, to apply for each of these body regions is required. The study population is relatively modest at 40. While adequate for overall population conclusions, subgroup BMI analysis is limited by sample size and the effect of BMI on the optimal ASiR strength to use may be underestimated. These results may not apply to other similar iterative reconstruction methods available from other vendors. Owing to the difference in image appearance, blinding of the radiologists between higher and lower strengths of ASiR during subjective image analysis was difficult. In an attempt to minimize potential recognition bias, the image datasets acquired with different dose levels and reconstruction techniques were randomized.

The 'waxy', 'plastic' and 'impasto' appearance of hybrid images reconstructed with the higher strengths of ASiR [72,81,83,87,163-164] may also introduce adaptation bias (i.e. when observers, accustomed to a certain image appearance and noise texture, prefer these images to clinically equivalent images with a slightly different appearance [111]). Images reconstructed with iterative reconstruction techniques can have an altered texture with a smoothened appearance, the degree of which increases with the degree of noise suppression used. This can lead to reduced sharpness of tissue margins, a smoothened appearance of solid organs, and reduced perception of small objects [18],

particularly with the higher percentage ASiR hybrid blends (90-100%). In the lungs, the over smoothing of images has been reported to obscure visibility of the major lung fissures [165]. A radiologist unaccustomed to viewing and interpreting such images will have less diagnostic confidence with the altered and unfamiliar image texture. The lower subjective image quality scores at the highest ASiR increments may be partially a consequence of the reader being uncomfortable with the image rather than a truly sub-optimal image from a diagnostic quality point of view. Because images generated with iterative reconstruction have a different texture to FBP images, a gradual implementation of iterative reconstruction and dose reduction is advised, avoiding drastic changes in CT protocols [81]. We have demonstrated that the degree of image texture change is variable with the ASiR strength used. Such knowledge can be exploited so that the level that strikes the best balance between noise reduction and image familiarity can be used or adopted to taper radiologists' experience with the new altered image texture by gradually increasing the strength applied.

Conclusion:

In conclusion, the strength of ASiR in the hybrid iterative reconstruction algorithm applied can greatly impact on the quality of the image generated from the CT raw data. Selection of the optimal strength of ASiR to use depends on the degree of radiation dose reduction, the maximum tolerable noise level in the resultant image, and the desired spatial resolution and these factors differ among scanning protocols. With modified dose CT imaging, it is vital that the appropriate radiation dose level as well as the correct associated strength of

iterative reconstruction is selected to maximize image quality for the clinical task while keeping radiation exposure to a minimum.



Chapter 5

A prospective feasibility study of sub-millisievert
abdominopelvic CT using model based iterative
reconstruction in Crohn's disease

Iterative Reconstruction as a Novel Method of Radiation Dose Reduction
at Computed Tomography in Patients with Crohn's Disease

Introduction:

Patients with Crohn's disease are exposed to high lifetime cumulative doses of ionising radiation, primarily due to the more widespread and repeated use of CT [13,146, 166-168]. At present there is considerable research and industry drive to reduce radiation exposure during CT imaging while preserving image quality and diagnostic accuracy.

We, and others, have validated the use of hybrid reconstruction algorithms such as Adaptive Statistical Iterative Reconstruction (ASiR) in facilitating dose reductions of up to 73.5% over traditional Filtered Back Projection (FBP) in patients with Crohn's disease [118,161-162,169]. Dose reductions of a similar magnitude have been achieved in other patient populations with good preservation of diagnostic accuracy [71,85,116,158-159,170-173]. Hybrid iterative reconstruction has certain limitations, however, including reliance on an ideal statistical model of photon and electronic noise. Blending with comparatively noisy filtered back projection images is required to improve image acceptability among radiologists [174].

Pure iterative reconstruction algorithms such as MBIR differ significantly from their hybrid predecessors in that they operate using a model of the actual physical characteristics of the individual scanner including the focal spot, the x-ray fan beam, the three dimensional interaction of the x-ray beam within the patient, and the two dimensional interaction of the x-ray beam within the detector [174]. In chapter 2, phantom and cadaveric studies yielded favourable results suggesting the superiority of MBIR over ASiR in terms of image quality

with less image noise for images acquired at even submillisievert doses. Early clinical data suggest that abdominal CT reconstructed with MBIR is superior to hybrid iterative reconstruction and may facilitate dose reductions in the order of 75% over filtered back projection [83].

The advantages of emerging dose optimisation technology such as MBIR may have the greatest benefit in patient cohorts like those with Crohn's disease, who often present at an early age and sometimes have decades of active disease requiring repeated CT imaging [13].

This is a prospective intra-individual feasibility study involving the contemporaneous acquisition of modified (circa 1mSv) and conventional (circa 5mSv) CT of the abdomen and pelvis in patients with active Crohn's disease with the following aims:

1. To demonstrate the feasibility of an optimally developed modified dose CT protocol to enable reduction of the effective dose of a CT of abdomen and pelvis to within the one-millisievert range using MBIR in a clinical setting (in patients with active Crohn's disease).
2. To compare objective noise and subjective image quality indices when modified dose CT images are reconstructed with model based iterative reconstruction (MBIR), 40% and 70% adaptive statistical iterative reconstruction (ASiR) and filtered back projection (FBP).
3. To determine the diagnostic accuracy of modified dose CT using MBIR in the assessment of patients with Crohn's disease with suspected extramural complications when compared with conventional dose CT.

Methods:

This is a secondary analysis of CT data acquired for the validation of adaptive statistical iterative reconstruction in achieving diagnostic quality CT at markedly reduced radiation doses. Concise methods have been published elsewhere [161-162] and are described in detail in chapter 3.

Briefly, 50 consenting patients with known Crohn's disease with a suspected acute complication, who required a CT of abdomen and pelvis for clinical indications, underwent both conventional dose and modified dose CT of abdomen and pelvis on a 64-slice CT scanner (GE Lightspeed VCT-XTe) as part of an IRB-approved research protocol [ClinicalTrials.gov Identifier NCT 01244386]. The conventional dose protocol comprised CT of abdomen and pelvis acquired at approximately 90% of the radiation dose of the standard departmental CT of abdomen and pelvis protocol (tube voltage 120kV, noise index 38%, gantry rotation time 0.8s). The modified dose protocol comprised CT of abdomen and pelvis acquired at approximately 10% of the radiation dose of standard departmental CT of abdomen and pelvis (tube voltage 100kV, noise index 70%, gantry rotation time 0.5s). All patients were imaged in the portal venous phase of intravenous contrast with the low dose protocol first, followed by the conventional dose protocol 6.2s later. For both protocols z-axis automated tube current modulation resulted in a variable tube current, with minimum and maximum tube current thresholds of 20 and 350mA respectively.

Of these 50 patients, 34 patients had raw data appropriately saved for retrospective reconstruction with adaptive statistical iterative reconstruction

and model based iterative reconstruction. The discrepancy in numbers is accounted for by the failure to save 10 datasets in an appropriate format for retrospective reconstruction (as outlined in chapter 4) as well as corruption of the hard-drives containing 6 of the studies during the MBIR reconstruction process with loss of the raw data.

The modified dose image raw data were retrospectively reconstructed with filtered back projection, ASiR 40% (a blend of 40% ASiR reconstruction and 60% FBP), ASiR 70% (a blend of 70% ASiR and 30% FBP) and with MBIR (standard setting), each to a slice thickness of 2mm. This yielded a total of 4 modified dose series per patient. The corresponding conventional dose raw data were reconstructed with ASiR 40% as per standard departmental protocol and consistent with manufacturers’ recommendations.

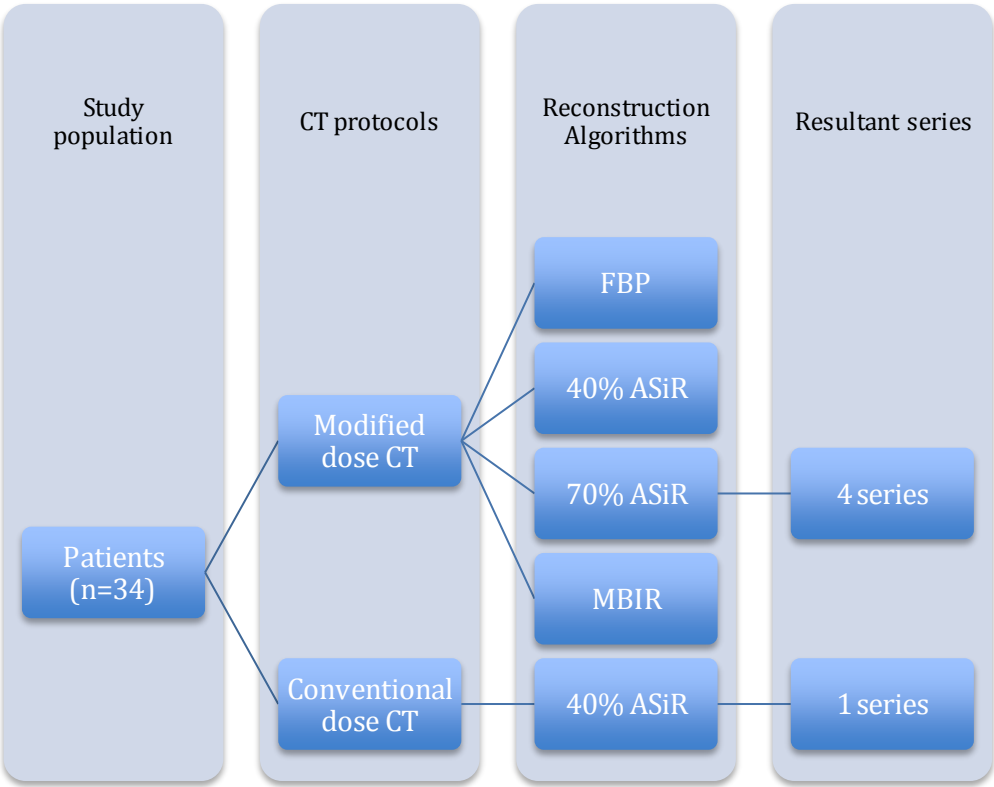


Image review – diagnostic accuracy:

Reconstructed CT data sets were reviewed in a Digital Imaging and Communications in Medicine (DICOM) format on imaging workstations (Advantage Workstation VolumeShare 2, Version 4.4, GE Medical Systems, Milwaukee, USA).

Two fellowship-trained abdominal radiologists, with 9 and 8 years of radiology experience, respectively, performed image review for diagnostic findings independently. Importantly, these radiologists were different to those used in chapter 3 as we wished to avoid any possibility of recall bias given that the CT images were reconstructed from the same CT raw data. The modified dose with MBIR and conventional dose with ASiR 40% series were reviewed for diagnostic findings. To minimise the effects of recall bias, all datasets were anonymised and studies identified merely by a randomly generated four-digit number. Similarly, to avoid recall bias from repetition arising from reading the modified and conventional dose images, reviewers were made aware that the patient had a history of Crohn's disease but blinded to the clinical history and clinical query posed. Previous imaging studies were not available for comparison. Images were reviewed in a random patient order with a delay period 6 weeks instituted between review of modified and conventional dose CT images to minimise recall bias. In all cases, modified dose CT images were reviewed first. CT data were reconstructed into axial and coronal reformats of 2mm thickness and images were reviewed using a soft tissue window setting (window width, 400HU; window level, 40HU).

Diagnostic findings for both the modified and conventional dose CT protocols were assessed separately and reported in a similar manner to standard clinical practice. The presence and nature of previous surgery was documented. Crohn's disease related findings such as the extent and severity of active inflammation and the presence of strictures of the small and large intestine were recorded. Changes in the peri-enteric and peri-colonic tissues substantiating the presence of active inflammation or indicative of transmural disease were also recorded. Extraintestinal manifestations of Crohn's disease and any non-Crohn's disease related findings were noted.

Crohn's disease activity was graded and scored radiologically according to the presence and severity of morphologic changes in both the large and small bowel, changes suggestive of active inflammation and penetrating disease, and the presence or absence of acute complications such as acute obstruction, ileus or visceral perforation [table 5.1]. This is an adaptation of a scoring system grading severity of radiological Crohn's disease activity that has been validated by our group [153] and is a summation of the presence and severity of findings in the small bowel, large bowel, mesentery and peri-enteric/peri-colonic tissues. In addition, a designation of A+ or A- was assigned to patients with or without acute complications (obstruction, ileus, perforation), respectively. Utilising this Crohn's disease activity score, disease severity was categorised into grade 0 (0/12), grade I (1-4/12), grade II (5-8) and grade III (9-12/12).

Table 5.1: Crohn's disease activity score [153]

| | | |
|---------------------|---|----|
| Small bowel disease | Normal small bowel | 0 |
| | Wall thickening >3mm | 1 |
| | Stricture(s) without obstruction | 2 |
| | Stricture(s) with obstruction | 3 |
| Large bowel disease | Normal large bowel | 0 |
| | Wall thickening >3mm | 1 |
| | Stricture(s) without obstruction | 2 |
| | Stricture(s) with obstruction | 3 |
| Inflammation | No inflammatory change | 0 |
| | Mesenteric hypervascularity | +1 |
| | Mesenteric fat stranding | +1 |
| | Mesenteric lymphadenopathy | +1 |
| Penetration | No penetrating disease | 0 |
| | Fistulating disease | 1 |
| | Phlegmon | 2 |
| | Abscess | 3 |
| Acute complications | Acute obstruction, ileus, perforation, etc. | A+ |
| | No acute complications | A- |

Image quality – subjective:

Parameters for the assessment of image quality were selected based on previous studies using the European Guidelines on Quality Criteria for CT document [71,102,119]. These methods are described in detail in chapter 3. A senior reader, having used these methods previously [154-156], trained the second reader prior to commencing analysis using a training set of five standard CTs. Anatomical sites for measurement of image quality indices were chosen to be reproducible and comparable for assessment across reconstructed series.

Image quality was assessed in terms of diagnostic acceptability, subjective image noise, the presence of streak artifact, and contrast resolution. The grading systems described in chapter 3 were felt too crude for differentiation of subtle

image quality variations between the reconstructed series and therefore a more refined 10-point scale was introduced for diagnostic acceptability, subjective image noise and contrast resolution, as in chapter 4.

Diagnostic acceptability was assessed by means of a 10-point visual grading scale with 1 = unacceptable, 5 = adequate, 10 = excellent. Five different structures were assessed subjectively with this method: the solid organs, large bowel, small bowel, peri-colonic fat and peri-enteric fat. Superior scores were awarded for clear depiction of these structures with lesser scores when images were degraded from noise or artefacts. The median score from all 5 levels was taken as an overall score of diagnostic acceptability.

Subjective image noise was assessed by means of an inverse 10-point visual grading scale with 10 = unacceptable, 5 = adequate, 1 = excellent. Assessment was made at 5 anatomical levels (the right hemidiaphragm, the porta hepatis, the right renal hilum, the right iliac crest, the right acetabulum). Images were assessed for graininess or mottle affecting depiction of small anatomic structures such as blood vessels and tissue interfaces. Lesser scores were awarded for a lack of appreciable graininess or mottle with greater scores when graininess interfered with structure depiction.

Streak artefact was scored on a 3-point visual grading scale at the same 5 anatomical levels, with 0 = absent, 1 = present but not interfering with image interpretation, 2 = present and interfering with image interpretation.

Contrast resolution was assessed at three locations (liver, spleen, buttock musculature) on a 10-point visual grading scale with 1 = unacceptable, 5 = adequate, 10 = excellent. The depiction of contrast between the abdominal soft tissues was rated with superior scores awarded for clear fat planes and crisp organ margins, and lesser scores when these structures were less well visualised.

Image quality – objective

Spherical regions of interest (ROI) of standard size (diameter, 10mm; volume, 523mm³) were drawn by a single reader in 5 individual anatomical regions: liver parenchyma at the right hemi-diaphragm, liver parenchyma at the porta hepatis, erector spinae at the right renal hilum, psoas at the right iliac crest and gluteus maximus at the roof of the right acetabulum. In each structure, the ROIs were placed in as homogeneous an area of tissue as possible (away from blood vessels, fat planes etc.) so that the attenuation value within was representative of the underlying tissue. Using a propagation feature on the image review software, the ROI was placed at an identical location on each modified dose series, possible as all series were reconstructed from the same CT raw data set. The region of interest was manually placed in as close a location as possible on the conventional dose images using direct visual comparison. Objective CT noise was measured as the standard deviation of the pixel values within these ROIs. Subtracting the objective noise on the modified dose ASiR 40%, ASiR 70% and MBIR images from the objective noise presence on the modified dose FBP images subsequently derived the magnitude of noise reduction.

Method of reference case review:

From chapter 3, we felt that blinding of the readers to the clinical information and history and previous imaging placed them at a disadvantage in terms of image interpretation. For this reason, a final method of reference case review of the 34 patient examinations was performed in consensus by 2 readers, designed to simulate a more realistic reporting setting and provide a reference standard with which to compare the study findings. These readers were allowed access to all available current and prior imaging, results of prior radiological and non-radiological investigations, complete clinical histories, cellular pathology results (if acquired in the 1-month period before or 1-month period after CT examination) and surgical correlation (where available). This method of reference assessment of radiological findings utilized the same format as used in the initial clinical image review. The information from the initial blinded clinical review was not available for the method of reference case review.

Importantly, these method of reference readers were different to those used in the blind diagnostic reads for this chapter and for chapter 3 as we used the method of reference case review to establish the standard against which these blinded reads were compared, without the restriction of limited clinical information. In contrast, intra-individual comparison of the blinded reads allowed direct comparison to be made between modified and conventional dose images under identical circumstances with the blinding facilitating a reduction in recall bias.

Estimation of radiation dose:

CTDI_{vol} and DLP measurements were recorded from the scanner dose report. SSDE was calculated in accordance with AAPM methodology, as previously described, by application of a conversion factor extrapolated from the effective body diameter at the midslice level to the CTDI_{vol} for an individual patient [97]. The imaging performance and assessment in CT (ImPACT) patient dosimetry calculator was used to calculate effective doses using original scanning parameters for each protocol, also previously described.

Statistical methods:

Data compilation and statistical analyses were performed using Microsoft Excel (Microsoft Corporation, Redmond, WA) and GraphPad Prism version 6.0 (GraphPad Software Incorporated, San Diego, CA). Descriptive statistics are provided in terms of means with standard deviations and medians with interquartile ranges (IQR) for parametric and non-parametric values. Variables were compared with paired t-tests and repeated measures ANOVA (with Tukey's and Dunnett's multiple comparison tests if ANOVA showed a significant difference) if parametric. If non-parametric, Wilcoxon matched pairs, Kruskal-Wallis and Friedman tests (with Dunn's multiple comparison test) were used. Pearson and Spearman correlations were used for parametric and non-parametric variables, respectively. For cases where testing for inter-observer concordance was required, the Cohen's κ test was used. The criterion for significance was taken as $P < 0.05$.

Results:

Thirty-four patients were included in this study. The study population is described in table 5.2.

Table 5.2: Patient demographics and clinical characteristics

| | | |
|---|--------|-----------------------|
| Sex (n) | Male | 13 |
| | Female | 21 |
| Age (y), mean±SD (range) | | 37.8±13.7 (16-74) |
| BMI (kg/m ²), mean±SD (range) | | 24.7±4.97 (17.4-38.8) |
| Effective diameter (cm), mean±SD (range) | | 28±3.88 (20.82-36) |

Measurements of radiation exposure:

The mean radiation dose, regardless of metric used (CTDI_{vol}, DLP, SSDE, effective dose), was significantly less for the modified dose protocol when compared with the conventional dose protocol ($p < 0.0001$ for all comparisons). Radiation dose for each dose protocol in terms of CTDI_{vol}, DLP, SSDE and effective dose and the dose reductions achieved are summarized in table 5.3. Comparing effective doses between protocols [100], there was a 72.9% reduction in radiation dose with the modified dose CT protocol compared with the conventional dose protocol.

Table 5.3: A summary of radiation dose from modified and conventional dose CT protocols and absolute and percentage dose reductions achieved

| | Conventional dose | Modified dose | Absolute reduction | % Reduction |
|---------------------------|-------------------|---------------|--------------------|-------------|
| CTDI _{vol} (mGy) | 6.33±3.67 | 2.03±1.22 | 4.3 | 67.9% |
| DLP (mGy.cm) | 303±186 | 88±58 | 215 | 71% |
| Effective diameter (cm) | 28±3.88 | 28±3.88 | - | - |
| SSDE (mGy) | 7.93±3.06 | 2.53±1.06 | 5.4 | 68.1% |
| Effective dose (mSv) | 4.8±2.99 | 1.3±0.87 | 3.5 | 72.9% |

Data are presented as means with standard deviations

$P < 0.0001$ for all comparisons

The radiation dose for each protocol stratified by BMI group is summarized in table 5.4 and figure 5.1. A statistically significant increase in DLP, CTDI_{vol}, SSDE and effective dose was encountered with increasing BMI for both modified and conventional dose protocols (Pearson correlations; $r=0.91-0.94$, $p<0.0001$ for all comparisons).

Table 5.4: A summary of radiation dose from modified and conventional dose CT protocols for patients categorised by BMI $<25 \text{ kg/m}^2$ or BMI $\geq 25 \text{ kg/m}^2$

| | Conventional dose | | Modified dose | |
|---------------------------|-------------------|------------------|------------------|------------------|
| | BMI < 25 | BMI ≥ 25 | BMI < 25 | BMI ≥ 25 |
| CTDI _{vol} (mGy) | 4.34 \pm 0.75 | 9.54 \pm 4.14 | 1.36 \pm 0.31 | 3.11 \pm 1.37 |
| DLP (mGy.cm) | 204 \pm 37 | 463 \pm 220 | 57 \pm 13 | 137 \pm 69 |
| Effective diameter (cm) | 25.56 \pm 1.95 | 31.84 \pm 2.94 | 25.56 \pm 1.95 | 31.84 \pm 2.94 |
| SSDE (mGy) | 6.27 \pm 0.77 | 10.62 \pm 3.49 | 1.95 \pm 0.35 | 3.46 \pm 1.17 |
| Effective dose (mSv) | 3.24 \pm 0.61 | 7.33 \pm 3.5 | 0.83 \pm 0.21 | 1.98 \pm 1.06 |

Data are presented as means with standard deviations
 $P<0.0001$ for all comparisons

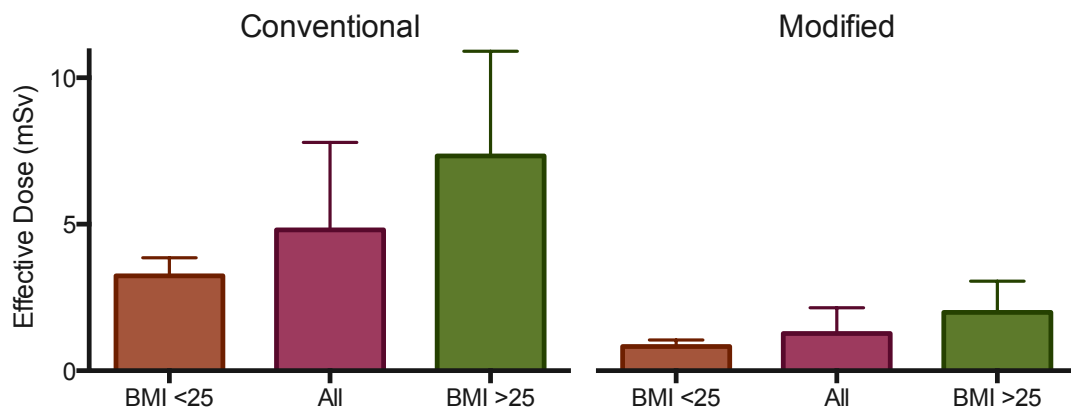


Figure 5.1: Column bar graph summarising the effective doses overall and for the BMI subgroups with both conventional and modified dose CT protocols. The box represents the mean dose and the whiskers the standard deviation. The mean radiation doses are significantly less with the modified dose protocol when compared with the conventional dose protocol, both overall and for both BMI subgroups.

Diagnostic accuracy:

The Crohn's disease related CT findings demonstrated on the method of reference reads (with all clinical information and imaging made available to the readers) are as follows:

Table 5.5: Crohn's disease related CT findings demonstrated on the method of reference reads (n)

| | |
|-----------|----|
| Enteritis | 20 |
| Colitis | 24 |
| Stricture | 5 |
| Fistula | 5 |
| Abscess | 5 |

The Crohn's disease activity scores for the method of reference reads are summarized in figure 5.2.



Figure 5.2: Bar chart of the number of patients within each Crohn's disease activity score grade. The median (interquartile-range) overall value of CDAS was 4 (2).

The median Crohn's disease activity scores for modified dose with MBIR and conventional dose with ASiR 40% are summarized in table 5.6 below, with the median method of reference score provided for comparison. The median Crohn's disease activity score was comparable for modified dose CT with MBIR and conventional dose CT with ASiR 40% images for both readers.

Table 5.6: Comparison of median Crohn's disease activity scores between modified dose CT with MBIR and conventional dose CT with ASiR 40%

| | Reader 1 | Reader 2 | Method of reference |
|---|----------|----------|---------------------|
| Modified dose CT with MBIR | 4±3 | 5±1.75 | |
| Conventional Dose with CT ASiR 40% | 4±3 | 5±2 | |
| All available imaging and clinical information | | | 4±2 |
| Data are expressed as medians ± interquartile range (IQR) | | | |

10 patients had pathological correlation and 5 patients had surgical resection, the results of which corroborated the method of reference clinical reads and resultant scores. Crohn's disease activity score grades showed excellent intra-observer and method of reference agreement (table 5.6). Agreement for the detection of Crohn's related findings in the small intestine, colon, peri-enteric and peri-colonic tissues on modified dose CT with MBIR vs. conventional dose CT with ASiR 40% images is also summarized in Table 5.7.

Table 5.7: Cohen's Kappa agreement scores for CDAS and clinical findings comparing modified dose CT with MBIR and conventional dose CT with ASiR 40% with the method of reference read and with each other for each reader.

| | Reader 1 | | | Reader 2 | | |
|-------------|---------------|-----------------------|----------------|---------------|-----------------------|----------------|
| | Modified MBIR | Conventional ASiR 40% | Intra-observer | Modified MBIR | Conventional ASiR 40% | Intra-observer |
| CT findings | | | | | | |
| CDAS | 0.857 | 0.669 | 0.717 | 0.697 | 0.702 | 0.894 |
| Enteritis | 0.939 | 0.879 | 0.816 | 0.746 | 0.746 | 1.00 |
| Colitis | 0.746 | 0.805 | 0.816 | 0.866 | 1.00 | 0.866 |
| Stricture | 0.598 | 0.531 | 0.799 | 0.675 | 0.157* | 0.622 |
| Fistula | 0.719 | 0.719 | 1.00 | 0.617 | 0.617 | 1.00 |
| Abscess | 1.00 | 1.00 | 1.00 | 1.00 | 1.00 | 1.00 |

Statistical Agreement between gold standard read and MDCT MBIR or CDCT ASiR 40% is assessed using Cohen's kappa analysis (* denotes p value of >0.05). Intra-observer values compare the modified dose MBIR and conventional dose ASiR 40% findings for each reader.

There was perfect intra-observer agreement between modified dose MBIR and conventional dose ASiR 40% detection of abscesses and fistulas for both readers in addition to complete agreement for the detection of abscesses for both readers when compared with the Method of Reference reads, yielding sensitivity and specificity scores of 100% for each of these findings. There was almost complete intra-observer and Method of Reference agreement for modified dose MBIR and conventional dose ASiR 40% images for the detection of enteritis and colitis. Individual agreement was weakest, for the detection of strictures (table 5.7). All strictures recorded were subjectively short and were non-obstructing on both the modified dose MBIR and conventional dose ASiR 40% images. The sensitivity and specificity scores for strictures for reader 1, when compared with the Method of Reference reads, were 100% and 96.5%, respectively. For reader 2, the sensitivity and specificity scores for strictures were 60% and 96.9%, respectively.

Data regarding the detection of extra-intestinal findings in the abdomen and pelvis on modified dose MBIR vs. conventional dose ASiR 40% images are summarized in table 5.8. Reviewer 2 missed a single 3mm renal calculus and a 6mm hepatic simple cyst when interpreting the conventional dose ASiR 40% images. No additional extra-intestinal findings were demonstrated on the conventional dose CT with ASiR 40% images when compared with the modified dose MBIR images. Reader 1 had sensitivity and specificity scores of 100%. Reader 2 had sensitivity and specificity scores of 83.3% and 100%, respectively.

Table 5.8: Comparison of extra-intestinal CT findings between modified dose CT with MBIR and conventional dose CT with ASiR 40% for each reader.

| CT findings (n) | Reader 1 | | Reader 2 | |
|------------------------|---------------|-----------------------|---------------|-----------------------|
| | Modified MBIR | Conventional ASiR 40% | Modified MBIR | Conventional ASiR 40% |
| Hepatic Steatosis | 2 | 2 | 5 | 5 |
| Renal Calculi | 2 | 2 | 2 | 1* |
| Hepatic/Renal Cysts | 4 | 4 | 4 | 3* |
| Intraperitoneal fluid | 1 | 1 | 1 | 1 |
| Sacroiliitis | 2 | 2 | 3 | 3 |
| Ankylosing Spondylitis | 1 | 1 | 1 | 1 |

Data are expressed as absolute number (n) of each diagnostic finding identified on each CT series. Discrepant values are marked with *.

Image quality – objective analysis:

Overall and at each anatomical level, quantitatively measured objective image noise (defined as the standard deviation of the Hounsfield value within a region of interest) decreased progressively when modified dose CT images were reconstructed with FBP (117±18.3HU), ASiR 40% (77.7±12.2HU), ASiR 70%

($59.6 \pm 8.2\text{HU}$) and MBIR ($27.5 \pm 6.7\text{HU}$), respectively ($p < 0.0001$ for all comparisons). Objective image noise levels across the reconstruction protocols are summarized in figure 5.3. No significant difference in objective noise was found when modified dose MBIR images were compared with conventional dose ASiR 40% ($27.5 \pm 6.7\text{HU}$ vs. $26.2 \pm 5\text{HU}$) (paired t test; $P = 0.0549$).

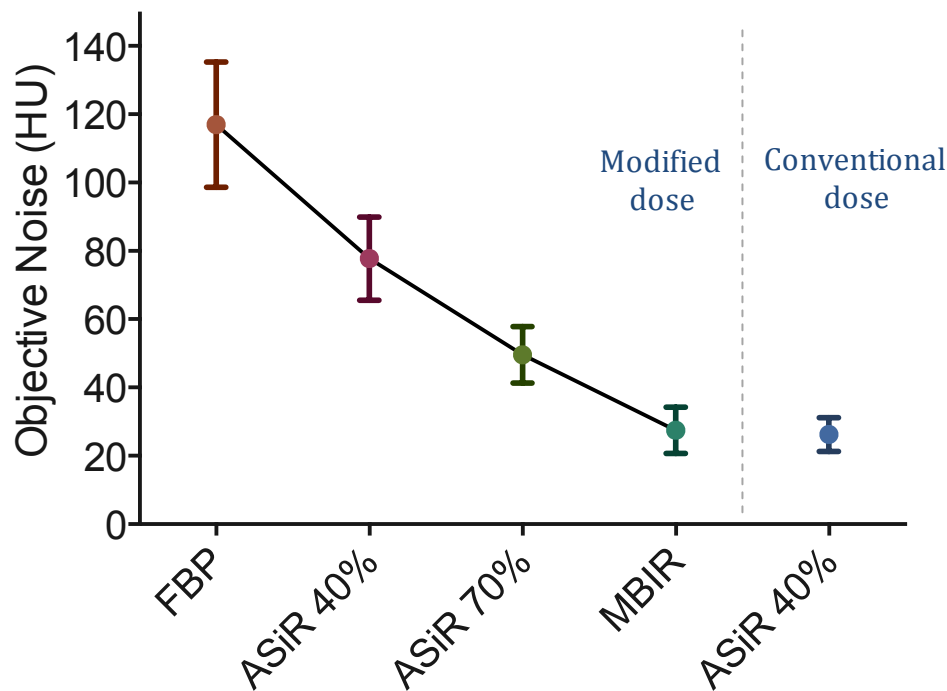


Figure 5.3: Line graph demonstrating the objective noise across the reconstruction protocols. There was no significant difference in objective noise between the modified dose MBIR images and conventional dose ASiR 40% images ($P = 0.0549$).

The effect of reconstruction protocol on absolute and percentage noise reduction is summarized in figure 5.4. Absolute noise reduction is calculated by subtracting the objective noise on modified dose images reconstructed with ASiR 40%, ASiR 70% and MBIR from the objective noise present on the modified dose FBP images and percentage noise reduction is derived by dividing this value by the objective noise on the modified dose images with FBP. Mean objective noise

reduction values in terms of absolute values and percentages for ASiR 40%, ASiR 70% and MBIR when compared with modified dose FBP are 39.23HU (33.5%), 67.38HU (57.6%) and 89.5HU (76.5%), respectively ($P<0.0001$).

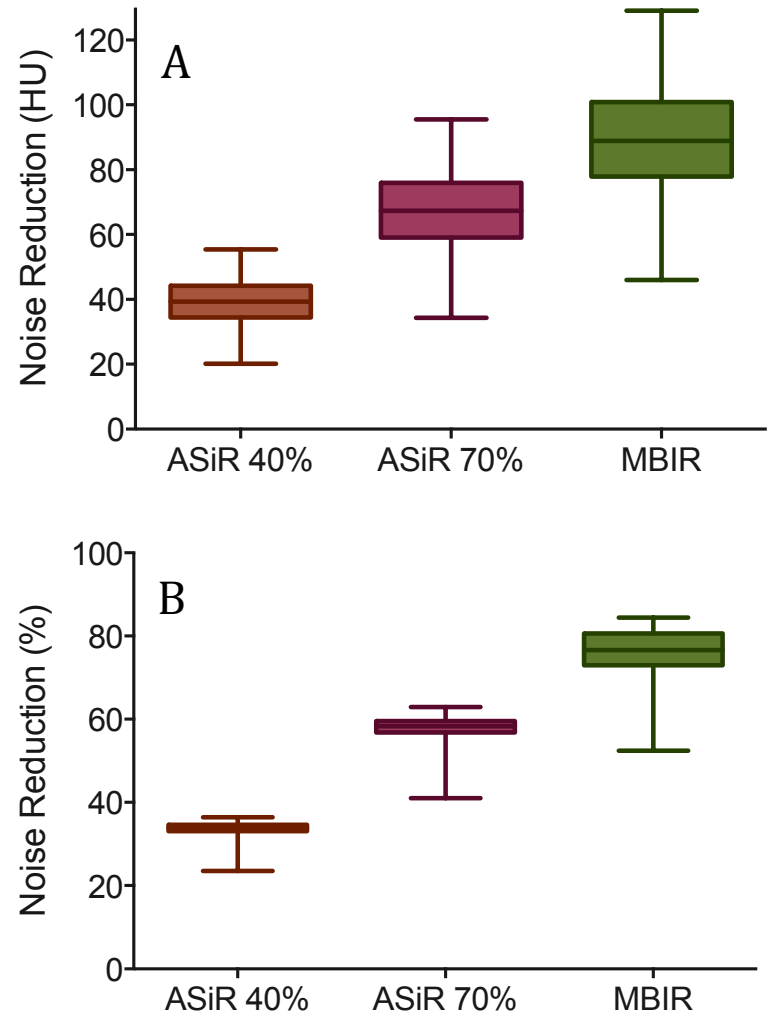


Figure 5.4 (A-B): Box and whisker plots demonstrating absolute (A) and percentage (B) noise reductions achieved with ASiR 40% and 70% and MBIR with modified dose CT using FBP as the reference comparison.

Effect of BMI on noise reduction:

Objective image noise was significantly higher in patients with a BMI of $<25\text{kg/m}^2$ compared with a BMI of $\geq 25\text{kg/m}^2$ on the modified dose MBIR images ($24.9\pm 3.9\text{HU}$ vs. $31.6\pm 8.2\text{HU}$, $P<0.0001$). There was also a significant difference in objective noise between patients with $\text{BMI}<25\text{kg/m}^2$ and those patients with $\text{BMI}\geq 25\text{kg/m}^2$ for the modified dose images reconstructed with FBP and ASiR 40% (P values of 0.03 and 0.042, respectively), but the difference for ASiR 70% was not significant ($P=0.093$). For conventional dose images reconstructed with ASiR 40% ($26.1\pm 4.9\text{HU}$ vs. $26.4\pm 5\text{HU}$) the difference was not significant ($P=0.7106$). For those reconstruction algorithms that demonstrated a statistically significant difference in objective noise between BMI groups, the actual magnitude of such differences is small ($<7\text{HU}$) so clinical significance is questionable.

The magnitude of noise reduction for each reconstruction protocol was then compared between patients with $\text{BMI}<25\text{kg/m}^2$ and $\text{BMI}\geq 25\text{kg/m}^2$. There was no significant difference in objective noise reduction between patients in each of the BMI groups on modified dose images reconstructed with MBIR (unpaired t test; $P=0.88$). There was a significant difference in mean objective noise between BMI groupings for the modified dose images reconstructed with ASiR 40% and 70% (p values from unpaired t tests of 0.025 and 0.027, respectively). Again, however, the difference between the means in each case is small ($<5\text{HU}$) suggesting a statistically but not clinically significant difference.

The difference in percentage of noise reduction between patients with BMI<25kg/m² and BMI≥25kg/m² was not significantly different for the ASiR 40% and 70% reconstructions of the modified dose dataset a P value of 0.55 for each comparison on unpaired t test. However, there is a statistically significant difference between percentage noise reductions for MBIR between BMI groups (P<0.0001). Interestingly, the percentage noise reduction is greater in the BMI<25kg/m² group (77.8±4.5%) than in the BMI≥25kg/m² group (73.5±6.7%). This mirrors the finding of greater overall objective noise in the BMI≥25kg/m² group when modified dose CT data are reconstructed with MBIR.

Image quality – subjective analysis:

Subjective image quality indices across the examined reconstruction protocols are graphically demonstrated in figure 5.5 (A-E). Median diagnostic acceptability, spatial resolution and contrast resolution scores were significantly greater and subjective noise significantly lower on the conventional dose CT images with ASiR 40% compared with all modified dose datasets (FBP, ASiR 40%, ASiR 70%, MBIR) (Friedman test with Dunn's multiple comparisons test, p<0.0001 for all comparisons). Subjective image quality scores were significantly better for modified dose MBIR images compared with the modified dose CT datasets reconstructed with ASiR 40%, ASiR 70% and FBP (p<0.0001 for all comparisons). Modified dose MBIR images had above average to excellent diagnostic acceptability, subjective noise, spatial and contrast resolution scores. Median streak artifact scores were significantly less on the modified dose MBIR images compared with the conventional dose ASiR 40% images (p<0.001).

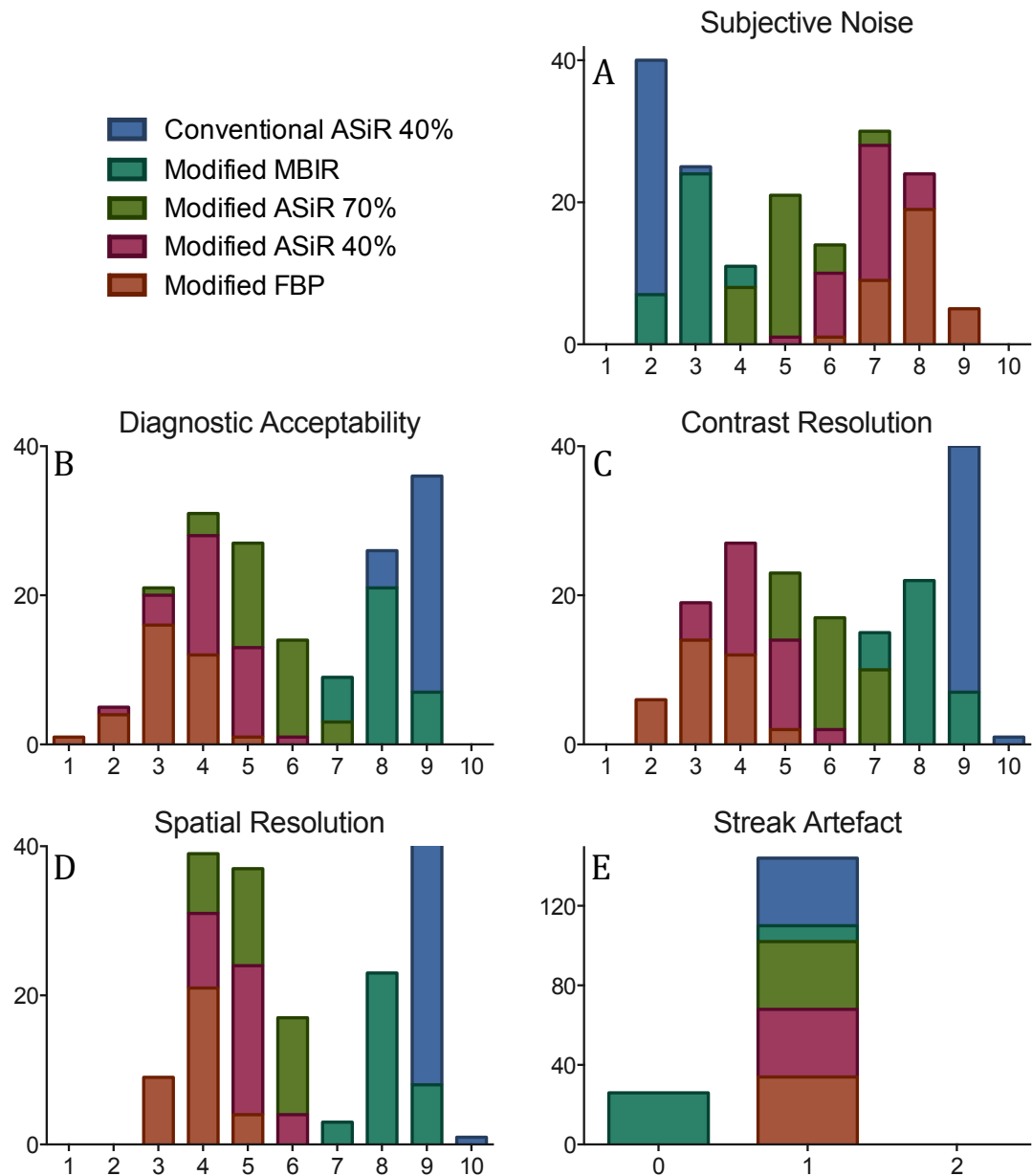


Figure 5.5 (A-E): Stacked bar graphs demonstrating the distribution of overall median image quality scores [subjective noise (A), diagnostic acceptability (B), contrast resolution (C), spatial resolution (D), streak artifact (E)] for each of the reconstruction protocols studied. The y-axis in each graph represents the number of patients with a given score.

There was no significant difference between the subjective image quality indices (diagnostic acceptability, subjective image noise, contrast resolution, spatial resolution and streak artifact) for patients with BMI<25kg/m² and those with

BMI $\geq 25\text{kg/m}^2$ for any of the modified or conventional dose reconstruction algorithms used (Kruskal-Wallis test with Dunn's multiple comparisons test; $p > 0.05$ for all comparisons).

Figures 5.6-5.10 below demonstrate both modified and conventional dose CT images of Crohn's disease related findings. Figure 5.11 demonstrates an incidental finding of a porcelain gallbladder.

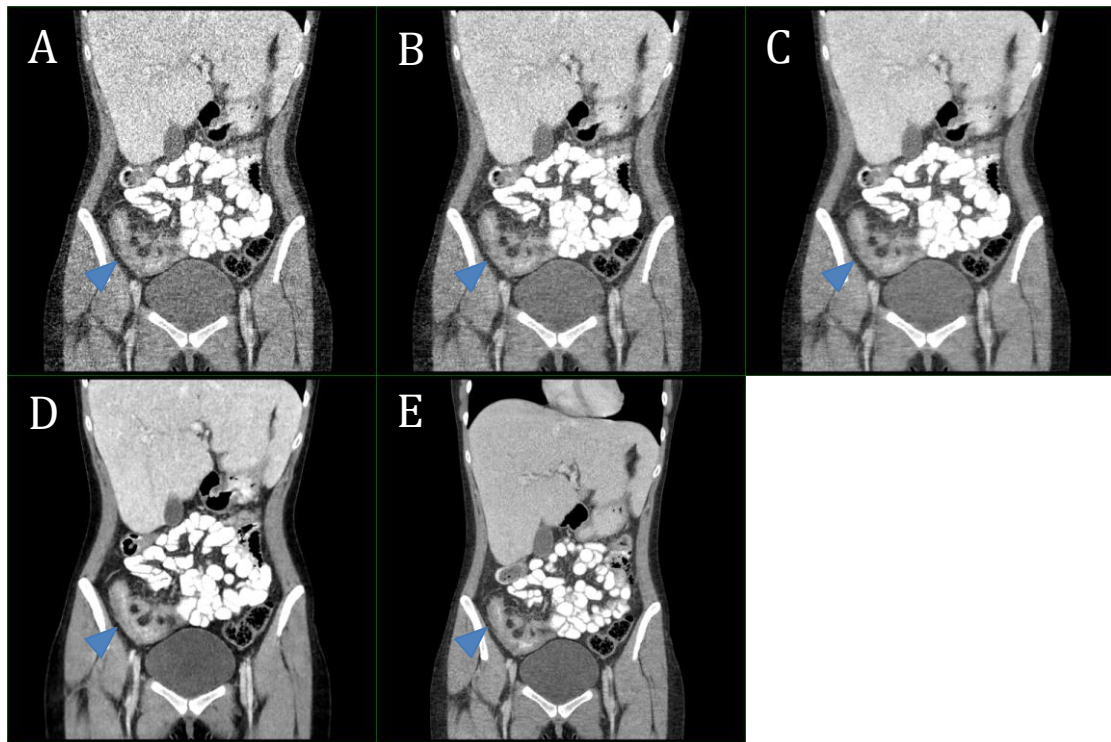


Figure 5.6 (A-E): Coronal reconstructions of modified dose CT images with FBP (A), ASiR 40% (B), ASiR 70% (C) and MBIR (D) with conventional dose CT with FBP for comparison (E). Images depict active Crohn's enteritis in the right iliac fossa (blue arrowhead) in a 26 year old lady with a BMI of 17.8kg/m^2 . The modified dose CT was acquired at 0.52mSV and the conventional dose CT at 2.3mSV .

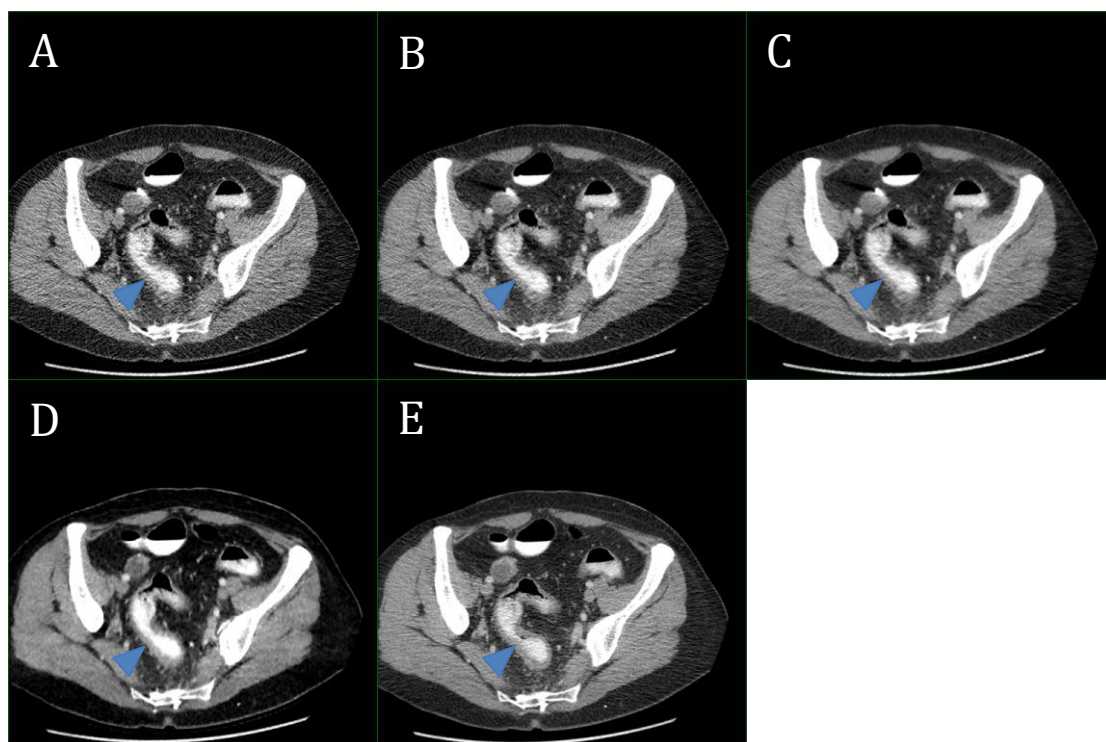


Figure 5.7 (A-E): Axial reconstructions of modified dose CT images with FBP (A), ASiR 40% (B), ASiR 70% (C) and MBIR (D) with conventional dose CT with FBP for comparison (E). Images depict active Crohn's colitis of the sigmoid colon with local mesenteric fat stranding and vascular injection (blue arrowhead) in a 43 year old lady with a BMI of 24.2 kg/m². The modified dose CT was acquired at 1mSV and the conventional dose CT at 4mSV.

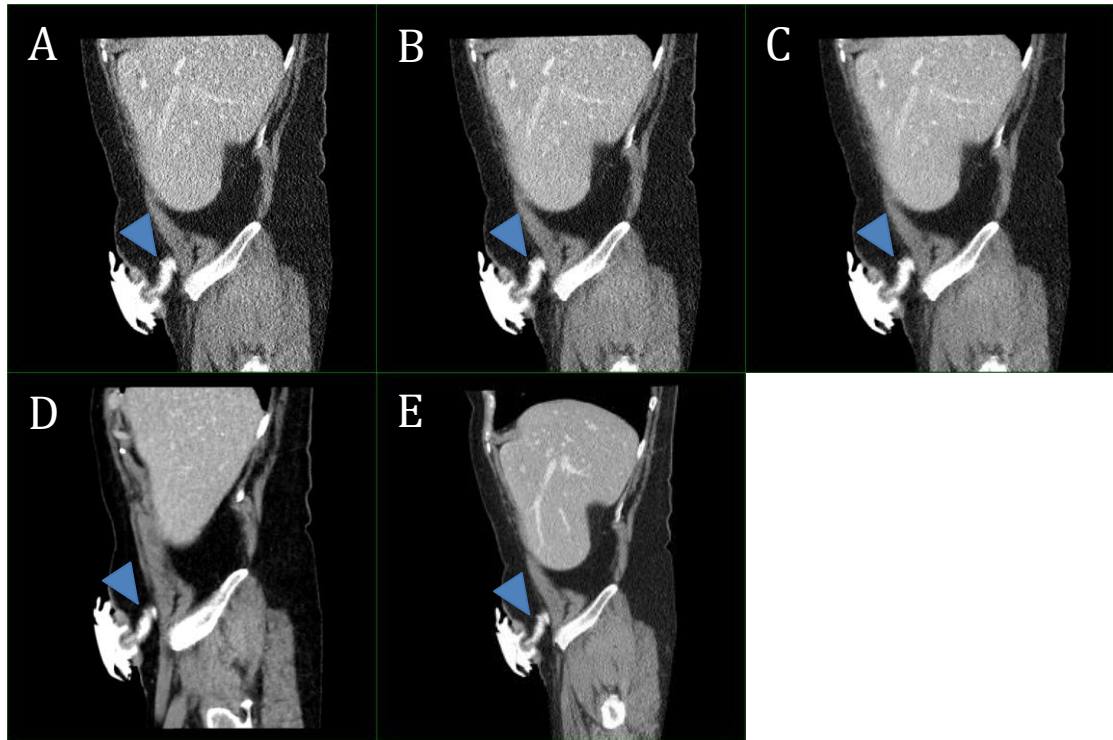


Figure 5.8 (A-E): Sagittal reconstructions of modified dose CT images with FBP (A), ASiR 40% (B), ASiR 70% (C) and MBIR (D) with conventional dose CT with FBP for comparison (E). Images demonstrate an uncomplicated end ileostomy in the right iliac fossa (blue arrowhead) in a 68 year old lady with a BMI of 22.8 kg/m². The modified dose CT was acquired at 1mSV and the conventional dose CT at 3.7mSV.

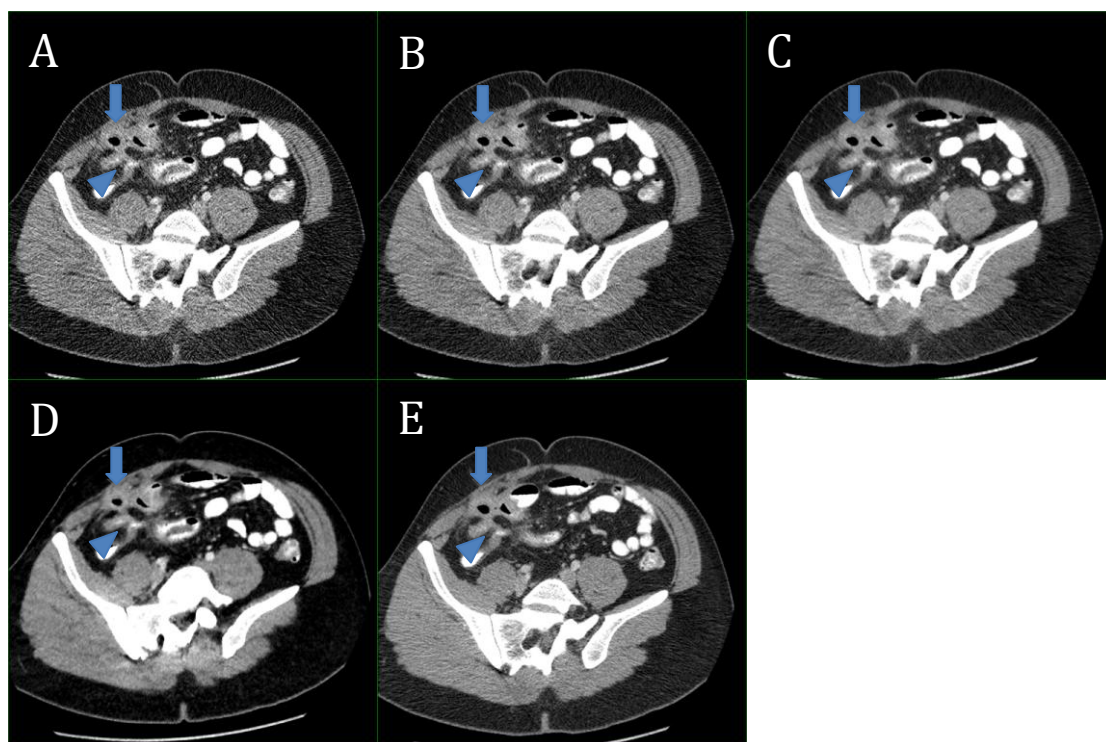


Figure 5.9 (A-E): Axial reconstructions of modified dose CT images with FBP (A), ASiR 40% (B), ASiR 70% (C) and MBIR (D) with conventional dose CT with FBP for comparison (E). Images demonstrate penetrating disease with an ileo-ileal fistula in the right iliac fossa (blue arrow) with local extraluminal gas indicating perforation (blue arrowhead) in a 31 year old man with a BMI of 26.9 kg/m². The modified dose CT was acquired at 1.6mSV and the conventional dose CT at 6.5mSV.

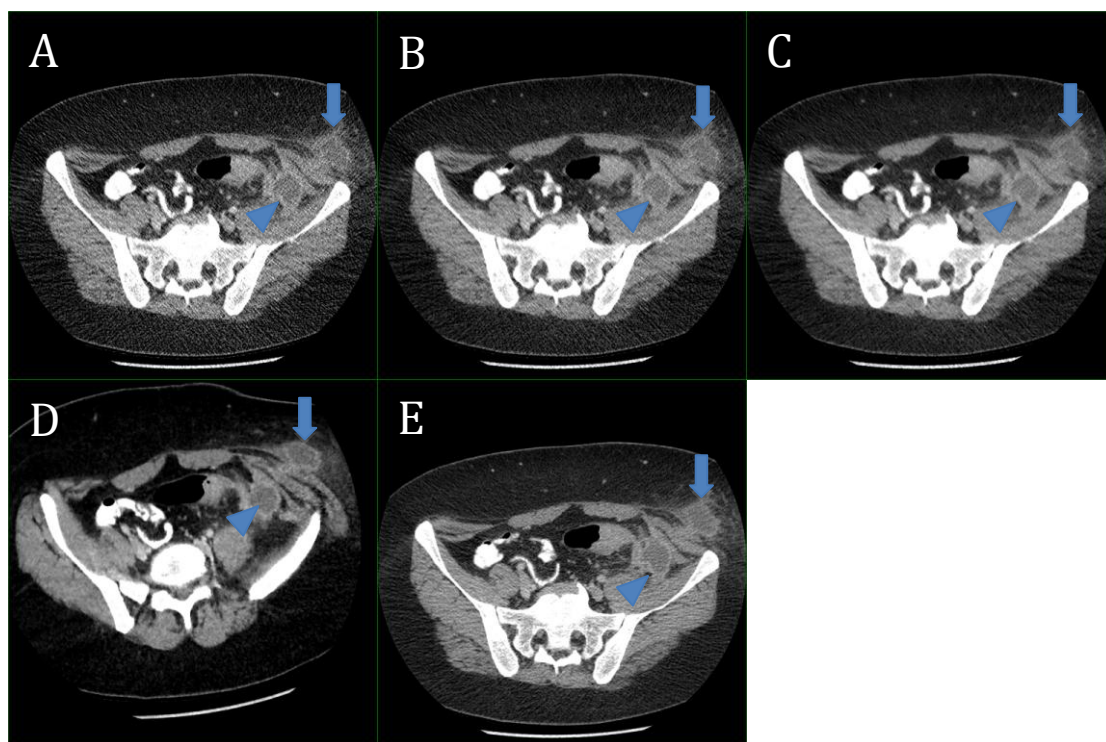


Figure 5.10 (A-E): Axial reconstructions of modified dose CT images with FBP (A), ASiR 40% (B), ASiR 70% (C) and MBIR (D) with conventional dose CT with FBP for comparison (E). Images depict two abscess collections (one superficial labelled with blue arrow and one deep labelled with blue arrowhead) in the left iliac fossa in a 28 year old lady with a BMI of 32.3 kg/m². The modified dose CT was acquired at 3.2mSV and the conventional dose CT at 10mSV.

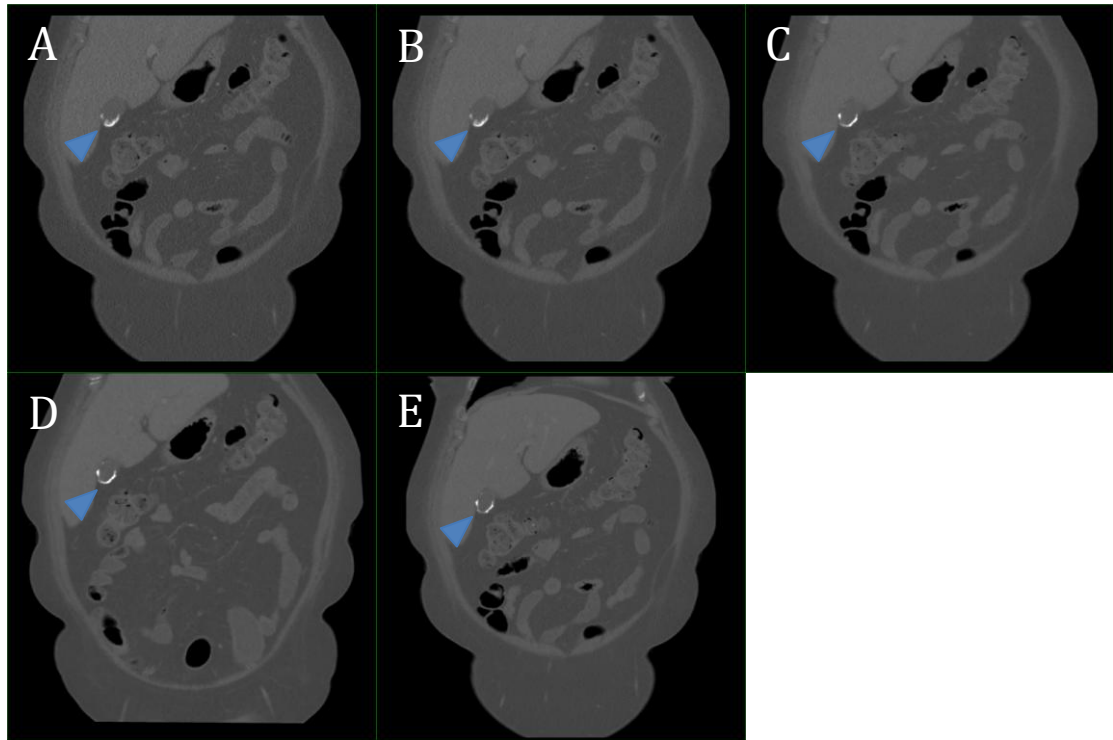


Figure 5.11 (A-E): Coronal reconstructions of modified dose CT images with FBP (A), ASiR 40% (B), ASiR 70% (C) and MBIR (D) with conventional dose CT with FBP for comparison (E). Images demonstrate an incidental porcelain gallbladder (blue arrowhead) in a 66 year old lady with a BMI of 35.5 kg/m². The modified dose CT was acquired at 2.8mSV and the conventional dose CT at 11mSV.

Discussion:

The primary aim of this study was to demonstrate the feasibility of a modified dose CT protocol, which would reduce the effective dose of a CT abdomen and pelvis to within the one-millisievert range using MBIR in patients with active Crohn's disease. The mean effective dose achieved using the modified dose CT protocol was 1.27mSv (DLP 88mGy.cm), which compares favorably with other recent low dose CT studies including Kambadakone et al who achieved a DLP of 380.3mGy.cm when performing low dose MDCT with hybrid IR on a cohort of 48 patients with Crohn's disease and a DLP of 408mGy.cm when performing low dose CT enterography with hybrid IR on a cohort of 16 Crohn's patients [169]. Lee et al achieved a DLP of 182 mGy.cm when performing low dose CT Enterography with hybrid IR in a further 91 patients with CD [118]. Vardhanabhuti et al [66] reported dose reductions of 76% with preservation of image quality but suboptimal assessment at 85% dose reduction at low dose abdominal CT with MBIR.

The scale of dose reduction desired for our modified dose CT protocol (less than 50% of DLP reported in other low dose studies involving Crohn's patients) necessitated a feasibility study with careful intra-individual control using contemporaneously acquired conventional dose CT as the reference standard. Comparison of the diagnostic yield of the index test (modified dose CT with MBIR) and reference standard (conventional dose CT with ASiR 40%) in our study indicates that sub-100mGy.cm abdominopelvic CT is feasible in patients with active Crohn's disease when MBIR reconstruction is used. The clinical indication for CT was addressed and answered satisfactorily in all cases. There

was perfect agreement for the detection of extramural penetrating complications that would significantly alter patient management such as abscess, albeit affecting a small number (n=5, 14.7%) of patients in this study. Nevertheless, a large proportion of patients had enteritis or colitis (n=20 (58.8%) and n=24 (70.6%), respectively), and this was appropriately detected and characterized. There was almost complete agreement between modified dose CT with MBIR and conventional dose CT with ASiR 40% images for the detection of enteritis and colitis but agreement was admittedly weaker for the detection of intestinal strictures, similar to chapter 3. The strictures imaged in this study sample were uniformly low grade, which may have contributed to subjective interpretational discrepancies, and importantly no stricture was missed on the modified dose CT with MBIR images. The issue of detection and characterization of strictures is a difficult one. CT abdominopelvic acquisitions and even CT enterography are disadvantaged compared to MR enterography or barium studies because CT relies on a single image acquisition compared to MR enterography or barium studies where multiple views and even cine views (MR) are feasible. Therefore, peristalsis can be confused with non-obstructing strictures; this is a possible explanation of lower than expected correlation between image sets. Similarly, there were discrepant interpretations of the presence of other Crohn's disease complications such as colitis. It is important to remember that interpretation of findings such as these, in everyday practice is very often subjective even among experts in the field. The clinical review in this study was performed by two experienced fellowship-trained abdominal radiologists. As in the case of the strictures, only five patients each had endoscopy or surgery, therefore it is not possible to make a judgment of who "over-called" or "under-called". We would

argue however, that the purpose of this study is the assessment of whether modified dose CT studies reconstructed with full IR can retain diagnostic accuracy versus a standard dose protocol and that intra-reader agreement is vitally important in answering that question. Intra-reader correlation for detection of a wide range of Crohn's complications for modified dose CT with MBIR and conventional dose CT with ASiR 40% was overall very satisfactory (see table 5.7). In addition it is reassuring that, in the five patients who had surgery during the follow-up period, findings on CT were confirmed in all cases at the time of surgery.

Image quality analysis demonstrated no statistically significant difference in objective image noise between the modified dose CT with MBIR and conventional dose CT with ASiR 40% images acquired at almost four times the radiation dose of the modified dose protocol. Interestingly, we found that objective image noise was greater in patients with a BMI $\geq 25\text{kg/m}^2$ when the modified dose protocol was reconstructed with MBIR, FBP and ASiR 40%. This finding was not replicated with conventional dose CT reconstructed with ASiR 40%. In an attempt to determine the cause of this difference we retrospectively reviewed the peak mA data from the both arms of the split dose CT protocol and found that the automated tube current modulation maximum tube current threshold (350mA) was not reached in any case while using the modified or conventional dose protocol. It is therefore likely the statistical difference in image noise between the BMI $< 25\text{kg/m}^2$ and BMI $\geq 25\text{kg/m}^2$ subgroups for the modified dose CT protocol maybe related to the reduced tube voltage of 100kV employed in the modified dose protocol. CT of the abdomen and pelvis using a

reduced tube voltage has previously been shown to accentuate beam hardening and streak artifacts in patients with an increased BMI [132]. This may also account for the superior percentage noise reduction achieved with $\text{BMI} < 25 \text{ kg/m}^2$ when compared with $\text{BMI} \geq 25 \text{ kg/m}^2$ when the modified dose protocol is reconstructed with MBIR – artifacts and beam hardening may interfere with noise reduction in larger patients.

In a previous study using an identical CT acquisition protocol (chapter 3), we found that diagnostic accuracy was maintained when the modified dose images were reconstructed with ASiR 40% [161-162]. The key difference between that work and the present study is that we now demonstrate that image quality is compromised to a far less degree when a pure iterative reconstruction algorithm such as MBIR is employed. Subjective analysis of the modified dose images in this study showed reduced subjective noise and significantly superior diagnostic acceptability, contrast and spatial resolution when the modified dose MBIR images were compared with modified dose CT images reconstructed with hybrid iterative reconstruction (ASiR). Diagnostic acceptability, spatial resolution and contrast resolution were graded as acceptable to poor when ASiR 40% was employed. In comparison, the MBIR images were graded as above average to excellent. Median image quality scores were significantly lower when the modified dose MBIR images were compared with conventional dose CT with ASiR 40% and subjective image noise was also graded to be significantly worse on the modified dose MBIR images. We therefore found a discrepancy between the subjective comparison of image noise, which demonstrated superiority of the conventional dose with ASiR 40% dataset, and objective image noise analysis,

which showed no significant difference between the modified dose with MBIR and conventional dose with ASiR 40% images. One possible explanation for this discrepancy was that the reviewers who performed the subjective analysis were not accustomed to the different appearance of the images reconstructed with MBIR. We would describe the different quality of the modified dose with MBIR images as being mildly “mottled” or “pixelated” but expert opinion in this area suggests that imagers tend to adapt to the new quality of these images in a relatively short period of time [174].

There are a number of limitations to this study. As outlined in chapter 3, we calculate dose reduction compared with the conventional dose dataset (80-90% of standard dose) rather than with the standard of care departmental CT dose (7.84mSv) – therefore, a more accurate estimation of overall dose reduction achieved with the modified dose protocol is 83.4% when comparison is made to standard CT imaging. Our scanning protocol was designed to improve the detection of extramural complications, which were clinically suspected in all recruited patients. Positive rather than neutral oral contrast agents were used to increase the conspicuity of small abscesses and localized perforations. The delay in imaging after administration of IV contrast in our study was (40 seconds after ‘peak aortic opacification’ which works out at 60-65 seconds; use of this protocol in patients with known Crohn’s disease has been shown to result in satisfactory depiction of small and large intestinal inflammation when compared with magnetic resonance enterography [143]. However, as addressed in chapter 3, a change in thinking in the time period of this work mean that CT enterography now occupies a more prominent position in imaging of Crohn’s disease. Our

research group has addressed this by running a tandem clinical trial of modified dose CT enterography with ASiR and MBIR [115].

It should be emphasized that the reduction in dose achieved in this study was achieved by design of the modified dose protocol, which included a lower tube voltage of 100kV, selected to allow sufficient mA range for effective tube current modulation. The role of MBIR was to reduce noise, improve spatial resolution and ultimately improve diagnostic acceptability and yield from these modified dose images. With regard to the modified dose protocol, the tube potential difference was not varied with BMI or patient size, in order to standardize the protocol (i.e. kept at 120kV for the conventional dose and 100kV for the modified dose). It is worth noting that encouraging results have been shown with automated attenuation-based tube voltage selection [175-178] with dose reductions of up to 56% reported. Automated tube voltage modulation was not examined in our study, as this technology was not locally available. Blinding of the reviewers as to the scanning protocol during clinical interpretation was also not possible as the modified dose MBIR images had an obviously different appearance compared with conventional dose CT images with ASiR 40%. Hybrid and pure iterative reconstruction algorithms from only a single vendor (GE Healthcare, Waukesha, WI) were assessed and MBIR currently has a relatively long reconstruction time (10-90 minutes per dataset) compared with FBP and ASiR, which are computationally efficient and quick. Perhaps the greatest limitation of our study is the narrow subgroup included, namely patients with an exacerbation of known Crohn's disease who had a clinically suspected extramural complication. It is therefore not possible to extrapolate our study

findings to other gastrointestinal and abdominal disorders. We did not include pediatric Crohn's patients and we did not include patients who presented to the emergency department acutely. The results of our study would therefore not be entirely applicable to these groups at present. Importantly our findings also do not apply to patients who do not yet have a confirmed diagnosis of Crohn's disease; direct endoscopy, magnetic resonance or CT enterography would be more appropriate for imaging in that clinical context [179].

Conclusion:

MBIR reduces image noise in modified dose CT data to the level found in images acquired at a 269% higher dose reconstructed with 40% ASiR and results in images that allow complete clinical agreement for the detection of extramural complications of Crohn's disease and satisfactory agreement for the detection of enteritis and colitis. Abdominopelvic CT using MBIR is feasible in patients with active Crohn's disease. Dose reductions in the range of 72.9% over the conventional dose protocol (83.4% over standard departmental CT of abdomen and pelvis) are possible with little compromise in image quality using MBIR. Further research should focus on the dose limits of this technique, particularly in patients with a high BMI and the interpretation of IR images, which have an unfamiliar quality.



Chapter 6

Dose-equivalent CT with model based iterative reconstruction as a replacement for the abdominal radiograph in patients with Crohn's disease

Iterative Reconstruction as a Novel Method of Radiation Dose Reduction
at Computed Tomography in Patients with Crohn's Disease

Introduction:

Radiation dose to the population from medical imaging is increasing with strong and growing concern among the medical and lay populations. With approximately 50% of the average radiation dose to the population coming from medical exposures and a quarter due to computed tomography (CT) alone, justification and optimisation of all medical imaging that utilises ionising radiation is of utmost importance [180]. The population we examine in this thesis, namely patients with Crohn's disease, have been demonstrated 'at risk' for exposure to high levels of cumulative radiation during years, and sometimes decades, of active disease [13]. The ALARA (as low as reasonably achievable) principle is employed to optimise CT imaging, aiming to keep radiation doses to patients as low as practicable whilst ensuring the CT images are of sufficient quality for accurate diagnosis. The magnitude of dose reduction possible with traditional CT data reconstruction was limited by a parallel relationship between image quality and dose, where a reduction in radiation dose at CT resulted in an increase in image noise and poorer image quality. In chapters 3 and 5 we demonstrated the superior noise reduction properties of ASiR and MBIR, respectively, when applied to modified dose CT protocols in which dose reductions in the order of 73% still yielded sufficient quality images that were non-inferior to conventional dose CT in terms of diagnostic findings.

Before the advent of cross-sectional imaging, the plain abdominal radiograph was an essential component in the evaluation of patients presenting with an 'acute abdomen' [181]. The plain abdominal radiograph is now largely defunct in terms of imaging in patients with suspected acute or active Crohn's disease, with

few specific indications. The American College of Radiologists recommend abdominal radiograph only when the patient is unstable with a high suspicion of visceral perforation [182]. The Royal College of Radiologists suggest abdominal radiographs are only indicated in cases of suspected acute bowel obstruction and for the diagnosis and monitoring of acute toxic dilatation [183]. The European evidence based consensus on the diagnosis and management of Crohn's disease do not even mention abdominal radiograph in the diagnostic pathway [142]. The two main generally-accepted purposes that plain abdominal radiograph serve in patients with Crohn's disease serve are (1) to assess for the presence of intestinal obstruction and (2) to evaluate for pneumoperitoneum prior to further radiological/surgical work-up.

The estimated mean ionising radiation exposure (i.e. effective dose) from a single abdominal radiograph is approximately 0.7mSv (equivalent to 35 chest radiographs) [150]. The European mean effective dose for an abdominal radiograph is 0.9mSv [31]. Despite being essentially obsolete with its results contributing to patient management in only a small percentage of cases, the abdominal radiograph remains a commonly requested radiological examination in the emergency setting [184-187]. Suggested reasons for this include: force of habit, relatively low cost, ease of availability, to 'be seen to do something' while waiting for CT, and lower radiation exposure compared with CT. Looking generally at the yield of abdominal radiographs in emergency departments, it has been suggested that their excessive use adds financial strain, increases patient discomfort and may even be a source of future litigation [188].

Diagnostic imaging is frequently essential for patients with Crohn's disease at initial diagnosis, for monitoring response to therapy, and for peri-operative evaluation and these patients may undergo repeated imaging studies over years of illness [13,167]. A large retrospective study by our group of imaging patterns in 409 patients with Crohn's disease over a 15 year period demonstrated that plain film radiography, including abdominal radiographs, accounts for approximately 60% of all imaging studies in these patients [13]. Worryingly, during the study period (1992-2007), while the use of CT increased almost fourfold from 5.2% (46.3% of diagnostic radiation exposure) of imaging studies in the first five years to 19.7% (84.7% of diagnostic radiation exposure) in the final five year period, the use of plain radiography remained constant [13]. Normal and abnormal radiographs are equally likely to result in progression to further imaging, usually CT, within 5 days [189]. While the radiation dose of abdomino-pelvic CT (circa 8mSv) greatly exceeds that of an abdominal radiograph (circa 0.7mSv), the higher diagnostic yield often justifies the use of CT.

The use of modified dose CT with iterative reconstruction at radiation doses approximating to that of an abdominal radiograph has been validated for abdominal CT and, particularly, in assessment for suspected acute complications of Crohn's disease [115,118,161-162,169]. The aims of this study are (1) to compare the diagnostic yield of contemporaneous modified dose CT with MBIR with plain abdominal radiograph in patients with Crohn's disease, (2) to establish whether modified dose CT with MBIR represents a feasible replacement for initial radiograph in the assessment of these patients and (3) to

explore whether modified dose CT may obviate the need for progression to conventional dose CT.

Methods:

This is a secondary analysis of CT data acquired for the validation of model based iterative reconstruction in achieving diagnostic quality CT at markedly reduced radiation doses. Concise methods have been published elsewhere [161-162] and are described in detail in chapters 3 and 5.

Briefly, 50 consenting patients, who required a CT of abdomen and pelvis for clinical indications, underwent both conventional dose and modified dose CT of abdomen and pelvis on a 64-slice CT scanner (GE Lightspeed VCT-XTe) as part of an IRB-approved research protocol [ClinicalTrials.gov Identifier NCT 01244386]. Of these 50 patients, 23 underwent a contemporaneous plain abdominal radiograph (within 24 hours of the CT scan) and this cohort form the population for the current study (summarized in figure 6.1 below).

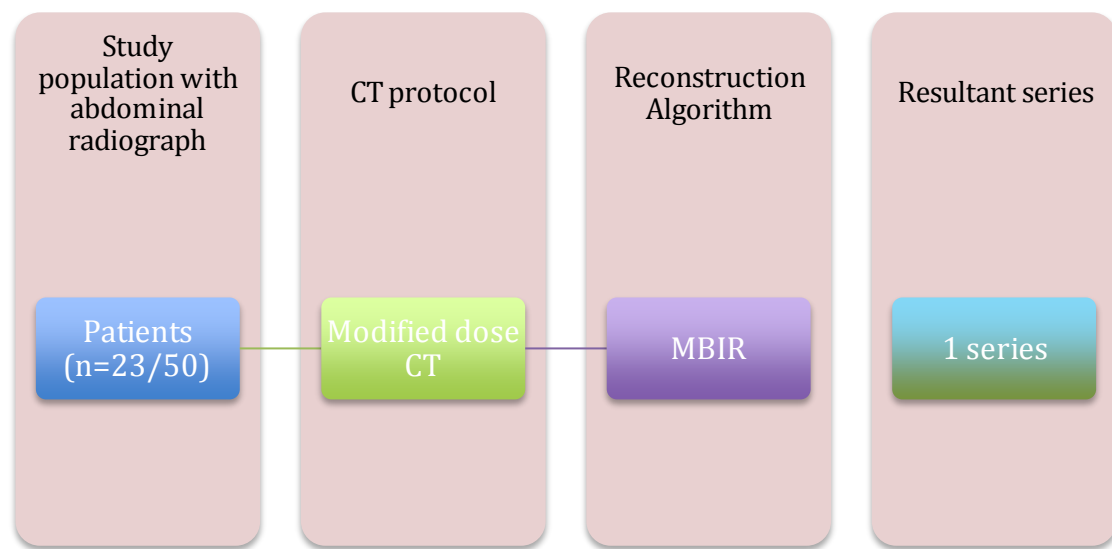


Figure 6.1: summary of the study population. Twenty-three of fifty patients who underwent the split dose CT protocol had a contemporaneous plain abdominal radiograph.

The conventional dose protocol comprised CT of abdomen and pelvis acquired at approximately 90% of the radiation dose of the standard departmental CT of abdomen and pelvis protocol (tube voltage 120kV, noise index 38%, gantry rotation time 0.8s). The modified dose protocol comprised CT of abdomen and pelvis acquired at approximately 10% of the radiation dose of standard departmental CT of abdomen and pelvis (tube voltage 100kV, noise index 70%, gantry rotation time 0.5s). All patients were imaged in the portal venous phase of intravenous contrast with the low dose protocol first, followed by the conventional dose protocol 6.2s later. For both protocols z-axis automated tube current modulation resulted in a variable tube current, with minimum and maximum tube current thresholds of 20 and 350mA respectively.

For this study, we examined the modified dose series only, with the prior knowledge that this series is non-inferior to conventional dose CT in terms of diagnostic accuracy (see chapter 5). Modified dose CT raw data were reconstructed with MBIR (standard) only for direct comparison with the abdominal radiographs. Studies were anonymised and reviewers were blinded to all clinical details other than a known history of Crohn's disease with a suspected current complication. Reviewers were informed that the CT images were from a modified dose CT protocol with MBIR reconstruction. They were unable to access the conventional dose CT images, any previous imaging, or the reports of these.

All CT images were reviewed on a dedicated advanced imaging workstation (Advantage Workstation, VolumeShare 3, version 4.4, GE Medical Systems,

Milwaukee, USA) on a soft tissue window setting (window width, 400HU window level, +40HU) with axial reconstructions only and a slice thickness of 3mm. Images were reviewed in consensus by two radiologists. The abdominal radiographs were reviewed, again in consensus, nine months later by the same two readers on a PACS workstation (Impax 6.3.1, Agfa Healthcare, Morstel, Belgium). CT and radiographic images were reported in a standard manner, with particular reference to the presence and/or severity of bowel, peritoneal, or penetrating disease, as well as previous surgery and incidental findings. The presence/absence of the following features were specifically mentioned: large/small bowel oedema, large/small bowel dilatation, small bowel displacement, toxic megacolon, pneumatosis, pneumoperitoneum, abscess, ileus/obstruction. Disease severity was also graded using an adapted version of a validated Crohn's specific coding system [153].

All patients had their weight (kg) and height (m) measured and their body mass index (BMI, kg/m²) calculated at time of CT. CTDI_{vol} (mGy) and DLP (mGy.cm) values for each study were obtained from the scanner dose report. The effective diameter for each patient was derived as per AAPM methods from the mid-slice antero-posterior and lateral diameters [97]. The SSDE was then calculated by multiplying the CTDI_{vol} by the corresponding correction factor [97]. The imaging performance and assessment in CT (ImPACT) patient dosimetry calculator was used to calculate the effective doses using the original scanning parameters for the modified dose CT. Departmental audit [unpublished audit over a two year period] established the mean standard dose for an abdominal radiograph to be 0.7mSv. Due to difficulties in precise calculation of effective dose from the Dose

Area Product (DAP) for each radiograph, for simplicity the mean departmental value was taken as the mean dose for a single abdominal radiographic exposure. In many cases of larger size patients, a dose estimate of 0.7mSv is conservative due to the need to increase dose to achieve tissue penetrance and due to the relatively frequent need for more than one exposure to adequately cover the entire abdominal volume. In cases where more than one film was acquired, total dose was calculated by multiplying the film dose by that number.

Statistical analysis

Data compilation and statistical analyses were performed using Microsoft Excel (Microsoft Corporation, Redmond, WA) and GraphPad Prism version 6.0 (GraphPad Software Incorporated, San Diego, CA). Descriptive statistics are provided in terms of means with standard deviations for parametric values. Parametric variables were compared with paired t-tests. Pearson correlations were used for parametric variables. The criterion for significance was taken as $P < 0.05$.

Results:

Study population:

The included population comprised 23 patients with Crohn's disease (15 female; 8 male) with a mean age of 37.9 ± 14.6 years (range, 19-69 years). The mean population BMI was $24.4 \pm 4.7 \text{ kg/m}^2$ (range, 17.4-35.5 kg/m^2).

Radiation dose of abdominal radiograph:

Extrapolating from the departmental audit radiation dose for abdominal radiographs of 0.7mSv, the mean effective dose for abdominal radiographs in this study was $0.97 \pm 0.35 \text{ mSv}$ (range, 0.7-1.4mSv). The abdominal radiograph study comprised of a single radiograph for 14 patients (mean BMI $22.8 \pm 4.2 \text{ kg/m}^2$; mean effective diameter $26.3 \pm 2.9 \text{ cm}$) and two radiographs for nine patients (mean BMI 26.8 kg/m^2 ; mean effective diameter $29.9 \pm 5 \text{ cm}$). The BMI and effective diameter were significantly greater for those patients who required greater than one film to complete the study ($P=0.05$ and 0.039 , respectively).

Radiation dose of modified dose CT:

The mean radiation doses for the modified dose CT protocol are summarised in table 6.1. Because this study compares CT with conventional radiographs, effective dose expressed in mSv is used as the dose metric in all further comparisons [100]. Comparison with the corresponding conventional dose CT protocol (mean effective dose $4.73 \pm 2.59 \text{ mSv}$; range, 2.1-11mSv) demonstrated a 74% reduction in effective dose ($P<0.0001$) with the modified dose protocol.

Table 6.1: Summary of radiation dose for the modified dose CT protocol

| Radiation dose metric | Dose | Range |
|---------------------------|--------------|--------------|
| CTDI _{vol} (mGy) | 1.99±1.09mGy | 0.72-4.75 |
| DLP (mGy.cm) | 84.15±45.59 | 32.45-195.23 |
| Effective diameter (cm) | 27.67±4.14 | 20.84-38.42 |
| SSDE (mGy) | 2.51±0.99 | 1.25-4.28 |
| Effective dose (mSv) | 1.22±0.7 | 0.46-2.8 |

As before, with the modified dose CT protocol there are significant and very strong correlations between increasing radiation dose and patient BMI (Pearson coefficient 0.91, $P < 0.0001$) and effective diameter (Pearson coefficient 0.89, $P < 0.0001$). The mean effective dose for underweight or normal patients (with a BMI of $< 25 \text{ kg/m}^2$, $n=14$) was $0.8 \pm 0.24 \text{ mSv}$ (range, 0.46-1.4mSv). The mean effective dose for overweight or obese patients (with a BMI of $\geq 25 \text{ kg/m}^2$, $n=9$) was $1.81 \pm 0.64 \text{ mSv}$ (range, 1-2.8mSv).

Dose comparison:

Figure 6.1 summarises the effective dose relationships of abdominal radiographs, modified dose CT with MBIR, conventional dose CT and standard of care departmental CT. Paired t testing comparing the mean effective doses of the plain abdominal radiograph with modified dose CT demonstrates no significant difference ($P=0.09$, mean difference 0.22mSv). For patients with a BMI of $< 25 \text{ kg/m}^2$, the mean effective dose for the modified dose CT was not significantly different from that of the corresponding abdominal radiographs ($P=0.1021$). For patients with a BMI of $\geq 25 \text{ kg/m}^2$, the mean effective dose of the modified dose CT exceeded that of the abdominal radiographs ($P=0.0015$, mean difference 0.8mSv). See figure 6.2 below.

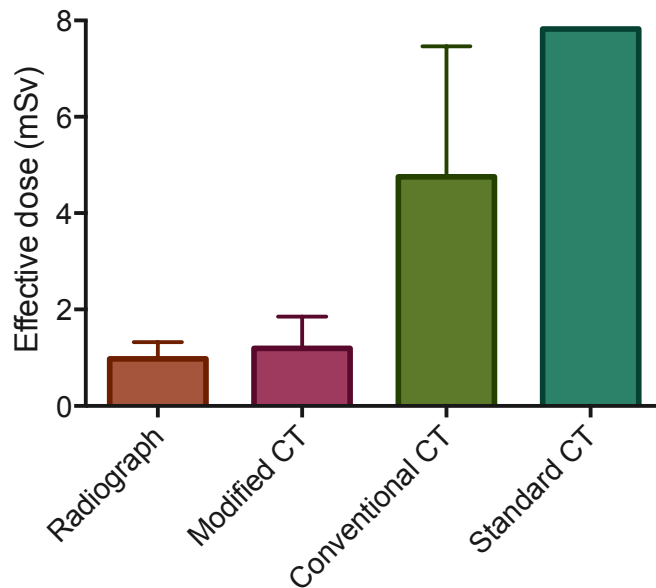


Figure 6.1: Column bar graph summarising the effective dose for abdominal radiograph and modified dose CT, with conventional CT (from split dose protocol) and mean standard of care departmental CT doses for comparison. The columns represent the mean values with the error bars representing standard deviations. There is no significant difference between the mean effective dose of abdominal radiographs and modified dose CT.

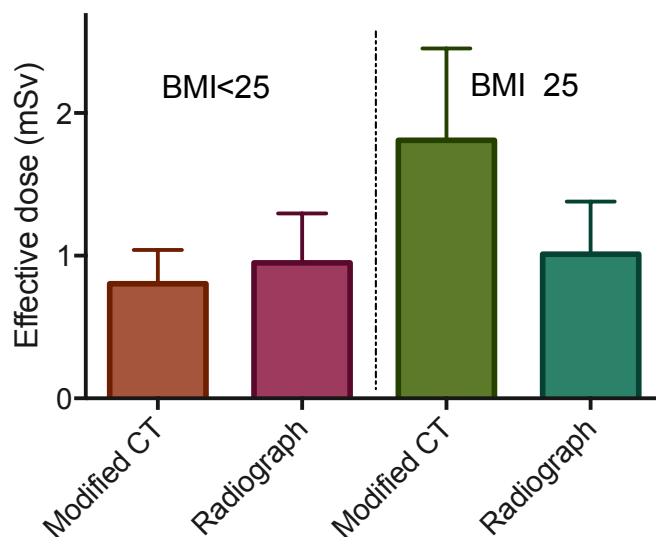


Figure 6.2: Column bar graph summarising the effective dose for abdominal radiograph and modified dose CT, stratified for BMI values of $<25\text{kg/m}^2$ and $\geq 25\text{kg/m}^2$, respectively. The columns represent the mean values with the error bars representing standard deviations. There is no significant difference between the mean effective dose of abdominal radiographs and modified dose CT for BMI $<25\text{kg/m}^2$ but the difference is significant with BMI $\geq 25\text{kg/m}^2$.

Diagnostic accuracy:

Only 4 of the abdominal radiographs demonstrated significant abnormal findings. In total, 20 of the modified dose CT examinations had significant abnormal findings. These are summarised in figure 6.4 and listed in table 6.2 below. There were discrepancies between the findings on modified dose CT and abdominal radiograph in 20 patients (86.9%). Complete agreement between the radiograph and CT findings was observed in 3 patients only (13%) – this complete agreement was observed only when the abdominal radiograph and modified dose CT had no abnormal findings.

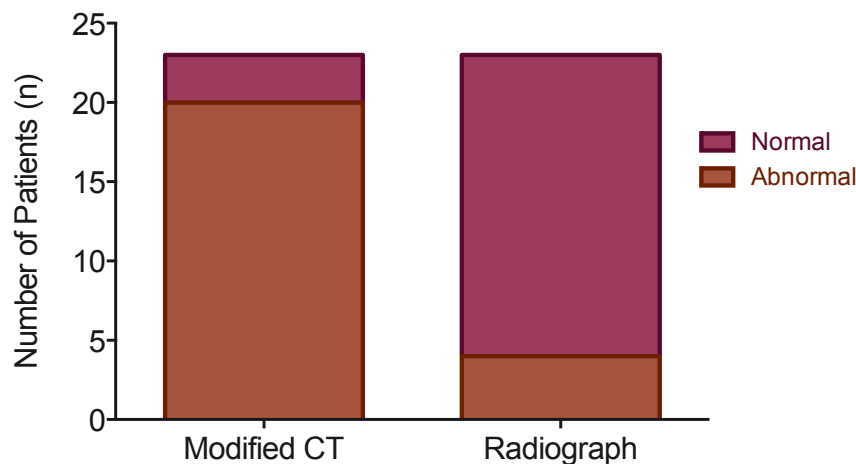


Figure 6.4: summary of the number of normal and abnormal examinations for each imaging modality.

Table 6.2: Summary of the Crohn's disease related imaging findings on each modality

| | Modified dose CT with MBIR (n) | Abdominal radiograph (n) |
|-----------------------------|-----------------------------------|-----------------------------|
| Enteritis | 14 | 1 |
| Colitis | 12 | 3 |
| Ileus/obstruction | 4 | 0 |
| Localised bowel perforation | 1 | 0 |
| Abscess | 1 | 0 |
| Pneumatosis | 0 | 0 |
| Pneumoperitoneum | 0 | 0 |

Clinically significant Crohn's disease related findings detected on modified dose CT that were missed on abdominal radiograph included: abscesses (n=1), localised bowel perforations (n=1), acute bowel obstruction (n=4), colitis (n=9), enteritis (n=13). The presence of acute-on-chronic disease was also better depicted with modified dose CT. Modified dose CT also detected radiographically occult Crohn's disease specific incidental findings such as sacro-ileitis. Modified dose CT also detected more clinically significant non-Crohn's disease related incidental findings (e.g. 1 case of advanced cervical cancer with unilateral hydroureter and hydronephrosis; 1 indeterminate pancreatic lesion that required further imaging to characterise), which were not demonstrated on the corresponding abdominal radiographs. Figures 6.5-6.8 demonstrate some examples of modified dose CT examinations with MBIR and their clinical findings. In each case the corresponding contemporaneous abdominal radiograph was normal.

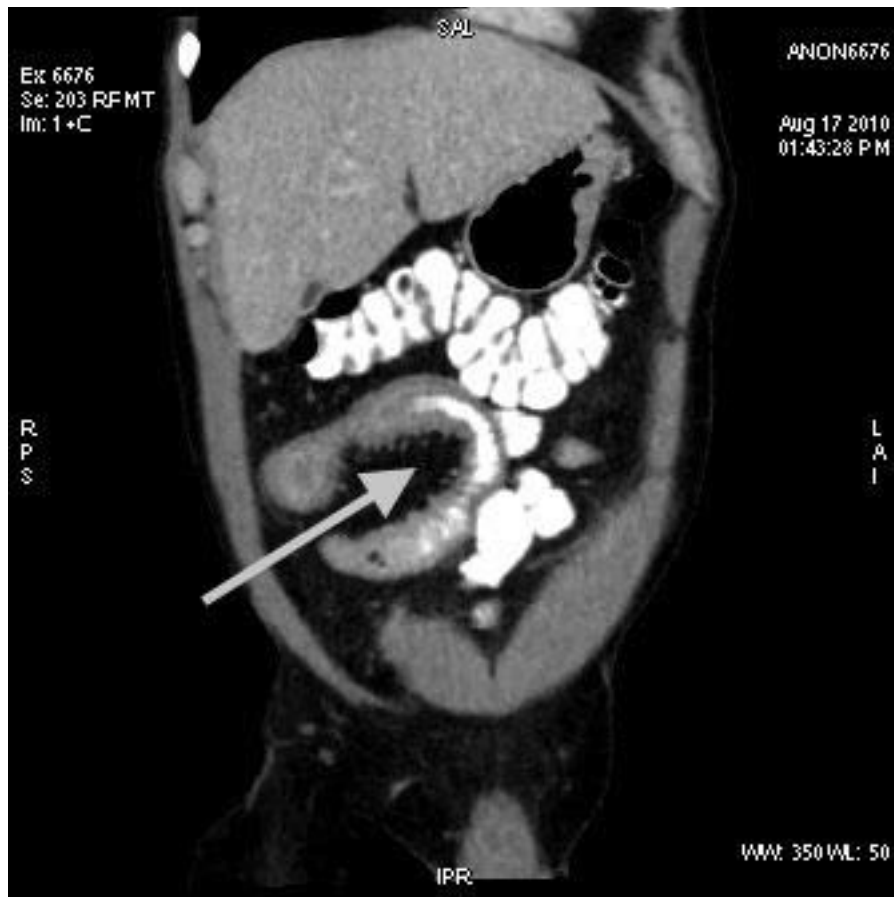


Figure 6.5: Coronal reconstruction of modified dose CT of the abdomen and pelvis with MBIR of a 48 year old man with a BMI of 25.9 kg/m². The arrow points to a segment of mural thickening of the distal ileum with local mesenteric injection in keeping with acute enteritis. This CT study was acquired with a radiation dose of 1.1mSv.

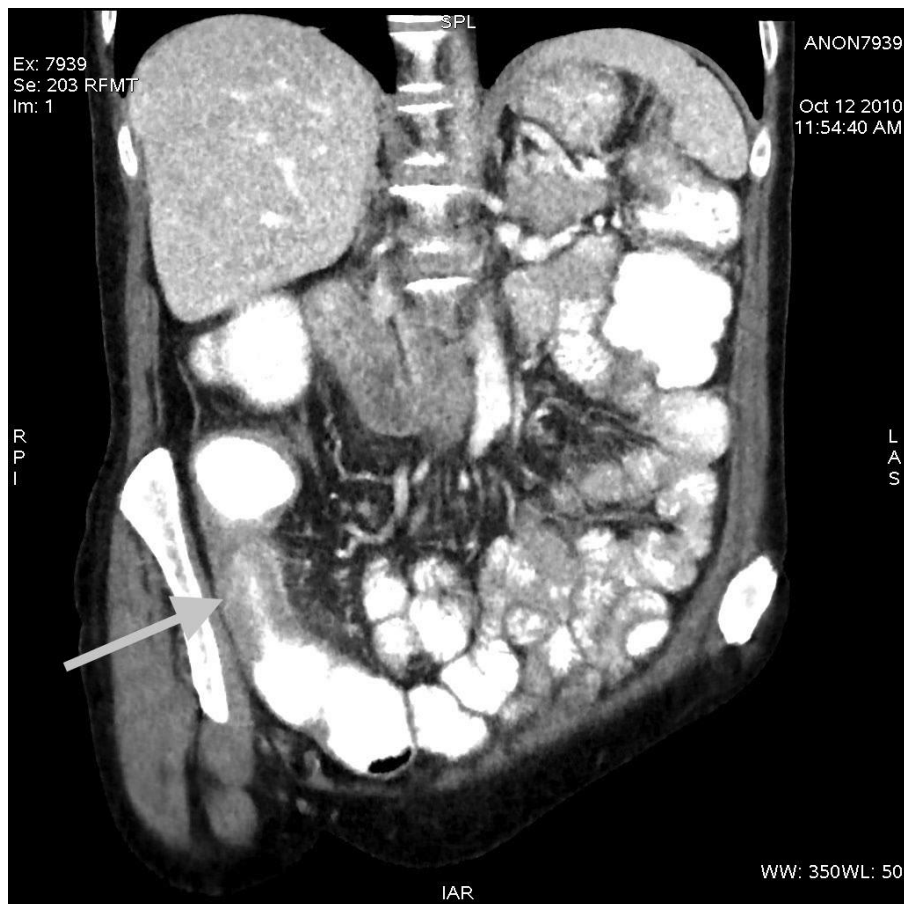


Figure 6.6: Coronal reconstruction of modified dose CT of the abdomen and pelvis with MBIR of a 59 year old lady with a BMI of 17.4 kg/m². The arrow points to a segment of mural thickening of the distal ileum with local mesenteric injection in keeping with acute enteritis. In this case the segment is more focal with proximal bowel dilatation suggesting a non-obstructing stricture. This CT study was acquired with a radiation dose of 0.65mSv.



Figure 6.7: Coronal reconstruction of modified dose CT of the abdomen and pelvis with MBIR of a 41 year old lady with a BMI of 29.4 kg/m². The arrows point to sclerosis and fusion of the sacroiliac joints bilaterally in keeping with sacroiliitis, a known extraintestinal manifestation of Crohn's disease. This CT study was acquired with a radiation dose of 1.4mSv.

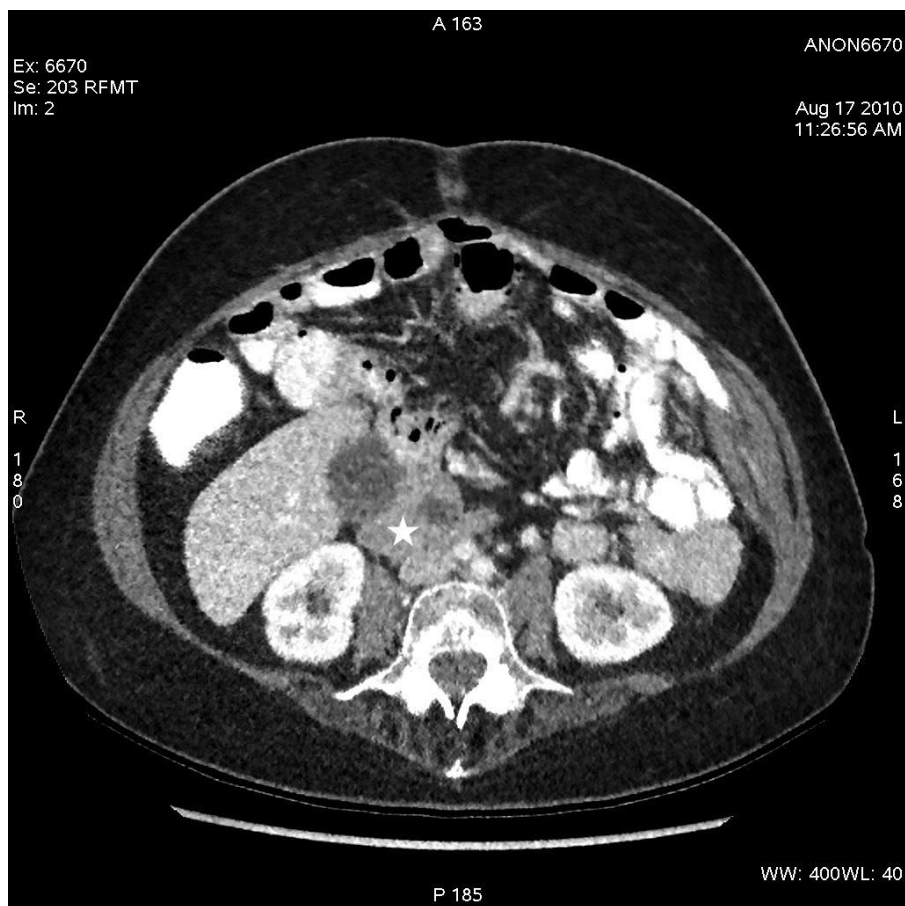


Figure 6.8: Axial reconstruction of modified dose CT of the abdomen and pelvis with MBIR of a 41 year old lady with a BMI of 29.4 kg/m^2 . The star lies adjacent to a low attenuation lesion within the pancreas that is of indeterminate aetiology. This was an incidental finding and required follow-up imaging of this lesion. This CT study was acquired with a radiation dose of 1.4 mSv .

Discussion:

The role of the abdominal radiograph in modern imaging practice is dwindling. In particular, the role of the abdominal radiograph in the diagnosis, management and follow-up of Crohn's disease is limited with few appropriate clinical indications for this imaging modality [182]. Despite guidelines and accepted practice to the contrary, in the acute setting, 57.5% of this cohort of consecutive patients with a suspected complication of known Crohn's disease underwent abdominal radiograph prior to CT. The yield is demonstrably low and the contribution to clinical management negligible. Indeed, all of these patients proceeded to CT of abdomen and pelvis within 24 hours of radiographic examination to achieve a definitive diagnosis and guide management so the necessity for any of the abdominal radiographs is questionable [189]. The continued high levels of plain radiograph use in patients with Crohn's disease despite the increasing use of CT mirrors the findings of Desmond et al [13].

Our institution is not unique with abdominal radiographs being performed that do not meet referral criteria. This failure of clinical practice to adapt to changing imaging recommendations has been suggested due to the fact that abdominal radiographs are cheap, quick and available [184,188]. Unfortunately, sometimes referral for abdominal radiograph is out of habits of old from when CT imaging was less readily available. Clinicians often erroneously assume that the dose for an abdominal radiograph is negligible, in the realms of that of a chest radiograph when in fact average doses approximate to 35 times this dose. Worryingly, this mistaken belief can be felt to justify getting an abdominal radiograph to 'be seen

to do something' and keep the patient occupied while waiting for CT. In patients with Crohn's disease who are 'at risk' for large cumulative doses, such 'bonus' radiation may be detrimental.

The number of films forming the abdominal radiograph examination for a given patient depends on patient size (among other factors such as operator technique and fitness of the patient for positioning)– the larger the patient/abdomen, the greater the chance that the full field might not be adequately covered in a single exposure. The mean BMI and effective diameter for patients requiring a single film were significantly less than those for patients requiring more than one film.

The mean overall effective dose for modified dose CT of abdomen and pelvis was 1.22mSv, ranging from 0.46 to 2.8mSv. The impact of patient size, as measured by BMI and effective diameter, on dose is evident with very strong correlations observed meaning the bigger the patient, the bigger the dose. For patients with a BMI < 25 kg/m², there was no significant difference between the effective dose from modified dose CT and corresponding abdominal radiograph with a mean effective dose for modified dose CT of 0.8mSv, approximating to the dose of the equivalent abdominal radiograph. For those patients with an overweight or obese habitus, the mean effective dose from modified dose CT (1.81mSv) approximates to 2 to 3 abdominal radiographic films. The mean effective dose for a plain abdominal radiograph for patients with BMI ≥ 25 kg/m², taking the number of exposures into account, is 1 ± 0.4mSv. Therefore, the modified dose CT for this BMI subset actually equates to less than two abdominal radiographic

examinations. This suggests dose equivalence for lower BMI patients and near-dose equivalence for higher BMI patients between the modalities in this study.

The principle of optimisation with regard to medical imaging using ionising radiation highlights the need to achieve image quality appropriate to the clinical objective of the examination but to generate these diagnostic quality images with the least possible radiation exposure. Modified dose CT of abdomen and pelvis, when reconstructed with MBIR, yielded images of acceptable diagnostic quality for the diagnosis of Crohn's disease related complications including obstructing strictures, localised perforations and abscesses, as well as the detection of and assessment of the extent of active colitis and enteritis. Crohn's and non-Crohn's disease related incidental findings of clinical significance were also demonstrated, including an unsuspected case of cervical cancer with ureteric impingement and hydronephrosis.

The superiority of modified dose CT with MBIR over abdominal radiographs at comparable doses is demonstrated by the gross discordance of clinically significant findings between modalities. Complete agreement was observed in only three patients, and these were normal studies. Sixteen other radiographs were deemed normal despite the corresponding CT demonstrated abnormalities. False reassurance by a normal radiograph may be detrimental to patient management.

This study highlights how blunt and insensitive abdominal radiographs are as a tool for abdominal assessment with, often, gross underestimation of underlying

pathology. Indeed, with the declining reliance on radiographic interpretation and the increasing use of CT imaging, interpretation skills of radiologists for plain radiograph subtleties and diagnostic nuances are waning due to lack of experience [190]. Radiologists are now less comfortable with making a diagnostic call on radiographic findings, preferring to correlate with cross-sectional imaging for definitive diagnosis. For this reason, a senior fellowship-trained abdominal radiologist experienced in abdominal radiograph interpretation was one of the readers in this study to maximise the yield from radiographic review.

The fact that all patients in this study proceeded to CT with 24 hours of abdominal radiograph, regardless of the findings, underlines the lack of diagnostic merit placed on these studies, even by those physicians who request them despite guidelines to the contrary. As such, these represent a not-insignificant source of ‘wasted’ radiation dose to patients already at risk for high levels of cumulative radiation exposure [13]. We propose that the use of the abdominal radiograph generally, but particularly in Crohn’s disease, should be tightly restricted to indications in the recognised guidelines or even abandoned.

This study had some limitations. The included study population is small; this is a result of this being a secondary analysis of a previously recruited study sample of which just over half met criteria for inclusion (contemporaneous abdominal radiograph). The use of a departmental audit value for abdominal radiograph dose is an approximation necessitated by inability to convert recorded DAP values from radiographs into effective dose values for direct comparisons. Our

departmental audit value of 0.7mSv is less than the European mean of 0.9mSv meaning our results will tend, if anything, to underestimate the radiation dose from abdominal radiographs [31]. Finally, we are comparing a novel imaging protocol with an imaging study that, in most cases, is not indicated by current referral guidelines for imaging of Crohn's disease so our conclusions about 'replacing' abdominal radiographs with modified dose CT are a little misplaced. However, the literature and our experience in this study suggest that the abdominal radiograph is still widely used in patients with Crohn's disease so we use this to justify our recommendations [13].

Abdominal radiographs in patients with suspected acute complications of Crohn's disease are over-used and of negligible, if not no, clinical value. Modified dose CT reconstructed with MBIR represents a feasible replacement for initial abdominal radiograph in the assessment of patients with Crohn's disease with a suspected acute complication. The radiation doses required to acquire these CT studies are equivalent or near equivalent to the doses of a corresponding abdominal radiographic examination. Detection of clinically significant intra-abdominal findings may provide a definitive diagnosis sufficient to allow initiation of clinical management and may obviate the need for a conventional dose CT [161-162]. In cases of indeterminate findings or an apparently normal modified dose CT in the context of high levels of clinical concern, the modified dose CT can be used as a stepping stone to conventional dose CT and may guide optimisation of technique (oral contrast preparation, phases of IV contrast, limited scan range, etc.) for the conventional dose study.

Conclusion:

Replacing the abdominal radiograph in the investigation of suspected acute complications of Crohn's disease with a modified dose CT of abdomen and pelvis acquired at an equivalent radiation dose yields significantly increased diagnostic information and avoids any false assurance derived from a normal radiograph.



Chapter 7

Quantitative comparison of tissue attenuation values
across traditional and novel reconstruction algorithms

Iterative Reconstruction as a Novel Method of Radiation Dose Reduction
at Computed Tomography in Patients with Crohn's Disease

Introduction:

In the simplest terms, a CT image is a density map depicting the absorption properties of the imaged structures. Fundamental to CT image interpretation is differentiation and measurement of attenuation values in various anatomical and pathological tissues and lesions. This generally occurs on a background level, where the reader appreciates a whiter structure as being dense, such as bone, calcification or exogenous contrast material, and a blacker structure as being a less dense substance/tissue such as gas or fat. However, precise measurement of the attenuation values of the pixels within a drawn region of interest is of value to assess for subtle differences from the norm or to characterize the constituent tissues of a lesion. For example, the liver parenchyma in a patient with fatty infiltration is less dense than normal healthy parenchyma, whereas the liver parenchyma in a patient with iron deposition from haemochromatosis is more dense than normal. An adrenal adenoma is an example of an adrenal mass lesion that can be definitively characterized based on the presence of macroscopic tissue of fat density within. The preservation and conformity of accurate attenuation measurements in CT images, irrespective of the reconstruction algorithm used, is vital for both the reporting and characterization of disease entities.

Objective image noise is an image property that impacts negatively on image quality and has traditionally been the fundamental limiting factor with reduced dose CT protocols. With filtered back projection, as radiation dose decreases, there is a corresponding increase in image noise, as measured by the standard deviation of the attenuation of a tissue. Image noise is not uniform throughout

the imaged volume, affected by adjacent structures and body thickness at that site. Iterative reconstruction algorithms decrease image noise by processing data at the level of the raw data domain or image domain. This non-uniform reduction in inherent image noise by advanced modeling techniques improves image quality [17,71,158,172,191-197].

In order to routinely replace conventional FBP with any of the iterative reconstruction algorithms available, it is mandatory that both qualitative and quantitative information is retained in the image. CT numbers or Hounsfield Units provide information on the x-ray attenuation characteristics of the corresponding voxel in a patient relative to the HU of water:

$$HU = 1000 \times (\mu_x - \mu_{\text{water}}) / \mu_{\text{water}}$$

The attenuation coefficient is energy dependent so consequently CT number values depend on the kilovoltage at which the scanning is performed. We also know that CT attenuation measurements can be affected by beam hardening, scatter, CT system stability, and CT reconstruction kernel [52]. The effect of iterative reconstruction algorithms on Hounsfield Unit conformity in patients is, as yet, undetermined. Chapter 2 examined in detail the effects of changes in CT input parameters and resultant changes in radiation dose on image quality across reconstruction algorithms using cylindrical and anthropomorphic phantoms and cadaveric models. Our brief examination of image noise across reconstruction algorithms in these models suggests no statistically or clinically significant difference in objective noise with given acquisition parameters. In

chapters 3 and 5 we examined the image noise and its effects on the qualitative aspects of image interpretation with ASiR and MBIR reconstruction, respectively, when applied to modified dose CT imaging in patients with Crohn's disease. In this chapter we examine the quantitative aspects of image interpretation, namely attenuation but also encompassing the related value noise.

The objective of this study is to compare attenuation values in various substances and tissues with differing reconstruction algorithms across multiple acquisition protocols in phantom and cadaveric models. The effect on attenuation of each of these reconstruction algorithms on modified and conventional dose CT examinations of the abdomen and pelvis in live human subjects will then be assessed. We hypothesise:

- That tissue attenuation values will not change significantly across reconstruction algorithms in phantom, cadaveric or live human subjects.
- That objective image noise values for MBIR will be more favourable than with ASiR or FBP.

Methods:

The methodology can be divided into three sections:

1. Phantoms
2. Cadavers
3. Patients.

Phantoms:

Anthropomorphic: As described in detail in chapter 2, the Kyoto CTU-41 torso phantom (Kyoto Kagaku, Fushimi-ku, Kyoto, Japan) is a life-size male anthropometric phantom with a height of 100cm and a body weight of 45kg constructed from urethane and epoxy base resins. It has synthetic internal organs with each organ having a particular CT attenuation corresponding to the matched structure in the human body. The phantom is placed supine on the CT table and centred by means of lateral and antero-posterior CT localiser radiographs, as would a human subject. The scan length extended from the lung bases to the pubic symphysis as per standard of care CT protocol.

Cylindrical: The Catphan 600 phantom (The Phantom Laboratory Inc., Salem, NY) is a cylindrical phantom for measurement of image quality. The phantom's long axis (z-axis) is placed longitudinally on the CT table and aligned with the scanner's isocentre so the modules are in transverse planes to the phantom z-axis (x-y plane). For this section, the CTP404 module was used for sensitometry (CT number accuracy) analysis [106]. This module comprises seven high contrast sensitometric targets as demonstrated in figure 7.1 and listed in table 7.1. These can be used to verify and compare CT numbers from the phantom

specifications with the system's imaging capability. The CT numbers for these attenuators range from -1000 to +1000HU (note: the estimated target HU values provided by the phantom specifications are within $\pm 5\%$).

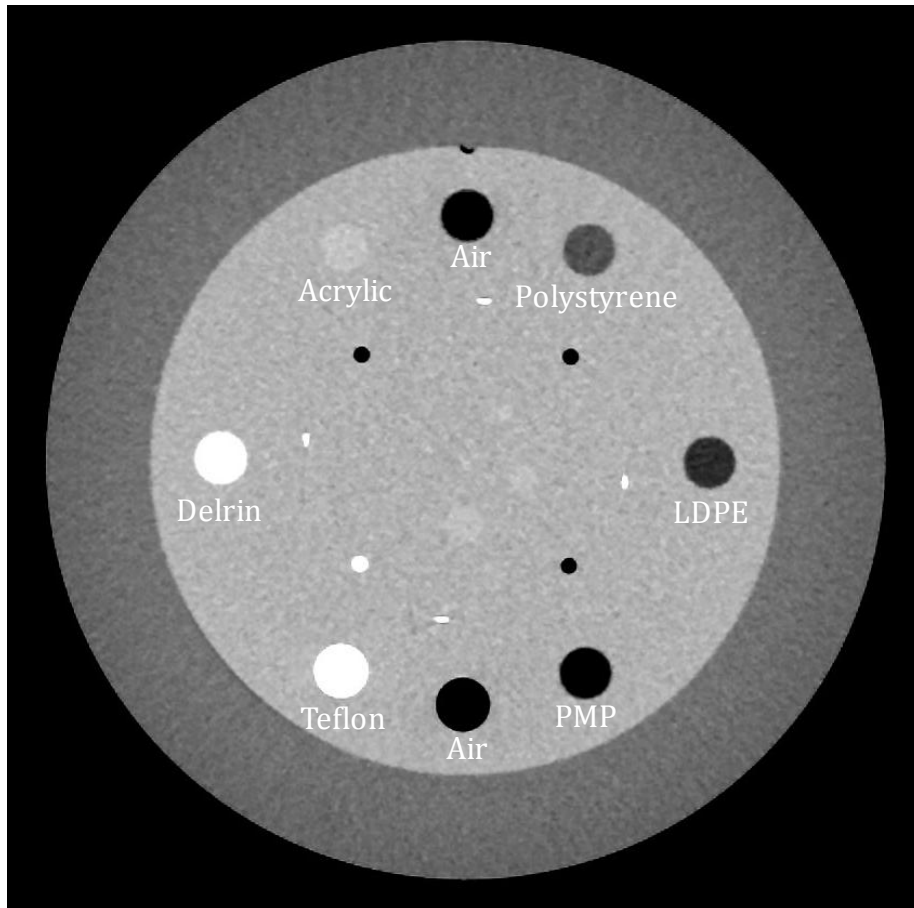


Figure 7.1: The CTP404 module of the Catphan 600 phantom with each of the 7 attenuators labeled. Note that there are two air chambers making a total of 8 targets.

Table 7.1: CTP404 sensitometry target specifications [106]

| Material | Formula | Estimated CT number ($\pm 5\%$) |
|-------------|---|-----------------------------------|
| Water | H ₂ O | 0 |
| Air | 78%N, 21%O, 1%Ar | -1000 |
| PMP | C ₆ H ₁₂ (CH ₂) | -200 |
| LDPE | C ₂ H ₄ | -100 |
| Polystyrene | C ₈ H ₈ | -35 |
| Acrylic | C ₅ H ₈ O ₂ | 120 |
| Delrin | N/A | 340 |
| Teflon | CF ₂ | 950 |

Cadavers:

This is a secondary analysis of the cadaveric CT data acquired in chapter 2. These human cadavers were used in compliance with the Helsinki Declaration and approval was granted for their use by the institutional ethical review board. Five cadavers (3 male, 2 female) were obtained from anatomical bequests to the Department of Anatomy in University College Cork. All were embalmed with using the Thiel methodology [129-130], resulting in well-preserved organs and tissues. The cadavers were placed supine and headfirst on the CT table in an arms-down position. Appropriate isocentre alignment was achieved by use of lateral and antero-posterior CT localiser scans. The scan length extended from the lung bases to the pubic symphysis as per standard of care CT protocol.

Patients:

This is a secondary analysis of CT data acquired for the validation of adaptive statistical and model based iterative reconstruction in achieving diagnostic quality CT at markedly reduced radiation doses. No additional CT examinations of live patients were performed. Concise methods have been published elsewhere [161-162] and are described in detail in chapter 3. Briefly, 32 of 50 consenting patients with a known diagnosis of Crohn's disease with a suspected acute complication had modified and conventional dose CT raw data appropriately saved for inclusion in this study (table 7.2).

| Table 7.2: Patient demographics and clinical characteristics | |
|--|----------------------------|
| Sex (n) | |
| Male | 11 |
| Female | 21 |
| Age (y), mean \pm SD (range) | 39 \pm 13.5 (20-69) |
| BMI (kg/m ²), mean \pm SD (range) | 24.6 \pm 4.9 (17.4-38.8) |
| Effective diameter (cm), mean \pm SD (range) | 28 \pm 3.6 (23.4-36) |

CT acquisition protocols:

All CT acquisitions were performed on either a GE Discovery CT750 HU 64 slice CT scanner (GE Healthcare, Milwaukee, Wisconsin, USA) with inbuilt ASiR capability and upgraded with MBIR reconstruction capability or a GE Lightspeed VCT-XTe 64 slice CT scanner with inbuilt ASiR capability and remote MBIR reconstruction. The following standard parameters were applied to all acquisition protocols (table 7.3):

| Table 7.3: Standard scan parameters applied to all CT acquisition protocols | |
|---|--|
| Pitch: | 1 |
| Rotation time: | 0.8 sec for all protocols other than 100kV with ATCM acquisitions with variable noise index where 0.5 sec was used |
| Image matrix: | 512 x 512 |
| Field of view: | 36cm for Kyoto phantom and cadavers, 26.5cm for Catphan phantom 36.5cm for patients |
| Acquisition slice thickness: | 0.625mm |

Phantoms and cadavers:

Repeated CT acquisitions were performed on both phantoms and the five cadavers with variation of the user-selected parameters for each protocol. With a fixed tube voltage of 120kV, examinations were performed with tube currents of

400mA, 200mA and 100mA. With a fixed tube current of 225mA, examinations were performed with tube voltages of 140kV, 120kV, 100kV and 80kV. With use of tube current modulation and fixed kV settings of 120kV and 100kV, examinations were performed with noise index setting of 20, 30, 40, 50, 60 and 70. The acquisition protocols are summarised in figure 2.7 in chapter 2.

Patients:

All 32 patients underwent both conventional dose and modified dose CT of abdomen and pelvis on a 64-slice CT scanner as part of an IRB-approved research protocol [ClinicalTrials.gov Identifier NCT 01244386]. The conventional dose protocol comprised CT of abdomen and pelvis acquired at approximately 90% of the radiation dose of the standard departmental CT of abdomen and pelvis protocol (tube voltage 120kV, noise index 38%, gantry rotation time 0.8s). The modified dose protocol comprised CT of abdomen and pelvis acquired at approximately 10% of the radiation dose of standard departmental CT of abdomen and pelvis (tube voltage 100kV, noise index 70%, gantry rotation time 0.5s). All patients were imaged in the portal venous phase of intravenous contrast with the low dose protocol first, followed by the conventional dose protocol 6.2s later. For both protocols z-axis automated tube current modulation resulted in a variable tube current, with minimum and maximum tube current thresholds of 20 and 350mA respectively.

Raw data reconstruction:

For the phantom and cadaveric models, the raw data from each examination were reconstruction with filtered back projection, adaptive statistical iterative

reconstruction with a strength of 40% (40% ASiR is a blend of 40% ASiR reconstruction and 60% FBP), and MBIR RP05 and MBIR NR05 model based iterative reconstruction (see figure 7.2 below). A soft tissue reconstruction kernel was used.

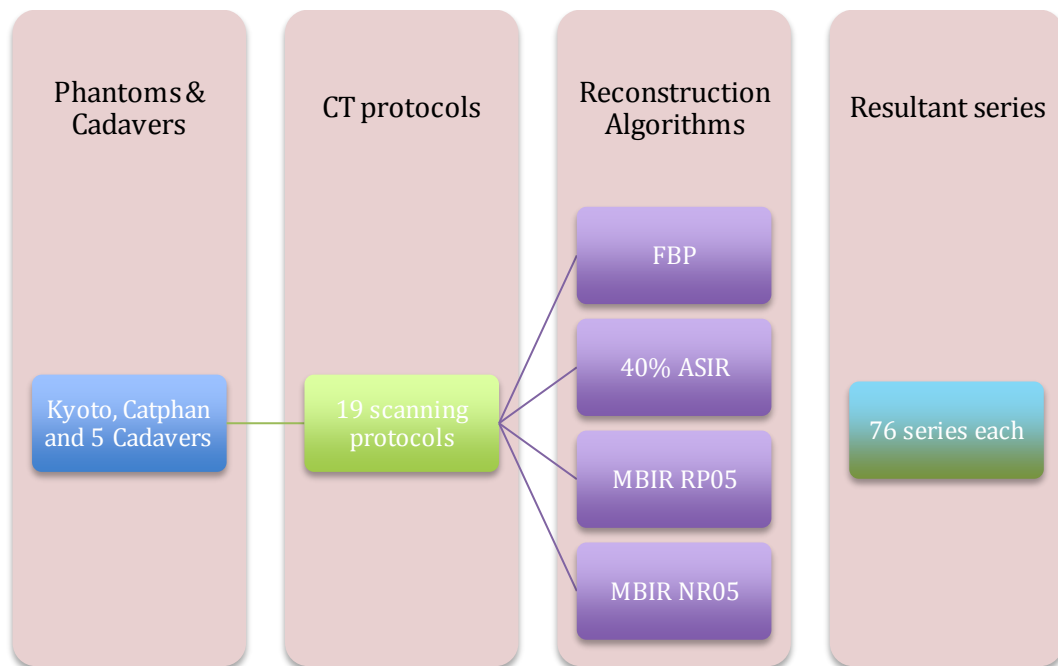


Figure 7.2: Series reconstructed from the phantom and cadaveric raw data

For the patients, the CT modified dose raw data were reconstructed with filtered back projection, adaptive statistical iterative reconstruction with a strength of 50% (50% ASiR is a blend of 50% ASiR reconstruction and 50% FBP), and Standard model based iterative reconstruction. The corresponding conventional dose CT raw data from these patients were reconstructed with FBP (see figure 7.3 below). A soft tissue reconstruction kernel was used.

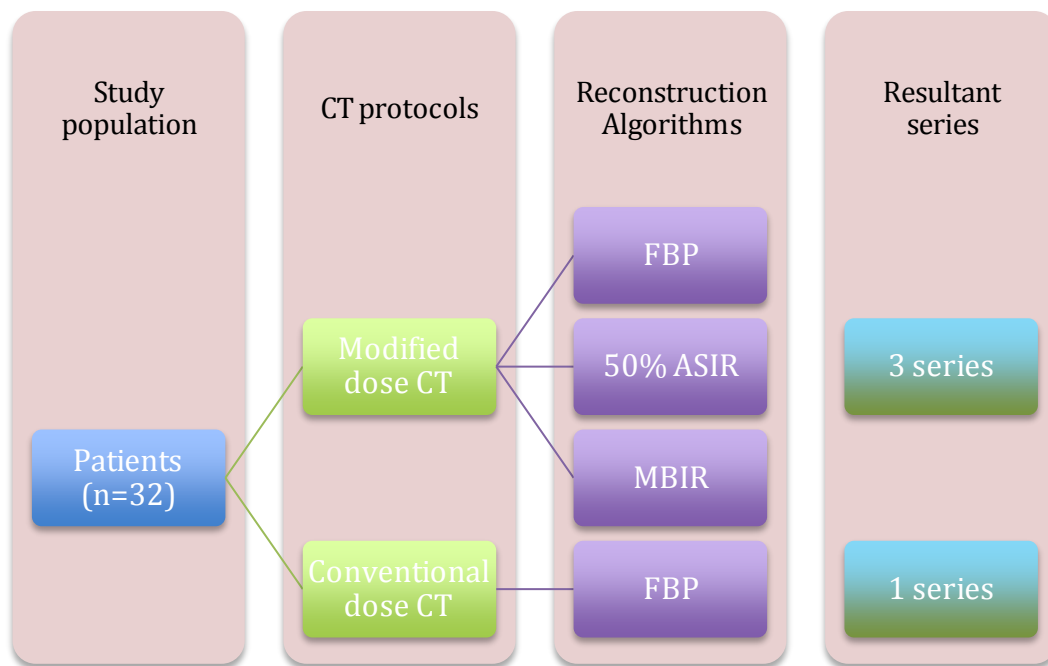


Figure 7.3: Series reconstructed from the clinical patient raw data

Image review:

Images were reviewed on a dedicated advanced image review workstation (Advantage Workstation VolumeShare 2, Version 4.4, GE Medical Systems, Milwaukee, USA). A soft-tissue window setting (window width, 400 HU; window level, 40HU) was chosen.

For the Catphan phantom, identical spherical regions of interest (diameter 10mm, volume 519mm³) were placed in each sensitometry target (n=8) at a mid-module slice with care taken to place the ROIs away from the target edges to ensure sampling of the target tissue only. This was performed on a single slice for each series (see figure 7.4).

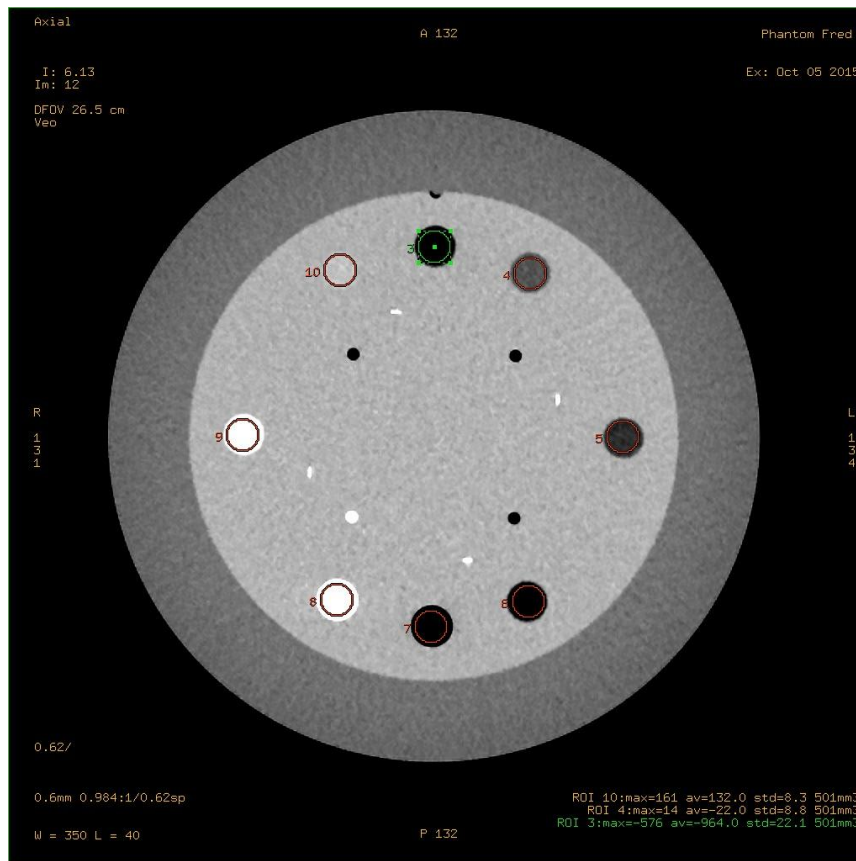
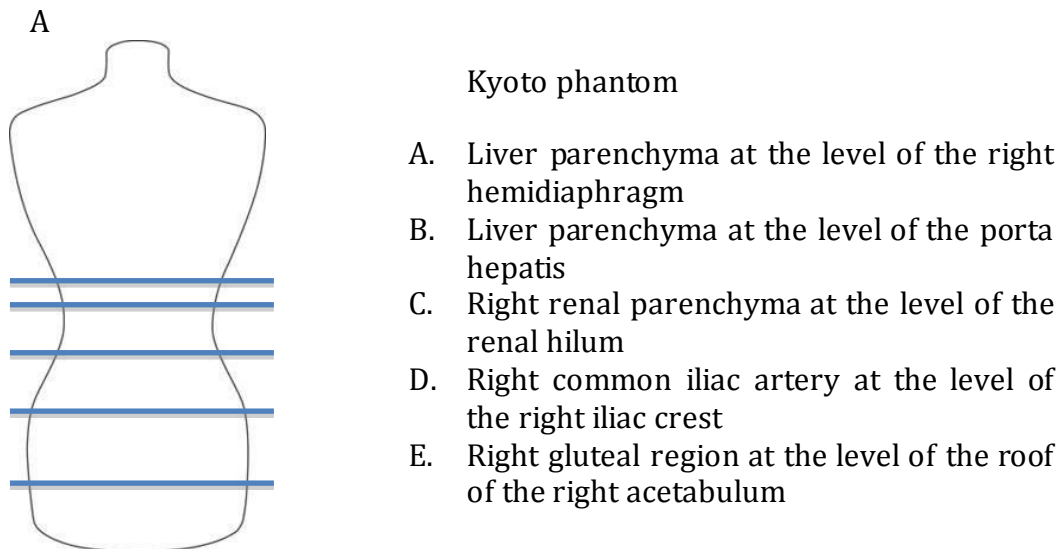


Figure 7.4: CTP404 module of the Catphan 600 phantom with regions of interest drawn in all 8 sensitometry targets. The mean pixel values within the regions of interest are taken as the attenuation measurements.

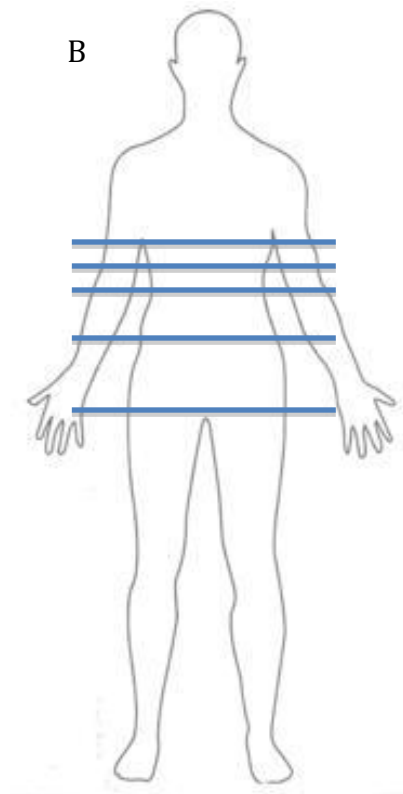
For the anthropomorphic phantom and cadavers, attenuation and objective noise were measured by placing spherical regions of interest in anatomical tissues/organs at five different anatomical levels. For the anthropomorphic phantom, these locations were chosen to approximate to anatomical levels used in human models, but with slight deviation due to phantom composition. These comprised the liver parenchyma at the level of the right hemidiaphragm, the liver parenchyma at the level of the porta hepatis, the right renal parenchyma at the level of the renal hilum, the right common iliac artery at the level of the right iliac crest and the right gluteal region at the level of the roof of the right acetabulum (see figure 7.5 below). In the cadavers, the sites varied at the level of

the renal hilum where the right erector spinae was measured and the right iliac crest where psoas was measured. Care was taken to place the ROIs in as homogenous an area of tissue as possible, away from blood vessels, fat planes and organ edges. Identical spherical regions of interest (diameter 10mm, volume 519mm³) were used and propagated to identical loci on each series by means of a cut and paste function to ensure consistency and repeatability.

Figures 7.5 (A-B) below depict the slice levels where ROIs are placed in both anthropomorphic phantom (A) and cadaveric (B) models to assess attenuation.



Cadavers



- A. Liver parenchyma at the level of the right hemidiaphragm
- B. Liver parenchyma at the level of the porta hepatis
- C. Right erector spinae muscle belly at the level of the right renal hilum
- D. Right psoas muscle belly at the level of the right iliac crest
- E. Right gluteus maximus muscle belly at the level of the roof of the right acetabulum

For the clinical patients, quantitative measurements of objective image noise in the resultant CT images were obtained at 13 distinct anatomical sites, as summarised in table 7.4 and figure 7.6 below. Again, this was achieved by drawing a standard region of interest (ROI, diameter 10mm, volume 393mm³) at each of these sites. A spherical region of interest was chosen to take into account both in and out of plane variation. Using a propagation feature on the image review software, the ROI was placed at an identical location on each modified dose series, possible as all series were reconstructed from the same data set. The region of interest was manually placed in as close a location as possible on the conventional dose images.

Table 7.4: Anatomical sites in patients at which regions of interest were placed to measure objective image noise

1. Liver at the diaphragm
2. Liver at the porta hepatis
3. Spleen
4. Gallbladder
5. Intravenous contrast within the aorta
6. Right erector spinae
7. Right psoas muscle
8. Right gluteus maximus
9. Buttock fat
10. Ischiorectal fossa fat
11. Bowel gas
12. Oral contrast within the bowel
13. Background – ROI placed within the field of view but outside of the patient

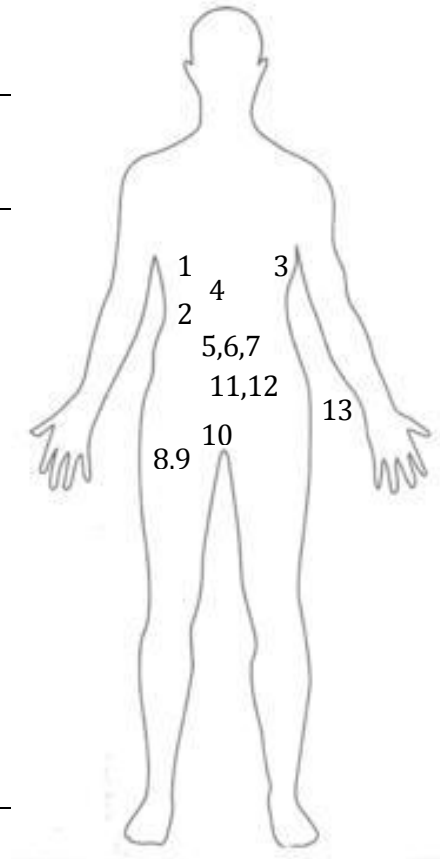


Figure 7.6 depicts the physical locations of these regions of interest

For clinical patients, the mean attenuation value within the ROI was recorded, as was the standard deviation of this value, which acted as a measure of objective noise [198]. The *signal to noise ratio* (SNR) within each ROI was calculated by dividing the mean attenuation value by its standard deviation [132]. For the CT number accuracy of water, the AAPM Task Group 66 has defined a tolerance of $\pm 5\text{HU}$ so we used this as our tolerance level [136].

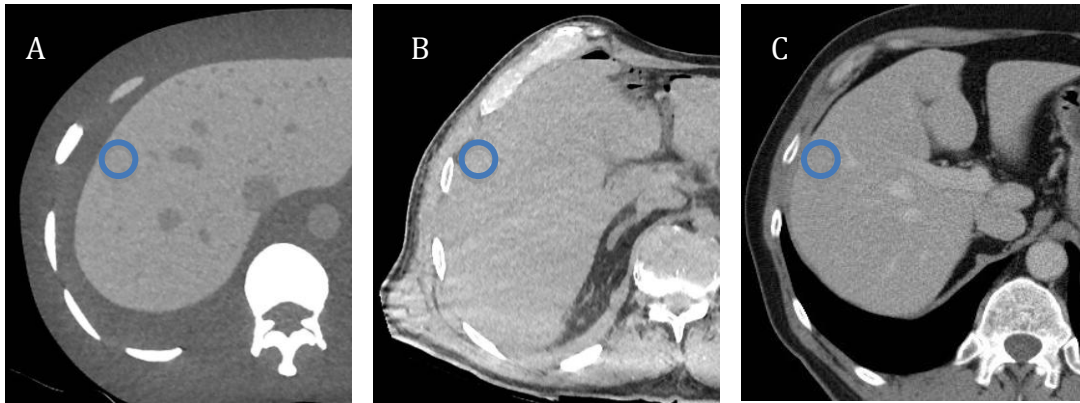


Figure 7.7: Details of individual axial slices from CT of abdomen and pelvis for the anthropomorphic phantom (A), a cadaver (B) and a live human subject (C). Fixed volume spherical regions of interest (ROIs) are placed in the liver parenchyma at the level of the porta hepatis. The value of the pixels within the ROI is indicative of attenuation and the standard deviation of this value is a measure of objective image noise. The ratio of these two values is the signal to noise ratio.

Statistical methods:

Data compilation and statistical analyses were performed using Microsoft Excel (Microsoft Corporation, Redmond, WA) and GraphPad Prism version 6.0 (GraphPad Software Incorporated, San Diego, CA). Descriptive statistics are provided in terms of means with standard deviations for parametric values. Variables were compared with t-tests or repeated measures and one-way ANOVA (with Tukey's and Dunnett's multiple comparison tests if ANOVA showed a significant difference) if parametric. Pearson correlations were used for parametric variables. The criterion for significance was taken as $P < 0.05$.

Results:

Catphan:

The mean overall attenuation values of each of the targets for the 19 protocols are summarised in figure 7.8. Values for each target are not significantly different from the estimated target HU values provided by the phantom specifications, allowing for $\pm 5\%$.

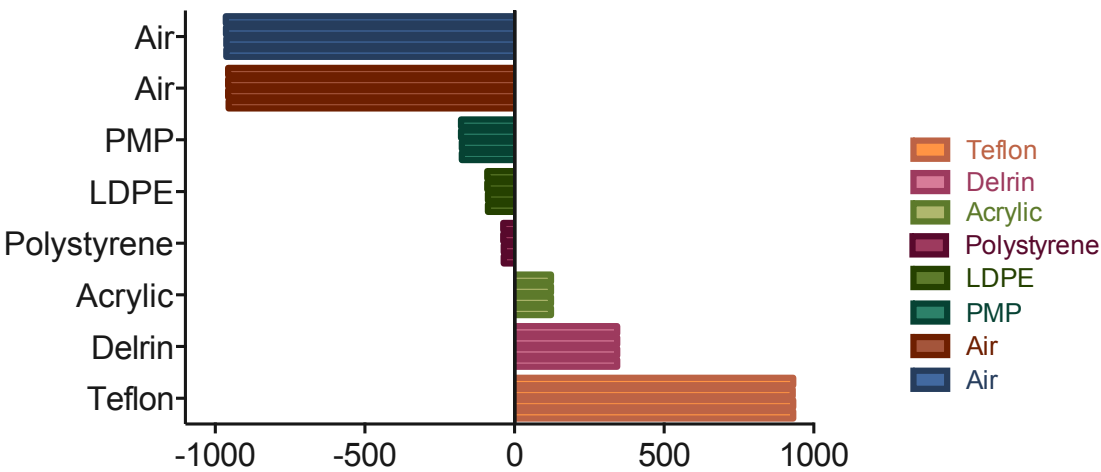


Figure 7.8: Graphical representation of the mean overall attenuation values of each of the sensitometry targets of the CTP404 module of the Catphan phantom.

Comparisons of the mean attenuation values overall across the 4 reconstruction protocols are graphically demonstrated in figure 7.9 below with figure 7.10 depicting the mean composite attenuation for each acquisition protocol. Repeated measures ANOVA testing overall suggested a statistically significant difference between algorithms ($P=0.0073$) but Tuckey's multiple comparisons test demonstrated the maximal value of this difference to be $<5U$ (1.4HU) and therefore not clinically significant.

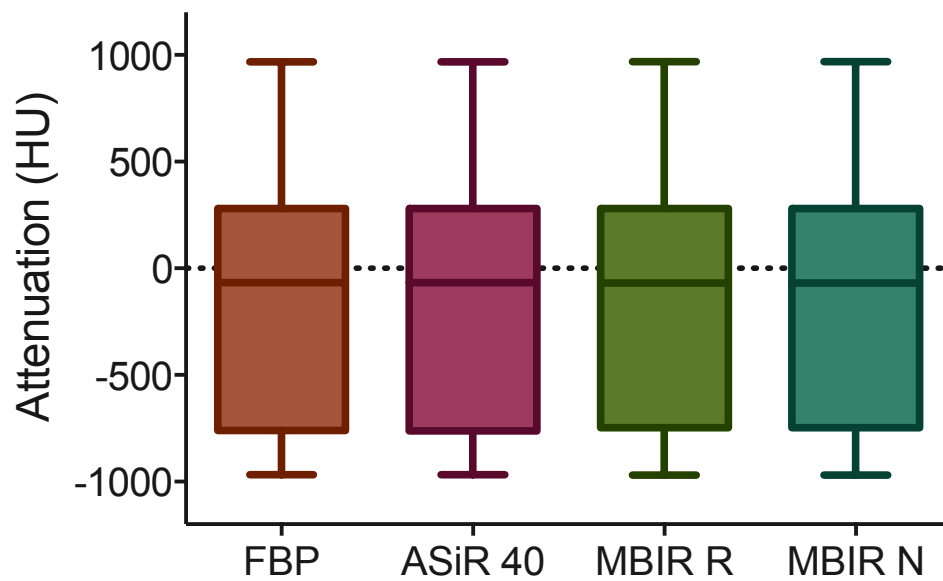


Figure 7.9: Box-plot of attenuation values in the sensitometric targets in the CTP404 module across all nineteen of the acquisition protocols. The line represents the mean, the box the standard deviations and the error bars the minimum and maximum values.

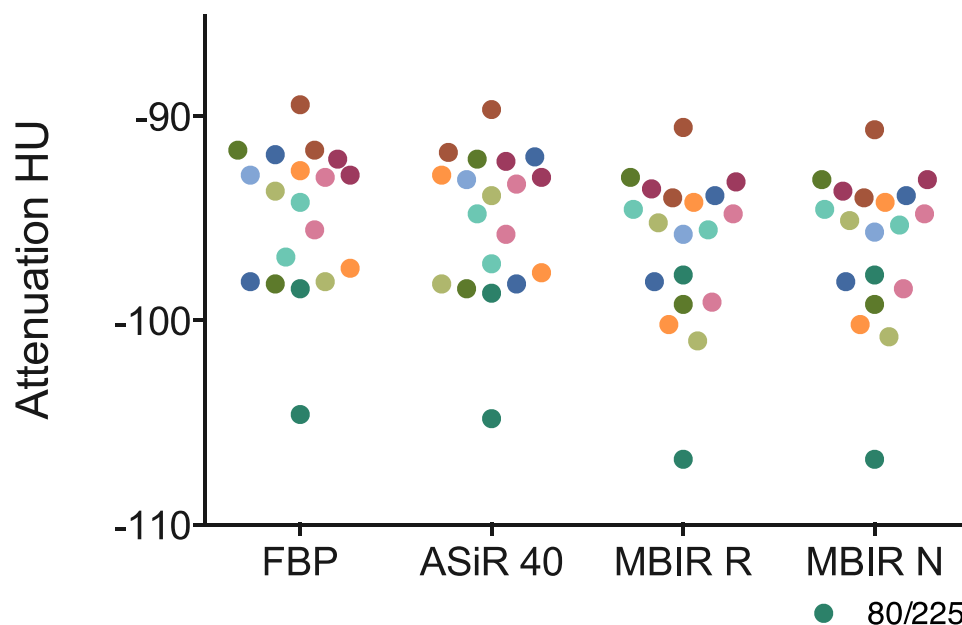


Figure 7.10: Scatter graph demonstrating the mean attenuation from a composite of 8 sensitometric targets in the CTP404 module of the Catphan phantom with each reconstruction algorithm. Each dot represents the mean attenuation from a different acquisition protocol. Note that the 80kV/225mA protocol (teal dot) is an outlier.

Figure 7.11 compares the mean attenuation values for each target across the 4 reconstruction protocols. When subdivided for each target, statistically significant differences were observed only for polystyrene, LDPE and PMP (P values of <0.0001, 0.0017 and 0.0331, respectively) but the maximal difference observed in was 3.2HU, again not clinically significant.

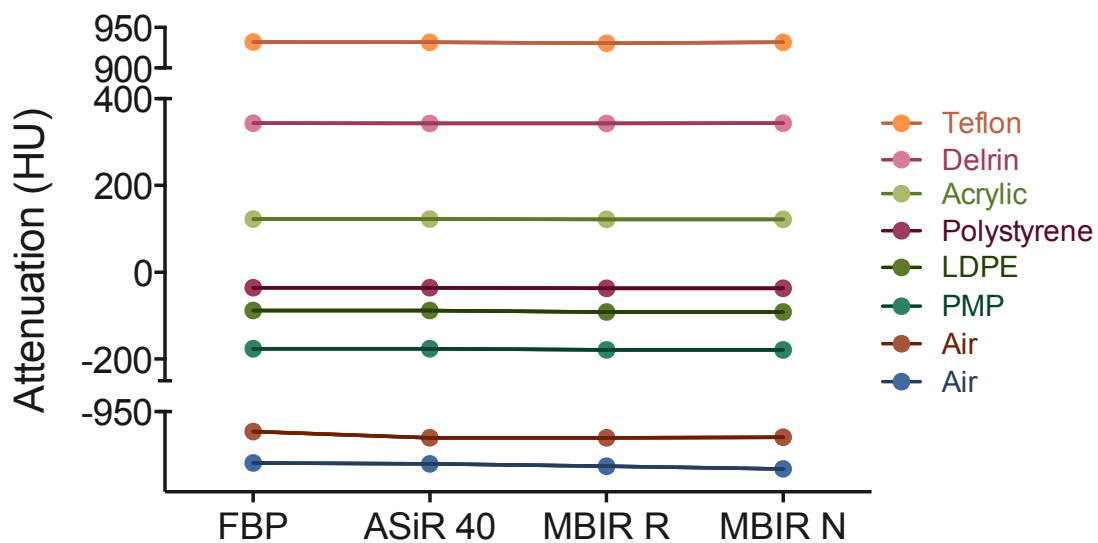


Figure 7.11: Line plot of the mean attenuation for each of the individual sensitometric targets across reconstruction algorithms.

Anthropomorphic phantom:

Tissue attenuation was measured at five distinct anatomical locations the anthropomorphic phantom. The mean attenuation from a composite of these locations for the anthropomorphic phantom with each reconstruction algorithm is demonstrated in figure 7.12 below. There is no significant correlation between radiation dose and measured attenuation values ($P > 0.05$ for all comparisons).

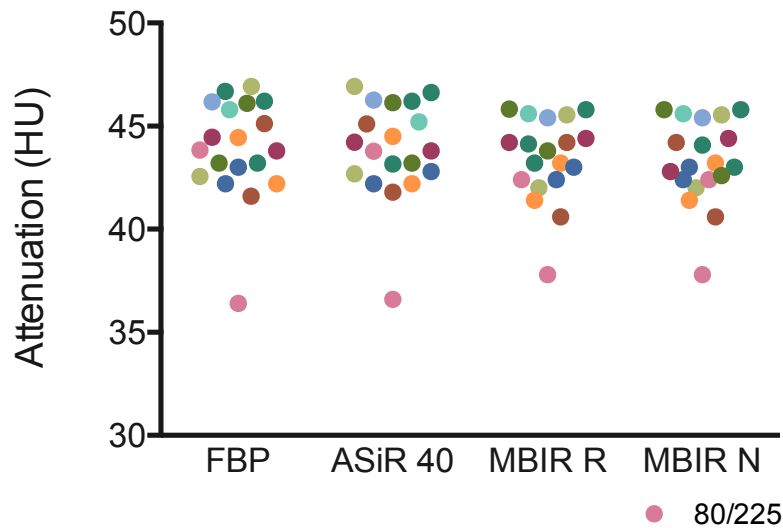


Figure 7.12: Scatter graph demonstrating the mean attenuation from a composite of 5 anatomical sites in the anthropomorphic phantom with each reconstruction algorithm. Each dot represents the mean attenuation from a different acquisition protocol. Note that the 80kV/225mA protocol (pink dot) is an outlier.

Comparison across scanning protocols: When the mean attenuation values for the protocols were compared with one another, a statistically significant ($P=0.0014$) difference was observed between some protocols. This was most evident with the 80kV with 225mA protocol when compared with the others – well demonstrated on figure 7.12 above as an outlier. If this protocol was excluded, statistically significant differences were observed between some protocols but the magnitude of each was $<5\text{HU}$ so did not prove clinically significant [136].

Comparison across reconstruction algorithms: Repeated measures ANOVA testing with Tukey's multiple comparisons test demonstrated a statistically significant difference between measured Hounsfield units across reconstruction protocols ($p=0.0086$) but this difference is $<1\text{HU}$ so, again, is not of clinical

significance. This indicates that fidelity in HU values is preserved with iterative reconstruction.

Cadavers:

For the cadaveric models, no statistically significant difference was observed in attenuation values between scanning protocols ($P=0.3107$) or reconstruction algorithms ($P=0.0943$) with repeated measures ANOVA. See figure 7.13 below.

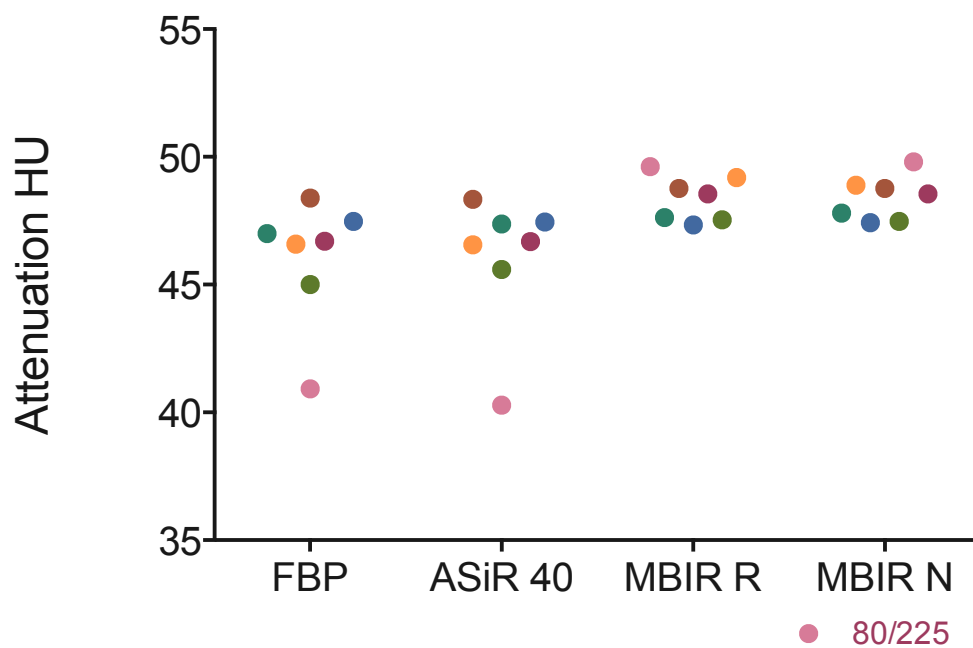


Figure 7.13: Scatter graph demonstrating the mean attenuation from a composite of 5 anatomical sites in the 5 cadavers with each reconstruction algorithm. Each dot represents the mean attenuation from a different acquisition protocol. Note that again the 80kV/225mA protocol (pink dot) is an outlier, though not significantly difference.

Patients:

Comparison of the mean attenuation values overall of the three modified dose CT protocol reconstructions (FBP, ASiR 50%, MBIR) with the conventional dose protocol demonstrated no statistically significant difference in attenuation ($P=0.8277$). Comparison of the mean overall attenuation values between the three modified dose datasets demonstrated no statistically significant difference in overall attenuation between reconstruction algorithms. See figure 7.14.

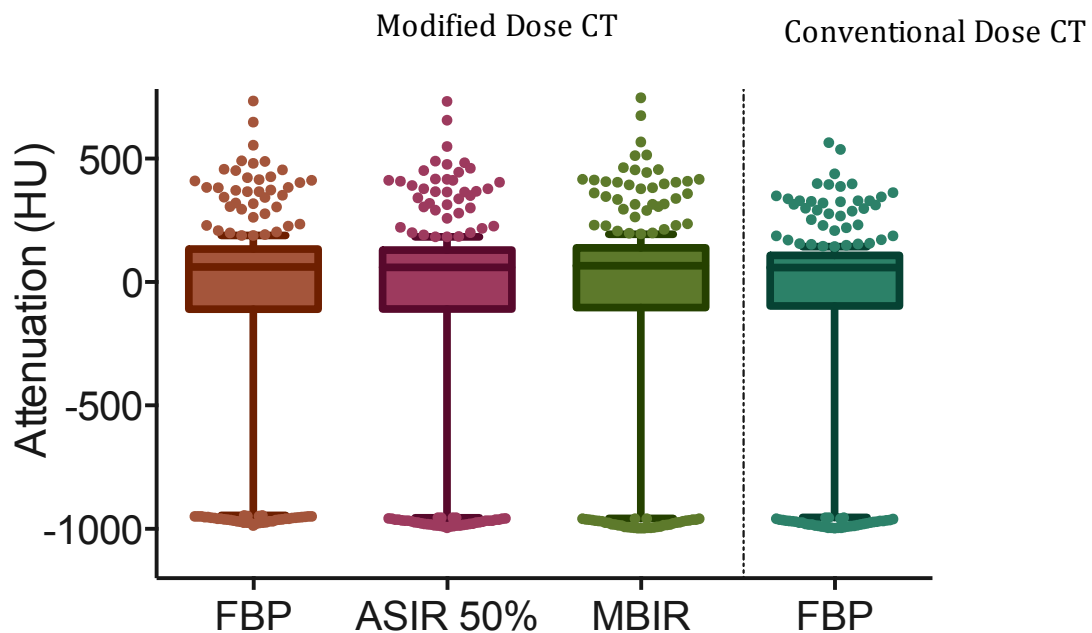


Figure 7.14: Box and whisker plot demonstrating no significant difference between attenuation values at 13 measured sites across modified dose CT data reconstructions with FBP, ASiR 50% and MBIR. There was also no significant difference overall between the modified and conventional dose CT protocols in terms of attenuation. The lines represent the mean attenuation, the boxes the standard deviation and the whiskers representing the 10th and 90th percentiles.

ANOVA testing compared the mean attenuation at each of the 13 anatomical sites measured (see figure 7.15 below). There was no statistically significant difference in attenuation at these sites ($P>0.05$), except for the ischiorectal fossa fat. Here the mean attenuation values for FBP, ASiR 50% and MBIR for the modified dose series were $-129.6\pm19.2\text{HU}$, $-131.3\pm19.5\text{HU}$ and $-106.3\pm23.8\text{HU}$, respectively, while the mean attenuation of ischiorectal fat for conventional dose CT with FBP was $-94.9\pm9\text{HU}$ (see figure 7.16). There was no significant difference between the pairing of modified dose FBP and ASiR 50% ($P=0.9855$) or the pairing of modified dose MBIR and conventional dose FBP ($P=0.0776$). Tuckey's multiple comparisons test demonstrated a statistically significant difference between all other comparisons for ischiorectal fossa fat attenuation.

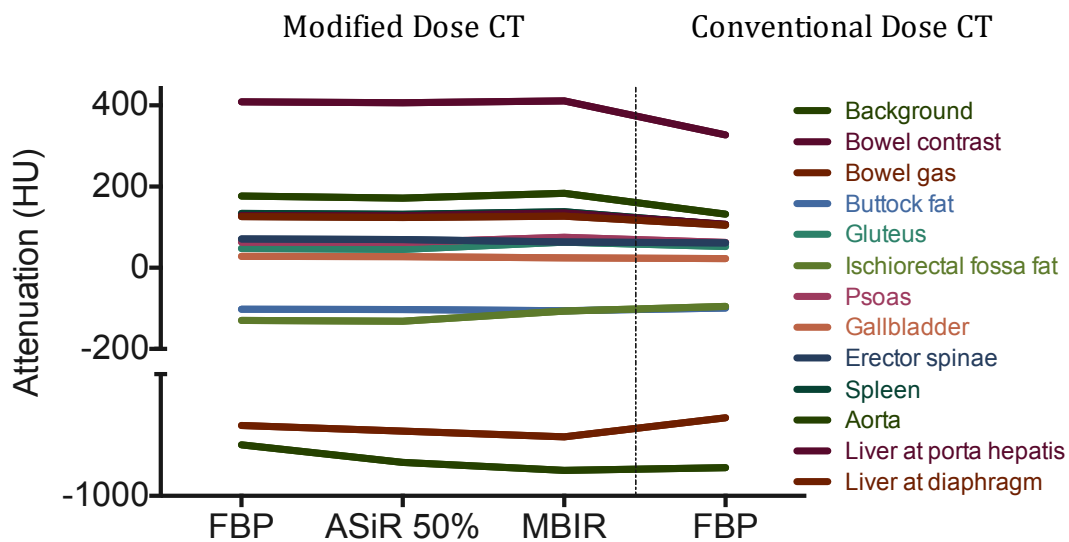


Figure 7.15: Line graph depicting the effect of reconstruction algorithm on objective image noise at each of 13 anatomical sites.

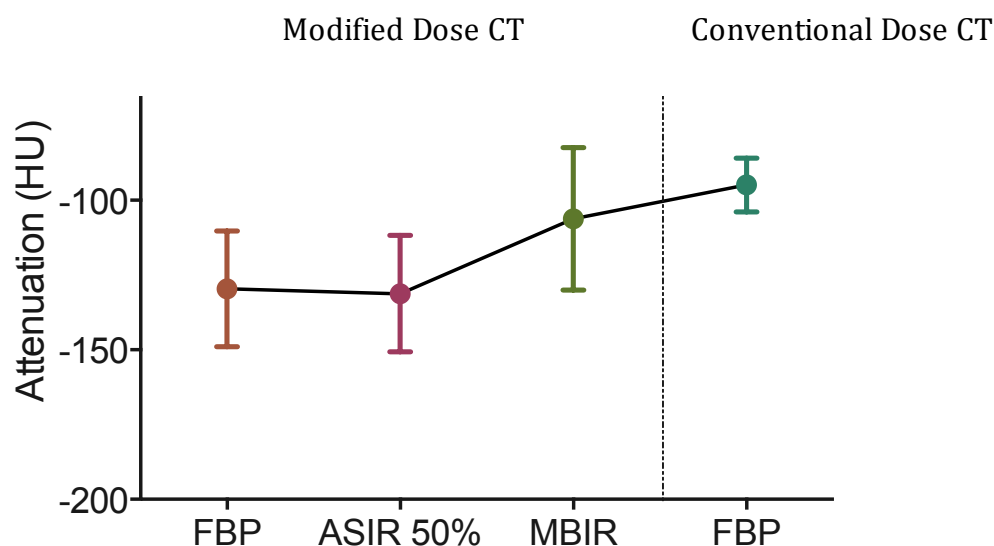


Figure 7.16: Graphical representation of the attenuation values in the right ischiorectal fossa across reconstruction algorithms. While there was no statistically significant difference between the modified dose datasets reconstructed with FBP and ASiR 50% at this site, attenuation values were significantly difference between all other comparisons with mean differences of 11-36HU.

For completion, the attenuation data from chapter 4 which examined the effects differing strengths of ASiR on image quality indices in clinical patients are also included here. The modified dose CT raw data from clinical patients were retrospectively reconstructed with filtered back projection (0% ASiR) then with escalating increments of ASiR 10% up to ASiR 100% yielding a total of 11 modified dose series (0%, 10%, 20%, 30%, 40%, 50%, 60%, 70%, 80%, 90%, 100%). The percentage of ASiR refers to a blend of that level of iterative reconstruction with the remainder being filtered back projection. Tissue attenuation values were measured as the mean value of the pixels within a region of interest. With escalating strength of ASiR, the mean attenuation at each of the anatomical sites did not change significantly indicating preserved fidelity of attenuation measurements for tissue characterization. Figure 7.17 below demonstrates the relationship of attenuation with ASiR strength.

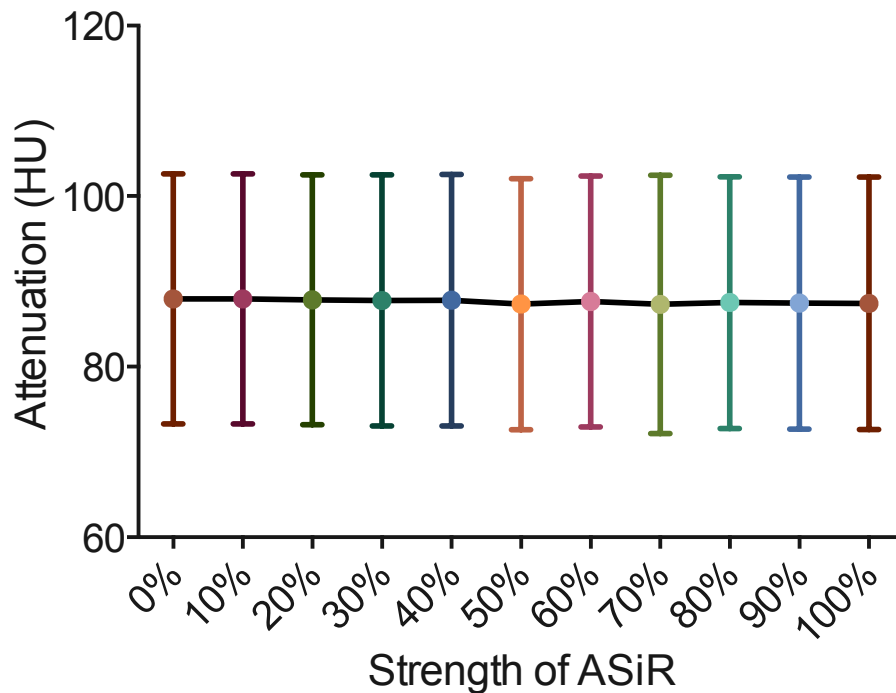


Figure 7.17: The mean attenuation values (symbols) with standard deviations (error bars) for increasing strengths of ASiR for modified dose CT imaging. There is no significant change in attenuation with change in ASiR strength.

Mean noise across algorithms:

Noise measurements were performed in clinical patients only – phantom noise has been examined in depth in chapter 2. Image noise is taken as the standard deviation of the attenuation value in HU within the ROI. While the absolute attenuation values are not strictly directly comparable across CT acquisition protocols (due to differences in kVp), image noise is as this is a measure of variance. The mean overall image noise across the 13 sites measured for each reconstruction algorithm is summarised in figure 7.18. With a 74% reduction in radiation dose between the conventional dose and modified dose CT protocols, there is a 52% increase in objective image noise when both are reconstructed in an identical manner with FBP (51.5HU v 107.2HU), highlighting the effect of reducing dose on image noise.

The mean overall objective image noise for the modified dose series was greatest for FBP ($107.2 \pm 25.1 \text{HU}$), intermediate for ASiR 50 ($47.2 \pm 12.1 \text{HU}$) and least for MBIR ($26.5 \pm 9 \text{HU}$) ($p < 0.0001$). For each individual tissue examined on the modified dose protocol, objective noise was greatest with FBP reconstruction and least with MBIR ($P < 0.0001$) (See figure 7.19 below). The objective noise measured on the conventional dose images reconstructed with FBP ($51.5 \pm 14.2 \text{HU}$) was greater than the modified dose CT images reconstructed with ASiR and MBIR despite the 74% reduction in radiation dose ($P < 0.0001$). When modified dose CT images reconstructed with FBP and MBIR are compared, there is a 75.3% reduction in objective image noise on this same raw data set.

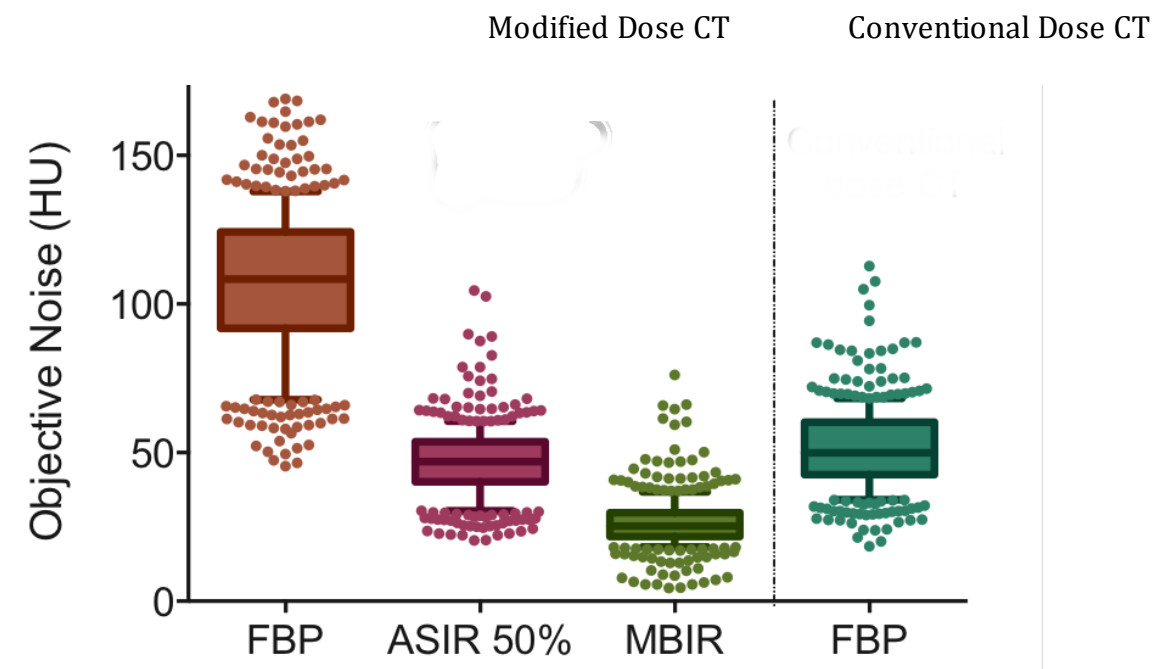


Figure 7.18: Box and whisker plot demonstrating the objective noise values overall across the reconstruction algorithms. The boxes represent means with standard deviations and the whiskers represent the 10th and 90th percentiles. The mean noise was greatest in the modified dose CT images with FBP reconstruction, decreasing with each of ASiR 50% and MBIR. Modified dose CT with ASiR 50% and MBIR reconstruction had less objective noise than conventional dose CT with FBP.

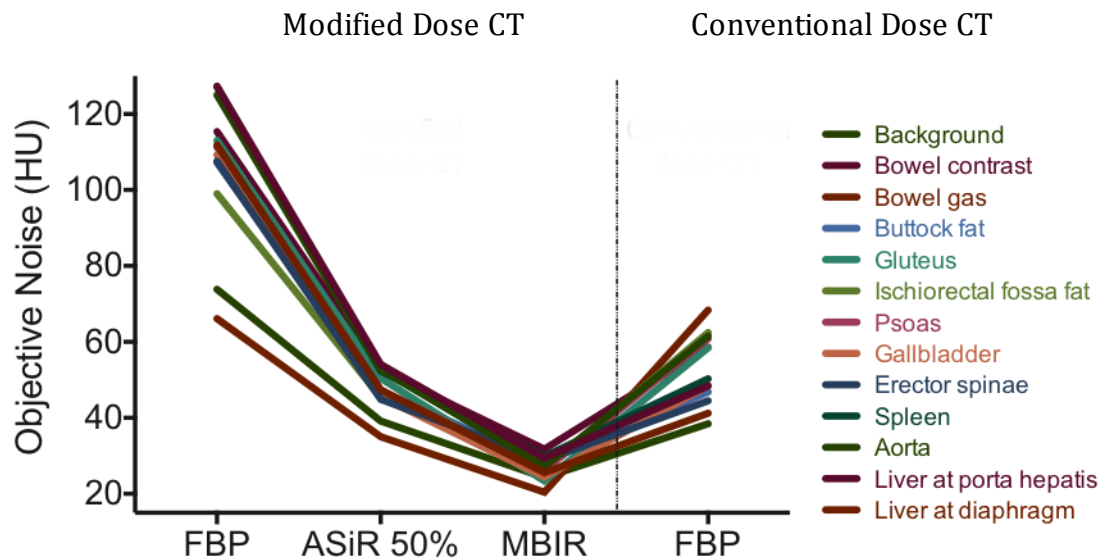


Figure 7.19: Line graph depicting the effect of reconstruction algorithm on objective image noise at each of 13 anatomical sites. For the modified dose CT protocol, in all cases FBP > ASiR 50% > MBIR in terms of objective noise values. Modified dose CT with MBIR is uniformly superior to conventional dose CT with FBP for objective noise also.

Signal to noise ratio:

For the modified dose dataset, the signal to noise ratio increases from FBP, through ASiR 50% to MBIR ($P < 0.0001$) as demonstrated in figure 7.20 below. There was no statistically significant difference between the mean signal to noise ratio for conventional dose CT with FBP and the modified dose protocol reconstructed with FBP and ASiR 50% with the mean of this dataset (SNR 5.9 ± 9.8) lying between those of the other two (3.2 ± 5 and 6.8 ± 10.5 , respectively). Given the absence of a significant change in attenuation with reconstruction algorithm, this change in signal to noise ratio relates to changes in levels of objective image noise.

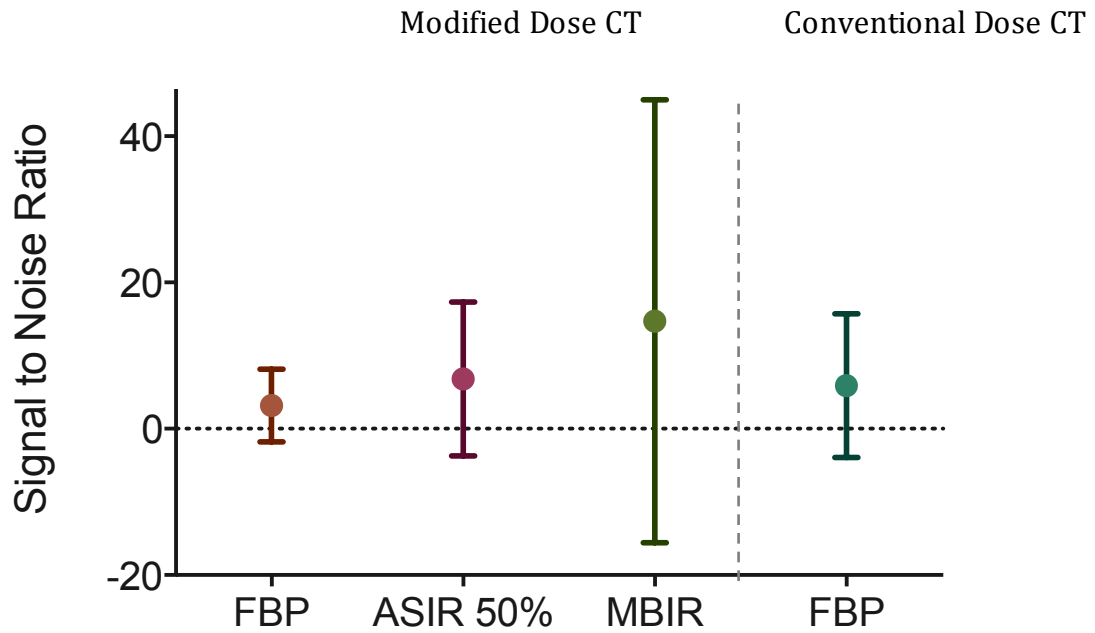


Figure 7.20: Graphical representation of the signal to noise ratio with each reconstruction algorithm. Symbols represent means and the error bars represent standard deviations. Iterative reconstruction increases the signal to noise ratio when compared with FBP.

Discussion:

The introduction of new image reconstruction techniques into routine clinical practice requires evaluation of qualitative and quantitative parameters of image quality and comparison with the conventional standard of reference [199-200]. Chapters 3 and 5 examined subjective image quality with ASiR and MBIR reconstruction as compared with conventional reconstruction with FBP and demonstrate superiority of these iterative algorithms in terms of diagnostic findings and image quality indices. In chapter 2 we examined the effects of each reconstruction algorithm on image quality indices, including attenuation measurements, in phantoms and cadavers. The present study examines specifically the effect of reconstruction algorithms on the quantitative metric of attenuation and the fidelity of this measurement with novel iterative reconstruction algorithms. As previously, there is a progression from cylindrical phantoms to anthropomorphic phantoms to cadavers to clinical human subjects.

The assessment of attenuation values of anatomical and pathological structures is core to interpretation of CT images, whether at a conscious or subconscious level. Attenuation can help differentiate disease states when examined overall in an organ, such as a steatotic liver, or more focally in a lesion, such as the presence of macroscopic fat in an adrenal lesion suggesting it to be a benign adenoma and less likely a neoplastic process. Loss of such applied benefits would impact negatively on the diagnostic ability and accuracy of CT interpretation, therefore preserved accuracy of attenuation values is a core quality of any new CT reconstruction algorithm. We have demonstrated that the mean attenuation

values overall across a wide range of CT acquisition protocols reconstructed with FBP, ASiR and MBIR were not significantly different, meaning the ability to characterise tissue composition was not affected. The impact of differing tube voltages across protocols was less evident than expected with significant differences observed only with the 80kV protocol for the anthropomorphic phantom only.

In clinical patients, when the 13 different anatomical tissues were examined in isolation, only the ischiorectal fossa fat demonstrated statistically significant differences between all measurements other than between the modified dose series reconstructed with FBP and ASiR 50%. Reasons for why this difference exists here are unclear, particularly given that buttock fat (a structure with similar attenuation values and at a similar axial slice level as the ischiorectal fossa) did not demonstrate a significant difference (see figure 7.21 below). This may relate to differing levels of streak artefact from the osseous pelvic girdle impacting on structures within the pelvis to a greater degree than those outside. This would explain why findings were more evident with FBP and ASiR 50% reconstruction than with MBIR, as MBIR would reduce this artefact. The lack of a significant difference between the modified dose MBIR value and the conventional dose CT with FBP suggest this value to be more representative of true attenuation rather than artefactual degradation.

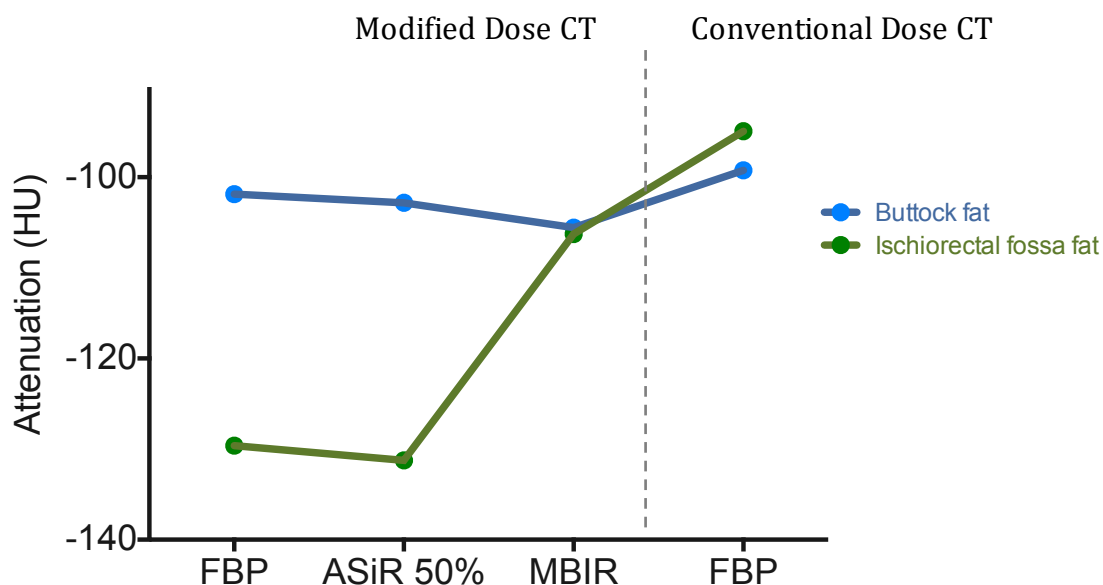


Figure 7.21: Expanded detail of line graph (figure 7.15 above) depicting the effect of reconstruction algorithm on objective image noise in the fat in the buttock and ischiorectal fossa.

Objective image noise is the main limiting factor with reduced dose CT protocols. High levels of image noise impact on image quality and, thus, diagnostic interpretation. For the clinical patients, comparing FBP reconstructions of each data set, we see that for a 74% reduction in radiation dose there is a 52% increase in image noise. Use of iterative reconstruction algorithms such as ASiR and MBIR reduced this image noise, such that noise values for modified dose CT images reconstructed with these algorithms are less than the corresponding conventional dose CT images reconstructed with FBP. Indeed, within the modified dose CT series, MBIR allows a 75.3% reduction in image noise compared with FBP. These findings are true for overall measurements but also when stratified for individual measured tissues with widely varying mean attenuation values.

By using a variety of scanning subjects (phantoms, cadavers, clinical patients) and scanning protocols for each reconstruction algorithm, we have attempted to achieve an overall impression as to how attenuation behaves with each algorithm under a variety of settings. Nevertheless, this study has some limitations. The main limitation is that two different CT scanners were used – one for the clinical patients and another for all other acquisitions. Measurement of attenuation is known to vary between CT scanners, as well as between phantoms. In this study, this is not a major issue as all comparisons are made between differing reconstructions of identical datasets, i.e. comparisons are intra-scanner rather than inter-scanner. Similarly comparison was not made between attenuation measurements from different phantoms.

Conclusions:

Attenuation values in phantom and human models do not change significantly across reconstruction algorithms meaning preserved tissue characterisation capabilities with ASiR and MBIR. Iterative reconstruction algorithms allow marked improvement in image noise on modified dose CT images when compared to FBP, with MBIR superior to ASiR. Modified dose CT images with ASiR and MBIR also demonstrate superior objective noise characteristics when compared with conventional dose FBP.



Chapter 8

Conclusions

Iterative Reconstruction as a Novel Method of Radiation Dose Reduction
at Computed Tomography in Patients with Crohn's Disease

Once the principle of justification of a medical imaging examination is satisfied, there is an onus on the imaging team to endeavour to produce diagnostic quality CT images at the lowest possible radiation dose to that patient. The renaissance, rediscovery and refinement of iterative reconstruction is, perhaps, one of the more valuable recent developments in CT imaging, finally uncoupling administered radiation dose from observed image noise. This thesis is fundamentally an exercise in optimisation in clinical CT practice, examining, analysing and applying the qualitative and quantitative effects of iterative reconstruction in modified dose CT.

The context of this thesis arose from an important paper from our research team that quantified the alarming levels of radiation dose to patients with Crohn's disease from medical imaging and the shift to CT in more recent years [13]. CT delivers some of the highest doses of ionising radiation in diagnostic radiology. During the course of this work, the estimated risks from medical radiation extrapolated from studies of atomic bomb survivors [39-40] as the linear no-threshold model were validated by Pearce et al [9] in their landmark paper proving a causal link between ionising radiation from medical imaging and carcinogenesis. The introduction of adaptive statistical iterative reconstruction by GE Healthcare in 2008 heralded the dawn of an era of change in how we reconstruct CT data and the radiation doses we use to image patients.

The main objectives of this thesis were to assess iterative reconstruction as a method for improvement of image quality in CT, to explore the associated potential for radiation dose reduction, and to develop a new split dose CT

protocol with the aim of achieving diagnostic quality submillisievert CT imaging in patients with Crohn's disease.

The following conclusions can be drawn from the individual chapters:

In chapter 2, phantoms and cadavers were used to examine the interplay of user-selected parameters on radiation dose and image quality, comparing traditional filtered back projection with iterative reconstruction algorithms. Both forms of iterative reconstruction examined (ASiR and MBIR) were superior to FBP across a wide variety of imaging protocols, with MBIR superior to ASiR in all areas other than reconstruction speed. We established that ASiR appears to work to a target percentage noise reduction whilst MBIR works to a target residual level of absolute noise in the image. This work resulted in the development of an optimised, refined and appropriate split dose protocol for CT of the abdomen and pelvis in clinical patients with Crohn's disease that aims to achieve diagnostic quality submillisievert CT by applying iterative reconstruction to the CT raw data. We have also confirmed that an anthropomorphic phantom (Kyoto) is a good model for human research and protocol tailoring.

Chapter 3 was designed to validate the use of ASiR with modified dose CT protocols for imaging of the abdomen and pelvis in patients with Crohn's disease by applying this reconstruction algorithm to the aforementioned split dose CT protocol. The contemporaneously acquired conventional dose study provided a reference against which diagnostic findings and image quality could be measured. Modified dose CT with ASiR, acquired with a mean effective dose of

1.26mSv (73.5% dose reduction), was demonstrated non-inferior to the conventional dose study in terms of diagnostic findings, despite reduced subjective and objective indices of image quality.

The differing strengths of ASiR available to CT users were examined in chapter 4 in an attempt to determine the optimal strength to apply to this modified dose CT protocol. The overall optimal ASiR strength for the modified dose protocol used in this work is ASiR 80%, as this provides the most favourable balance of peak subjective image quality indices with less objective image noise than the corresponding conventional dose CT images reconstructed with FBP. Reconstruction of modified dose CT raw data in this dose range with ASiR strengths of 20% or less should be avoided, as the low level of ASiR employed is insufficient to overcome the excessive noise in the images leaving them inadequate for diagnosis. With modified dose CT imaging, it is vital that the appropriate radiation dose level as well as the correct strength of iterative reconstruction is selected to maximise image quality for the clinical task while keeping radiation exposure to a minimum.

The use of MBIR for modified dose CT protocols for imaging of the abdomen and pelvis in patients with Crohn's disease was validated in chapter 5. With methodology mirroring that in chapter 2, MBIR was demonstrated to preserve diagnostic accuracy for Crohn's disease related CT findings on modified dose CT images when compared with conventional dose CT with FBP. When compared with ASiR and FBP, MBIR provides superior subjective and objective image quality for modified dose CT images and mean dose reductions of 72.9% were

achieved over the conventional dose CT protocol with little compromise to image quality. Overall, modified dose CT with MBIR represents a feasible method of imaging patients with Crohn's disease in a clinical setting.

Despite guidelines to the contrary, abdominal radiographs are still often used in the initial imaging of patients with a suspected complication of Crohn's disease. In chapter 6, we demonstrated the negligible clinical benefit (and possible false reassurance) obtained from radiographs in this population and the superiority of modified dose CT with MBIR over abdominal radiographs at comparable doses in detection of Crohn's disease and non-Crohn's disease related findings. We suggest a move toward modified dose CT with MBIR as the initial investigation of choice for suspected acute complications of Crohn's disease – this avoids the 'wasted radiation' of abdominal radiographs and may obviate the need for a conventional dose CT of the abdomen and pelvis if the clinical question is satisfied.

Finally, chapter 7 is an examination of the quantitative information obtained from CT, namely attenuation measurements, across a variety of reconstruction algorithms (FBP, ASiR, MBIR) and imaging protocols in phantom and cadaveric models and in clinical patients. Attenuation measurements are important in characterisation of tissues and lesions for differentiation of disease states and the fidelity of their values is important to image interpretation. We concluded that attenuation values do not change significantly across reconstruction algorithms meaning preserved tissue characterisation capabilities.

Clinical impact:

The essence of translational research, such as this, is that positive study results should lead to clinical implementation of the observed advances. In depth examination of iterative reconstruction and its impact on image quality and noise has improved our understanding and, thus, our confidence with its use. During the course of this thesis, adaptive statistical iterative reconstruction has been adopted into routine clinical practice for all CT examinations performed in our institution, with real and immediate dose savings. It remains that clinical examinations at submillisievert radiation doses are not yet routine practice. The superiority of MBIR over ASiR in terms of image quality is evident and there is a reluctance to commence routine abdominal imaging at such low radiation doses until MBIR becomes available as a clinical tool (currently it is approved for research uses only). However, we have instituted a prospective clinical trial of modified dose CT of abdomen and pelvis in patients with Crohn's disease using the protocol validated in this thesis and reconstructed with MBIR, without the corresponding conventional dose study. The inferiority of plain abdominal radiographs as an assessment tool in patients with Crohn's disease as demonstrated by this study has underlined the importance of adherence to imaging guidelines and has solidified our departmental practice against such 'wasted' radiation. The impact of iterative reconstruction as a dose-saving strategy in CT imaging has been felt, not only by patients with Crohn's disease, but also by a wide range of clinical patients [114-115, 201].

With continuing advances in CT technology, further improvements in image quality can be expected. An important outcome of this research is that we now have a radiation dose centred multi-disciplinary team in place with expert levels of knowledge to apply. Current research projects centre on radiation dose monitoring software (DoseWatch, GE Healthcare) and assessment of patient knowledge regarding radiation dose from medical imaging, as well as more tailored diagnostics centred projects such as modified dose CT at doses equivalent to a chest radiograph in patients with cystic fibrosis on novel medication trials and in patients requiring CT follow-up of indeterminate pulmonary nodules.



References

Iterative Reconstruction as a Novel Method of Radiation Dose Reduction
at Computed Tomography in Patients with Crohn's Disease

1. Mettler FA Jr, Bhargavan M, Faulkner K, et al. Radiologic and nuclear medicine studies in the United States and worldwide: frequency, radiation dose, and comparison with other radiation sources – 1950-2007. *Radiology* 2009; 253(2):520-31.
2. IMV 2014 CT Market Summary Report. Des Plaines, IL: IMV Medical Information Division, 2015.
3. Brenner DJ, Hall EJ. Computed tomography – an increasing source of radiation exposure. *NEJM* 2007; 357:2277-2284.
4. Hricak H, Brenner DJ, Adelstein SJ, et al. Managing radiation use in medical imaging: a multifaceted challenge. *Radiology* 2010; 258(3):889-905.
5. Koenig TR, Wolff D, Mettler FA Jr, Wagner LK. Skin injuries from fluoroscopically guided procedures: part 1, characteristic of radiation injury. *AJR Am J Roentgenol* 2001; 177:3-11.
6. Cardis E, Vrijheid M, Blettner M, et al. The 15-country collaborative study of cancer risk among radiation workers in the nuclear industry: estimates of radiation-related cancer risks. *Radiat Res* 2007; 167:396-416.
7. Brenner D, Elliston C, Hall E, Berdon W. Estimated risks of radiation-induced fatal cancer from pediatric CT. *AJR Am J Roentgenol* 2001; 176:289-96.
8. Smith-Bindman R, Lipson J, Marcua R, et al. Radiation dose associated with common computed tomography examinations and the associated lifetime attributable risk of cancer. *Arch Intern Med* 2009; 169:2078-86.

9. Pearce MS, Salotti JA, Little MP, et al. Radiation exposure from CT scans in childhood and subsequent risk of leukaemia and brain tumours: a retrospective cohort study. *Lancet* 2012; 380:499-505.
10. Boone JM, Hendee WR, McNitt-Gray MF, Seltzer SE. Radiation exposure from CT scans: How to close our knowledge gaps, monitor and safeguard exposure – proceedings and recommendations of the Radiation Dose Summit, sponsored by NIBIB, February 24-25, 2011. *Radiology* 2012; 265(2):544-54.
11. Malone J, Guleria R, Craven C, et al. Justification of diagnostic medical exposures: some practical issues. Report of an International Atomic Energy Agency Consultation. *BRJ Radiol* 2012; 85(1013):523-538.
12. Kinsella SM, Coyle JP, Long EB, et al. Maintenance haemodialysis patients have high cumulative radiation exposure. *Kidney Int* 2010; 78:789-93.
13. Desmond AN, O'Regan K, Curran C, McWilliams S, Fitzgerald T, Maher MM, et al. Crohn's disease: factors associated with exposure to high levels of diagnostic radiation. *Gut* 2008 Nov.;57(11):1524–1529.
14. O'Connell OJ, McWilliams S, McGarrigle A, et al. Radiologic imaging in cystic fibrosis: cumulative effective dose and changing trends over 2 decades. *Chest* 2012; 141:1575-83.
15. Primak AN, McCollough CH, Bruesewitz MR, Zhang J, Fletcher JG. Relationship between noise, dose, and pitch in cardiac multi-detector row CT. *Radiographics* 2006; 26:1785-1794.
16. Geyer LL, Schoepf UJ, Meinel FG, et al. State of the art: iterative CT reconstruction techniques. *Radiology* 2015; 276(2):339-357.

17. Silva AC, Lawder HJ, Hara A, Kujak J, Pavlicek W. Innovations in CT dose reduction strategy: application of the adaptive statistical iterative reconstruction algorithm. *AJR Am J Roentgenol* 2010; 194(1):191-9.
18. Kaza RK, Platt JF, Goodsitt MM, et al. Emerging techniques for dose optimisation in abdominal CT. *Radiographics* 2014; 34:4-17.
19. Hounsfield GN. Nobel Lecture, 8 December 1979. Computed Medical Imaging. *J Radiol* 1980; 61(6-7):459-68.
20. Hounsfield GN. Computerized transverse axial scanning (tomography), Part 1: description of the system. 1973. *Br J Radiol* 1995; 68(815):H166-72.
21. Mould RF. *A century of x-rays and radioactivity in medicine*. CRC Press, 1993. Print.
22. Di Chiro G, Brooks RA. The 1979 Nobel Prize in Physiology or Medicine. *J Comput Assist Tomogr* 1980; 4(2):241-5.
23. The Times, 20 April 1973, p19, "The Queen's Award to Industry'.
24. Hounsfield GN. Potential uses of more accurate CT absorption values by filtering. *AJR Am J Roentgenol* 1978; 131(1):103-6.
25. Bushberg JT, Seibert JA, Leidholdt EM, Boone JM. *The essential physics of medical imaging, 3rd ed*. Philadelphia, PA: Lippincott Williams & Wilkins, 2012. Print.
26. Kalender WA. *Computed tomography: fundamentals, system technology, image quality, applications, 3rd ed*. Erlangen, Germany: Publicis Publishing, 2011. Print.
27. Levi C, Gray JE, McCullough EX, Hattery RR. The unreliability of CT numbers as absolute values. *AJR Am J Roentgenol* 1982; 139:443-447.

28. Zerhouni EA, Spivey JF, Morgan RH, Leo FP, Stitik FP, Siegelman SS. Factors influencing quantitative CT measurements of solitary pulmonary nodules. *J Comput Assist Tomogr* 1982; 6:1075–1087.
29. Hunter TB, Pond GD, Medina O. Dependence of substance CT number on scanning technique and position within scanner. *Comput Radiol* 1983; 7:199–203.
30. Birnbaum BA, Hindman N, Lee J, Babb JS. Multidetector row CT attenuation measurements: assessment of intra- and interscanner variability with an anthropomorphic body CT phantom. *Radiology* 2007; 242:109–119.
31. European Commission. Radiation Protection N° 180. Medical Radiation Exposure of the European Population. Part 1/2. Contract ENER/2010/NUCL/SI2.581237. Luxembourg: European Union, 2014. Available from: <https://ec.europa.eu/energy/sites/ener/files/documents/RP180.pdf>
32. United Nations Scientific Committee on the Effects of Atomic Radiation (UNSCEAR). Sources and Effects of Ionising Radiation, Volume 1. UNSCEAR 2008, United Nations, New York, 2010.
33. Davies HE, Wathen CG, Gleeson FV. The risks of radiation exposure related to diagnostic imaging and how to minimise them. *BMJ* 2011; 342:d947.
34. Berrington de Gonzales A, Darby S. Risk of cancer from diagnostic x-rays: estimates for the UK and 14 other countries. *Lancet* 2004; 363:345-51.

35. Sodickson A, Baeyens PF, Andriole KP, et al. Recurrent CT, cumulative radiation exposure, and associated radiation-induced cancer risks from CT of adults. *Radiology* 2009; 251(1):175-84.
36. Brenner DJ, Hricak H. Radiation exposure from medical imaging: time to regulate? *JAMA* 2010; 304(2):208-9.
37. Ding GX, Munro P, Pawlowski J, Malcolm A, Coffey CW. Reducing radiation exposure to patients from kV-CBCT imaging. *Radiother Oncol* 2010; 97(3):585-92.
38. Paterson A, Frush DP, Donnelly LF. Helical CT of the body: are settings adjusted for pediatric patients? *AJR Am J Roentgenol* 2001; 176(2):297-301.
39. Pierce DA, Preston DL. Radiation-related cancer risks at low doses among atomic bomb survivors. *Radiat Res* 2000; 154(2):178-86.
40. Preston DL, Shimizu Y, Pierce DA, Suyama A, Mabuchi K. Studies of mortality of atomic bomb survivors. Report 13: Solid cancer and noncancer disease mortality: 1950-1997. *Radiat Res* 2012; 178(2):AV61-87.
41. Kathren RL. Pathway to a paradigm; the linear non-threshold dose-response model in historical context. The American Academy of Health Physics 1995; Radiology Centennial Hartman Oration. *Health Phys* 1996; 70(5):621-35.
42. ICRP, Publication 102: Managing patient dose in multi-detector computed tomography. *Ann ICRP* 2007; 37(1).
43. Brink JA, Amis ES Jr. Image Wisely: a campaign to increase awareness about adult radiation protection. *Radiology* 2010; 257(3):601-2.

44. Goske MJ, Applegate KE, Bulas D, et al. Image Gently: progress and challenges in CT education and advocacy. *Pediatr Radiol* 2011; 41 Suppl 2:461-6.
45. Brink JA, Miller DL. US National Diagnostic Reference Levels: closing the gap. *Radiology* 2015; 277:3-6.
46. ICRP, Publication 26: Recommendations of the International Commission on Radiological Protection. *Ann ICRP* 1977; 1(3).
47. Slovis TL. Children, computed tomography radiation dose, and the As Low As Reasonably Achievable (ALARA) concept. *Pediatrics* 2003; 112(4):971-2.
48. Slovis TL. The ALARA concept in pediatric CT: myth or reality? *Radiology* 2002; 223(1):5-6.
49. Kalra MK, Maher MM, Toth TL, et al. Strategies for CT radiation dose optimisation. *Radiology* 2004; 230(3):619-28.
50. McCollough CH, Primak AN, Braun N, Kofler J, Yu L, Christner J. Strategies for reducing radiation dose in CT. *Radiol Clin North Am* 2009; 47:27-40.
51. Dougeni E, Faulkner K, Panayiotakis G. A review of patient dose and optimisation methods in adult and paediatric CT scanning. *Eur J Radiol* 2012; 81(4):e665-e683.
52. Seeram E. *Computed tomography: physical principles, clinical applications, and quality control*, 4th ed. Elsevier Health Sciences, 2015. Print.
53. Maldjian PD, Goldman AR. Reducing radiation dose in body CT: a primer on dose metrics and key CT technical parameters. *AJR Am J Roentgenol* 2013; 200:741-7.

54. Kalra MK, Maher MM, Sahani DV, et al. Low-dose CT of the abdomen: evaluation of image improvement with use of noise reduction filters – pilot study. *Radiology* 2003; 228(1):251-6.
55. Hsieh J. Adaptive statistical iterative reconstruction. Whitepaper, GE Healthcare 2008.
56. Hsieh J, Nett B, Yu Z, Sauer K, Thibault JB, Bouman CA. Recent advances in CT image reconstruction. *Curr Radiol Rep* 2013; 1:39-51.
57. Thibault JB. Veo CT model-based iterative reconstruction. GE Healthcare Whitepaper 2010.
58. Patino M, Fuentes JM, Hayano K, Kambadakone AR, Uyeda JW, Sahani DV. A quantitative comparison of noise reduction across five commercial (hybrid and model-based) iterative reconstruction techniques: An anthropomorphic phantom study. *AJR Am J Roentgenol* 2015; 204:W176-W183.
59. Koral KF, Rogers WL. Application of ART to time-coded emission tomography. *Phys Med Biol* 1979; 24(5):879-94.
60. Pelc NJ, Chesler DA. Utilization of cross-plane rays for three-dimensional reconstruction by filtered back-projection. *J Comput Assist Tomogr* 1979; 3(3):385-95.
61. De Jonge FA, Blokland KA. Statistical tomographic reconstruction: how many more iterations to go? *Eur J Nucl Med* 1999; 26(10):1247-50.
62. Beister D, Kolditz D, Kalender WA. Iterative reconstruction methods in x-ray CT. *Physica Medica* 2012; 28:94-108.

63. Buxi TBS, Yadav A, Singh Rawat K, Singh Ghumna E. Effect of iterative reconstruction in low dose computed tomography. *J Biomed Graph Comput* 2014; 4(3):1-9.
64. Chen B, Ramirez Giraldo JC, Solomon J, Samei E. Evaluating iterative reconstruction performance in computed tomography. *Med Phys* 2014; 41(12):121913.
65. Smith EA, Dillman JR, Goodsitt MM, et al. Model-based iterative reconstruction: effect of patient dose and image quality in pediatric body CT. *Radiology* 2014; 270:526-534.
66. Vardhanabhuti V, Loader R, Roobottom CA. Assessment of image quality effects of varying tube voltage and automatic tube current modulation with hybrid and pure iterative reconstruction techniques in abdominal and pelvic CT. *Invest Radiol* 2013; 48(3):167-74.
67. Vardhanabhuti V, Loader RJ, Mitchell GR, Riordan RD, Roobottom CA. Image quality assessment of standard- and low-dose chest CT using filtered back projection, adaptive statistical iterative reconstruction, and novel model-based iterative reconstruction algorithms. *AJR Am J Roentgenol* 2013; 200(3):545-52.
68. Willemink MJ, de Jong PA, Leiner T, et al. Iterative reconstruction techniques for computed tomography. Part 1. Technical principles. *Eur Radiol* 2013; 23:1623-1631.
69. Raman SP, Johnson PT, Deshmukh S, et al. CT dose reduction applications: available tools on the latest generation of CT scanners. *J Am Coll Radiol* 2013; 10:37-41.

70. Hara AK, Wellnitz CV, Paden RG, Pavlicek W, Sahani DV. Reducing body CT radiation dose: beyond just changing the numbers. *AJR Am J Roentgenol* 2103; 210:33-40.
71. Singh S, Kalra MK, Hsieh J, Licato PE, Do S, Pien HH, et al. Abdominal CT: comparison of adaptive statistical iterative and filtered back projection reconstruction techniques. *Radiology* 2010 Nov.;257(2):373–383.
72. Flicek KT, Hara AK, Silva AC, Wu Q, Peter MB, Johnson CD. Reducing the radiation dose for CT colonography using adaptive statistical iterative reconstruction: A pilot study. *AJR Am J Roentgenol* 2010; 195(1):126-31.
73. Yu Z, Thibault JB, Bouman CA, Sauer KD, Hsieh J. Fast model-based x-ray CT reconstruction using spatially nonhomogenous ICD optimization. *IEEE Trans Image Process* 2011; 20:161-175.
74. Veo™ user manual and technical reference manual. GE Healthcare 2014.
75. Pickhardt PJ, Lubner MH, Kim DH, et al. Abdominal CT with model-based iterative reconstruction (MBIR): initial results of a prospective trial comparing ultra low-dose with standard-dose imaging. *AJR Am J Roentgenol* 2012; 199:1266-1274.
76. Yoon Ma, Kim SH, Lee JM, et al. Adaptive statistical iterative reconstruction and Veo: assessment of image quality and diagnostic performance in CT colonography at various radiation doses. *J Comput Assist Tomogr* 2012; 36:596-601.
77. Deák Z, Grimm JM, Treitl M, et al. Filtered back projection, adaptive statistical iterative reconstruction, and a model-based iterative reconstruction in abdominal CT: an experimental study. *Radiology* 2013; 266(1):197-206.

78. Katsura M, Masuda I, Akahane M, et al. Mode-based iterative reconstruction technique for radiation dose reduction in chest CT: comparison with the adaptive statistical iterative reconstruction technique. *Eur Radiol* 2012; 22(8):1613-23.
79. Miéville FA, Gudinchet F, Brunelle F, Bochud FO, Verdun FR. Iterative reconstruction methods in two different MDCT scanners: physical metrics and 4-alternative forced-choice detectability experiments – a phantom approach. *Phys Med* 2013; 29(1):99-110.
80. Hérin E, Gardavaud F, Chiaradia M, et al. Use of Model-Based Iterative Reconstruction (MBIR) in reduced-dose CT for routine follow-up of patients with malignant lymphoma: dose savings, image quality and phantom study. *Eur Radiol* 2015; 25:2362-2370.
81. Padole A, Khawaja RDA, Kalra MK, Singh S. CT radiation dose and iterative reconstruction techniques. *AJR Am J Roentgenol* 2015; 204(4):W384-W392.
82. Samei E, Richard S, Lurwitx L. Model-based CT performance assessment and optimisation of iodinated and non-iodinated imaging tasks as a function of kVp and body size. *Med Phys* 2014; 41(8):081910.
83. Singh S, Kalra MK, Do S, Thibault JB, Pien H, O'Connor OJ, et al. Comparison of hybrid and pure iterative reconstruction techniques with conventional filtered back projection: dose reduction potential in the abdomen. *J comput assist tomogr* 2012 May;36(3):347–353.
84. Leipsic J, Labounty TM, Heilbron B, et al. Estimated radiation dose reduction using adaptive statistical iterative reconstruction in coronary

- CT angiography: the ERASIR study. *AJR Am J Roentgenol* 2010; 195(3):655-60.
85. Prakash P, Kalra MK, Digumarthy SR, et al. Radiation dose reduction with chest computed tomography using adaptive statistical iterative reconstruction technique: initial experience. *J Comput Assist Tomogr* 2010; 34(1):40-5.
 86. Schindera ST, Diedrichsen L, Müller HA, et al. Iterative reconstruction algorithm for abdominal multidetector CT at different tube voltages: assessment of diagnostic accuracy, image quality, and radiation dose in a study. *Radiology* 2011; 260(2):454-62.
 87. Singh S, Kalra MK, Gilman MD, et al. Adaptive statistical iterative reconstruction technique for radiation dose reduction in chest CT: a pilot study. *Radiology* 2011; 259(2):565-73.
 88. Protik A, Thomas K, Babyn P, Ford NL. Phantom study of the impact of adaptive statistical iterative reconstruction (ASiRO) on image quality for pediatric computed tomography. *J Biomed Sci Eng* 2012; 5:793-803.
 89. Singh S, Kalra MK, Shenoy-Bhangle AS, et al. Radiation dose reduction with hybrid iterative reconstruction for pediatric CT. *Radiology* 2012; 263(2):537-546.
 90. Ghetti C, Palleri F, Serreli G, Ortenzi O, Ruffini L. Physical characterisation of a new CT iterative reconstruction algorithm method operating in sinogram space. *J Appl Clin Med Phys* 2013; 14(4):4347.
 91. Metha D, Thompson R, Morton T, Dhanantwari A, Shefer E. Iterative model reconstruction: simultaneously lowered computed tomography

- radiation dose and improved image quality. *Med Phys Int J* 2013; 1(2):147-155.
92. Goenka AH, Herts BR, Obuchowski NA, et al. Effect of reduced radiation exposure and iterative reconstruction on detection of low-contrast low-attenuation lesions in an anthropomorphic liver phantom: an 18 reader study. *Radiology* 2014; 272(1):154-163.
 93. Kim M, Lee JM, Yoon JH, et al. Adaptive iterative dose reduction algorithm in CT: effect on image quality compared with filtered back projection in body phantoms of different sizes. *Korean J Radiol* 2014; 15(2):195-204.
 94. Klink T, Obmann V, Heverhagen J, Stork A, Adam G, Begemann P. Reducing CT radiation dose with iterative reconstruction algorithms: the influence of scan and reconstruction parameter on image quality and CTDIvol. *Eur J Radiol* 2014; 83:1645-1654.
 95. Khawaja RDA, Singh S, Blake M, et al. Ultra-low dose abdominal MDCT: Using a knowledge-based Iterative Model Reconstruction technique for substantial dose reduction in a prospective clinical study. *Eur J Radiol* 2015; 84:2-10.
 96. Mayo-Smith WW, Hara AK, Mahesh M, Sahani DV, Pavlicek W. How I do it: managing radiation dose in CT. *Radiology* 2014; 273(3):657-72.
 97. J. Boone, K. Strauss, D. Cody, C. McCollough, M. McNitt-Gray, and T. Toth, "Size-specific dose estimates (SSDE) in pediatric and adult body CT exams," Report of AAPM Task Group 204, 2011.
 98. ICRP 2007. 2007 Recommendations of the Internal Commission on Radiological Protection. ICRP Publication 103. *Ann ICRP* 37(2-4):1-332

99. ICRP 1991. 1990 Recommendations of the Internal Commission on Radiological Protection. ICRP Publication 60. *Ann ICRP* 21(1-3).
100. Bankier AA, Kressel HY. Through the looking glass revisited: the need for more meaning and less drama in the reporting of dose and dose reduction in CT. *Radiology* 2012; 265(1):4-8.
101. Goldman LW. Principles of CT: radiation dose and image quality. *J Nucl Med Technol* 2007; 35(4):213-25; quiz 226-8.
102. Bongartz G, Golding SJ, Jurik AG, et al. 2004 CT quality criteria. Office for Official Publications of the European Communities, Luxembourg.
103. Barrett JF, Keat N. Artifacts in CT: recognition and avoidance. *Radiographics* 2004; 24:1679-91.
104. Månsson LG. Methods for the evaluation of image quality: a review. *Radiat Prot Dosimetry* 2000; 90:89-99.
105. Report 54: Medical imaging – assessment of image quality. International commission on radiation units and measurements (ICRU), Bethesda, MD; 1996.
106. Catphan 500 and 600 manual. *The Phantom Laboratory*, Greenwich, NY; 2009.
107. Bath M. Evaluating imaging systems: practical applications. *Radiat Prot Dosimetry* 2010; 139:26-36.
108. Sackett DL. Bias in analytic research. *J Chronic Dis* 1979; 32(1):51-63.
109. Sica GT. Bias in research studies. *Radiology* 2006; 238:780-789.
110. Brealey S, Scally AJ. Bias in plain film reading performance studies. *Br J Radiol* 2001; 74(880):307-16.
111. Obuchowski NA. Special Topics III: bias. *Radiology* 2003; 229(3):617-621.

112. Obuchowski NA. How many observers are needed in clinical studies of medical imaging? *AJR Am J Roentgenol* 2004; 182(4):867-9.
113. Solomon J, Samei E. Quantum noise properties of CT images with anatomical textured backgrounds across reconstruction algorithms: FBP and SAFIRE. *Med Phys* 2014; 41(9):091908.
114. McLaughlin PD, Murphy KP, Hayes SA, et al. Non-contrast CT at comparable dose to an abdominal radiograph in patients with acute renal colic; impact of iterative reconstruction on image quality and diagnostic performance. *Insights Imaging* 2014; 5(2):217-30.
115. Murphy KP, Crush L, Twomey, et al. Model-Based Iterative Reconstruction in CT enterography. *AJR Am J Roentgenol* 2015; 205(6):1173-81.
116. Desai GS, Thabet A, Elias AYA, Sahani DV. Comparative assessment of three image reconstruction techniques for image quality and radiation dose in patients undergoing abdominopelvic multidetector CT examinations. *Br J Radiol* 2013; 86:20120161.
117. Zhao J, Jin Y, Lu Y, Wang G. A filtered backprojection algorithm for triple-source helical cone-beam CT. *IEEE Trans Med Imaging* 2009; 28:384-393.
118. Lee SJ, Park SH, Kim AY, et al. A prospective comparison of standard-dose CT enterography and 50% reduced-dose CT enterography with and without noise reduction for evaluating Crohn disease. *AJR Am J Roentgenol* 2011; 197:50-57.
119. Prakash P, Kalra MK, Kambadakone AK, et al. Reducing abdominal CT radiation dose with adaptive statistical iterative reconstruction technique. *Invest Radiol* 2012; 45:202-210.

120. Kalra MK, Woisetschlager M, Dahlstrom N, et al. Radiation dose reduction with sonogram affirmed iterative reconstruction technique for abdominal computed tomography. *J Comput Assist Tomogr* 2012; 36:339-346.
121. Maxfield MW, Schuster KM, McGillicuddy EA, et al. Impact of adaptive statistical iterative reconstruction on radiation dose in evaluation of trauma patients. *J Trauma Acute Care Surg* 2012; 73(6):1406-11.
122. Hara AK, Paden RG, Silva Ac, et al. Iterative reconstruction technique for reducing body radiation dose at CT: feasibility study. *AJR Am J Roentgenol* 2009; 193:764-771.
123. Kwon H, Cho J, Oh J, et al. The adaptive statistical iterative reconstruction-V technique for radiation dose reduction in abdominal CT: comparison with the adaptive statistical iterative reconstruction technique. *Br J Radiol* 2015; 88(1054):201540463.
124. Kulkarni NM, Uppot RN, Eisner BH, Sahani DV. Radiation dose reduction at multidetector CT with adaptive statistical iterative reconstruction for evaluation of urolithiasis: how low can we go? *Radiology* 2012; 265(1):158-66.
125. Ploussi A, Alexopoulou E, Economopoulos N, et al. Patient radiation exposure and image quality evaluation with the use of iDose4 iterative reconstruction algorithm in chest-abdomen-pelvis CT examinations. *Radiat Prot Dosimetry* 2014; 158(4):399-405.
126. McNitt-Gray MF. AAPM/RSNA physics tutorial for residents: topics in CT. *Radiographics* 2002; 22:1541-1553.

127. Gervaise A, Osemont B, Lecocq S, et al. CT image quality improvement using adaptive iterative dose reduction with wide-volume acquisition on 320-detector CT. *Eur Radiol* 2012; 22:295-301.
128. Rampado O, Bossi L, Garabello D, Davini O, Ropolo R. Characterisation of a computed tomography iterative reconstruction algorithm by image quality evaluations with an anthropomorphic phantom. *Eur J Radiol* 2012; 81:3172-3177.
129. Thiel W. Die Konservierung ganzer Leichen in natürlichen Farben. *Ann Anat* 1992; 174:185-95.
130. Thiel W. Ergänzung für die Konservierung ganze Leichen nach. W. Thiel *Ann Anat* 2002; 184:267-9.
131. Shrimpton P. Assessment of patient dose in CT. In: EUR. European guidelines for multislice computed tomography funded by the European Commission 2004: contract number FIGMCT2000-20078-CT-TIP. Luxembourg, Luxembourg: European Commission, 2004:Appendix C
132. Nakayama Y, Awai K, Funama Y, et al. Lower tube voltage reduced contrast material and radiation doses on 16-MDCT aortography. *AJR Am J Roentgenol* 2006; 187:W490-7.
133. Tang K, Wang L, Li R, Lin J, Zheng X, Cao G. Effect of low tube voltage on image quality, radiation dose and low-contrast detectability at abdominal multidetector CT: Phantom study. *J Biomed Biotechnol* 2012; 2012:130169.
134. Funama Y, Awai K, Nakayama Y, et al. Radiation dose reduction without degradation of low-contrast detectability at abdominal multisection CT with a low-tube voltage technique: phantom study. *Radiology* 2005; 237(3):905-10.

135. Verdun FR, Denys A, Valley JF, Schnyder P, Meuli RA. Detection of low-contrast objects: experimental comparison of single- and multi-detector row CT with a phantom. *Radiology* 2002; 31:2423-2442.
136. Mutic S, Palta JR, Butker EK, et al. Quality assurance for computed-tomography simulators and the computed tomography-simulation process: report of the AAPM Radiation Therapy Committee Task Group 66. *Med Phys* 2003; 30(10):2762-92.
137. Kanal KM, Stewart BK, Kolokythas O, Shuman WP. Impact of operator-selected noise index and reconstruction slice thickness on patient radiation dose in 64-MDCT. *AJR Am J Roentgenol* 2007; 189:219-25.
138. AAPM routine abdomen/pelvis CT protocol (updated 08/07/2015). Available from aapm.org.
139. Crohn BB, Ginzburg L, Oppenheimer GD. Regional ileitis; a pathologic and clinical entity. *Am J Med* 1952; 13(5):583-90.
140. Lockhart-Mammery HE, Morson BC. Crohn's disease (regional enteritis) of the large intestine and its distinction from ulcerative colitis. *Gut* 1960; 1:87-105.
141. Levy AD, Morteale KJ, Yeh BM. 2015, Rotations in Radiology: Gastrointestinal imaging, Oxford University Press, 198 Madison Avenue, New York.
142. Stange EF, Travis SP, Vermeire S, et al. European Crohn's and Colitis Organisation. European evidence based consensus on the diagnosis and management of Crohn's disease: definitions and diagnosis. *Gut* 2006; 55(Suppl 1):i1-i15).

143. Van Assche G, Dignass A, Panes J, et al. The second European evidence-based consensus on the diagnosis and management of Crohn's disease: definitions and diagnosis. *J Crohns Colitis* 2010; 4:7–27.
144. Schreyer AG, Seitz J, Feuerbach S, Rogler G, Herfarth H. Modern imaging using computed tomography and magnetic resonance imaging for inflammatory bowel disease (IBD). *Inflamm Bowel Dis* 2004; 10:45-54.
145. Fidler J. MR imaging of the small bowel. *Radio Clin North Am* 2007; 45:317-31.
146. Levi Z, Fraser A, Krongrad R, et al. Factors associated with radiation exposure in patients with inflammatory bowel disease. *Aliment Pharmacol Ther* 2009; 30:1128-36.
147. Herfarth H, Palmer L. Risk of radiation and choice of imaging. *Dig Dis* 2009; 27:278-84.
148. Bernstein CN, Blanchard JF, Kliever E, et al. Cancer risk in patients with inflammatory bowel disease: a population-based study. *Cancer* 2001; 91:854-62.
149. Jess T, Loftus JE, Velayos FS, et al. Risk of intestinal cancer in inflammatory bowel disease: a population-based study from Olmsted County Minnesota. *Gastroenterology* 2006; 130:1039-46.
150. Making the best use of a department of clinical radiology: guidelines for doctors. 5th ed. Royal College of Radiologists website. <http://rcr.ac.uk/index.asp?PageID=310&PublicationID=17>.
151. Harvey RF, Bradshaw JM. A simple index of Crohn's-disease specific activity. *Lancet* 1980; 1(8167):514.

152. Huda W, Ogden KM, Khorasani MR. Converting dose-length product to effective dose. *Radiology* 2008; 248(3):995-1003.
153. Desmond AN, O'Regan K, Malik N, et al. Selection of symptomatic patients with Crohn's disease for abdominopelvic computed tomography: role of serum C-reactive protein. *Can Assoc Radiol J* 2012; 63(4):267-74.
154. Kalra MK, Rizzo S, Maher MM, et al. Chest CT performed with z-axis modulation: scanning protocol and radiation dose. *Radiology* 2005; 237:303-8.
155. Kalra MK, Maher MM, Kamath RS, et al. 16-slice multidetector-row CT of the abdomen and pelvis: a study for optimization of z-axis modulation technique in 153 subjects. *Radiology* 2004; 233:241-249.
156. Kalra MK, Maher MM, Toth TL, et al. Comparison of z-axis automatic tube current modulation technique with fixed tube current CT scanning of the abdomen and pelvis. *Radiology* 2004; 232:347-53.
157. Jackson CP, Cushing T, Abujudeh HH, et al. RADPEER scoring white paper. *J Am Coll Radiol* 2009; 6:21-5.
158. May MS, Wüst W, Brand M, et al. Dose reduction in abdominal computed tomography: intraindividual comparison of image quality of full-dose standard and half-dose iterative reconstructions with dual-source computed tomography. *Invest Radiol* 2011 ;46(7):465-470.
159. Sagara Y, Hara AK, Pavlicek W, Silva AC, Paden RG, Wu Q. Abdominal CT: comparison of low-dose CT with adaptive statistical iterative reconstruction and routine-dose CT with filtered back projection in 53 patients. *AJR Am J Roentgenol* 2010 ;195(3):713-719.

160. Leipsic J, Heilbron BG, Hague C. Iterative reconstruction for coronary CT angiography: finding its way. *Int J Cardiovasc Imag* 2012; 28(3):613-20.
161. O' Neill SB, McLaughlin PD, Crush L, et al. A prospective feasibility study of sub-millisievert abdominopelvic CT using iterative reconstruction in Crohn's disease. *Eur Radiol* 2013; 23:2503-2512.
162. Craig O, O' Neill SB, O' Neill F, et al. Diagnostic accuracy of computed tomography using lower doses of radiation for patients with Crohn's disease. *Clin Gastroenterol Hepatol* 2012; 10(8):886-92.
163. Pontana F, Pagniez J, Flohr T, et al. Chest computed tomography using iterative reconstruction vs filtered back projection. Part 1. Evaluation of image noise reduction in 32 patients. *Eur Radiol* 2011; 21:627-35.
164. Gervaise A, Naulet P, Beuret F, et al. Low-dose CT with automatic tube current modulation, adaptive statistical iterative reconstruction, and low tube voltage for the diagnosis of renal colic: impact of body mass index. *AJR Am J Roentgenol* 2014; 2002:553-60.
165. Kalra MK, Woisetschlager, Dahlström N, et al. Sinogram-Affirmed iterative reconstruction of low-dose chest CT: effect on image quality and radiation dose. *AJR Am J Roentgenol* 2013; 201:W235-W244.
166. Peloquin JM, Pardi DS, Sandborn WJ, Fletcher JG, McCollough CH, Schueler BA, et al. Diagnostic ionizing radiation exposure in a population-based cohort of patients with inflammatory bowel disease. *Am J Gastroenterol* 2008; 103(8):2015-2022.
167. Newnham E, Hawkes E, Surender A, James SL, Gearry R, Gibson PR. Quantifying exposure to diagnostic medical radiation in patients with

- inflammatory bowel disease: are we contributing to malignancy? *Aliment Pharmacol Ther* 2007;26(7):1019–1024.
168. Kroeker KI, Lam S, Birchall I, Fedorak RN. Patients with IBD are exposed to high levels of ionizing radiation through CT scan diagnostic imaging: a five-year study. *J Clin Gastroenterol* 2011;45(1):34–39.
 169. Kambadakone AR, Chaudhary NA, Desai GS, Nguyen DD, Kulkarni NM, Sahani DV. Low-dose MDCT and CT enterography of patients with Crohn disease: feasibility of adaptive statistical iterative reconstruction. *AJR Am J Roentgenol* 2011; 196(6):W743–52.
 170. Mitsumori LM, Shuman WP, Busey JM, Kolokythas O, Koprowicz KM. Adaptive statistical iterative reconstruction versus filtered back projection in the same patient: 64 channel liver CT image quality and patient radiation dose. *Eur Radiol* 2011; 22(1):138–143.
 171. Vorona GA, Ceschin RC, Clayton BL, Sutcavage T, Tadros SS, Panigrahy A. Reducing abdominal CT radiation dose with the adaptive statistical iterative reconstruction technique in children: a feasibility study. *Pediatr Radiol* 2011; 41(9):1174–1182.
 172. Winklehner A, Karlo C, Puippe G, Schmidt B, Flohr T, Goetti R, et al. Raw data-based iterative reconstruction in body CTA: evaluation of radiation dose saving potential. *Eur Radiol* 2011; 21(12):2521-2526.
 173. Cornfeld D, Israel G, Detroy E, Bokhari J, Mojibian H. Impact of Adaptive Statistical Iterative Reconstruction (ASIR) on radiation dose and image quality in aortic dissection studies: a qualitative and quantitative analysis. *AJR Am J Roentgenol* 2011;196(3):W336–40.

174. Nelson R, Feuerlein S, Boll D. New iterative reconstruction techniques for cardiovascular computed tomography: How do they work, and what are the advantages and disadvantages? *J Cardiovasc Comput Tomogr* 2011; 5(5):286-92.
175. Hu L, Wang Y, Hou H, Wei F, Yang G, Chen Y. Radiation dose and image quality with abdominal computed tomography with automated dose-optimized tube voltage selection. *J Int Med Res* 2014; 42(4):1011-7.
176. Layritz C, Muschiol G, Flohr T, Bietau C, Marwan M, Schuhbaeck A, et al. Automated attenuation-based selection of tube voltage and tube current for coronary CT angiography: reduction of radiation exposure versus a BMI-based strategy with an expert investigator. *J Cardiovasc Comput Tomogr* 2013; 7(5):303–10.
177. Husarik DB, Schindera ST, Morsbach F, Chuck N, Seifert B, Szucs-Farkas Z, et al. Combining automated attenuation-based tube voltage selection and iterative reconstruction: a liver phantom study. *Eur Radiol* 2014; 24(3):657–67.
178. Gonzalez-Guindalini FD, Ferreira Botelho MP, Töre HG, Ahn RW, Gordon LI, Yaghmai V. MDCT of chest, abdomen, and pelvis using attenuation-based automated tube voltage selection in combination with iterative reconstruction: an inpatient study of radiation dose and image quality. *AJR Am J Roentgenol* 2013; 201(5):1075–82.
179. Schreyer AG, Hoffstetter P, Daneschnejad M, Jung E-M, Pawlik M, Friedrich C, et al. Comparison of conventional abdominal CT with MR-enterography in patients with active Crohn's disease and acute abdominal pain. *Acad Radiol* 2010; 17(3):352–357.

180. NCRP National Council of Radiation Protection and Measurements. Report No. 160 – ionizing radiation exposure of the population of the United States. Bethesda: NCRP; 2009.
181. Levine MS. Plain film diagnosis of the acute abdomen. *Emerg Med Clin North Am* 1985; 3(3):541-62.
182. Huprich JE, Rosen MP, Fidler JL, et al. ACR Appropriateness Criteria on Crohn's disease. *J Am Coll Radiol* 2010; 7:94–102.
183. iRefer guidelines: gastrointestinal system G15 – suspected small bowel disease (Crohn's disease). Available at: www.irefer.org.uk/index.php/features/gastrointestinal-system
184. Kellow ZS, MacInnes M, Kurzencwyg D, et al. The role of abdominal radiography in the evaluation of the nontrauma emergency patient. *Radiology* 2008; 248(3):887-93.
185. Tareen F, McLaughlin D, Cianci F, et al. Abdominal radiography is not necessary in children with intussusception. *Pediatr Surg Int* 2015 Nov 6. [Epub ahead of print]
186. Alshamari M, Norrman E, Geijer M, Jansson K, Geijer H. Diagnostic accuracy of low-dose CT compared with abdominal radiography in non-traumatic acute abdominal pain: prospective study and systematic review. *Eur Radiol* 2015 Sep 18 [Epub ahead of print]
187. Gans SL, Stoker J, Boermeester MA. Plain abdominal radiography in acute abdominal pain; past, present, and future. *Int J Gen Med* 2012; 5:525-33.
188. Maynard W. Reality or science fiction? A comparison of concordance in clinical presentation against referral forms in requests for abdominal

- radiographs in the emergency setting. ePoster presentation The UK Radiological Congress (UKRC) 2015 meeting.
189. O' Regan K O' Connor OJ, O' Neill SB, et al. Plain abdominal radiographs in patients with Crohn's disease: radiological findings and diagnostic value. *Clin Radiol* 2012; 67(8):774-81.
190. Thompson WM, Kilani RK, Smith BB, et al. Accuracy of abdominal radiography in acute small-bowel obstruction: does reviewer experience matter? *AJR Am J Roentgenol* 2007; 188:W233-8.
191. Korn A, Bender B, Fenchel M, et al. Sinogram affirmed iterative reconstruction in head CT: improvement of objective and subjective image quality with concomitant radiation dose reduction. *Eur J Radiol* 2013; 82:1431-5.
192. Marin D, Nelson RC, Schindera ST, et al. Low-tube voltage, high tube current multidetector abdominal CT: improved image quality and decreased radiation dose with adaptive statistical iterative reconstruction algorithm – initial clinical experience. *Radiology* 2010; 254:145-53.
193. Husarik DB, Marin D, Samei E, et al. Radiation dose reduction in abdominal computed tomography during the late hepatic arterial phase using a model-based iterative reconstruction algorithm: how low can we go? *Invest Radiol* 2012; 47:468-74.
194. Moscariello A, Takx RA, Schoepf UJ, et al. Coronary CT angiography: image quality, diagnostic accuracy, and potential for radiation dose reduction using a novel iterative image reconstruction technique – comparison with traditional filtered back projection. *Eur Radiol* 2011; 21:2130-8.

195. Meyer M, Klein SA, Brix G, et al. Whole-body CT for lymphoma staging: feasibility of halving radiation dose and risk by iterative image reconstruction. *Eur J Radiol* 2014; 83:315-21.
196. Kidoh M, Nakaura T, Nakamura S, et al. Low-dose abdominal CT: comparison of low tube voltage with moderate-level iterative reconstruction and standard tube voltage, low tube current with high-level iterative reconstruction. *Clin Radiol* 2013; 68:1008-15.
197. Vardhanabhuti V, Riordan RD, Mitchell GR, Hyde C, Roobottom CA. Image comparative assessment using iterative reconstructions: clinical comparison of low-dose abdominal/pelvic computed tomography between adaptive statistical, model-based iterative reconstructions and traditional filtered back projection in 65 patients. *Invest Radiol* 2014; 49(4):209–16.
198. Solomon JB, Christianson O, Sami E. Quantitative comparison of noise texture across CT scanners from different manufacturers. *Med Phys* 2012; 39:6048-6055.
199. Gordic S, Desbiolles L, Stolzmann P, et al. Advanced modelled iterative reconstruction for abdominal CT: qualitative and quantitative evaluation. *Clin Radiol* 2014; 69(12):e497-504.
200. Sudarski S, Apfaltrer P, Nance Jr JW, et al. Objective and subjective image quality of liver parenchyma and hepatic metastases with virtual mono-energetic dual-source dual-energy CT reconstructions: an analysis in patients with gastrointestinal stromal tumour. *Acad Radiol* 2014; 21:514-22.

201. Sullivan CJ, Murphy KP, McLaughlin PD, et al. Radiation exposure from diagnostic imaging in young patients with testicular cancer. *Eur Radiol* 2015; 25(4):1005-13.



Appendices

Iterative Reconstruction as a Novel Method of Radiation Dose Reduction
at Computed Tomography in Patients with Crohn's Disease



Tel: + 353-21-490 1901
Fax: + 353-21-490 1919

COISTE EITICE UM THAIGHDE CLINICIÚIL
Clinical Research Ethics Committee

Lancaster Hall,
6 Little Hanover Street,
Cork,
Ireland.

GE

Project
3 & 4

Coláiste na hOllscoile Corcaigh, Éire
University College Cork, Ireland

Our ref: ECM 3 (kk) 09/04/13

14th March 2013

Professor Michael Maher
Department of Radiology
Cork University Hospital
Wilton
Cork

Re: Low-dose CT using iterative reconstruction in patients with inflammatory bowel disease: prospective, randomised evaluation of safety and patient outcome.

Dear Professor Maher

The Chairman approved the following:

- Final version of consent form.

Full approval is now granted to carry out the above study.

We note that the co-investigators involved in this study will be:

- Dr Patrick McLaughlin, Dr Siobhan O'Neill, Dr Kevin O'Regan, Dr Sean MacSweeney, Dr Owen O'Connor, Anne Marie McGarrigle, Professor Fergus Shanahan, Professor Eamonn Quigley and Dr Lee Crush.

Yours sincerely

Professor Michael Molloy
Chairman
Clinical Research Ethics Committee
of the Cork Teaching Hospitals



Tel: + 353-21-490 1901
Fax: + 353-21-490 1919

COISTE EITICE UM THAIGHDE CLINICIÚIL
Clinical Research Ethics Committee

Lancaster Hall,
6 Little Hanover Street,
Cork,
Ireland.

Coláiste na hOllscoile Corcaigh, Éire
University College Cork, Ireland

Our ref: ECM 3 (bbb) 01/10/13

16th September 2013

Professor Michael Maher
Department of Radiology
Cork University Hospital
Wilton
Cork

Re: Sub-millisievert CT scanning of the abdomen and pelvis using model based iterative reconstruction (MBIR) in patients with inflammatory bowel disease: prospective, randomised evaluation of diagnostic efficacy, safety and patient outcome.

Dear Professor Maher

The Chairman approved the following:

- Revised Consent Form.

Full approval is now granted to carry out the above study.

We note that the co-investigators involved in this study will be:

- Dr Kevin Murphy, Dr Siobhan O'Neill, Dr Owen O'Connor, Dr Kevin O'Regan, Anne Marie McGarrigle, Dr Sean McSweeney and Professor Fergus Shanahan.

Yours sincerely

Professor Michael G Molloy
Chairman
Clinical Research Ethics Committee
of the Cork Teaching Hospitals

The Clinical Research Ethics Committee of the Cork Teaching Hospitals, UCC, is a recognised Ethics Committee under Regulation 7 of the European Communities (Clinical Trials on Medicinal Products for Human Use) Regulations 2004, and is authorised by the Department of Health and Children to carry out the ethical review of clinical trials of investigational medicinal products. The Committee is fully compliant with the Regulations as they relate to Ethics Committees and the conditions and principles of Good Clinical Practice.



Tel: + 353-21-490 1901
Fax: + 353-21-490 1919

Coláiste na hOllscoile Corcaigh, Éire
University College Cork, Ireland

COISTE EITICE UM THAIGHDE CLINICIÚIL
Clinical Research Ethics Committee

Lancaster Hall,
6 Little Hanover Street,
Cork,
Ireland.

Our Ref: ECM 4 (ii) 08/12/09

4th November 2009

Professor Michael Maher
Professor of Radiology
Cork University Hospital
Wilton
Cork

Re: Low-dose CT using iterative reconstruction in patients with inflammatory bowel disease.

Dear Professor Maher

Expedited approval is granted to carry out the above study in:

- Cork University Hospital.

The following documents were approved:

- Application Form
- Consent Form – Remove the word “sample” from the title prior to use
- Research Protocol
- Data Collection Summary.

We note that the co-investigators involved in this study will be:

- Dr Owen O'Connor, Dr Alan Desmond, Dr Kevin O'Regan, Dr Patrick McGloughlin, Ann Marie McGarrigle, Sebastian McWilliams, Dr Matrin Buckley, Professor Fergus Shanahan, Professor Eamonn Quigley.

Yours sincerely



Dr Michael Hyland
Chairman
Clinical Research Ethics Committee
of the Cork Teaching Hospitals



Index

Iterative Reconstruction as a Novel Method of Radiation Dose Reduction at
Computed Tomography in Patients with Crohn's Disease

A

Adaptive Statistical Iterative Reconstruction, ASiR 26, 32, 53, 146, 240, 264
Aims of thesis 48
ALARA XXV, 16, 38, 207
Anthropomorphic phantom 55, 57, 65, 67, 236, 243
ASiR strength 27, 144, 146, 166, 240, 255
Attenuation 4, 6, 65, 85, 118, 152, 182, 233, 242, 245, 260
Automated tube current modulation XXVI, XXVII, 12, 86, 91

B

Bias 43, 88, 140, 206
Brenner 14

C

Cadavers 56, 61, 65, 67, 236, 239, 243
Catphan phantom 41, 56, 58, 68, 236, 242
Contrast to noise ratio, CNR 41, 68
Cormack 3, 4
Crohn's disease 98
Crohn's disease activity score 116, 179, 215
CT enterography 100, 140, 142, 202, 206
CT history 3
CT scanner set-up 4, 5, 8
CT Dose Index, CTDI_{vol} 35, 36, 113

D

Data acquisition 10
Desmond 102, 211, 226, 264
Diagnostic acceptability 42, 117, 152, 181
Diagnostic accuracy 42, 115, 151, 178, 215, 220
Dose concerns 13, 101, 137, 207, 264
Dose determinants 17
Doses for various diagnostic radiology procedures 14
Dose Length Product, DLP 36, 113

E

Effective diameter 36, 113
Effective dose 36, 114

F

Filters 11
Filtered back projection 19, 86, 146, 233

H

Harvey Bradshaw Index 108
Helical scanning 9
Hounsfield 3, 4
Hounsfield Units 6, 40, 234
Hypotheses of thesis 48

I

Image processing 11
Ischiorectal fossa fat 254, 261

Iterative reconstruction XXVI,
21, 52, 260

J

Justification XXIV, 264

L

Linear no-threshold model
15, 264

Low contrast resolution 38,
41, 68, 118, 152, 182

M

**Method of reference case
review** 183

**Model Based Iterative
Reconstruction, MBIR** 26, 28,
32, 53, 174, 202, 205, 240

Multi-detector CT 8

N

Nobel Prize 4

Noise 39, 66, 118, 152, 182,
233

Noise index 18, 86

Noise Reduction, NR 29, 53,
241

O

Objectives 49

Optimisation XXIV, 228, 264

P

Paterson 14

Pearce 15, 264

Phantoms 46, 55, 236, 239

Plain abdominal radiograph
209, 213, 226, 230

R

Resolution Preference, RP 29,
53, 241

S

Sample size calculation 109

Signal to noise ratio, SNR 40,
66, 119, 152, 182, 246

**Size Specific Dose Estimation,
SSDE** 35, 36, 113

Spatial resolution 38, 41, 68

Split dose CT protocol 54, 92,
104, 110, 137, 146, 148, 176,
207, 213, 240

Strictures 123, 140, 189, 203

Streak artefact 118, 152, 181,
261

Subjective image noise 117,
152, 181

T

Tube current 18, 85

Tube voltage 18, 85, 89, 207,
261

V

**Vendor specific iterative
reconstruction algorithms** 25

Visual grading analysis 44